BODLEIAN LIBRARY OXFORD
DEPOSITED
THE818
30-3-79

STRUCTURAL AND CHEMICAL STUDIES IN THE NIOBIUM OXIDES AND RELATED COMPOUNDS

by

S. KAMAL E. FORGHANY
Wolfson College

A Thesis submitted for the degree of
Doctor of Philosophy
to the Board of the Faculty of
Physical Sciences at the
University of Oxford

September 1978

To the memory of

my father

ACKNOWLEDGEMENTS

I would like to express my gratitude to Professor J.S. Anderson F.R.S. for accepting me as a student in his eminent Solid State research group in the Inorganic Chemistry Laboratory, Oxford, and for introducing me to this interesting field of Science. His guidance, encouragement and constructive criticism are respectfully mentioned here.

My thanks are due to Dr. A.K. Cheetham (Chemical Crystallography Laboratory) who, after Professor Anderson's retirement, kindly undertook the supervision during the writing stage of this thesis. I am indebted to him for his critical reading of the Chapters and for his helpful comments and advice.

I am grateful to Dr. J.L. Hutchison for teaching me the principles of high resolution electron microscopy, to Dr. G.K.L. Cranstoun for giving me a place in his laboratory during the final part of the work and to Dr. G. Garton (Clarendon Laboratory) for the critical reading of Chapter II.

Mr. K. Waters very skilfully photographed diagrams and electron micrographs and my sincere thanks are due to him for his continuous and kind co-operation. I also wish to thank other members of the technical and administrative staff of the Inorganic Chemistry Laboratory for their helpful assistance and I acknowledge here colleagues for providing assistance in the computerizing of data.

Mr. G. Dixon-Brown (Department of Metallurgy and Science of Materials) kindly allowed me to use the Philips EM 300 electron microscope, the hot stage of which was needed for investigations reported in Chapter VI.

Mrs. P. Lawrence expertly typed the manuscript and I am grateful for her most valuable co-operation.

It is my wish to thank, in this place, my wife Janny for the careful reading of the drafts and for many constructive comments. Her understanding and encouragement in every stage of the work has been invaluable to me.

It is appropriate to mention here Mr. Kazem Keshvary whose invaluable personal influence earlier in my education has had a great impact on my career.

The financial support of the Ministry of Science and Higher Education of Iran, of the University of Azarabadegan, Tabriz, Iran and of the British Council is gratefully acknowledged here.

S.K.E. Forghany

Oxford, September, 1978

ABSTRACT

STRUCTURAL AND CHEMICAL STUDIES IN THE NIOBIUM OXIDES AND RELATED COMPOUNDS

S.K.E. Forghany

(Wolfson College, Oxford)

Thesis submitted for the degree of Doctor of Philosophy

Trinity Term

The chemistry and thermodynamics of the Nb-O system and the related Ti-Nb-O system were studied to elucidate: 1) Kinetic characteristics of block structure oxides at T>1300°C, 2) Thermodynamic properties of block structure oxides at T>1300°C and 3) Phase equilibria in the metastable Nb_2O_5 systems.

Single crystals of B- and P-Nb_2O_5 were prepared by the Chemical Vapour Transport Technique under predominantly convection controlled conditions. Phase equilibria experiments were carried out in a Cahn microbalance system and a newly designed Horizontal Quench Furnace line. Controlled oxygen potentials were generated from CO_2/CO or CO_2/H_2 gas mixtures. Structural studies of the oxides involved X-ray diffraction, electron diffraction and high resolution transmission electron microscopy (HRTEM).

Results of phase equilibria studies in the NbO_2 - (B-Nb_2O_5) system at 750°C <T<900°C indicated that the transformation of B- to the block structure phase takes place readily on the area of contact with the Pt. container, probably catalyzed by the platinum surface. The transformed oxides contained both disordered and ordered fragments. In diffraction studies, the disordered structures simulated the tetragonal symmetry of M-Nb_2O_5, the existence of which was contradicted by HRTEM results. A new phase $Nb_{43}O_{107}$ having monoclinic lattice parameters of a = 20.3 Å, b = 3.8 Å, c = 61.5 Å and β = 117° was detected in the ordered crystals. Its structural relationships with the neighbouring phases in the Nb-O system is discussed. At 700°C and controlled oxygen potentials, B-Nb_2O_5 transformed directly into NbO_2 on reduction. In the system NbO_2 - (P-Nb_2O_5) at isotherm 750°C and controlled oxygen potentials, $Nb_{12}O_{29}$ existed as the only stable intermediate phase.

Phase equilibria in the system (Ti-Nb-O) were determined by equilibrating $TiNb_2O_7$, $Ti_2Nb_{10}O_{29}$ and $TiNb_{24}O_{62}$ at 1400°C. The oxide-gas equilibrium was attained rapidly (<1 hr). The (p, x) isotherms showed complete bivariance in the systems $(Ti,Nb)O_2$ - $TiNb_2O_7$, $(Ti,Nb)O_2$ - $Ti_2Nb_{10}O_{29}$ and $(Ti,Nb)O_2$ - $TiNb_{24}O_{62}$. HRTEM results showed that the bivariance was due to coherent intergrowth of neighbouring phases in the host lattice, suggesting that Wadsley defects were thermodynamically stable. An abrupt process: $TiNb_2O_7$ → metastable transient $Me_{25}O_{60}$ → $Ti_2Nb_{10}O_{29}$ was also detected. Associated with the reduction of Ti-Nb oxides is the generation of a rutile phase $Ti_xNb_{1-x}O_2$, the composition of which is dependent upon the oxygen potential. The results are summarised in a ternary phase diagram.

SUMMARY

In the Nb-O system [i.e. mixed Nb (IV) and Nb (V) oxides] as well as in the related TiO_2-Nb_2O_5 compounds, two orthogonal sets of shear planes (CS planes) divide the ReO_3-type parent into blocks or columns.

Block structures are characterized by specific column dimensions i.e. length and width and by the modes of column linkage. A review of current knowledge of the Chemistry and Thermodynamics of crystallographic shear (CS) phases and block structure compounds is given in Chapter I of this Thesis. The review shows that the following aspects needed further investigation:

1) The kinetic characteristics of (CS) and block structure compounds at high temperatures - i.e. $T > 1300^{o}C$.
2) Thermodynamic properties of block structure oxides at high temperatures - i.e. $T > 1300^{o}C$.
3) Phase equilibria in the different metastable niobium pentoxides - i.e. B- and P-Nb_2O_5.

The investigation of these three aspects was the objective of the present study. The studies and their results are reported in seven Chapters of this Thesis as follows:

Non-stoichiometry and Thermodynamics of metal-oxide systems, notably (CS) and block-based oxides, are reviewed in Chapter I in which the aim of the present study is also discussed in detail.

In Chapter II, preparative methods are described for

single crystals of metastable modifications of niobium pentoxide (i.e. B-, P-, and N-Nb_2O_5) employing the Chemical Vapour Transport Technique with $NbCl_5$ / Cl_2 as transporters. The growth rate of the crystals was improved by employing sample tubes having a larger diameter (33 mm) and containing chlorine gas in a lower pressure (p_{Cl_2} = 0.5 atm. at 23°C) than have previously been reported. Prior to phase equilibria studies of B- and P-Nb_2O_5 crystals, impurities such as condensed niobium oxychloride on the surface of the crystals, as well as interstitial chlorine atoms trapped in the process of crystal growth, were removed by heat treatment of the crystals in the vacuum environment of a Cahn microbalance system. Thermogravimetric measurements suggested that crystals of B-, P- and N-Nb_2O_5, on average, had less than 0.01 Cl % impurities.

Thermogravimetric analysis of blue B-Nb_2O_5 crystals, also grown under oxidizing conditions, indicated that these crystals were substoichiometric.

Details of the methods applied in phase equilibria studies of metastable B- and P-Nb_2O_5 as well as of the Ti-Nb-O systems are given in Chapter III.

Reducing atmospheres were generated by CO_2-CO or CO_2-H_2 gas mixtures of known compositions. The phase equilibria studies were carried out in two different experimental set-ups, employing different temperature ranges. At the low temperatures (i.e. T < 1100°C) required in studies of metastable Nb-O systems, a Cahn microbalance line was utilized. At the high temperatures (i.e. T > 1300°C),

needed for the investigation of the Ti-Nb-O system, a newly designed Horizontal Quench Furnace was employed which permitted equilibration of oxides at fixed isothermal-isobaric conditions and also allowed quenching of the reduced oxides at a fast rate in a vacuum environment. Oxide compositions were determined by a thermogravimetric method at approximately 1100°C using a Cahn microbalance line.

For structural studies of the reduced oxides, X-ray powder diffraction, electron diffraction and high resolution transmission electron microscopy were employed. A brief description of the latter technique and a discussion on the interpretation of electron micrographs are given in Chapter IV.

Thermodynamic and structural aspects of B-Nb_2O_5 phase conversion, under oxidizing and reducing atmospheres at 950° - 700°C, are reported in Chapter V.

B-Nb_2O_5, at T > 900°C, transformed into an extensively disordered block-based structure. At T < 900°C, B-Nb_2O_5 was stable under atmospheric conditions but when a reducing atmosphere was introduced at temperature range 750°C < T < 900°C it transformed into block-type structures, particularly in areas where the sample was in contact with the surface of the platinum container. A further decrease in oxygen partial pressure resulted in the advancement of conversion from the bottom layer towards the uppermost part of the sample, probably through an autocatalytic effect of the first reduced crystals.

X-ray powder diffraction, electron diffraction and electron microscopy of the reduced B-Nb_2O_5 showed that two different kinds of crystals were present with ordered and extensively disordered block structures, respectively. In the disordered crystals, blocks of different sizes were packed coherently, giving rise to the apparent tetragonal symmetry of M-Nb_2O_5. However, the existence of M-Nb_2O_5 was contradicted by evidence obtained from the high resolution lattice images suggesting that M-Nb_2O_5 is not a crystallographic entity.

In ordered crystals, a new phase having the composition $Nb_{43}O_{107}$ was detected. This phase, which represents the second intermediate phase in the system (H-Nb_2O_5)-NbO_2, was shown to be monoclinic with lattice parameters of a = 20.3 Å, b = 3.8 Å, c = 61.58 Å and $\beta = 117^\circ$. The structural relationships between $Nb_{43}O_{107}$ and the neighbouring phases, i.e. $Nb_{28}O_{70}$ and $Nb_{53}O_{132}$ in the phase diagram, are discussed.

In the second part of Chapter V, the direct transformation of the rutile-based shear structure of B-Nb_2O_5 into NbO_2 under reducing atmospheres at 700°C is discussed.

Chapter VI deals with two basic aspects of chemical reactions of the P-Nb_2O_5 polymorph. The first aspect is the phase transformation of P-Nb_2O_5 into the high temperature stable modification H-Nb_2O_5. For this study, an electron microscope equipped with a single-tilt-axis heating holder was used. The transformation into H-Nb_2O_5, for the majority of the P-Nb_2O_5 crystals, was found to occur sharply at circa 850°C. Some crystals transformed at lower temperatures

under the heating influence of the incident electron beam. Other crystals converted at higher temperatures (900 - 930°C). The variation in transformation temperature is probably due to the presence of defects and impurities in the crystal matrix.

Observations further showed that a single crystal taken through the transition point breaks up into polycrystalline H-Nb_2O_5. The conversion is irreversible and does not proceed through the formation of hybrid crystals.

The orientation relationship between P-Nb_2O_5 and H-Nb_2O_5 at the point of transition could not be determined unambiguously due to thermal drift of the specimen. However, tentative indications of the following structural relationship were obtained:

$$[001]_{P\text{-}Nb_2O_5} \parallel [100]_{H\text{-}Nb_2O_5}$$

The second aspect studied involved phase equilibria in the system NbO_2 - (P-Nb_2O_5) at the isotherm 750°C (below the transformation temperature of P-Nb_2O_5). Results showed that $Nb_{12}O_{29}$ was generated abruptly and was the only stable intermediate phase in this system.

Phase equilibria measurements in the system Ti-Nb-O at isotherm 1400°C are reported in Chapter VII. The three distinct compounds present in the system (i.e. $TiNb_2O_7$, $Ti_2Nb_{10}O_{29}$ and $TiNb_{24}O_{62}$) were equilibrated with controlled oxygen partial pressures ranging from 10^{-6} - 10^{-12} (atm.).

Solid-gas equilibrium at the isotherm studied was attained in less than one hour. However, experiments were

run for more than 10 hours in order to attain structural equilibration.

The equilibrium (p, x) diagrams for the three systems $(Ti,Nb)O_2$ - $TiNb_2O_7$, $(Ti,Nb)O_2$ - $Ti_2Nb_{10}O_{29}$ and $(Ti,Nb)O_2$ - $TiNb_{24}O_{62}$, showed bivariant characteristics. This suggested, in terms of classical thermodynamics, the presence of single phases with wide ranges of non-stoichiometry. Structural studies (X-ray powder diffraction, electron diffraction and direct lattice imaging), however, revealed that in the majority of the reduced $TiNb_2O_7$ crystals, the neighbouring phases were intergrown coherently with the matrix, suggesting that these Wadsley defects (i.e. coherent intergrowths of domains or lamellae of the neighbouring phases in the host lattice) are thermodynamically stable species. Certainly, phase transformations in these block-based compounds proceed in a smeared and coherent manner.

Intermediate phases detected in the $(Ti,Nb)O_2$ - $TiNb_2O_7$ system were: o-$Nb_{12}O_{29}$; a solid solution of o-$Nb_{12}O_{29}$ and o-$Ti_2Nb_{10}O_{29}$; a solid solution of m-$Nb_{12}O_{29}$ and m-$Ti_2Nb_{10}O_{29}$; and a solid solution of (Nb_3O_7?) and $TiNb_2O_7$. In addition, during the reduction of $TiNb_2O_7$, a rutile phase ($Ti_xNb_{1-x}O_2$) was found to be rejected from the matrix. The composition of this phase would appear to be dependent upon the equilibrium oxygen partial pressures i.e. at high oxygen pressures the phase was richer in titanium than at lower oxygen potentials. Information obtained from one single crystal fragment suggested that a second reduction pathway i.e. an abrupt process, may also take place here. In this case, $TiNb_2O_7$, by rejecting a rutile phase, reduces

into an intermediate metastable phase ($Me_{25}O_{60}$). This in turn transforms into o-$Me_{12}O_{29}$ (Me = metal), again by rejecting a rutile phase.

A similar phase diagram was found in the $(Ti,Nb)O_2$ - $TiNb_{10}O_{29}$ system. Here, the intermediate phases were: o-$Nb_{12}O_{29}$; a solid solution of m-$Nb_{12}O_{29}$ and $Ti_2Nb_{10}O_{29}$; $Ti_xNb_{1-x}O_2$. The composition of the rejected rutile phase was again dependent on the oxygen potential.

In the $(Ti,Nb)O_2$ - $TiNb_{24}O_{62}$ system, X-ray powder diffraction patterns of the reduced intermediate oxides indicated that in the composition range of $(Ti,Nb)O_{2.417}$ - $(Ti,Nb)O_{2.480}$, the oxide reduction is confined to an oxygen dissociation reaction. However, in the composition range below x = 2.417, i.e. $(Ti,Nb)O_{2.000}$ - $(Ti,Nb)O_{2.417}$, a rutile phase $Ti_xNb_{1-x}O_2$ can also be identified. Below the composition $(Ti,Nb)O_{2.417}$, the oxide reduction follows an identical pathway to that found in the reduction of $Ti_2Nb_{10}O_{29}$. Based on the close similarity between the (Ti-Nb-O) system and that of the binary Nb-O system, the formation of several discrete intermediate phases is tentatively suggested.

The phase equilibria relationships determined in the above three systems are summarized in a triangular phase diagram.

CONTENTS

Page

CHAPTER I GENERAL INTRODUCTION ——— 1

CHAPTER II SINGLE CRYSTAL GROWTH OF B-, P- AND N-Nb_2O_5 APPLYING THE CHEMICAL VAPOUR TRANSPORT TECHNIQUE ——— 36

2.1. Introduction ——— 37

2.2. Materials and Methods ——— 40

2.2.1. Construction of the Chemical Vapour Transport Apparatus ——— 43

2.2.2. Charging of Transport Ampoules ——— 45

2.2.3. Crystal growth ——— 46

2.3. Results ——— 48

2.3.1. Characterisation of the Vapour Transport Products ——— 48

2.3.2. Purification and Impurity estimation of the Chemical Vapour Transport Products ——— 50

2.3.3. Chemical Composition of the blue B-Nb_2O_5 Crystals ——— 54

2.4. Summary and Discussion ——— 55

CHAPTER III EXPERIMENTAL METHODS FOR PHASE EQUILIBRIA STUDIES IN THE SYSTEMS Nb-O AND Ti-Nb-O; CONSTRUCTION OF APPARATUS ——— 57

Introduction ——— 58

3.1. Experimental methods applied in high-temperature thermodynamic measurements of metal-oxygen systems ——— 58

3.2. Design and Construction of Apparatus ——— 64

Page

3.2.1. The mixed gas buffer system ——— 64

3.2.2. The Cahn RG Thermobalance System ——— 70

3.2.3. The Horizontal Quench Furnace System ——— 77

CHAPTER IV ELECTRON MICROSCOPY ——— 86

CHAPTER V THERMODYNAMICS AND STRUCTURAL ASPECTS OF B-Nb_2O_5 REDUCTION ——— 96

5.1. Part A: Phase transformation of B-Nb_2O_5 into block-type structures ——— 97

5.1.1. Introduction ——— 98

5.1.2. Materials and Methods ——— 99

5.1.3. Results ——— 100

5.1.3.1. Thermodynamics ——— 100

5.1.3.2. Structural studies (Electron microscopy) ——— 116

5.1.4. Discussion ——— 143

5.2. Part B: Phase equilibria in the system NbO_2 - (B-Nb_2O_5) ——— 151

5.2.1. Introduction ——— 153

5.2.2. Materials and Methods ——— 153

5.2.3. Results ——— 155

5.2.4. Discussion ——— 159

CHAPTER VI THERMODYNAMICS AND STRUCTURAL ASPECTS OF P-Nb_2O_5 PHASE TRANSFORMATION ——— 161

Part A: Phase transformation of P-Nb_2O_5 into H-Nb_2O_5

Part B: Phase equilibria in the system NbO_2 - (P-Nb_2O_5) ——— 161

Page

6.1. Introduction ——— 162

6.2. Materials and Methods ——— 164

6.2.1. Materials ——— 164

6.2.2. Methods ——— 166

6.3. Results ——— 169

6.3.1. Part A ——— 169

6.3.2. Part B ——— 174

6.3.2.1. Phase equilibria in the system NbO_2 - (P-Nb_2O_5) ——— 174

6.3.2.2. Structural studies ——— 176

6.4. Discussion ——— 180

CHAPTER VII PHASE EQUILIBRIA IN THE SYSTEM Ti-Nb-O AT 1400°C ——— 187

Part A: $(Ti,Nb)O_2$ - $TiNb_2O_7$

Part B: $(Ti,Nb)O_2$ - $Ti_2Nb_{10}O_{29}$ ——— 187

Part C: $(Ti,Nb)O_2$ - $TiNb_{24}O_{62}$

7.1. Introduction ——— 188

7.2. Materials and Methods ——— 191

7.2.1. Materials ——— 191

7.2.2. Experimental method ——— 193

7.3. Results ——— 193

7.3.1. Part A: Phase equilibria in the system $(Ti,Nb)O_2$ - $TiNb_2O_7$ at isotherm 1400°C —195

7.3.1.1. Assessment of the purity of the starting material ($TiNb_2O_7$) ——— 197

7.3.1.2. Thermodynamics ——— 197

7.3.1.3. Structural Studies ——— 200

Page

7.3.1.3.1. X-ray powder diffraction studies ——— 200

7.3.1.3.2. Electron microscopy studies ——— 204

7.3.1.4. Summary ——— 212

7.3.2. Part B: Phase equilibria in the system $(Ti,Nb)O_2$ - o-$Ti_2Nb_{10}O_{29}$ at the isotherm 1400°C ——— 215

7.3.2.1. Assessment of the purity and structural homogeneity of the starting material (o-$Ti_2Nb_{10}O_{29}$) — 217

7.3.2.2. Thermodynamics ——— 217

7.3.2.3. Structural studies ——— 219

7.3.2.4. Summary and Discussion ——— 223

7.3.3. Part C: Phase equilibria in the system $(Ti,Nb)O_2$ - $TiNb_{24}O_{62}$ at isotherm 1400°C (Results and Discussion) ——— 225

7.3.3.1. Assessment of the purity of the starting material ($TiNb_{24}O_{62}$) —— 227

7.3.3.2. Thermodynamics ——— 227

7.3.3.3. Structural aspects ——— 231

7.3.3.3.1. Composition range $(Ti,Nb)O_{2.417}$ - $(Ti,Nb)O_{2.480}$ ——— 231

7.3.3.3.2. Composition range $(Ti,Nb)O_{2.000}$ - $(Ti,Nb)O_{2.417}$ ——— 238

7.3.3.4. Summary ——— 238

7.3.4. Phase relations in the system (TiO_2 - Nb_2O_5 - NbO_2) ——— 239

7.4. Discussion ——— 242

REFERENCES 255

CHAPTER I

GENERAL INTRODUCTION

In a perfect crystalline solid, the atomic arrangement extends indefinitely in three dimensions with a regular periodicity. Such a crystal has a definite stoichiometry which is expressed by the formula of the compound. The ideal stoichiometry occurs only in true thermodynamic equilibrium when the entropy is zero, that is at absolute zero temperature. Real crystals, occurring at temperatures above $0^{o}K$, have an aperiodically perturbed structure associated with small deviations in their chemical composition. The evolution of theories concerning such non-stoichiometry in crystalline compounds is briefly outlined below and the aim of the study presented in this thesis is explained.

In their classical paper on statistical thermodynamics of real crystals, Schottky and Wagner (1930) stated that, in principle, every solid crystalline compound at temperatures above absolute zero can exist as a single phase within a range of compositions. This implies that, for crystalline materials, the concept of a perfectly ordered system must be replaced by that of statistical order, indicating that under conditions of inner equilibrium an inherent degree of disorder persists. The existence of two kinds of point defects has been suggested in the literature: 1) Schottky defects, and 2) Frenkel defects.

(1) A Schottky defect (a in Fig. 1), consists of a vacant cation or anion site: the missing atoms are considered to have migrated to the crystal surface. In a crystal which contains equal numbers of cation and anion

Schottky defects, the ideal stoichiometry is retained.

(2) A Frenkel defect (b in Fig. 1) consists of a vacant lattice site with the atom, which ideally should have occupied that site, occupying a different position. In some crystals, Frenkel defects produce an incomplete cation lattice whereas other crystals have an incomplete anion lattice. The former is more common, since cations in general are smaller than anions and can be accommodated more readily into alternative interstitial positions.

Schottky and Frenkel defects are illustrated diagrammatically in Fig. 1 (after Addison, 1961) for a hypothetical two-dimensional crystal of type AB.

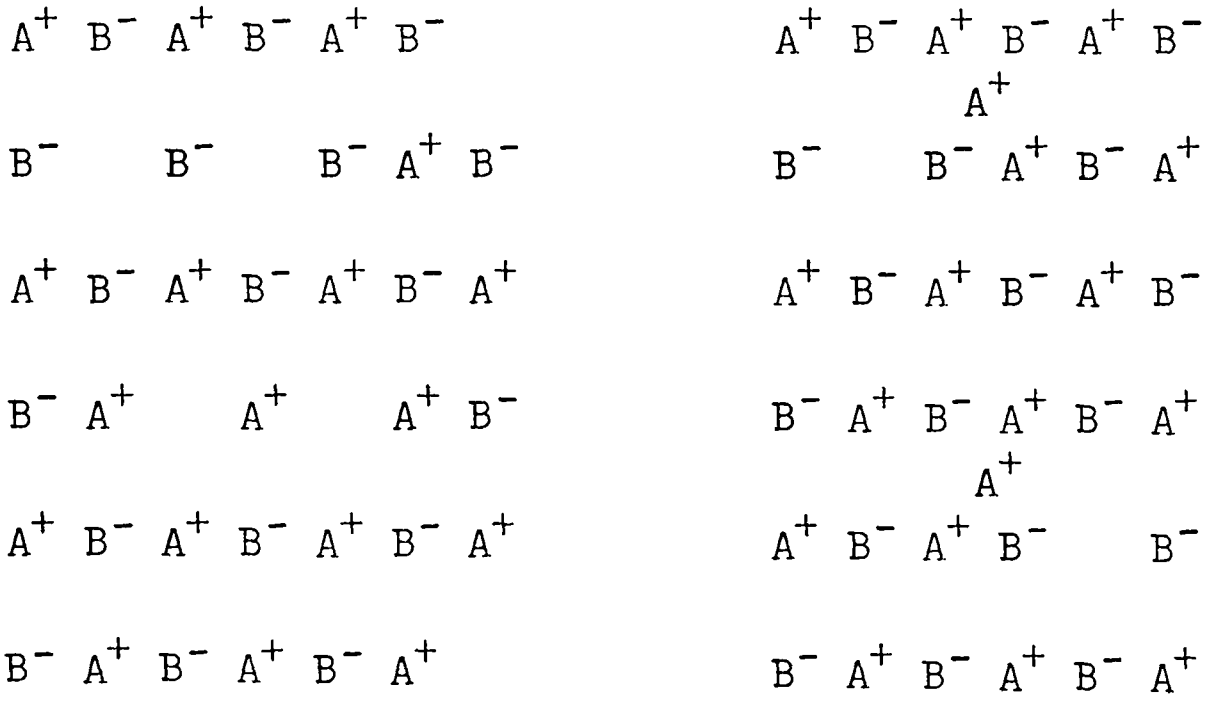

Fig. 1 Schottky and Frenkel defects.

According to Schottky and Wagner, the number of Schottky defects in a crystal AB is given by the formula:

$$n_s = Ne^{-\frac{W_s}{2kT}}$$

in which n_s is the number of Schottky defects per c.c. crystal at T^oK, N the number of ion pairs per c.c. of an

ideal crystal and W_s the work required to form a Schottky defect. The above expression for n_s assumes that $N>>n_s$ -- i.e. the crystal is not grossly defective.

Similarly, the number of Frenkel defects is given by:

$$n_f = \sqrt{NN'}\ e^{-\frac{W_f}{2kT}}$$

in which n_f is the number of Frenkel defects per c.c. of the crystal at T^oK, N the number of sites left vacant per c.c. of the ideal crystal, N' the number of alternative interstitial positions available per c.c. of the crystal and W_f the work required to form a Frenkel defect.

It is apparent that the concentration of defects of either type in a given crystalline system is dependent upon the energy required to produce them and upon the absolute temperature: the number of defects increases with an increase in temperature.

The theory of point defects was subsequently utilized by many investigators to explain the non-stoichiometric behaviour of many crystalline solids. For example, in the rutile (TiO_{2-x}) system (Kofstad, 1962; Forland, 1964) a small deviation of the composition was illustrated through an oxygen dissociation reaction:

$$TiO_2 \rightleftharpoons TiO_{2-x} + x/2O_2$$

In this equation, the quantitative relationship between the chemical potential of oxygen, crystal composition and conductivity can be expressed in terms of the point defect theory through the creation of oxygen vacancies:

TABLE 1

Table 1

Summary of Defect Models. (after Anderson,1972a)

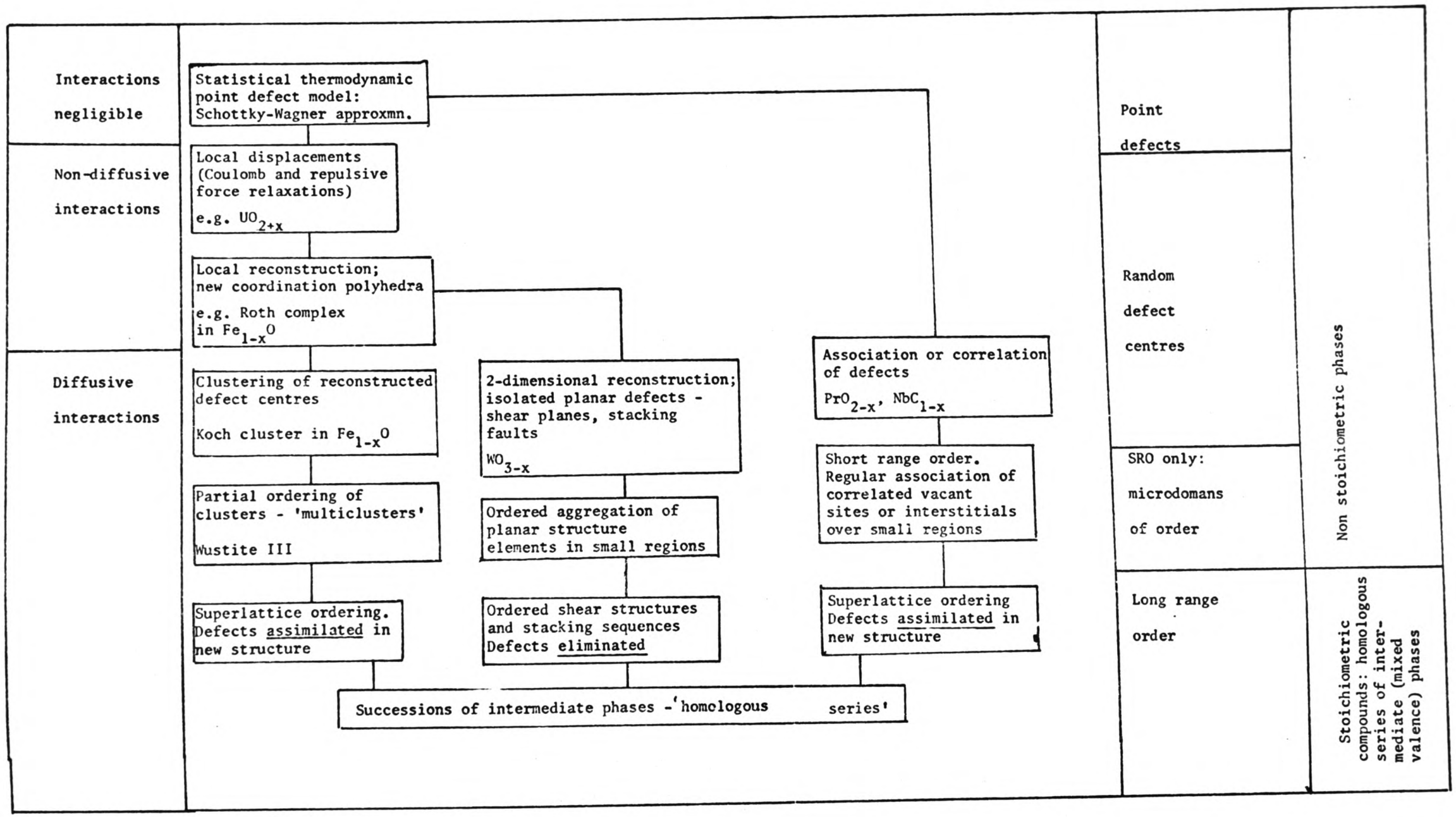

$$O_O^x \rightleftharpoons \tfrac{1}{2}O_2 + V_O^x$$

$$V_O^x \rightleftharpoons V_O^{\cdot} + e^-$$

$$V_O \rightleftharpoons V_O^{\cdot\cdot} + e^-$$

Based upon defect energy considerations, Anderson (1969 a and b, 1970, 1972a) gave a reappraisal of the theory that the formation of simple point defects is the major source of non-stoichiometry. He indicated that relaxation of the point defect system in a crystal may go far beyond a simple rebalancing of coulomb forces and may give rise to a structural transformation of the crystal lattice. Anderson (1972a) summarized the effects of such relaxations and defect interactions in a Table (see Table 1, after Anderson, 1972a). The essence of Anderson's argument is that the common property of a non-stoichiometric system is an inbuilt tendency towards attainment of order, at least on a local scale. Ordered configurations are advantageous as compared with random distributions at significant defect concentrations.

Depending both on the electronic structure of the elements and the compounds, Anderson (1972a) classified the thermodynamic defects (structural consideration) of oxides into five main groups:

1. An approximation of a simple defect model.
2. Non-reconstructive clusters.
3. Reconstructive clustering.
4. Elimination of defects by crystallographic shear.
5. Defects in block-type structures.

In the literature, non-stoichiometric systems have been reviewed and discussed extensively by Cheetham (1971), Fender (1972) and Bevan (1973). The five groups (above) are briefly described below:

(1) An approximation of a simple defect model. This involves a variety of defects within the NaCl-type structures, examplified by the VO and TiO systems (Watanabe et al, 1967 and 1970). Oxides which have a metallic character contain a high concentration of cation and anion vacancies in their structures. Stoichiometric variations alter the electron population within the conduction band. Hence cation and anion vacancies, as charged entities, are screened by the conduction electrons leading to rather weak defect interaction.

The non-stoichiometry of titanium monoxide extends as far as $TiO_{1.25}$. At low temperatures (<1000°C), defects are involved in an ordered configuration forming two superstructures, TiO and $TiO_{1.25}$. The two superstructures are topologically compatible and occur coherently within individual crystallites. The system thus conforms to the concept of microdomain defects of solids (Watanabe et al, 1970).

The microdomain theory, first proposed by Aria and Morozova (1958), suggests that non-stoichiometric crystals consist of microdomains of a different structure (i.e. different composition) intergrown coherently into the main lattice. The size of the microdomains was initially estimated (Aria and Popov, 1962) to be in the range of 200-1000 unit cells, but later, Anderson (1969b) suggested

that the ordering of defects may be restricted to regions of few unit cells in dimension.

(2) Non-reconstructive defect clusters. Due to coulombic forces and crystal field interactions in ionic crystals, point defects may undergo profound defect association reactions to form defect clusters. It is significant in this process that the crystal lattice around the defects might be slightly modified but without causing drastic atomic rearrangements of the parent lattice. A typical example of this type is the sub-stoichiometric structure of binary and ternary fluorite type oxides (Bevan et al, 1965; Parks et al, 1970; Thornber, et al., 1970).

(3) Reconstructive clustering -- i.e. assimilation of defects as structural elements. In interactions between the defects and the surrounding crystal structure, the latter may relax and thereby change the atomic occupancy of the parent lattice. As a result, a new structural configuration may form. Both the parent and new structure should occur in perfect coherency. The non-stoichiometric nature of ferrous oxide ($Fe_{1-x}O$) has been discussed according to this theory (Koch and Cohen, 1969; Fender and Riley, 1970; Cheetham, Fender and Taylor, 1971).

(4) Elimination of defects by crystallographic shear. In oxides containing highly charged transition metal cations -- e.g. Ti^{4+}, V^{4+}, V^{5+}, Nb^{5+}, Mo^{6+}, W^{6+} -- a deviation from stoichiometry does not occur via the formation of point defects, but through rearrangements within the parent structure -- e.g. ReO_3, rutile, etc. -- to form planar defects. This phenomenon, first reported by Magneli (1948, 1950, 1953) in structural studies of non-stoichiometric

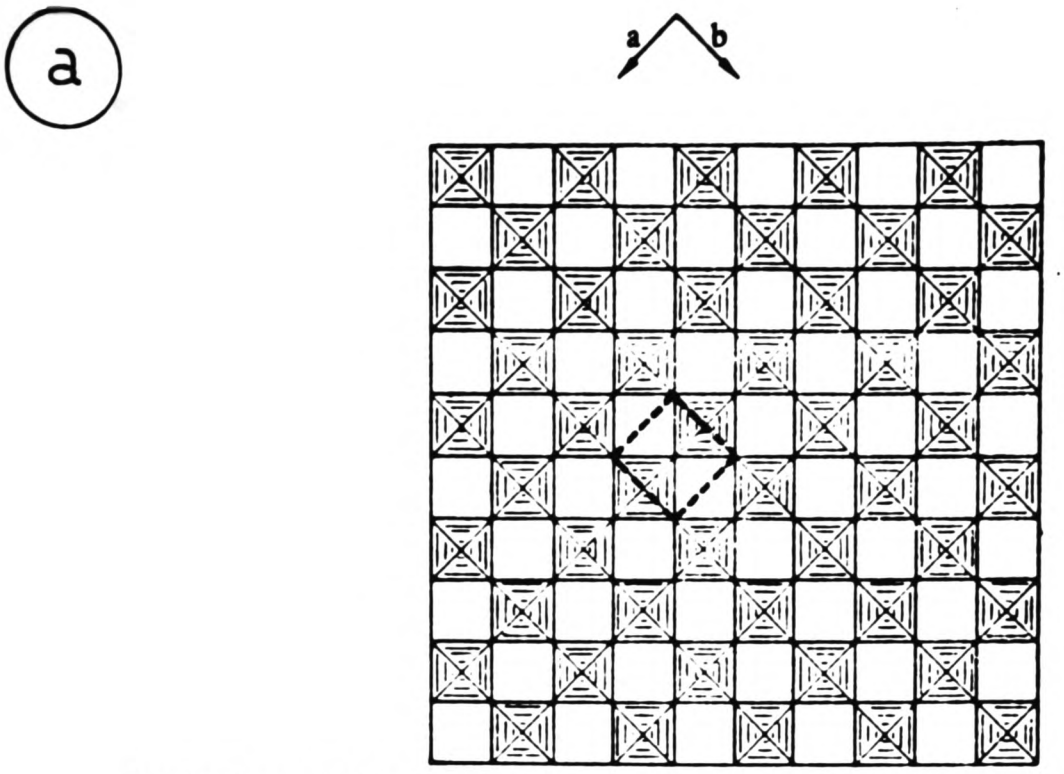

Projection of the ReO_3-type structure on the (001) plane. The unit cell is indicated.

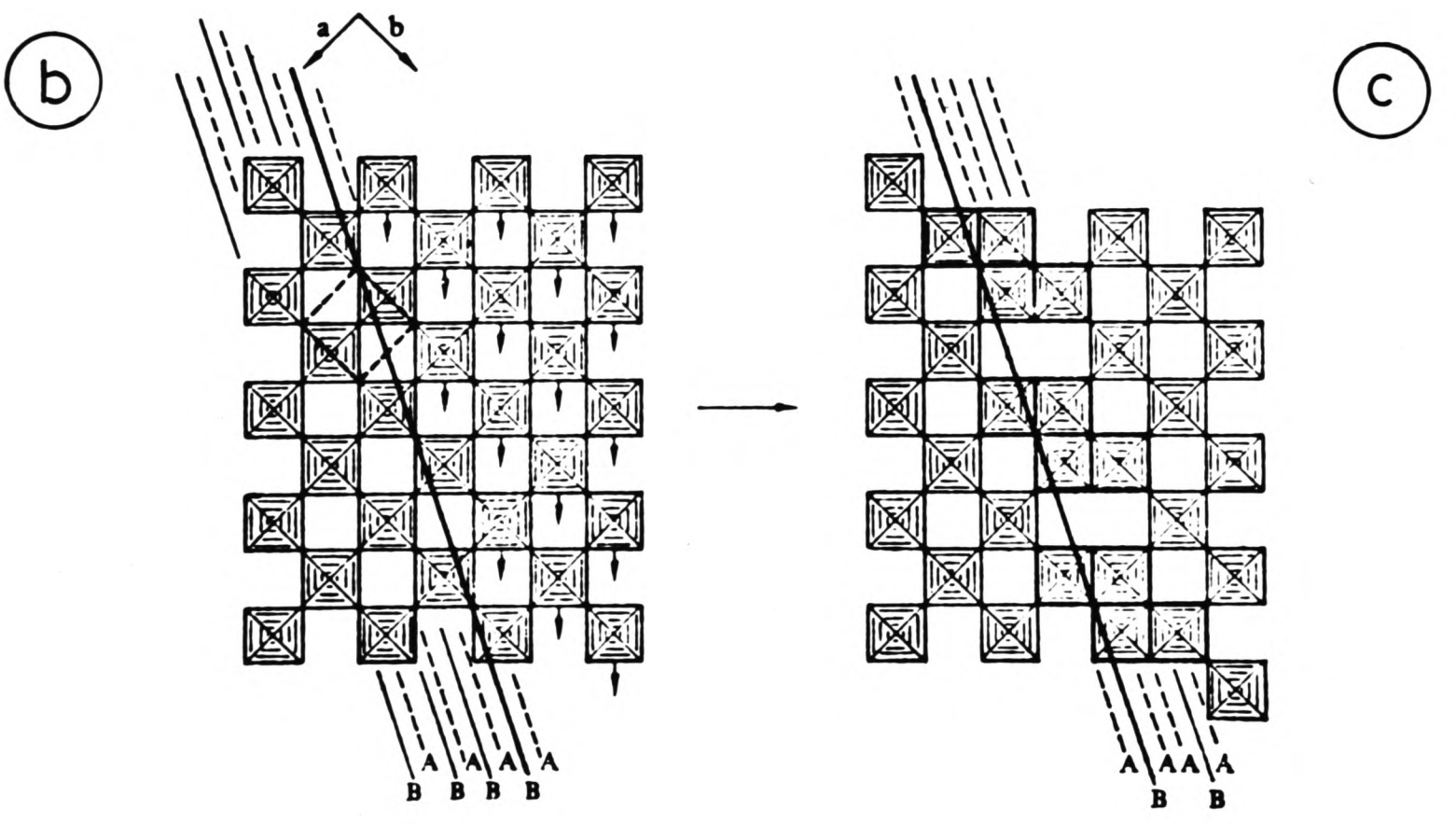

Representation of the formation of the type of CS plane which occurs in Mo_9O_{26}. (After Anderson and Hyde 1965,)

Fig.2

molybdenum and tungsten oxides, was subsequently described by Wadsley (1955) as "Crystallographic Shear" (CS). Below, a brief description of a typical crystallographic shear operation is given for the generation of the Mo_9O_{26} structure from an ReO_3-type parent.

An ReO_3-type structure in its idealized projection on the (001) plane is shown in Fig. 2-a. According to Anderson and Hyde (1965, 1967) two kinds of $(\bar{1}20)$ planes exist in the structure (labelled A and B in Fig. 2-b). The A-planes contain both metal and oxygen atoms and their stoichiometry is MeO_2 (Me = metal). In B-planes, only oxygen atoms are present and their number is half that of oxygen atoms in the A-plane. B-planes, therefore, have a composition of only "O". The sequence of A- and B-planes in the ReO_3 parent, as well as in slices of ReO_3 within Mo_9O_{26} (see Fig. 2-c) can be given as .....ABABA..... . Under reducing conditions, one whole B-plane of oxygen atoms (indicated by a solid line in Fig. 2-c) may be extracted and the two halves of the structure collapse and shear. Hence, at the shear discontinuity, the regularity is broken and the sequence becomes ....ABA*ABA....

* = discontinuity due to the generation of a shear plane (Fig. 2-c).

Along the shear plane, the new polyhedron linkage may involve a considerable distortion due to a cation-cation repulsion (Hyde and Bursill, 1970).

In a crystallographic shear, the co-ordination number of the cations is unchanged, but that of anions is increased. In ReO_3-type compounds, the oxygen co-ordination is raised

from 2 to 3; in the PdF_3-based compounds where crystallographic shear takes place by octahedra sharing faces (Andersson and Galy, 1970), the oxygen co-ordination is increased from 3 to 4).

The occurrence of shear planes with a particular orientation at fixed intervals produces an ordered new structure, the composition of which is dependent upon two factors: a) the number of anion sites per cation that are eliminated in the shear plane and b) the width of the slab of parent structure between shear planes (Anderson, 1972a). Changes in the oxide composition may have two consequences:

a) The breadth of the parent structure slab between successive CS planes will change without changing the CS plane orientation. In this case, some CS planes will necessarily be eliminated or new CS planes will be introduced.

b) The CS planes will undergo an orientation change (Anderson, 1974). Evidence for this process was provided by research of Bursill et al., (1971) on the Cr_2O_3-TiO_2 system. Subsequent thermodynamic data obtained from the reduction of TiO_2 under controlled oxygen partial pressures suggested that the rotation of CS planes is kinetically favoured (Merritt and Hyde, 1973).

A non-periodic CS defect, intergrown coherently into the matrix of a related phase is called a Wadsley defect. Wadsley defects account for small ranges of non-stoichiometry in CS or block-based structures and restrict the role of point defects to a very low, residual concentration.

Mechanisms of formation of crystallographic shear

Based on the fact that crystallographic shear can produce stoichiometric changes without the introduction of any point defects, three distinct mechanisms have been proposed in the literature. Important questions are:

1. What is the relaxation mechanism by which shear planes are created in the course of chemical reactions?
2. What is the relationship of such processes to the defect structure of the parent compound?
3. How does the interaction of shear planes as two-dimensional defects lead to their regular spacing and the formation of intermediate phases?

The three mechanisms are briefly described below:

Model 1 (Gado, 1965 - A in Fig. 3)

Oxygen diffuses out of the crystal, creating a relatively high concentration of anion vacancies. These vacancies order along zig-zag planes. The crystal then collapses and shears to annihilate the vacant sites and yields a CS plane. In this mechanism, a high concentration of point defects and the formation of a superlattice prior to a crystallographic shear process is essential. Evidence for these presuppositions has not been given in the literature (Hyde and Bursill, 1970). Furthermore, this mechanism does not explain the rearrangement of CS planes in the structure.

Model 2 (Anderson and Hyde, 1965, 1967 - B in Fig. 3)

A critical nucleation step takes place within the surface layers where the crystal is locally depleted in

oxygen. Adjacent anion vacancies aggregate into a vacancy disc which collapse to nucleate a CS plane. This nucleus is associated with a dislocation loop which can climb through the crystal acting as a sink for the annihilation of point defects from the immediately surrounding structure. The atomic positions at or near the bounding dislocation must undergo gross dislocation. Significant points in this mechanism are:

1. a slight deviation from stoichiometry is adjusted by a low density CS plane generation,
2. subsequent ordering of CS planes is left unexaplined,
3. nucleation and growth of CS planes takes place longitudinally.

Model 3 (Andersson and Wadsley, 1966 - C in Fig. 3)

This mechanism suggests that cation planes move co-operatively into the crystal. The removal of a layer of oxygen atoms in a reduction process displaces cations into adjacent empty interstitices. No anion vacancies or other kind of point defects appear to be necessary. The CS planes move laterally and the model can therefore explain the generation of ordered phases. The disadvantage of this mechanism is that the generation of an isolated CS plane across the middle of a crystal would require the movement of a vast number of atoms (Hyde and Bursill, 1970).

Literature findings concerning the reactions in CS structures indicate that the growth and extension of CS planes most likely is associated with a dislocation process -- i.e. the Anderson-Hyde mechanism. For example, this is

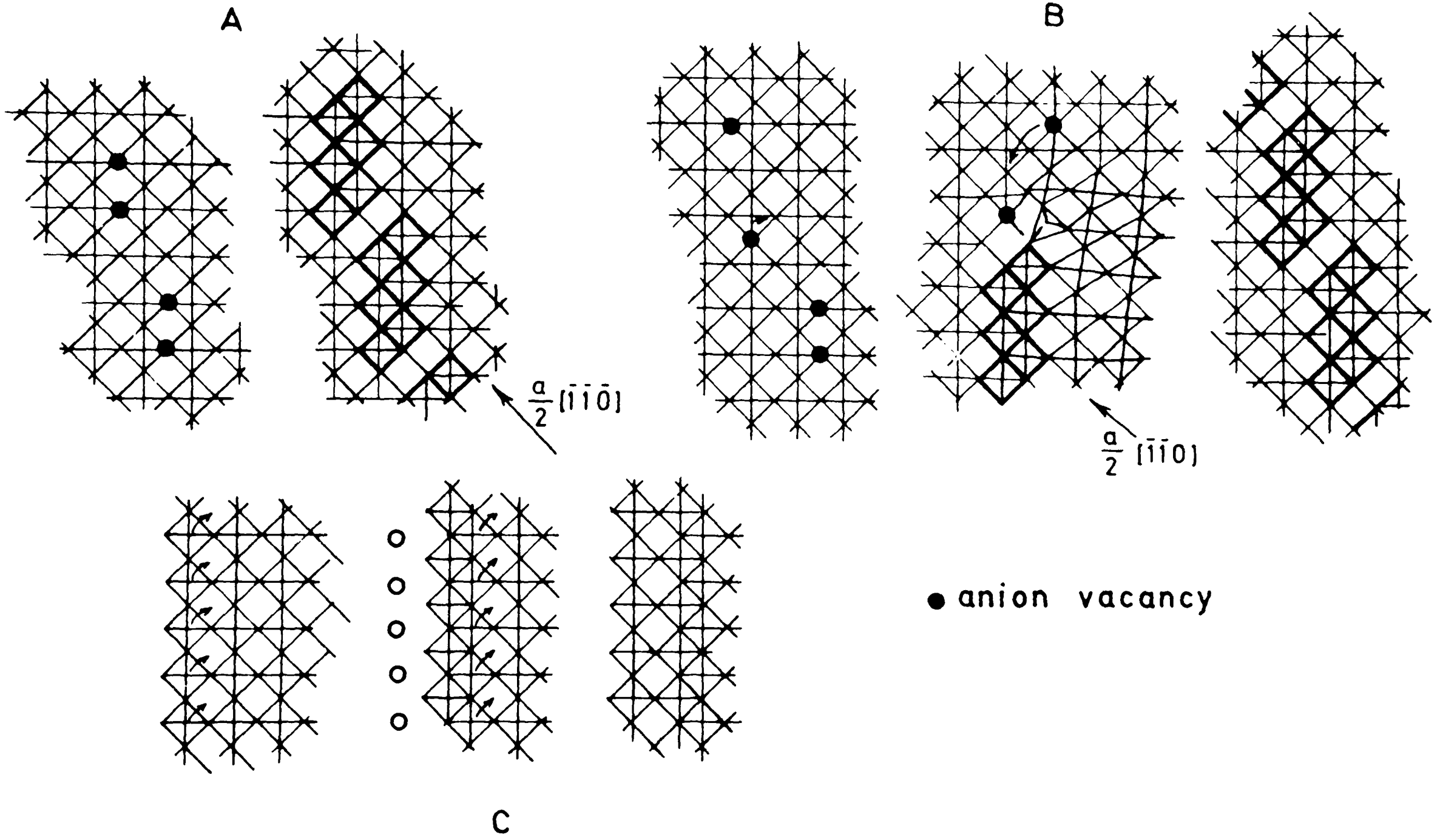

Figure 3 *Proposed mechanisms for formation of CS planes in reduction of oxides:* (A) *Gado*, (B) *Anderson and Hyde*, (C) *Wadsley and Andersson. In* (C), *oxygen atoms are removed and anion sites annihilated over the whole surface* (after Anderson,1972b)

found in the case of MoO_3 (Bursill, 1969), NbO_2F (Bursill and Hyde, 1969); TiO_2 (Anderson and Tilley, 1970; Van Landuyt and Amelinckx, 1970) and WO_3 (Allpress et al, 1971; Sundberg, 1977). Theoretical considerations of the formation energy of the isolated CS planes in ReO_3-related oxides have been given by Iguchi and Tilley (1978a and b).

Reactions in block-based structures have been reported to proceed via more complicated mechanisms: In an electron microscope study of the mechanism of the oxidation of $Nb_{12}O_{29}$ to Nb_2O_5, Browne and Anderson (1974) have demonstrated that, at high temperatures ($\sim 400^{o}C$), the reaction takes place via a co-operative mechanism -- i.e. an Andersson-Wadsley process -- for advancing the position of the CS boundary.

At lower temperatures ($\sim 110^{o}C$), however, there is a second mechanism in which interstitial diffusion of oxygen is predominant. Here, a well organized metastable superlattice structure is formed which transforms subsequently into regular CS planes. The essential step for this process is again a probable unit jump by cations into interstitial sites.

Crystallographic shear in specific systems

The most important systems involving crystallographic shear principles are:

1. ReO_3-related structures: tungsten oxides; molybdenum oxides; oxides related to NbO_2F, and niobium oxides -- i.e. block-based structures.

2. PdF_3-related structures: comprising two distinct groups of oxides:

   a) rutile-based oxides: TiO_2, VO_2, CrO_2, and

   b) α-PbO_2 type structures.

Literature findings in these systems (1-2 above) have been extensively reviewed by Anderson (1972b), Tilley (1972); Anderson and Tilley (1974) and recently by Tilley (1975). The involvement of crystallographic shear in silicate systems has recently been reviewed and summarized by Chisholm (1975)

Defects in block structures

There is a close analogy between the chemistry of crystallographic shear phases (discussed above) and that of complex niobium oxides and related compounds. The structural principles of the latter systems -- i.e. block-based oxides -- were determined by Wadsley (1961a and b) and by Gatehouse and Wadsley (1964) using X-ray diffraction. They showed that in the crystal structures of $TiNb_2O_7$, $Ti_2Nb_{10}O_{29}$ and H-Nb_2O_5, the ReO_3-type parent is adjusted by the operation of two sets of intersecting CS planes which divide the parent structure (i.e. ReO_3) into approximately rectangular blocks or columns extending infinitely along the third dimension (the b-axis of the crystal). Using electron microscopy, X-ray and neutron diffraction methods, Anderson et al (1975) have shown that these columns are essentially defect-free. Complete identification of the structure as idealised rectangular columns is inaccurate since the octahedra within the columns are slightly irregular with the niobium atoms displaced from the centres by a

polarization effect. Block structure systems have been further discussed in Chapter IV. Various review articles on the chemistry of block-structure compounds have appeared in the literature -- e.g. see Wadsley and Andersson, 1970; Anderson, 1972b; Anderson and Tilley, 1974; Tilley, 1972 and 1975; Eyring and Tai, 1973.

The defect chemistry of the binary Nb-O system has been studied by Anderson, et al., (1972a and b); Iijima (1973); Anderson et al, (1975); Iijima, et al., (1973 and 1974), and that of related ternary oxides -- i.e. Ti-Nb-O and W-Nb-O systems -- by Allpress and Wadsley (1969); Allpress (1969a and b, 1970), Allpress and Roth (1970). These authors have shown, using electron microscopy, that, due to the fact that the two intersecting sets of CS planes have different displacement vectors, the oxides possess a great flexibility for accommodating different kinds of defects. The most frequently encountered defects in the crystals include modes of twinning, planar defects, permitted wrong block combinations and point defects. These can be classified into two main groups:

1. stoichiometric defects and
2. non-stoichiometric defects.

(1) Stoichiometric defects, involving the coherent incorporation of planar domain boundaries while preserving the stoichiometry of the crystal, include:

a) Modes of twinning, changing the orientation of blocks in the twin boundary. Here, the ReO_3 substructure is preserved with minimum distortion, while blocks are linked at the same level. For example in the case of H-Nb_2O_5,

Anderson et al (1972a), examining crystals obtained via the chemical vapour transport technique, found frequent twinning on the $(10\bar{1})$ plane of the ReO_3 structure and concluded that in H-Nb_2O_5 the $(10\bar{1})_R$ plane is the only permitted twin boundary. Iijima (1973), studying defects, deliberately formed in crystals by quenching H-Nb_2O_5 from the melt, confirmed Anderson et al's finding.

b) Coherent intergrowth of different block-structres having the same stoichiometry. This has been shown to occur in the $(3 \times 4)_1 + (3 \times 5)_\infty$ structure of H-Nb_2O_5 and its block-structure modification, the $(4 \times 4)_\infty$ structure of N-Nb_2O_5 (Anderson et al., 1972a; Iijima, 1973).

The formation of a new modification of H-Nb_2O_5, namely $Nb_{10}O_{25}$ which occurs in full coherence with H-Nb_2O_5 has been reported by Iijima (1973). The $Nb_{10}O_{25}$ polymorph has the same structure as PNb_9O_{25} -- i.e. it is composed of $(3 \times 3)_1$ blocks.

(2) In non-stoichiometric defects, impurity structure(s) account for small deviations in oxide composition from the ideal stoichiometry. Such compositional fluctuations may take place in three different manners:

a) a localized change in spacing of CS planes,

b) rotation of CS planes

c) localized faulting within a finite coherent domain.

(a) In the localized change in spacing of CS planes, a small deviation of stoichiometry is adjusted by the insertion of rows or columns of a different size -- i.e. Wadsley defects. This is shown (↑T) in Plate 4-A (Chapter

IV) in which isolated strips of $Nb_{25}O_{62}$ ($NbO_{2.480}$) are incorporated coherently into the matrix of $Nb_{28}O_{70}$ (H-Nb_2O_5). If these defects are regularly recurrent, then a new ordered structure will form -- e.g. $Nb_{53}O_{132}$ which is a 1:1 intergrowth of $Nb_{28}O_{70}$ and $Nb_{25}O_{62}$ structures (Gruehn and Norin, 1967; Allpress, 1969a).

(b) Rotation of CS planes along certain discrete orientations results in the generation of a set of new structures having different compositions and occurring in perfect coherence with the matrix. This has been illustrated in Chpater V of this thesis, describing the formation of $Nb_{43}O_{107}$ ($NbO_{2.4884}$) due to the rotation by 4 degrees of the $(601)_R$ CS plane of $Nb_{53}O_{132}$ ($NbO_{2.4906}$) and $Nb_{28}O_{70}$ (H-Nb_2O_5).

(c) In localized faulting within a finite coherent domain, stoichiometric fluctuations appear as local elements of a new structure with a block size and/or block linkage different from that of the surrounding matrix. For example, in an oxidation reaction of $Nb_{12}O_{29}$ in air at 400°C, Browne and Anderson (1974) found that departure of $Nb_{12}O_{29}$ crystals from stoichiometry ($NbO_{2.417}$) was associated with the local formation of an ordered structure consisting of $(3 \times 3)_1$ blocks with tetrahedral sites at all block junctions -- i.e. the $Nb_{10}O_{25}$ polymorph of Nb_2O_5. $Nb_{10}O_{25}$ co-existed coherently with remnants of $Nb_{12}O_{29}$ within individual crystallites.

Structural inhomogeneities (which are indicative of departures from ideal stoichiometry) may also arise from

the incorporation of impurity atoms in the crystals rather than from changes in the oxidation state of the atoms. This phenomenon has been found by Anderson et al., (1972b) in an electron microscopy study of doped niobium oxides -- e.g. N-, M- and H-Nb_2O_5. They reported that impurity atoms -- e.g. F^-, OH^-, Mg^{2+}, etc. -- in such structures are segregated along domain walls, suggesting that the short-range ordering in the crystal is again preserved.

The contribution of point defects to the non-stoichiometry of block-based structures has been discussed by Anderson et al, (1975), studying metal-excess non-stoichiometry in GeO_2-$9Nb_2O_5$. According to these authors, the non-stoichiometry arises from the incorporation of interstitial cations in a set of sites with distorted octahedral co-ordinations which occur in square tunnels within the structure.

Skarnulis, Iijima and Cowley (1976), comparing calculated high resolution electron micrographs with experimental observations, confirmed Anderson et al's (1975) model though quantitatively their results differ from those of Anderson and co-workers.

Defect structures of niobium oxides have also been studied by Iijima, Kimura and Goto (1973, 1974) and Iijima (1975). They investigated reduced H-Nb_2O_5 samples prepared by Kimura,(1973) and found Wadsley defects as well as linear chains of point defects. The latter (appearing as dark spots within the block-structure) were suggested to arise from displacement of metal atoms from normal

octahedral sites either to interstitial octahedral or to tetrahedral sites.

Structural considerations of the nature of "defects" in non-stoichiometric compounds indicate that these systems will appear monophasic when the diffraction method is used as a mean of characterization (Anderson, 1969a and b). However, the structure, thermodynamics and statistical thermodynamics are inter-related in non-stoichiometric systems (Anderson, 1969a and b) and a thorough understanding of these systems clearly requires detailed thermodynamic studies.

Thermodynamic properties of non-stoichiometric compounds

Thermodynamic considerations of non-stoichiometric systems have been discussed by Anderson (1969a and b, 1970). Parts in his publications relevant to the present chapter, are summarised below:

Thermodynamically, the criterion for non-stoichiometric behaviour of oxide systems is that, over a range of chemical compositions in equilibrium with various chemical potentials of oxygen, the system simulates complete bivariance -- i.e. $\mu = f(T, X)$. In terms of the Gibbs phase rule, this would imply that a non-stoichiometric solid is a single phase across its composition range. By contrast, for a mixture of two phases (of defined compositions) in equilibrium, the equilibrium is univariant -- i.e. $\mu = f(T)$, independent of the total composition X.

In certain metal-oxide systems, a series of closely

spaced discrete phases exist. According to Anderson, the relation between the free energy minima indicates that tangents to adjacent phases differ only slightly from one pair to the next and merge into an almost continuous envelope. There is a possibility that many of the phases thought to be non-stoichiometric are actually mixtures -- i.e. domain intergrowth structures -- of closely spaced line phases. In the literature, this has been best illustrated in discussions of thermodynamic and structural aspects of the TiO_{2-x} system and fluorite-related systems. Since the two systems are relevant to the present work, significant points are briefly outlined below:

In a set of microbalance thermogravimetric studies, Merritt and Hyde (1973) equilibrated TiO_2 at 1300°K with H_2-H_2O gas buffer mixtures of various compositions. They found the following:

A solid-gas equilibrium was attained very slowly and the (p, x) isotherm of the system TiO_x ($1.67 < x < 1.98$), for both oxidation and reduction pathways showed pronounced hysteresis loops (1, 2 and 3 below) extending over the complete composition ranges of:

1. $TiO_{1.75}$ - $TiO_{1.90}$; this range covers the Andersson shear phases Ti_nO_{2n-1} ($4 < n < 9$) -- i.e. (121)

2. $TiO_{1.93}$ - $TiO_{1.98}$; in this range a new series of Ti_nO_{2n-1} phases with $\{132\}_r$ CS planes occur

3. $TiO_{1.981}$ - $TiO_{1.986}$; As described by Merritt and Hyde, a third hysteresis loop in this composition range may be present.

Between the first two loops (i.e. the region $1.90 < x < 1.93$), oxidation and reduction curves almost overlapped,

indicating the presence of equilibrium non-stoichiometric regions. In addition, the equilibrium reduction curve showed stepwise changes of phases, but the steps indicative of the intermediate phases were not sharp and did not correspond to the ideal compositions of the known CS phases.

Next, Merritt and Hyde correlated electron microscope findings with thermodynamic data for the reduced rutile phases. They concluded that both the apparent bivariance and the extreme hysteresis phenomena stem from the high activation energy needed for the nucleation of one structure out of the other. The authors demonstrated that the compositions of the discrete phases were closely-spaced and that single crystals contained neighbouring phases in a coherent intergrowth manner.

In fluorite related systems -- i.e. TbO_x (Hyde and Eyring, 1965) and PrO_x (Hyde, Bevan and Eyring, 1966) -- in which the intermediate phases are structurally inter-related, bivariance in the experimental isobars as well as gross hysteresis have again been reported. The thermodynamic behaviour in these systems is strongly influenced by coherent intergrowth of neighbouring phases, leading to the formation of diphasic single crystals.

Non-stoichiometry and thermodynamics of block-based compounds

Pure niobium oxides and mixed metal-niobium oxides were for a long time considered as classical non-stoichiometric systems extending within the composition range of MeO_x (Me = metal) where $2.4 < x < 2.7$.

It was in 1941 that investigations of NbO_2 - Nb_2O_5 were initiated by Brauer. On the basis of X-ray diffraction pattern analysis of oxides quenched from 1350°C, he concluded that Nb_2O_5 occurs as a single phase over the composition range of $NbO_{2.40}$ - $NbO_{2.50}$ (Brauer, 1941). Later this was apparently confirmed by Elliott (1960); Lavrent'ev et al., (1961); Kofstad and Anderson (1961) and Blumenthal et al., (1965).

In the TiO_2 - Nb_2O_5 system, Roth and Coughanour (1955) reported that Nb_2O_5 was able to take up 10 mole % TiO_2 in solid solution.

Subsequently, Goldschmidt (1960) described the WO_3 - Nb_2O_5 system and pointed out that Nb_2O_5 could incorporate 50 mole % WO_3 in solid solution -- i.e. a mixed tungsten-niobium oxide extended as the single phase in the composition range of $(W, Nb)O_x$; $2.5 < x < 2.7$.

Since then, important progress has been made in the structural identification of these non-stoichiometric block-based systems. The non-stoichiometric regions of the oxides have been seen to consist of several discrete but closely spaced and interrelated phases. In Table 2 of the present study, the oxides which have been observed as macroscopic crystals are listed. The Table also includes compounds identified by electron microscopy as domains of regular structures, at least a few unit cells in thickness.

In contrast, thermodynamic studies of the above systems have not kept pace with the detailed knowledge of structural aspects. The most extensively studied area in this respect has been the NbO_2 - (H-Nb_2O_5) system (Brauer, 1941; Elliott,

TABLE 2

KNOWN BLOCK STRUCTURES

(After Anderson, 1972b and Tilley, 1972, 1975)

Anion: cation ratio	Unit cell contents	Block structure	Known compounds References (in parenthesis; numbering according to literature references in this thesis)
2.3333	$M_{18}X_{42}$	$(3 \times 3)_\infty$	$TiNb_2O_7$ (216), $TiTa_2O_7$ (140)
2.4167	$M_{12}X_{29}$	$(3 \times 4)_\infty$	$Nb_{12}O_{29}$ (151), $Ti_2Nb_{10}O_{29}$ (152), $Mg_{2/3}Nb_{11\frac{1}{3}}O_{29}$ (mono and o-rh) (158), $Ni_{2/3}Nb_{11\frac{1}{3}}O_{29}$ (mono and o-rh) (157), $(Fe,Nb)_{12}O_{29}$ (85), $(Ga, Nb)_{12}O_{29}$ (85), $(Ni, Nb)_{12}O_{29}$ (85), $(Co,Nb)_{12}O_{29}$ (85), $(Cr, Nb)_{12}O_{29}$ (85), $Zn_{2/3}Nb_{11\frac{1}{3}}O_{29}$ (155), $AlNb_{11}O_{29}$ (153)
2.4490	$M_{49}X_{120}$	$(3x4)_\infty + (3x4)_2$	$Ti_5Nb_{44}O_{120}$ (3)
2.4545	$M_{22}X_{54}$	$(3x4)_\infty + (3x3)_1$	$Nb_{22}O_{54}$ (159)
2.4595	$M_{37}X_{91}$	$(3x4)_\infty + (3x4)_2$	$Ti_3Nb_{34}O_{91}$ (3)
2.4667	$M_{15}X_{37}$	$(3 \times 5)_\infty$	$MgNb_{14}O_{35}F_2$ (129), $TiNb_{14}O_{37}$ (104)
2.4681	$M_{47}X_{116}$	$(3x4)_\infty + (3x3)_1$	$Nb_{47}O_{116}$ (87), $Zr_2Nb_{45}O_{116}$ (85)
2.4800	$M_{25}X_{62}$	$(3 \times 4)_2$	$Nb_{25}O_{62}$ (159), $TiNb_{24}O_{62}$ (176), $Ni_{\frac{1}{3}}Nb_{24\,2/3}O_{62}$ (157), $Ga_{\frac{1}{3}}Nb_{24\,2/3}O_{62}$ (85), $FeNb_{24}O_{62}$ (85), $ZrNb_{24}O_{62}$ (6), $Al_{\frac{1}{3}}Nb_{24\frac{1}{3}}O_{62}$ (153)
2.4848	$M_{99}X_{246}$	$(3x4)_\infty + (3x3)_1 + (4x4)_1$	$ZrNb_{32}O_{82}$ (198)

2.4872	$M_{72}X_{194}$	$(3x4)_2 + (3x4)_1 + (3x5)_\infty$	$Nb_{39}O_{97}$ (3), $TiNb_{38}O_{97}$ (3) (33)
2.4906	$M_{53}X_{132}$	$(3x4)_2 + (3x4)_1 + (3x5)_\infty$	$Nb_{53}O_{132}$ (3) (86), $TiNb_{52}O_{132}$ (3)
2.50	$M_{28}X_{70}$	$(3x4)_1 + (3x5)_\infty$	H-Nb_2O_5 (77)
	$M_{16}X_{40}$	$(3x4)_\infty$	M-Nb_2O_5 (139), N-Nb_2O_5 (29), $(W_{0.35}V_{0.65})_2O_5$ (107)
	$M_{10}X_{25}$	$(3x3)_1$	PNb_9O_{25} (177, 127), $AsNb_9O_{25}$, VNb_9O_{25}, $AsTa_9O_{25}$, VTa_9O_{25}, VTa_9O_{25}, PTa_9O_{25} (127), $Nb_{10}O_{25}$ (47, 101, 33) $GeNb_{18}O_{47}$ (221, 19)
	$M_{46}X_{115}$	$(3x3)_1 + (3x4)_1$	$P_2Nb_{44}O_{115}$ (127)
2.5073	$M_{69}X_{173}$	$(3x4)_1 + (3x5)_\infty$	$WNb_{68}O_{173}$ (18)
2.5085	$M_{59}X_{148}$	$(3x4)_1 + (3x5)_\infty + (3x5)_2$	$Nb_{59}O_{147}F$ (84, 154)
2.5122	$M_{41}X_{103}$	$(3x4)_1 + (3x5)_\infty$	$WNb_{40}O_{103}$ (8)
2.5161	$M_{31}X_{78}$	$(3 x 5)_2$	$Nb_{31}O_{77}F$ (36)
2.5185	$M_{27}X_{68}$	$(3x4)_1 + (3x5)_\infty$	$WNb_{26}O_{68}$ (8)
2.5231	$M_{65}X_{164}$	$(3x5)_1 + (3x5)_2 + (3x6)_\infty$	$Nb_{65}O_{161}F_3$ (84, 154)

TABLE 2 cont.

TABLE 2 (cont.)

KNOWN BLOCK STRUCTURES

(After Anderson, 1972b and Tilley, 1972, 1975)

Anion: cation ratio	Unit cell contents	Block structure	Known compounds (in parenthesis; numbering according to literature references in this thesis)
2.5294	$M_{34}X_{86}$	$(3x5)_1 + (3x6)_\infty$	$Nb_{34}O_{84}F_2$ (142, 225)
2.5385	$M_{13}X_{33}$	$(3 \times 4)_1$	$WNb_{12}O_{33}$ (176), $MoNb_{12}O_{33}$ (63), $MoTa_{12}O_{33}$ (63)
2.5625	$M_{16}X_{41}$	$(3 \times 5)_1$	$WNb_{15}O_{40}F$ (85), $MoNb_{15}O_{40}F$ (76)
2.5667	$M_{30}X_{77}$	$(3x4)_1 + (4x4)_1$	$W_4Nb_{26}O_{77}$ (31)
2.5882	$M_{17}X_{44}$	$(4 \times 4)_1$	$WNb_{16}O_{44}$ (85), $Mo_3Nb_{14}O_{44}$ (63), $W_3Nb_{14}O_{44}$ - $W_7Nb_{10}O_{44}$ (85)
2.6190	$M_{21}X_{55}$	$(4 \times 5)_1$	$W_5Nb_{16}O_{55}$ - $W_7Nb_{12}O_{55}$ (85)
2.6538	$M_{26}X_{69}$	$(5 \times 5)_1$	$W_8Nb_{18}O_{69}$ - $W_{10}Nb_{16}O_{69}$ (85)
2.6770	$M_{31}X_{83}$	$(6 \times 5)_1$	$W_{11}Nb_{20}O_{83}$ (7)

1960; Lavrent'ev et al, 1961; Kofstad and Anderson, 1961; Blumenthal et al, 1965; Kovba et al, 1967; Abbatista et al, 1968; Burdeze et al, 1969; Schäfer et al, 1969; Kimura, 1973; Nimmo and Anderson, 1972; Marucco, 1974). Literature findings of the Nb-O system are briefly outlined here to highlight the significance of the present work.

Kofstad and Anderson (1961) equilibrated H-Nb_2O_5 with CO_2/CO gas buffer mixtures (10^{-7} atm > p_{O_2} > 10^{-18} atm.) at 900-1400°C and found that the relative isothermal weight change of the oxide was proportional to $p_{O_2}^{-1/6}$. They interpreted the observed non-stoichiometry of H-Nb_2O_5 in terms of classical point defect formation (oxygen vacancies). Similarly, Blumenthal et al., (1965) studied the non-stoichiometry of H-Nb_2O_5 by electrochemical cell measurements (over the range 800° - 1070°C) as well as by thermogravimetric gas-equilibrium measurements between 1000° and 1200°C. Their results, although not definitive, simulate a smooth relationship between the composition x (in Nb_2O_{5-x}) and the partial pressure of oxygen in equilibrium with the oxide. In 1960, Norin and Magneli identified three discrete phases having compositions of $NbO_{2.40}$, $NbO_{2.46}$ and $NbO_{2.48}$ corresponding to ideal formulae of $Nb_{12}O_{29}$ (O/Nb = 2.417), $Nb_{22}O_{54}$ (O/Nb = 2.454) and $Nb_{25}O_{62}$ (O/Nb = 2.480), respectively.

Kovba et al., (1967) studied the NbO_2 - Nb_2O_5 system by heating NbO_2/Nb_2O_5 mixtures in an evacuated silica tube at 1100°C. Their search for the $Nb_{22}O_{54}$ phase was not successful but they found $Nb_{25}O_{62}$ as the only phase occurring within the composition range of 2.474 > O/Nb > 2.454.

Burdeze et al., (1969) reacted NbO_2 and Nb_2O_5 mixtures of known compositions at 1200°C - 1400°C and they determined a stepwise (p, x) isotherm in the composition range NbO_2 - Nb_2O_5, which indicated that intermediate phases are formed. In their diagram, the occurrence of a new phase having the composition of $NbO_{2.432}$ is emphasized. A similar high temperature (p, x) isotherm (1250°C) has also been reported by Abbatistta et al., (1968) who equilibrated H-Nb_2O_5 with various compositions of CO_2/CO mixtures.

In 1967, Gruehn and Norin identified a new phase having the composition of $NbO_{2.483}$. This compound corresponds to the ideal formula of $Nb_{53}O_{132}$ with the ratio O/Nb = 2.491.

Subsequently, Wadsley and Andersson, in their review paper (1970), showed that all the intermediate phases present in the NbO_2 - Nb_2O_5 system are closely related and belong to two homologous series represented by the general formulae $Me_{3n}O_{8n-3}$ and $Me_{3n+1}O_{8n-2}$. [The two homologous series had previously been suggested by Gatehouse and Wadsley (1964) in structural studies of Nb-O as well as of the Ti-Nb-O system]. The thermodynamic stability of these intermediate phases was subsequently investigated by Schäfer et al., (1969) who equilibrated H-Nb_2O_5 with H_2O/H_2 gas buffer mixtures ($0.167 < H_2O/H_2 < 4.02$) at 1300°C and reported the formation of discrete intermediate phases (a stepwise p, x isotherm) in the composition range of $NbO_{2.00}$ - $NbO_{2.50}$. Their phase diagram depicts the presence of three stoichiometric phases: $NbO_{2.417}$ ($Nb_{12}O_{29}$); $NbO_{2.453}$ ($Nb_{22}O_{54}$) and $NbO_{2.483}$ ($Nb_{53}O_{132}$) as well as two other phases with a homogeneity range from $NbO_{2.464}$ - $_{2.467}$ ($Nb_{47}O_{116}$) and from

$NbO_{2.472}$ - 2.478 ($Nb_{25}O_{62}$). However, the compositions given for the latter phases do not correspond to the ideal formulae which can be determined from X-ray structural analyses.

In an attempt to correlate ultrastructure with thermodynamic behaviour, Nimmo and Anderson (1972) re-examined the $NbO_{2.00}$ - Nb_2O_5 system by equilibrating H-Nb_2O_5 with CO_2/CO gas mixtures and measuring the equilibria thermogravimetrically at 900-1050°C. A (T, x) scan recorded in constant gas buffer mixtures showed a continuous bivariant behaviour over the composition range $NbO_{2.417}$ - $NbO_{2.50}$ while electron microscopy on samples prepared between 800°C and 1050°C suggested a reaction sequence of:

$$H\text{-}Nb_2O_5 \longrightarrow Nb_{25}O_{62}\ [NbO_{2.480}] \longrightarrow \text{monoclinic-}Nb_{12}O_{29}\ [NbO_{2.417}].$$

In contrast, specimens prepared at 1200 - 1300°C by annealing NbO_2/Nb_2O_5 mixtures at appropriate proportions revealed the formation of intergrowth phases:

$$H\text{-}Nb_2O_5 \rightarrow Nb_{53}O_{132} \rightarrow Nb_{25}O_{62} \rightarrow Nb_{47}O_{117} \rightarrow Nb_{22}O_{54} \rightarrow Nb_{12}O_{29}.$$

On the basis of these observations, Nimmo and Anderson concluded that structures formed at 950 - 1050°C are not in true thermodynamic equilibrium whereas those prepared at higher temperatures kinetically favour the formation of intermediate intergrowth phases. The authors also state that transformation from one phase into another proceeds progressively by building a varying degree of the neighbouring structure into the matrix.

Concurrently, Kimura (1973) investigated H-Nb_2O_5 phase

equilibria in the composition range $NbO_{2.00}$ - $NbO_{2.50}$ at 1300° and 1400°C. H-Nb_2O_5 and NbO_2 were both equilibrated with fixed oxygen partial pressures generated from CO_2/CO gas mixtures and the products were chemically analysed and identified by X-ray powder diffraction. Important points in Kimura's report are:

1. A prolonged period was suggested for the equilibration of the oxides (15 - 17 hours).

2. At the same oxygen pressure, samples brought to equilibrium from Nb_2O_5 were often found to be more reduced than samples oxidized from NbO_2.

3. The phase equilibrium diagrams, established at 1300°C and 1400°C isotherms, show a succession of discrete phases with narrow ranges of homogeneity separated by univariant phase co-existence steps.

4. In a theoretical approach, a thermodynamic explanation of crystallographic shear planes and Wadsley defects was attempted, assuming the existence of four major oxygen sites in the crystal lattice. The four sites were:

a) in block-centres linked to two niobium atoms having an octahedral co-ordination;

b) in block-edges linked with three niobium atoms (Nb in octahedral co-ordination);

c) in block-corners bound with four niobium atoms (Nb in octahedral co-ordination) and

d) in sites where oxygen atoms are linked with one niobium atom in tetrahedral position and one in octahedral co-ordination.

Kimura concluded that the formation or annihilation of shear planes must alter the concentration of these four

different types of oxygen atoms in the lattice.

5. The observed oxygen deficiency of the intermediate phases was attributed to the formation of point defect, oxygen vacancies, rather than Wadsley defects -- i.e. Wadsley defects were considered to be of a non-equilibrium nature.

Morucco (1974) re-examined NbO_2 - Nb_2O_5 at 1000° - 1100°C isotherms by equilibrating H-Nb_2O_5 with CO_2/CO gas buffer mixtures and combined thermogravimetric measurements with those of electrical resistance of the solid phase. His findings suggested the presence of two non-stoichiometric phases having approximate compositions $NbO_{2.42}$ and $NbO_{2.47}$. Marucco, concluded that in the investigated temperature range, only two monophasic regions exist between NbO_2 and Nb_2O_5. The non-stoichiometry range of the phases in his diagram are $NbO_{2.422}$ - $NbO_{2.423}$, $NbO_{2.467}$ - $NbO_{2.474}$ and $NbO_{2.489}$ - $NbO_{2.500}$.

The possibility and nature of isolated oxygen vacancies in $Nb_{22}O_{54-x}$, $Nb_{25}O_{62-x}$ and $Nb_{28}O_{70-x}$ was examined thermodynamically by Kikuchi and Goto (1976). These authors, using Kimura's (1973) experimental data, stated that the singly ionized oxygen vacancies, the quasi-free electrons and the Nb^{4+} ions (formed as a consequence of retrapping of some of the electrons in the valence band of the constituent Nb^{5+} ions) are the most probable defects in slightly reduced $Nb_{22}O_{54}$, $Nb_{25}O_{62}$ and $Nb_{28}O_{70}$ phases. The concentration of oxygen vacancies in $Nb_{22}O_{54-x}$ and $Nb_{25}O_{62-x}$ was estimated to be proportional to $p_{O_2}^{-\frac{1}{2}}$, and, in $Nb_{28}O_{70}$, approximately to $p_{O_2}^{-\frac{1}{4}}$.

More recently, the non-stoichiometric nature of

H-Nb_2O_5 ($Nb_{28}O_{70}$) has been studied by Massiani et al., (1978) who measured the self diffusion co-efficient of oxygen by an isotopic solid-gas exchange reaction. Their results, obtained at a temperature range of 900 - 1200°C and oxygen partial pressures of 0.3 to 3.3 x 10^{-2} atmosphere, suggested that the self-diffusion co-efficient conforms to a $p_{O_2}^{-\frac{1}{4}}$ relationship. The authors confirmed that non-stoichiometry of Nb_2O_5, in the composition range close to stoichiometry -- i.e. $Nb_{28}O_{70}$ -- arises from singly ionized oxygen vacancies.

Aim of the present study

From the above survey of our current knowledge of crystallographic shear phases and block-based compounds, it would appear the area examined by Schäfer et al., (1969), Nimmo and Anderson (1972) and Kimura (1973) warrants further investigations on the following:

1) The kinetic characteristics of CS and block structure reactions at high temperatures -- i.e. T > 1300°C -- when a substantial atomic mobility is present.

In the literature, the attainment of redox equilibrium at medium temperatures ($\sim$ 1100°C) in TiO_{2-x} (Merritt and Hyde, 1973) as well as in the NbO_2 - Nb_2O_5 system (e.g. see Nimmo and Anderson, 1972; Schäfer et al., 1969) has revealed that equilibrium is approached very sluggishly, while the pseudo-equilibrium oxygen potentials showed gross hysteresis between oxidation and reduction. These observations at medium temperatures presently were re-assessed at higher temperatures (Chapter VII).

2) The thermodynamic properties of block-based compounds at high temperatures -- i.e. T > 1300°C. Literature data summarized earlier in the present Chapter show that two conflicting conclusions so far have been reported:

a) A stepwise phase equilibrium diagram suggesting the formation of discrete intermediate phases; Schäfer et al., (1969); Kimura (1973).

b) A continuous and coherent phase equilibrium diagram such as shown by Nimmo and Anderson (1972).

Clearly, to assess the validity of one of the two opinions, a re-investigation was needed. For this reason, we have studied (Chapter VII) phase equilibria in an alternate block-based system -- i.e. the ternary Ti-Nb-O system in which three distinct compounds : $TiNb_2O_7$, $Ti_2Nb_{10}O_{29}$, $TiNb_{24}O_{62}$ are present. They were reduced at the isotherm 1400°C under controlled oxygen partial pressures, using CO_2/CO gas buffer mixtures. Implicit in the reduction of the ternary Ti-Nb-O system is the question of the role of the altervalent cation (Ti^{4+}).

Another aspect of Nb_2O_5 systems which requires investigations is the phase equilibria of its metastable modifications. They are the subjects of Chapters V and VI.

Below, a survey of literature data so far reported on the chemistry and thermodynamics of these metastable Nb_2O_5 systems is given to underline the motivation of the present work.

Niobium pentoxide occurs in several polymorphs such as H-, N-, M-, P-, R-, B-, T-, TT-, etc. The preparation

of these compounds, using the chemical vapour transport technique, and their nomenclature and characterisation have been described by Schäfer et al., (1966). Structural aspects have been discussed by Wadsley and Andersson (1970).

Apart from the B-, T- and TT- forms, all modifications contain elements of ReO_3 in their structures. H-Nb_2O_5 is the only stable form at high temperatures ($T > 1000^oC$) and other modifications transform into the H-form on heating. The crystal structure of the H-form has been determined by Gatehouse and Wadsley (1964).

The N- and M-Nb_2O_5 polymorphs are closely related and contain ribbons of $(4 \times 4)_\infty$ blocks in their structures. The N-Nb_2O_5 structure has been studied by Andersson (1967) and the M-form by Mertin, et al., (1970).

There is a close similarity between P- and R-Nb_2O_5 as both compounds contain crystallographic shear planes in parallel to two of the cube axis of ReO_3. The CS planes divide the parent structure into blocks of $2 \times \infty \times \infty$. The crystal structure of the P- form has been investigated by Petter and Laves (1965) while R-Nb_2O_5 has been characterised by Gruehn (1966).

The structure of B-Nb_2O_5 is derived from the PdF_3-type parent in which octahedra groups are sharing corners in a similar manner to that in ReO_3. However, unlike the latter structure in which the anion arrangement is based on cubic close-packing, the anion configuration in PdF_3 is based upon hexagonal close-packing. The B-Nb_2O_5 structure, first solved by Laves, et al., (1964), consists of rutile-like ribbons of edge sharing octahedra. Blocks, two

octahedra wide, are joined through octahedral corners (Andersson and Galy, 1970).

Browne (1973), applying electron microscopy in a structural investigation of niobium oxides, studied the defect chemistry of these materials (see Anderson, et al., 1972a and b). Browne and Anderson (1974) also investigated the solid state oxidation of $Nb_{12}O_{29}$ to Nb_2O_5 using electron diffraction and high resolution electron microscopy. They reported that the reaction proceeds through a reorganization of the block structure at low temperatures ($T \leq 400^{o}C$) and found that highly correlated atom movements create a well-ordered superstructure which transforms into a new modification of Nb_2O_5, namely $Nb_{10}O_{25}$. The authors were able to advance a reaction mechanism.

Thermodynamic stabilities of metastable niobium pentoxides at one atmosphere pressure have been the subject of many investigations (Brauer, 1941; Schäfer and Roy, 1958; Holtzberg et al., 1957; Taylor and Doyle, 1957; Terao, 1963 and 1965; Schäfer et al., 1966). More recently, Kodama et al., (1972) determined relative stabilities of T-, B-, P- and H-Nb_2O_5 at 600 and 800°C at one atmosphere pressure. They reported that the relative stabilities, of these compounds, increase in the order $T \rightarrow H \rightarrow P \rightarrow B$ at 600°C and in the order $T \rightarrow P \rightarrow B \rightarrow H$ at 800°C.

High pressure phase relationships of various Nb_2O_5 modifications were studied by Tamura (1972). He reported

that direct transformation from the H- into the T-form and from the H- into the B-form takes place at high pressures, while the formation of the TT-form at high pressures is conditional upon the presence of trace impurities.

Further pressure-temperature relationships in niobium pentoxides have been found by Waring et al., (1973) who describe four single phase regions -- i.e. H-, B- and two regions of L-Nb_2O_5 (Schäfer's T and TT-forms).

It is clear from the above literature review that aspects of the phase equilibria of the different niobium pentoxide forms had not been given attention. Chapters V and VI of this thesis, therefore, deal with two aspects of phase relationships of B- (Chapter V) and of P- (Chapter VI) modifications of Nb_2O_5:

Aspect 1) The structural relationships between the metastable modifications and the high temperature form H-Nb_2O_5 are reported in Part A in the respective Chapters.

Aspect 2) Phase equilibria in the systems NbO_2 - (B-Nb_2O_5) and NbO_2 - (P-Nb_2O_5) are described in Part B in the respective Chapters.

For the studies reported in Chapters V and VI, carefully controlled crystal growth of the metastable modifications was essential. The application of the chemical vapour transport technique for such growth of single crystals under specific conditions of predominantly convection control is reported in Chapter II.

Phase equilibria measurements (above) were carried out utilizing a newly designed "Horizontal Quench Furnace" combined with a Cahn microbalance reduction line. In Chapter III, the

design of the apparatus is discussed in detail.

To identify the structures of the reduced oxides, electron diffraction and high resolution electron microscopy (direct lattice imaging) were employed. A brief description of the electron-optical techniques is given in Chapter IV.

CHAPTER II

SINGLE CRYSTAL GROWTH OF B-, P- and N-Nb_2O_5, APPLYING THE CHEMICAL VAPOUR TRANSPORT TECHNIQUE

2.1. INTRODUCTION

The chemical vapour transport reaction was introduced as a method for crystal growth by Schäfer *et al* (1956). Since then, significant improvements in experimental conditions as well as in the theoretical approach of this technique have been reported (Nitsche *et al*, 1961; Schäfer, 1964; Faktor and Garrett, 1974). The method is particularly useful for the preparation of materials which because of their high melting points or instability at high temperatures can not be obtained from melt.

The principle underlying the chemical vapour transport technique is the following: in a chemical system in which a solid is in equilibrium with n gaseous components, transport of the solid will take place if the equilibrium constant of the system is perturbed locally (Nitsche, 1960). Such perturbation can be brought about by introducing a temperature gradient in the reaction tube.

By this method, Schäfer, Gruehn and Schulte (1966) synthesized fourteen structurally distinct polymorphs of niobium pentoxide, including B-; P-; N-; T-; TT- and H-;. An additional polymorph having a composition of $Nb_{10}O_{25}$ was recently found to occur as a domain intergrowth structure in disordered H-Nb_2O_5 (Iijima, 1973). The latter polymorph was also obtained by Browne and Anderson (1974) as a product of $Nb_{12}O_{29}$ reoxidation in air at a low temperature -- i.e. $T < 400^{o}C$.

The above Nb_2O_5 modifications, in general are thermodynamically metastable i.e. they transform at high temperatures ($T > 1000^{o}C$) into H-Nb_2O_5 (Schäfer *et al*, 1966;

Reisman and Holtzberg, 1970; Kodama et al, 1972). The stability ranges of these oxides, as reported in the literature, have been reviewed and compiled by Browne (1973).

It is appropriate to discuss here briefly the definition of "oxide modification". According to Reisman and Holtzberg (1970), a modification (at 1 atmosphere pressure) is a phase which can be generated thermally from two directions, namely, the reversible transformation of two adjacent phases, one into the other. The authors concluded that three genuine forms of crystalline Nb_2O_5 occur, namely α (the high temperature form); β (the low temperature form) and ε which is a stable phase only at T > 1350°C. (According to the nomenclature of Schäfer et al (1966), the above oxides are H-Nb_2O_5; T-Nb_2O_5 and "I" (high), respectively). The question whether the other modifications are ternary phases with a low concentration of impurity species -- e.g. SiO_2, Al_2O_3, alkali metal oxides, etc. -- or metastable structures nucleated and catalytically grown in the presence of impurities, is left open by Reisman and Holtzberg.

With regard to the role of foreign ions in the formation of different modifications, the following should be noted. Crystal growth of some Nb_2O_5-modifications is known to be promoted by deliberately doped foreign ions e.g. F^- stabilizes N-Nb_2O_5 and OH^- promotes the growth condition of B-Nb_2O_5 (Schäfer et al, 1966; Emmenegger and Robinson, 1968; Browne, 1973; the present study.)

Additional contamination of the crystals has been

reported for the chemical vapour transport method. Schäfer et al., (1966), who obtained B-, P- and N-Nb_2O_5 from a $NbCl_5/Cl_2$ transport reaction, found that the crystals contained chlorine in a quantity less than 0.01%. In addition, between 0.05 - 0.1% F had been incorporated in the N-Nb_2O_5 crystals. Emmenegger and Robinson (1968), studying dielectric properties of B-, P-, H-, M- and T-Nb_2O_5, reported that a variable amount of silicon (250-900 ppm, as SiO_2) impurity was present in the crystals.

Anderson, Browne and Hutchison (1972, b) studied, by high resolution electron microscopy, the role of foreign ions in the structural formation of metastable Nb_2O_5 modifications. They found that foreign ions, in the impurity level, were not uniformly dispersed in solid solution with the matrix, but were often segregated in the crystal in such a way that the structure could be modified locally.

The following literature findings are of interest in view of the present preparation of single crystals of niobium pentoxide. Schäfer et al (1966) used a closed quartz ampoule (dia. 16-18 mm) and a small amount of $NbCl_5 + Cl_2$ (p_{Cl_2} = 1 atm at 25°C). This suggestes that due to the small diameter of the reaction tube and the high pressure (ca. 5 atm) of the gas phase at the transport temperature, the transport of matter took place predominantly via a diffusion mechanism. Such diffusion, which is the rate determining factor (Schäfer, 1972), normally causes a low efficiency of crystal growth -- i.e. a transport of

approximately 1 mg Nb_2O_5 in 100 hours (Browne, 1973). For this reason, Schäfer et al's method was not applicable in the present study in which large quantities of well-ordered materials (ideally obtained from one crystal growth run) were needed for the investigation of their phase equilibria systems. This stimulated us to modify the crystal growth condition from diffusion to convection control.

The present Chapter describes this modified method of the chemical vapour transport reaction applied to the growth of single crystals of B-, P- and N-Nb_2O_5. The products obtained were thermogravimetrically purified and their impurity levels determined.

2.2. MATERIALS AND METHODS

The starting material i.e. high purity "spectrographically standardized" Nb_2O_5 was obtained from Johnson Matthey Chemicals Ltd. This material, according to the manufacturers, contained the following detectable impurities:

Fe 2 ppm, Mg < 1 ppm, Ta < 100 ppm

The growth of single crystals of B-; P- and N-Nb_2O_5 involved the following endothermic reactions:

$$Nb_2O_5(s) + NbX_5(g) \underset{\text{cold}}{\overset{\text{hot}}{\rightleftharpoons}} 5\ NbOX_3(g) \qquad (1)$$

$$Nb_2O_5(s) + 3X_2(g) \underset{\text{cold}}{\overset{\text{hot}}{\rightleftharpoons}} 2NbOX_3(g) + 3/2\ O_2(g) \qquad (2)$$

where X = Cl, Br or I.; (s) = solid; (g) = gas.

The different equilibrium constants of equations (1) and (2), present in the hot and cold ends of a closed reaction tube, leads to the deposition of crystalline Nb_2O_5 in the low temperature zone by transport via the gaseous component $NbOCl_3$ (see Schäfer et al, 1966). In all experiments aimed at obtaining stoichiometric compounds, $NbCl_5$ presently was employed as a transport agent since the use of an iodine or bromine atmosphere would result in the formation of partially reduced Nb_2O_5 crystals (Schäfer et al, 1964; Schafer and Huesker, 1962; Emmenegger and Robinson, 1968). Chlorine gas (Cl_2) was included in the system as an oxidizing agent since it is known that in its absence, the formation of sub-stoichiometric oxides may take place. This is based on the fact that $NbCl_5$, at the elevated temperatures used, can partially dissociate into $NbCl_4$ and Cl_2 according to the equation (3):

$$NbCl_{5(g)} \rightleftharpoons NbCl_{4(g)} + \tfrac{1}{2}Cl_{2(g)} \qquad (3)$$

Cl_2 subsequently reacts with Nb_2O_5 -- see equation (2) -- and produces a small oxygen pressure which can control the stoichiometry of the NbO_x solid phase (Schäfer, 1972); hence, sub-oxides of Nb_2O_5 may be formed.

The rate of the transport reaction. For a given temperature gradient, the transport rate is approximately proportional to: a) the length and cross-section of the tube, b) the physical nature of the transport mechanism -- i.e. diffusion, convection or laminar flow, and c) the square of the transporter concentration (Nitsche et al., 1961).

In the present experiments, the mechanism of the

TABLE 3

TABLE 3

Crystal growth conditions of Nb_2O_5 modifications

Compound	Ampoule dia. mm	Ampoule length mm	Charge Nb_2O_5 g	Charge $NbCl_5$ mg.Cm^{-3}	Charge Other	Charge Cl_2 atm. at 23°C	Temperature °C T_1 (source) end	Temperature °C T_2 (deposition) end
B-Nb_2O_5	33	120	3	1.33	H_2O (trace)	0.5	750	700
P-Nb_2O_5	33	120	3	-	H_2O (trace)	0.5	850	750
N-Nb_2O_5	33	120	3	1.33	LiF (trace)	0.5	950	820

vapour transport reaction was altered from predominantly diffusion to convection by increasing the diameter of the reaction tube from 18 mm to 33 mm and by decreasing the total pressure of the gas phase (p_{Cl_2} = ½ atm. at 23°C). This produced satisfactory crystal growth in a shorter experimental period. A large quantity and high quality (large size and structural homogeneity) of the crystals was obtained.

Growth conditions: Table 3 gives details of the growth conditions applied in the preparations of B-, P- and N-Nb_2O_5.

2.2.1. Construction of the Chemical Vapour Transport Apparatus

The experimental set-up for a typical ampoule charging process is illustrated in Fig. 4. The system consisted of three main sections:-

1. The Gas Generation Line. The chlorine gas used (British Oxygen Company Ltd.) had a purity grade of 99.5% minimum. Moisture was its major contaminant and for this reason the system was equipped with drying columns containing $Mg(ClO_4)_2$. The columns are labelled A in Fig. 4.

2. Ampoule Charge Line. Quartz ampoules (C and E in Fig. 4), having approximately identical volumes, were incorporated in the system. Connections with the Pyrex-glass line were made by vacuum standard ball-socket joints, or cone and sockets, using "Apiezon T" as a lubricant. Three double-way taps connected the ampoules to the gas generation line (tap 1), the vacuum line (tap 2) and the

FIGURE 4

FIGURE 4

Typical Ampoule Charging Apparatus (Section 2.2.1.) to grow single crystals of Nb_2O_5 polymorphs by The Chemical Vapour Transport Technique. The system consists of:

(A) Gas-drying columns packed with Mg $(ClO_4)_2$.

(B) A gas-bubbler, containing condensed sulfuric acid.

(C and E) Quartz ampoules (dia. 33 mm., length 120 mm):

(a) a $NbCl_5$ preparation chamber (Section 2.2.2.).

(c) Nb_2O_5 source end.

(d) Nb_2O_5 crystallization zone (Section 2.2.3.).

(b and e) places where ampoules can be sealed off by heating.

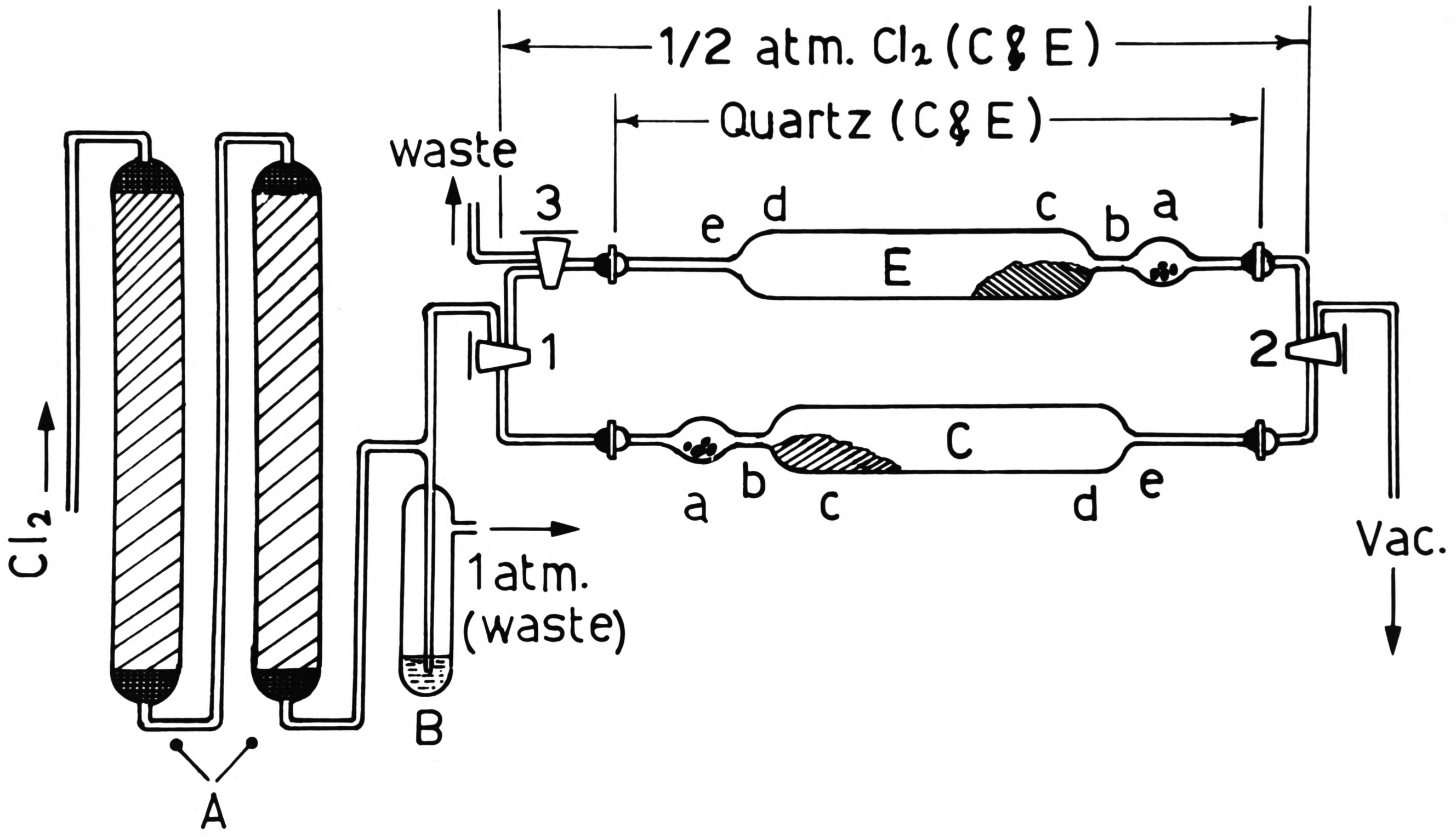
1/2 atm. Cl₂ (C & E)
Quartz (C & E)
waste
3
e
d
c
b
a
E
1
2
C
a
b
c
d
e
Vac.
Cl₂
1 atm.
(waste)
B
A

Fig. 4

waste (tap 3), respectively.

3. The vacuum line. An ordinary rotary pump was used to evacuate the ampoule charge line.

2.2.2. Charging of the Transport Ampoule (see Fig. 4)

The charging involved the following steps:

1. Approximately 3 gm of dry and degased feed material (Nb_2O_5) was put into the ampoules (C and E) at c and a prescribed amount of niobium metal (Johnson Matthey specpure Chemicals) was charged at a (both C and E). Trace amounts of H_2O for the growth of B-Nb_2O_5 and 0.1% LiF (Johnson Matthey Chemicals) for the preparation of N-Nb_2O_5 were also added, as dopants, in ampoules (C and E) at c.

2. Ampoules C and E were evacuated via tap 2. (taps 1 and 3 closed to the gas generation line and to the waste). When a good vacuum was attained, the ampoules were closed to the vacuum line and dry chlorine was admitted via tap 1. At 1 atmosphere Cl_2 pressure in the ampoules, the excess gas escaped from the gas bubbler (sulphuric acid), labelled B. Then, tap 3 was opened to the waste, allowing a constant flow of Cl_2 (approximately 10 ml/min) to stream through the system.

Preparation of the Transport Agent ($NbCl_5$)

Niobium pentachloride was prepared in compartments a and charged in ampoules (C and E) by direct chlorination of niobium metal at 300-350°C (Fairbrother, 1967). The lemon-yellow pentachloride, which sublimed in the gas stream, was subsequently condensed in the ampoules by cooling

the tubes between c-d.

Preparation of ½ atm. Cl_2 To reduce the gas pressure to approximately ½ atm. at room temperature, ampoule E (containing 1 atm. pressure Cl_2) was isolated from the system. (taps 1, 2 and 3 closed). Next, Ampoule (C) was evacuated via tap 2. After a good vacuum was obtained, re-connection of ampoules C and E (taps 1 and 2 closed) led to a Cl_2 pressure of approximately ½ atm. The two ampoules (C and E), again, were isolated from each other and were drawn off at points indicated b and e.

2.2.3. Crystal growth

A two-zone tube furnace, wound with "Kanthal A" wire and having an inner diameter of 4.5 cm and length of 50 cm, was utilized for the growth of crystals. The design and the construction method for the furnace have been described in detail by Browne (1973).

A characteristic temperature profile of the furnace for the preparation of N-Nb_2O_5 is shown in Fig. 5. The Figure also illustrates the method of a typical growth run consisting of the following steps: the ampoule, containing the feed material at (c), was first placed in the furnace at position (I) for approximately 5 hours to clean the crystallization region (d). Next, it was moved to a preset temperature gradient (labelled II) to transport Nb_2O_5 from (c) and deposit crystals at (d). The typical growth period was in the range of 200-300 hours.

At the end of each experiment, the ampoule was withdrawn following a reverse procedure to the one described

FIGURE 5

FIGURE 5

A typical Crystal Growth Temperature Profile in a Chemical Vapour Transport Run (Section 2.2.3.):

At the start of the experiment)	The ampoule is in Position (I) to clean the crystallization zone (d).
During the Growth Run)	The ampoule in Position II. The material is transported from the source end (c) and deposited in (d).
At the end of the experiment)	The ampoule in Position (I). The source end (c) is quenched. Next, the ampoule is withdrawn.

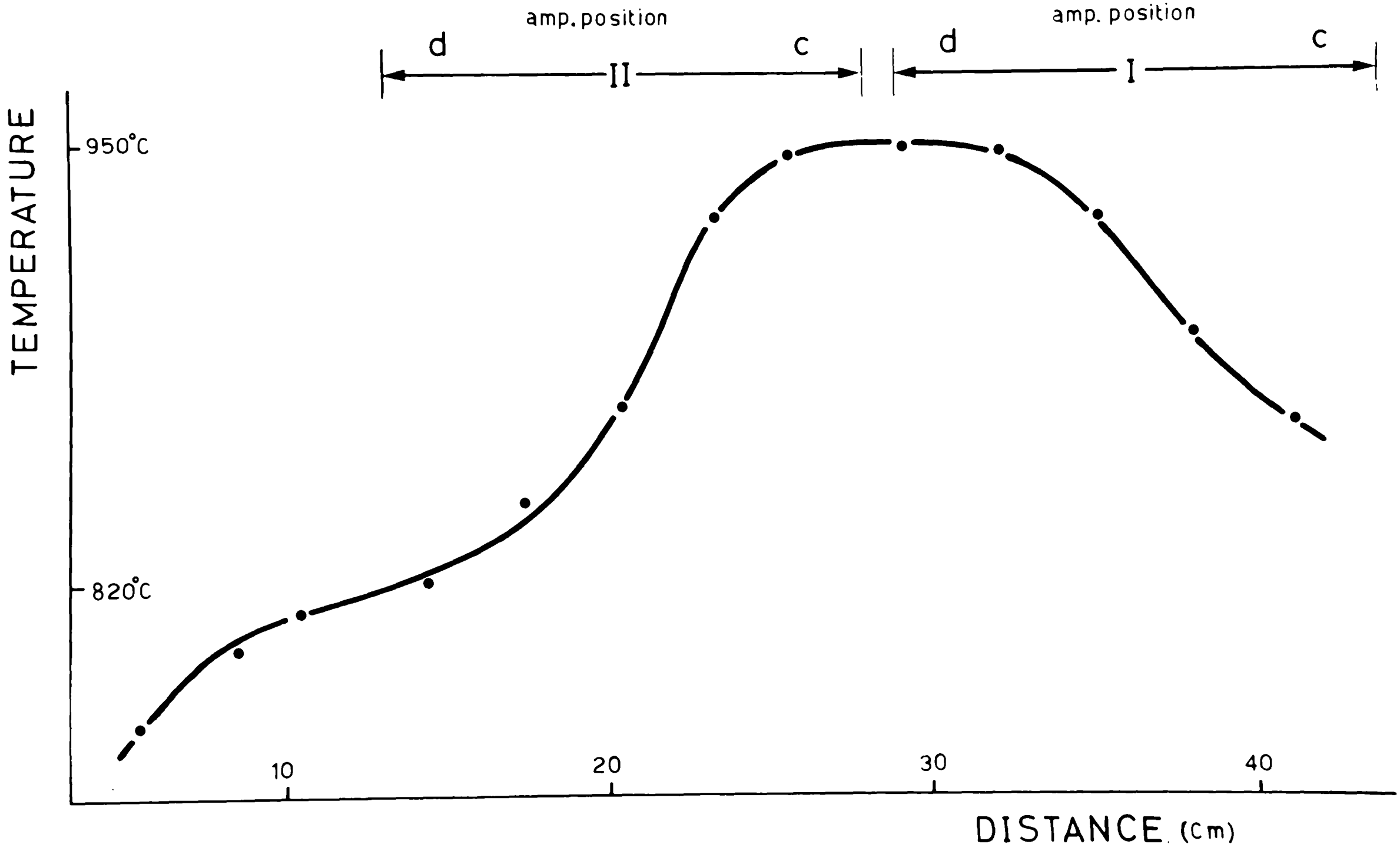
CRYSTAL GROWTH FURNACE
TEMP. PROFILE (e.g. N-Nb2O5)
amp. position
d
c
II
amp. position
d
c
I
TEMPERATURE
950°C
820°C
10
20
30
40
DISTANCE (cm)

FIG. 5

above -- i.e. the ampoule was first moved to position (I) and source end (c) quenched in order to condense the vapour phase at (c). Here, care was taken to keep the high temperature zone of the furnace below the transition temperature of the grown crystals. Finally, the ampoule was withdrawn from the furnace.

2.3. RESULTS

2.3.1. Characterisation of the vapour transport products

B (Blätter)-Nb_2O_5

In Plate (1-A), a typical colourless (stoichiometric) single crystal of B-Nb_2O_5 is shown. These stoichiometric crystals as well as the bluish (sub-stoichiometric) B-Nb_2O_5 crystals (see Plate 1-B) have a plate-like morphology. The crystals have a monoclinic symmetry in which c is unique with the b and c axis in the flat plane of the crystal and the a axis extends at $\gamma = 105^{\circ}\ 5'$ to this plane (Laves et al, 1964). A characteristic feature is the presence, on the flat surface of the crystals, of strips which are running in parallel to the b axis (Emmenegger and Robinson, 1968). Some thin crystals, however, do not show these strips.

Both colourless and bluish-tinted B-Nb_2O_5 crystals were separately identified by their Guinier X-ray powder diffraction patterns (see Plate 13-a). The patterns of the blue as well as of the colourless crystals showed no extraneous lines and were indexed by using the monoclinic cell dimensions a = 12.73 Å, b = 5.56 Å, c = 4.88 Å and $\gamma = 105^{\circ}\ 5'$ (Laves et al, 1964).

PLATE 1

PLATE 1

Crystal Morphology of Chemical Vapour Transport Products (Section 2.3.1.):

A) $\underline{B\text{-}Nb_2O_5}$: A representative single crystal with a plate-like morphology is shown here. max. crystal size: 5 x 5 x 1 mm^3 approx.

B) $\underline{Blue\ B\text{-}Nb_2O_5}$: A cross-section (perpendicular to the vapour transport direction) of a crystallization zone of the $B\text{-}Nb_2O_5$ reaction ampoule is shown here. Blue $B\text{-}Nb_2O_5$ crystals, grown in an oxidizing atmosphere (Cl_2), are sub-stoichiometric (Section 2.3.3.).

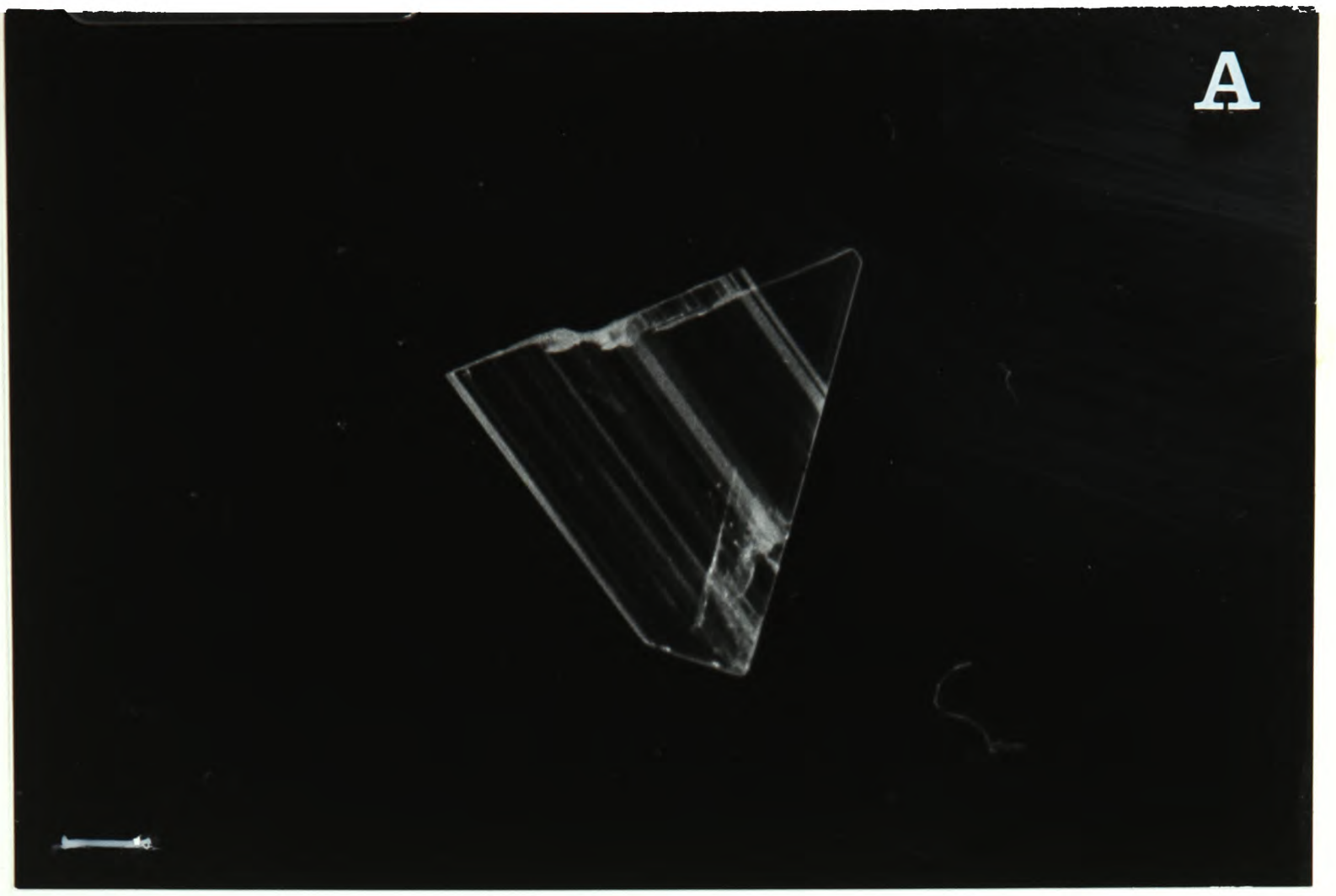

B–Nb_2O_5

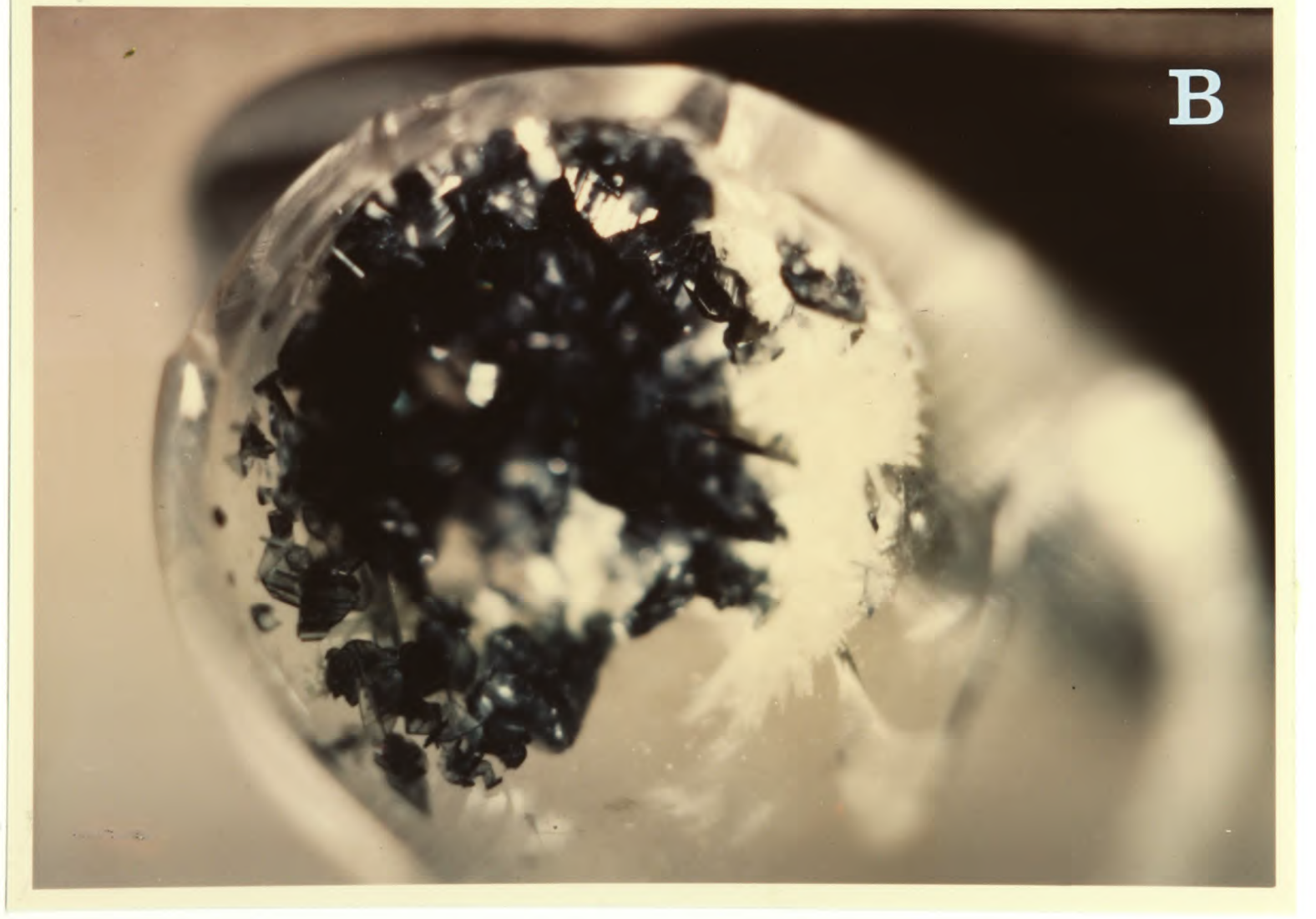

blue B–Nb_2O_5

Plate 1

P (Prism)-Nb_2O_5

Representative P-Nb_2O_5 single crystals are shown in Plate 2-B. Individual crystals, according to Petter and Laves (1965), have a rectangular morphology with the short axis of its tetragonal lattice (a = b = 3.89 Å) in the plane of the platelet and the long axis (c = 25.43 Å) perpendicular to the large face of the crystal.

The crystallographic identification of the sample was established by means of X-ray powder diffractometry (see Plate 16-A) as well as by electron diffraction and by the direct lattice imaging method (see Plate 14). Lattice parameters of the crystals were consistent with the above values given in the literature (Petter and Laves, 1965). Results of the X-ray powder diffraction analysis are given in Table 13.

N-(needle)-Nb_2O_5

Single crystals of N-Nb_2O_5 generally grow with an elongated needle habit. The b-axis of the monoclinic lattice extends in parallel to the direction of rapid growth (Anderson et al, 1972b). In Plate 2-A, a cross-section (in parallel to the transport direction) of a typical N-Nb_2O_5 growth morphology is shown. The crystals were identified by X-ray powder diffraction, electron diffraction and microscopy using data given by Andersson (1967).

2.3.2. Purification and Impurity Estimation of the Chemical Vapour Transport Products

Impurities present in single crystals of Nb_2O_5 can be classified into two groups:-

PLATE 2

PLATE 2

Crystal Morphology of Chemical Vapour Transport Products (Section 2.3.1.):

A) N-Nb_2O_5 single crystals. A cross-section (in parallel to the vapour transport direction) of a crystallization region of an N-Nb_2O_5 reaction tube is depicted. The crystals have a needle shape. Tube size: dia. 33 mm, length 120 mm. Max. crystal size: ~10 mm.

B) Typical single crystals of P-Nb_2O_5. The crystals are rectangular platelets. Max. crystal size: 5 x 3 x 1 mm^3 approx.



N-Nb_2O_5

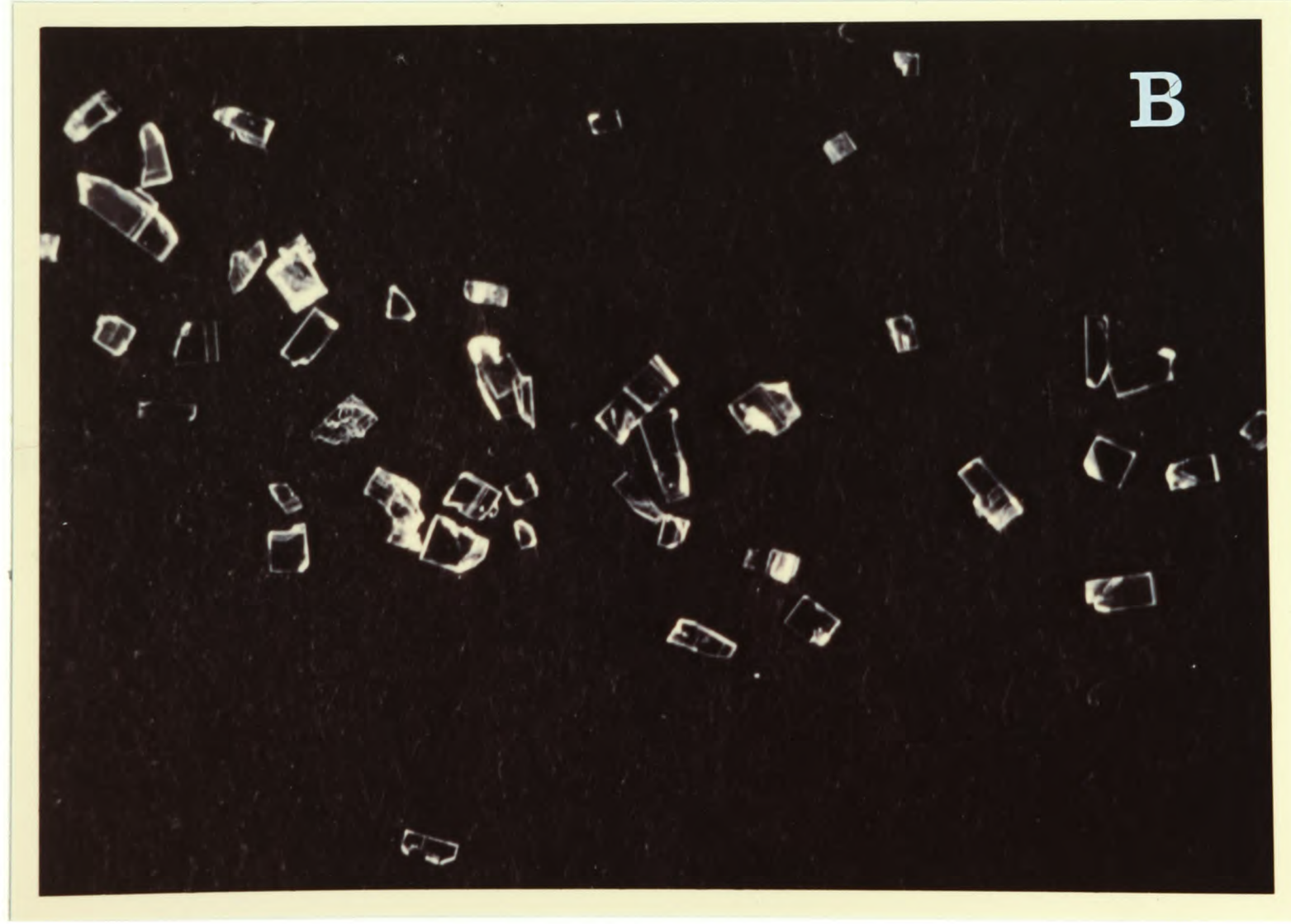

P-Nb_2O_5

Plate 2

1. External contaminations. They are caused - possibly during the process of crystal growth and withdrawl of the ampoule from the furnace -- by fractional condensation of the gas phase (i.e. $NbCl_5$, $NbOCl_3$) on the crystal surface.

2. Inner contamination -- i.e. impurity atoms such as F, Li, Cl, Si etc., which are probably occupying interstitial sites as well as normal lattice sites.

The adsorbed contaminations (1) and the non-metallic impurities (i.e. Cl_2) present in interstitial sites of the lattice (2) are susceptible to heat treatment of the crystals. Such impurities can therefore be eliminated by subjecting the crystals to heat (ca. 500°C) in a vacuum environment. Thus, prior to phase equilibria experiments on the samples B-, P-Nb_2O_5 * (see Chapters V and VI) the following procedure was adopted:

Approximately 100 mg of finely ground single crystals of B-, P- and N-Nb_2O_5 of different samples (Experiments 1-4, Table 4) were heated at 500-600°C in a high vacuum (ca. 10^{-4} torr) environment of the Cahn-microbalance line. It was found that, at the start of each experiment, an appreciable amount of weight loss took place rapidly. The sample weight thereafter remained constant, indicating that evaporation of the volatile species was completed. The weight losses, interpreted in terms of per cent chlorine in the samples, are listed in Table 4.

Footnote *: Phase equilibria studies in the system NbO_2-(N-Nb_2O_5) are not included in this thesis.

TABLE 4

Weight loss in % Cl_2

Experiment	B-Nb_2O_5	P-Nb_2O_5	N-Nb_2O_5
1	0.01	0.01	0.02
2	0.01	0.00(7)	0.01
3	0.02	0.00(6)	0.01
4	0.00(8)	0.00(7)	0.00(5)

It is apparent from Table 4 that there is a variation in the degree of contamination between individual samples of one compound. This might be attributed to slight differences in the conditions under which the materials were prepared -- i.e. temperature differences between source end and deposition end, slight variations in ampoule length and, also, in the care with which ampoules were withdrawn from the furnace.

Impurity atoms incorporated in proper lattice sites, are unlikely to be eliminated by a simple heat treatment of the oxides. The concentration of such impurities, was assessed by the thermogravimetric method: it was assumed that after heat treatment of the crystals impurity atoms could be driven out of the lattice by reduction of the crystalline Nb_2O_5 into NbO_2. In a reverse process -- i.e. reoxidation of NbO_2 into Nb_2O_5 -- the excess of oxygen uptake, thus, could lead to the assessment of the structural impurity level. However, experiments carried out on colour-

less B-; P- and N-Nb_2O_5 revealed no significant weight difference in the reduction-reoxidation process. This suggested that the crystals were pure with a stoichiometry of $NbO_{2.500}$.

2.3.3. Chemical Composition of the blue B-Nb_2O_5 Crystals

The composition of blue B-Nb_2O_5, by Schäfer *et al*, (1966) was estimated to be $Nb_2O_{4.994}$. They reported that the crystals could hardly be decolourized (i.e. oxidation of Nb^{4+} into Nb^{5+}) by prolonged heating in air at 800°C. Emmenegger and Robinson (1968) suggested that blue B-Nb_2O_5 crystals (obtained from a halogen transport process using $NbCl_5/Cl_2$ and a trace of H_2O) were contaminated with SiO_2.

In a present attempt to determine the chemical composition of blue B-Nb_2O_5 crystals, the following thermogravimetric method was applied:

After eliminating the volatile impurities (see Section 2.3.2.), approximately 25 mg of finely ground crystals were reduced to NbO_2 in a Cahn-balance using a stream (~ 10 ml/min) of CO at 1000°C for 20 hours. Next, the product was reoxidized back into Nb_2O_5 in air (flow rate ca. 10 ml/min) at 1000°C for 60 hours.

A comparison between total weight loss in the reduction and weight gain in the reoxidation processes showed, however, an appreciable difference -- i.e. there was a greater weight after the reoxidation process. It was assumed that this was due to oxygen deficiency of the starting material, and an average composition of $NbO_{2.4948}$

was tentatively assigned to the blue crystals.

2.4. SUMMARY AND DISCUSSION

Single crystals of B-, P- and N-Nb_2O_5 were grown by a chemical vapour transport method using $NbCl_5/Cl_2$ as transporters. As compared to literature reports, the crystal growth rate was improved by increasing the diameter of the transport tube (to 33 mm) and decreasing the total pressure of the gas phase (to ca. 0.5 atm. at 23°C). The improvement was probably due to an increased transport reaction via convection as opposed to diffusion. Growth of larger single crystals under these conditions requires precise temperature control to keep the number of nucleation sites to a minimum. The present process offered two distinct advantages over the growth procedures described by others (Schäfer et al, 1966; Emmenegger and Robinson, 1968).

1. The sample preparation is facile -- i.e. it is easier to prepare the transport ampoule at a low (ca. 0.5 atm. at 23°C) than at a high (1 atm.) pressure.

2. Large quantities of Nb_2O_5 single crystals can be grown in, at least, half of the time required by other methods.

Impurities present within the crystals were found to consist predominantly of chlorine. Thermogravimetric measurements showed that B-, P- and N-Nb_2O_5 contained, on average, % Cl $\leq$ 0.01. This finding confirms the assessment of Schäfer et al (1966) that chlorine impurity in vapour transport products is less than 0.01%.

The occurrence of other contaminations have also been

reported in the literature. Schäfer et al (1966) detected SiO_2 in N-Nb_2O_5 crystals. Similarly, Emmenegger and Robinson (1968) found that B-Nb_2O_5 crystals were contaminated by as much as 9000 ppm SiO_2. Reisman and Holtzberg (1970), on the basis of literature findings, concluded that the vapour transport products are probably Nb-Si-O ternary phases. Anderson et al (1972b), studying the ultrastructure of N- and transformed M-Nb_2O_5 crystals, found that impurity atoms were segregated as extended defects. They, therefore, suggested that metastable structures are formed due to a catalytic effect of the segregated impurities. A similar observation has been reported in Chapter V of the present thesis (Section 5.1.3.2.).

In the present samples, impurity atoms other than chlorine could not be detected by thermogravimetric analysis nor by X-ray spectrums obtained from an analytical electron microscope (Jeol 100 CX, TEMSCAN Instrument). We therefore assumed that after their purification (Section 2.3.2.) the oxides were pure, having a stoichiometry of $NbO_{2.5000}$.

By contrast, a thermogravimetric analysis of the blue B-Nb_2O_5 crystals indicated that the crystals were sub-stoichiometric having a composition of $NbO_{2.4948}$ and this is in close agreement with the value reported by Schäfer et al (1966) -- i.e. $Nb_2O_{4.996}$. The nature of the blue crystals is further discussed in Chapter V (Discussion, Part B).

CHAPTER III

EXPERIMENTAL METHODS FOR PHASE EQUILIBRIA STUDIES IN THE SYSTEMS Nb-O AND Ti-Nb-O

CONSTRUCTION OF APPARATUS

INTRODUCTION

Various methods generally used in investigations of thermodynamics of metal-oxygen systems are discussed in section 3.1. of this Chapter.

Section 3.2. deals with the present application of gas buffer methods -- i.e. CO_2-CO and CO_2-H_2 gas mixtures -- for studies of phase equilibria in pure niobium pentoxides (B- and P-Nb_2O_5) as well as in mixed niobium-metal oxides (i.e. the Ti-Nb-O system). The latter investigation -- i.e. reduction of $TiNb_2O_7$, $Ti_2Nb_{10}O_{29}$ and $TiNb_{24}O_{62}$ at 1400°C -- required the construction of a newly designed apparatus, the "Horizontal Quench Furnace System".

3.1. Experimental methods applied in high-temperature thermodynamic measurements of metal-oxygen systems

The chemical potential of oxygen in metal-oxide systems is generally determined by the application of one of two distinguished (groups of) methods:

a) The electromotive force (EMF) method

b) Measurements of oxygen dissociation pressures.

(a) In the EMF method, the chemical reaction under investigation is harnessed in such a way that the generated energy produces an electromotive force. The change in Gibbs free energy (ΔG) of the reaction is directly related to the EMF (E) according to the equation below (1) provided that all intensive parameters of the electrochemical system are kept constant.

$$\Delta G = -ZFE \qquad (1)$$

Z represents the number of equivalents of electrical charge transported when one formula amount (in moles) of the overall cell reaction takes place; F is the Faraday constant.

The relation between E and the chemical potential of oxygen can be determined as follows:-

In a solid state cell, formulated:

$$Pt,\ O_2\ (p'_{O_2})\ /\ ZrO_2(CaO)/O_2\ (p''_{O_2}),\ Pt$$

the halfcell reaction is:

$$O_{2(g)} \rightleftharpoons 2O^{2-} \quad -4e$$

and, the cell reaction:

$$O_2\ (p'_{O_2}) \rightleftharpoons O_2\ (p''_{O_2})$$

The standard free energy change for the cell reaction at temperature T (in ^{o}K), is given by equation (2):

$$G^{o}_{0} = -RT\mathrm{Ln}\ Kp \qquad (2)$$

where $Kp = p''_{O_2} / p'_{O_2}$

Combination of equations (1) and (2) results in:

$$E = \frac{RT}{ZF}\ \mathrm{Ln}\ \frac{p''_{O_2}}{p'_{O_2}} = \frac{\mu''_{O_2} - \mu'_{O_2}}{ZF} \qquad (3)$$

where Z, the number of electrons transferred per mole oxygen, = 4.

Equation (3) indicates that the measured voltage (E) is a measure of the oxygen partial pressure at each side of the electrolyte. Hence, a combination of a reference

electrode (e.g. Pt/Me, MeO) with an auxiliary oxygen ion conducting electrolyte provides a means by which unknown oxygen potentials can be measured.

The use of solid electrolytes in EMF measurements has developed significantly since Kiukkola and Wagner (1957) reported that the transport number of oxygen ion in a solid solution of lime in Zirconia (ca. 15 mole % CaO) is near to 1 (at 1 atm. > p_{O_2} > 10^{-22} atm. O_2 at 870°C).

Recent progress in solid state electrolyte research and the application of the EMF method for the determination of thermochemical data have been reviewed by Etsell and Flengas (1970) and Schmalzried and Pelton (1972).

(b) The second group of methods employed for the determination of oxygen partial pressures comprises dynamic, static, effusion and the more commonly applied gas equilibrium methods (Kubaschewski, Evans and Alcock, 1967). The methods are briefly described below:

In the dynamic method, known as the transpiration or transportation method, an inert gas is passed over a heated substance at a known rate which is slow enough to achieve saturation of the "carrier" gas with the sample vapour. The vapour is then condensed in cooler parts of the apparatus and the dissociation pressure calculated from the amount of the sample material collected in a known time period (Merten, 1959).

In the static method, the sample is placed in a vacuum compartment connected to a sensitive manometer system. After adjustment of the reaction equilibrium, the vapour pressure is recorded directly from the manometer.

The effusion method, based on principles devised by Knudsen (1909), Langmuir (1913) and Volmer (1931), employs a gas-tight sample container (i.e. reaction chamber) with a capillary opening through which vapour of the reaction pressure can be determined by its rate of evaporation in vacuum. In a complex vapour, the different species present can subsequently be analysed and identified by means of a mass spectrometer.

The gas-equilibrium method involves the equilibration of oxides with pure oxygen gas, dilute oxygen (O_2 + inert gases), or gas buffers (i.e. H_2O/H_2 or CO_2/CO mixtures) which are subsequently described below.

For high oxygen partial pressures (1 - 10^6 atm), pure oxygen is employed for the determination of dissociation pressures in the metal/oxide systems (Reed, 1970). According to Reed, oxygen can be supplied from ordinary cylinders or generated from the decomposition of CrO_3 or MnO_2 which have decomposition pressures of 10^4 - 10^6 atm. at 1000°K.

For low oxygen partial pressures (1 - 10^{-6} atm.), mixtures of oxygen with inert gases have been used (Muan, 1958; Reed, 1970).

Gas buffer mixtures of H_2O/H_2 or CO_2/CO are used to generate oxygen partial pressures as low as approximately 10^{-22} at 1000°C. Because of the inevitable presence of water vapour in an experimental system, the application of this method is restricted to studies of metal oxide systems in which the metal has a moderate affinity for oxygen (Kubaschewski and Slough, 1969).

Equilibrium constants at different temperatures, for

the reactions:

$$CO_2 = CO + \tfrac{1}{2}O_2 \quad \text{and} \quad H_2O = H_2 + \tfrac{1}{2}O_2$$

are compiled in the literature (Nat. Bur. Standards, 1945 U.S. Bureau of Mines, 1950; JANAF, thermodynamic tables, 1968.). By fixing the ratio of CO_2/CO or H_2O/H_2, the oxygen potential of the gas mixture can be calculated at a given equilibrium temperature. The gases are interchangeable i.e. CO may be mixed with H_2O and H_2 with CO_2. The interdependence of the equilibrium ratios H_2O/H_2, CO_2/CO, CO_2/H_2 and H_2O/CO at a certain oxygen pressure is expressed by the equilibrium constant for the "water gas equation" $CO_2 + H_2 = CO + H_2O$ (Darken and Gurry, 1945; Muan, 1958). The effective gas ratios of CO_2/CO or H_2O/H_2 fall in the range of 1000/1 - 1/1000 at 1000°C. Outside this range, the kinetics of oxygen exchange from the gas phase to the solid surface are too slow (Reed, 1970). Tables and monograms for the calculation of oxygen pressures for various gas ratios and temperatures have been given by Porter (1965), Khan (1968) and Nimmo (1971).

Still lower oxygen partial pressures (ca. 10^{-40} atm. at 1000°C) can be retained by the isopiestic technique in which the sample is equilibrated with alkaline-earth metal vapours of known partial pressures and solid alkaline-earth metal oxides -- e.g. Ca/CaO, Mg/MgO, Zn/ZnO. Using this technique, Komark and Silver (1962) investigated thermodynamic properties of Zr-O, Ti-O and Hf-O systems by equilibrating solutions of oxygen in the metals with magnesium oxide and magnesium vapour.

Solid metal-metal oxide buffer systems can also be employed to generate requisite oxygen partial pressures. In this method, the sample, enclosed in an evacuated silica tube, is equilibrated with a fixed oxygen partial pressure generated from mixtures of a reference metal and its lowest oxide or of successive oxides of the same metal -- e.g. Fe-FeO or Ni-NiO. Details of the technique have been given by Khan (1968); Reed (1970) and Nimmo (1971).

Differing methods applied for the determination of dissociation pressures in oxide systems as discussed above are summarized in Table 5, which shows the practical range of application of the methods in terms of calories per mole O_2 at 1000°C (after Kubaschewski and Slough, 1969).

TABLE 5

Method	G_{O_2} Kcal.
Direct dissociation	0-40
H_2O/H_2 and CO_2/CO equilibria	20-130
EMF (solid oxide electrolytes)	25-150
Equilibration with Mg/MgO	200-240

In the present study, the requisite oxygen partial pressures were generated using the gas buffer method, involving the equilibration of CO_2-CO or CO_2-H_2 gas mixtures with oxides at isotherms ranging from 750-1400°C.

The standard free energy (per mole oxygen) for the reaction

$$2Nb_2O_5\ (s) \rightleftharpoons 2Nb_2O_4\ (s) + O_2\ (g)$$

,at 750-1400°C, according to literature data (e.g. see Kubaschewski, Evans and Alcock, 1967), ranges from -114.63 to -96.45 Kcal. These values are practically obtainable by the gas buffer method.

3.2. Design and Construction of Apparatus

The apparatus described below was designed and constructed by the present author to investigate phase equilibria in the binary Nb-O and ternary Ti-Nb-O systems. The apparatus consisted of three main sections or systems:

(1). A mixed gas buffer system

(2). A Cahn-RG4 electro-balance system

(3). A horizontal quench furnace system

3.2.1. The mixed gas buffer system (Fig. 6)

This system consisted of the following parts: Carbon monoxide (or Hydrogen) and carbon dioxide cylinders including constant pressure inlet regulators; two capillary gas flow-meters (a) in Fig. 6; a gas bubble-meter (c) equipped with a soap solution reservoir; drying columns (b); gas mixing chambers (d); a non-return gas bubbler (e). The various parts in this system are described in detail below:

Gas flowmeter (Fig. 7)

The gas flowmeter, the mechanism of which was based on principles given by Barr (1934), consisted of a 115 cm long U-tube monometer (d in Fig. 7) to measure differences in pressure between the two ends of the capillary tube (a).

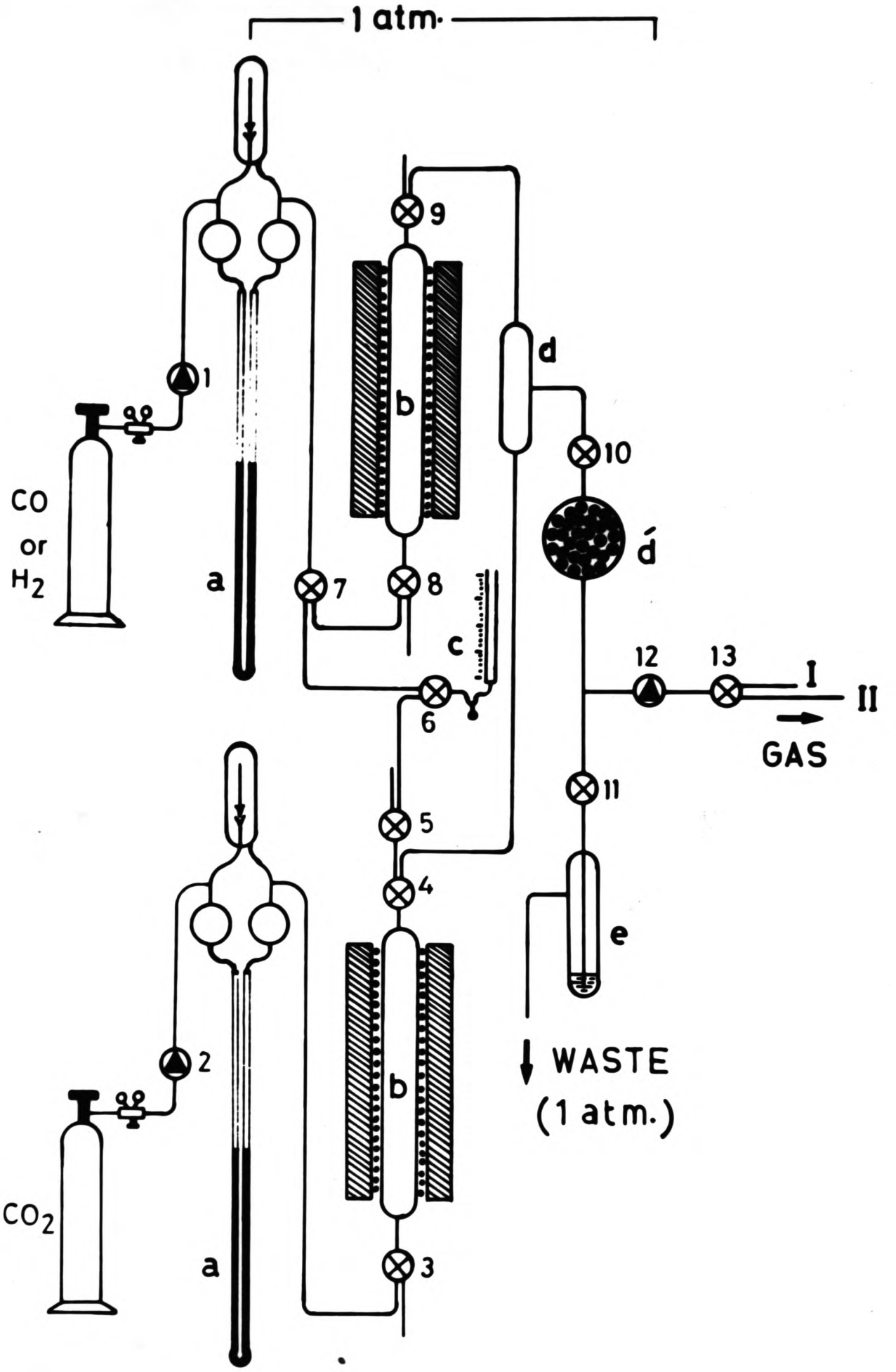

FIGURE 6

Diagrammatic drawing of the mixed gas buffer system (Section 3.2.1.).

The manometric liquid was dibutylphtalate which has a low vapour pressure at ambient temperature. Between the manometer and the capillary head two blow-off glass bulbs (c) were inserted. The capillary tube, approximately 7 cm long and arranged vertically, was connected to the glass bulbs using a B7 cone and socket. Over the capillary an end-closed demountable glass cap (b) was placed which was joined to the manometer system by a B24 cone and socket. The advantage of the present design is the facile method of changing the capillary with others having different diameters. This, in combination with the long arms of the U-shaped manometer, permits a continuous supply of gas flows with a wide range of rates.

The flowmeters were calibrated using a bubble-meter (c in Fig. 6) identical to the one described by Barr (1934) and Levy (1964). The bubble-meter employed in the present work was a 50 ml graduated burette equipped with a rubber reservoir containing a dilute soap solution. The meter was connected with the two gas flowmeters through taps Nos. 5 and 7. The gas stream to be measured entered the bubble-meter driving a thin film of soap ahead. This film was produced by the operator, by obstructing the gas passage temporarily with the soap solution by compressing the rubber soap reservoir. The film in the bubble-meter was mobile and stable when the inner surface of the tube was wet. The time required for the film to travel between two gradations at atmospheric pressure was measured by means of a stopwatch and the resulting flow rates were subsequently plotted against the manometer readings. The maximum and minimum

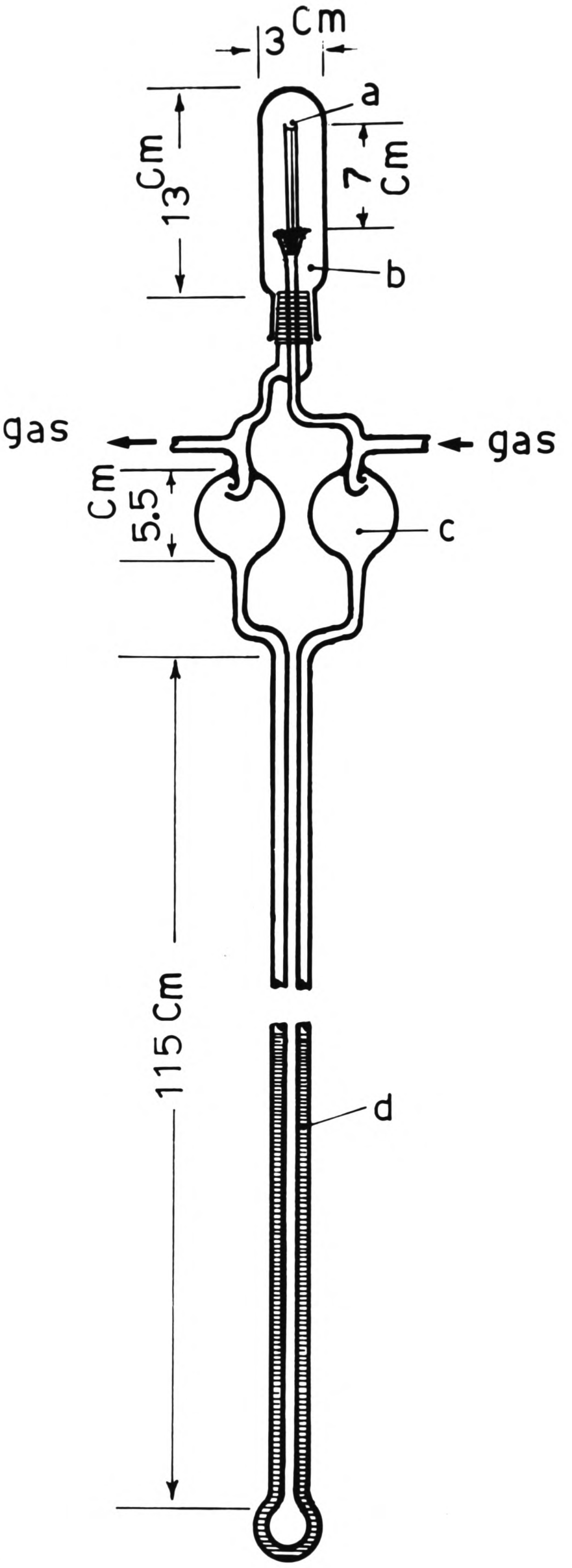

FIGURE 7

A gas flowmeter scheme designed for the supply of a wide range of mixed gas compositions (Section 3.2.1.)

flow rates measured in the present study were 60 and 0.2 ml. min^{-1}, respectively, with a probable error of $\pm$ 1%.

The impurity level of input gases

The purity grades and typical chemical analysis of the three gases used -- i.e. CO, H_2 and CO_2 -- as quoted by the manufacturers, are as follows:-

Carbon monoxide (supplied by Air Products)

Purity 99.5%. Impurities: oxygen - 800 ppm; carbon-dioxide - 550 ppm; hydrocarbons - 50 ppm; moisture - 5 ppm; nitrogen - 0.32% (by volume).

Hydrogen (Air Products)

Purity 99.5%. Impurities: oxygen - <1 ppm; nitrogen - <100 ppm; moisture - <1 ppm; hydrocarbons - <1 ppm.

Carbon dioxide (Distillers Co. Ltd)

Total residue	<0.2 vol.%, of which approximately one fifth is oxygen
moisture	<0.05%

Before preparing the CO_2-CO or CO_2-H_2 gas mixtures, the gases were purified. A possible source of error in later experiments arises from the presence of impurities such as CO_2, CO, O_2 and moisture in the constituent gases. Gases were purified by passage through columns (b in Fig. 6) of pre-dried molecular sieves (see 1 and 2 below) type 4A and 5A. CO gas was dried by sieve 4A which is capable of adsorbing CO_2 impurities as well as water vapour at room

temperature. CO_2 was dried by passing through sieve 5A column.

1) Molecular Sieves (B.D.H. Chemicals Ltd) are synthetic zeolites (aluminosilicates) with pore sizes capable of selectively adsorbing molecules of a narrow size range (Brack, 1964; Fieser and Fieser, 1967).

2) To activate (i.e. to dry the molecular sieves), the columns (b in Fig. 6) were externally wound with nichrome wire (17.94 Ω /yard) supplied by British Driver-Harris Co. Ltd. The column was insulated with asbestos strings and heated at approximately 300°C by a 3 amp variac. Concurrently, the columns were flushed with nitrogen gas using taps (Nos. 5-3) and (Nos. 9-8).

Note. The relatively small oxygen impurity of the gases was not removed. Its presence, however, reduces the effectiveness of CO_2/CO or CO_2/H_2 mixtures, particularly, at ratios departing from 1/1. Therefore, in the calculation of oxygen dissociation pressures of oxides, the effect of this impurity was taken into account.

Gas mixing chambers (d and d' in Fig. 6)

Measured and dried streams of CO_2 and CO (or CO_2 and H_2) were mixed initially in an empty chamber (d) and ultimately in a chamber (d') packed with glass beads. The mixed gases were subsequently admitted to the Cahn RG thermobalance system (I in Fig. 6) or the Horizontal Quench Furnace system (II) via a double-way tap (No 13), regulating the input gas rate by an Edwards needle value (12). The two systems are shown in Fig. 8-A and B respectively.

To prevent a continuous build-up of pressure within

the capillary system, a small fraction of the mixed gas was bled-out to the waste (at atmospheric pressure), using a fine-jet bubbler (e in Fig. 6) filled with dibutylphtalate.

Thermal diffusion effect; (adapted gas flow rates)

Due to the asymmetric flow of mixed gases through the Cahn RG electrobalance system, the effect of thermal diffusion in the reaction zone of the balance has to be considered. The thermal diffusion effect, basically, arises from different molecular weights of mixed gases flowing through a system in which a temperature gradient occurs. The diffusion effect, which has been discussed extensively in the literature (Darken and Gurry, 1945; Kubaschewski et al, 1967), can be minimised by using a sufficiently fast speed of gas flow. According to Darken and Gurry (1945), linear CO_2/CO gas velocites greater than 30 $ml.min^{-1}$ should be employed to avoid thermal segregation at 1100°C. However, high gas flow rates also have a disturbing effect on the microbalance zero point setting. For this reason, using a microbalance line at 750°-1000°C, gas flow rates of approximately 30 $ml.min^{-1}$ were adopted.

Calculation of oxygen partial pressures

Equilibrium oxygen partial pressures generated from CO_2/CO or CO_2/H_2 mixtures were calculated using data given in tables of the National Bureau of Standards (see Rossini et al, 1945).

FIGURE 8

FIGURE 8

Experimental set-up for measurements of phase equilibria in metal-oxide systems.

A) The Cahn-RG thermobalance system (Section 3.2.2.).

B) The Horizontal Quench Furnace System (Section 3.2.3.).

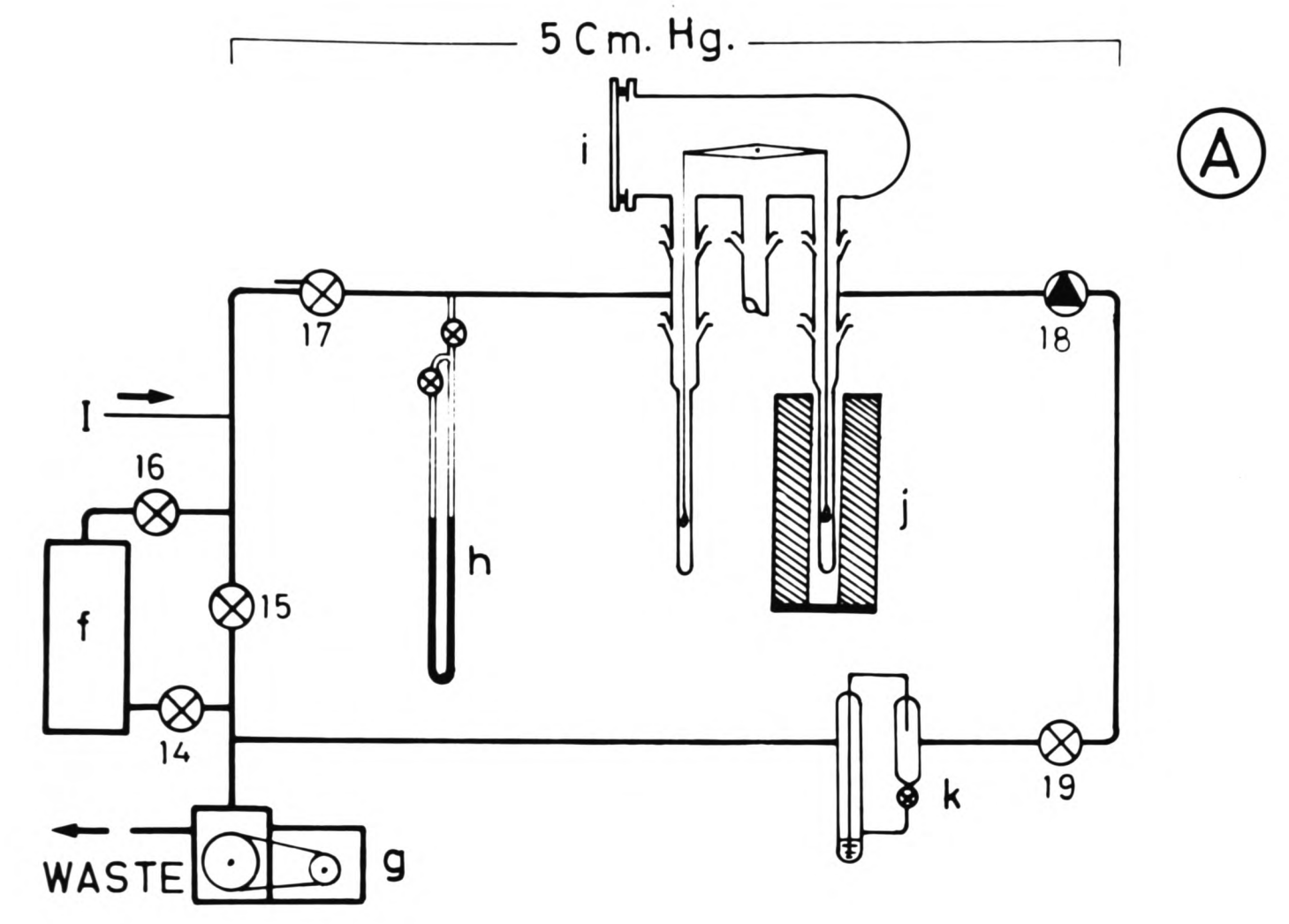
5 Cm. Hg.
A
i
17
18
I
16
h
j
f
15
14
k
19
WASTE
g
1atm.
B
II
20
21
22
m
l
h
n
23
k
24
25
26
f
27
WASTE
g
Edwards needle valve
4mm or 6 mm HV tap

Fig. 8

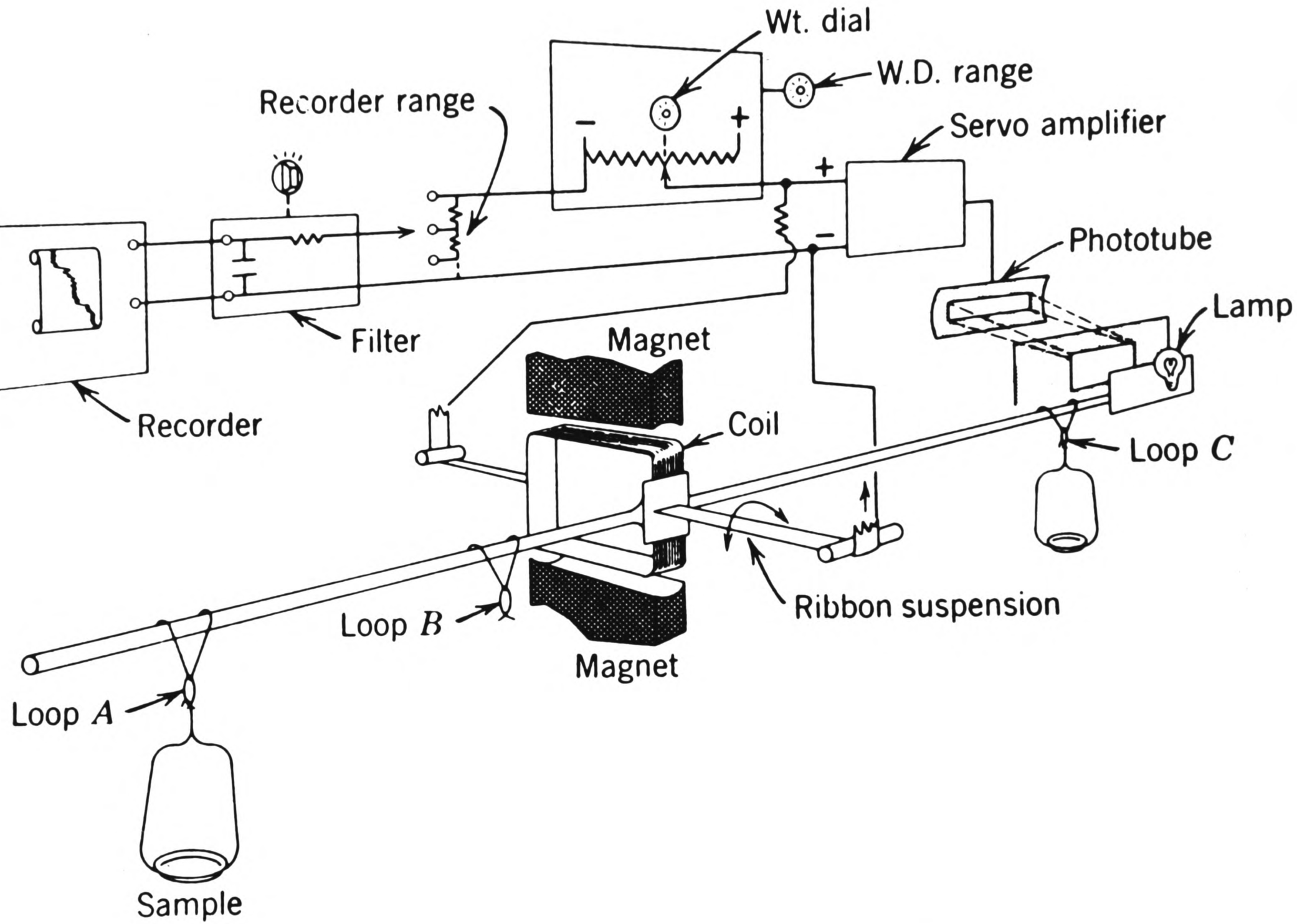

Figure 9 Schematic diagram of the Cahn Electrobalance.

3.2.2. The Cahn RG Thermobalance System

Weight changes of samples in phase equilibria studies of the binary Nb-Osystems and chemical analysis (i.e. -- re-oxidation) of the reduced Ti-Nb oxides were monitored using a model-RG Cahn Thermobalance system a schematic drawing of which is shown in Fig. 8-A. The system consisted of the following: a Cahn RG electrobalance (i); a vertical heating furnace (j); a mercury manometer (h); a non-return gas bubbler (k); a rotary pump (g); and a mercury diffusion pump (f).

Since the design and construction of the system has been previously described by Nimmo (1971), only significant parts are discussed here.

The Cahn RG electrobalance. The principle of the electrobalance functioning i.e. the null-balance principle with the sample being suspended from the indicating needle (balance beam), has been discussed in detail in the literature (Cahn and Schultz, 1963). Changes in sample mass cause the balance beam to deflect, changing the photo-cell current which is then amplified and applied to the coil attached to the balance beam. This coil is located in a magnetic field so that current flowing through it exerts a moment on the beam, restoring it to a null position. The coil current is thus an exact measure of the sample mass.

A diagram of the mechanism of the balance is shown in Fig. 9. The balance has a maximum capacity of 1 gm on a more sensitive loop and of 2.5 gm on a less sensitive one. The maximum sample weight variation is 200 mg; the balance sensitivity is 10^{-6} of the load with a limit of 2×10^{-7} gm.

An amplifier with a gain of 10 (constructed in this Laboratory) was fitted to the output of the Cahn balance to make the recorder sensitive to a 1 millivolt full scale. The amplifier also supplied positive and negative outputs to a centre zero recorder, thus facilitating the detection of both weight gain or loss.

The balance was mounted in an elongated horizontal glass flask (i in Fig. 8-A) which could be used for pressures down to approximately 10^{-8} torr or lower (Cahn balance manual). The flask was clamped rigidly to a 2.5 mm cast iron mount securely bolted to the wall.

The hang-down tubes had dimensions of 25 mm internal diameter and 35 cm length. From the lower conical joint onwards, the sample tube was constructed of fused quartz. The sample, contained in a platinum bucket having 9-10 mm internal diameter in which samples from 25-100 mg could be investigated, was suspended 45 cm below the balance using a 0.005 inch pure platinum wire (Johnson Matthey Ltd).

The vertical heating furnace

A Kanthal "A" wire ($3.7\Omega\ m^{-1}$) wound vertical furnace (j in Fig. 8-A) was used to heat the sample during the experiments. The furnace dimensions were 15 x 15 x 40 cm; the inner diameter of the refractory tube was 30 mm.

The furnace temperature was controlled by an Ether Transitrol type 991 instrument activated by a T_1/T_2 thermocouple.

The furnace, mounted on a hoist, could be raised or lowered to enclose or quench the sample. To minimize the

disturbing effect of gas convection, the microbalance head was cooled by means of an electric fan.

The sample temperature was measured by a Pt vs Pt-13% Rh thermocouple located in the vicinity of the bucket. The EMFs developed were measured on a Servoscribe Potentiometric, double channel, Recorder. To achieve greater accuracy, a Cambridge Vernier Potentiometer was also employed.

The high vacuum line consisted of a high-speed rotary pump (g in Fig. 8-A and B) and a mercury diffusion pump (f in Fig. 8-A and B) with a liquid nitrogen cold trap.

Pirani and Penning gauges were incorporated in the system near to the microbalance head, the vacuum pressures being measured on an Edwards control box.

General functioning of the microbalance system

Even when a balance is properly installed and operated, a considerable error in weight readings may still arise from 1) Zero point drift and 2) random noise:

Zero point drift

Zero stability depends primarily on the mechanical stability of the balance beam and its bearings. It is also dependent on the stability of the balance's Servo system (Cahn balance manual).

Mechanical instability could be due to: a) temperature differences between sample and counter-poise during heating experiments; b) the mounting and demounting of the sample on the balance; c) handling of the furnace; d) the rate of gas flow through the balance head; e) mechanical distur-

bances originating from the immediate environment of the balance.

Factors (a), (b) and (c) are inevitable, but their effects can be minimized by careful handling of the system.

Factor (d), the rate of the input gas flow, was optimised at approximately 30 $ml.min^{-1}$. This was found to be a satisfactory compromise in efforts to reduce both the thermal diffusion effect and the zero point drift of the balance.

The major mechanical disturbance (a) affecting the balance in the present experimental set up was due to vibrations transmitted from the rotary pump of the system. This problem was eliminated by connecting the all-glass microbalance system to the rotary pump by a high vacuum rubber tube.

The microbalance Servo stability was attained by following the instructions given in the Cahn balance manual -- i.e. the balance electronics were not switched off throughout the studies and the balance was operated close to the zero current condition of the coil.

Noise in the balance system

Random noise registered by the electrobalance recorder may stem from:

a) sample and suspension wire rubbing;

b) line voltage variations;

c) defective electronics in the system -- e.g. fluctuations and errors in the weighing mechanism, amplifier and recorder;

d) Stray light striking the phototube of the Cahn

balance weighing mechanism;

e) inaccurate control of the furnace temperature;

f) gaseous forces -- i.e. buoyancy forces, thermal convection, thermomolecular and aerodynamic effects ;

g) electrostatic forces.

In the present work, problems arising from (a), (b), (c) and (d) were checked and eliminated following the instructions given by Cahn balance manual.

Control of the heating furnace temperature (e) has been discussed above. The temperature fluctuations in all of the isothermal experiments were well inside $\pm$ 5°C.

The gaseous forces (f) and problems arising from turbulance in the hot gas around the sample were reduced to a minimum by operating the thermobalance at a constant 5 cm Hg gas pressure and using hang down tubes with narrow bores. To avoid a thermal convection effect, the micro-balance head was insulated by a 1" marinate case and cooled by cold air, blown from an electric fan. Problems of gaseous forces, to which all microbalances are subjected, have been studied theoretically as well as practically by many investigators (Czanderna, 1961; Boggs, 1961; Pierotti, 1967; Poulis et al, 1965; Evans and White, 1967; Steensland and Førland, 1966; Thomas and Poulis, 1963; Robens, 1971).

Accumulation of electro-static charge (g) on the surface of the hang-down tubes is a most serious problem occurring frequently during the experiments. This phenomenon leads to a random variation in the sample weight reading and, more often, to a complete interruption of the

experiments by attracting the sample and its hang-down wire to the tubes.

To eliminate the electrostatic charge, two methods have been suggested in the literature:

1) The precipitation of a (platinum or gold) conducting film on the internal surface of the tubes and earthing of the film (Cahn balance instruction manual; Evans and White, 1967).

2) Winding of earthed spirals of platinum wire or Kanthal wire around the heated parts of the hang-down tube (Sharp and Mortimer, 1968; Nimmo, 1971).

Method (1) was tested in the present study but was found to be unsatisfactory because platinum and gold films cracked at high temperatures (approx. 1000°C) into small segregated patches, each accumulating static charge locally. The induced charge then could not be removed and noticeably attracted the specimen and hang-down wire.

Method (2). Nimmo (1971) inserted an earthed and closely wound Kanthal wire between furnace and specimen tube but, after a heating/cooling cycle, he found that the spiral introduced stress and cracked the silica tube.

Evans and White (1967) suggested that static charge could be removed by platinum gauze (cyclinders) placed inside each hang-down tube and earthed through a tungsten wire seal. Their method could not be applied in the present study, since the platinum cylinder would be deformed during prolonged and frequent heating/cooling cycles. As a result, the free suspension of the sample would be obstructed. In addition, fixed platinum cylinders can accumulate dirt

causing nucleation of electrostatic charge.

In the present experiments, the following method was devised to remove electrostatic charge. The hang-down tubes were completely enclosed in fine mesh nichrome wire (gauge 32); gauze cylinders and the remaining upper parts of the hang-down tubes were wrapped with earthed Kanthal gauze. Satisfactory results were obtained and prolonged experiments could be carried out without serious electrostatic effects.

Description of one complete run of a microbalance experiment

After calibrating the microbalance (see Cahn balance manual), an amount of finely ground sample was pre-weighed (Stanton precision balance) directly into the platinum bucket. The bucket was hooked onto the suspension wire of the microbalance and the hang-down tube was replaced using Apiezon "T" grease as lubricant for the cone and socket junction.

Next, the microbalance system was evacuated via taps 15 and 19 using a rotary pump (g in Fig. 8-A). At approximately 10^{-3} torr pressure, the mercury diffusion pump (f in Fig. 8-A) was switched on. The sample was then heated at 100-150°C to degas and remove the adsorbed moisture (for the purification of B-, P- and N-Nb_2O_5 samples, see Chapter II, section 2.3.2.).

After obtaining a high vacuum (approximately 10^{-5} torr), taps 15, 16 and 19 were closed and the diffusion pump switched off. The gas buffer mixture (CO_2/CO or CO_2/H_2) with fixed composition (see above) was then admitted via the inlet tap 13-I (see Fig. 6). At 5 cm Hg pressure indicated

on a mercury manometer (h in Fig. 8-A), the inlet tap was closed and the "static" sample weight (i.e. in the absence of gas flow) recorded. The gas supply was again admitted by opening the inlet tap and Needle valve (12), and the exit Needle valve (18) was adjusted until the weight reading was identical to that under static gas conditions. The gas flow through the system then was maintained at these needle valve settings; the gas flow rates were estimated at approximately 30 $ml.min^{-1}$. The exit gas was pumped out by a rotary pump (g in Fig. 8-A) to the waste via a non-return oil gas bubbler (k in Fig. 8-A).

To start the reduction experiment, the furnace, pre-heated to a fixed isotherm, was raised around the specimen. Within several seconds, the specimen heated up to the working temperature and the reduction commenced.

At the end of the experiment, the furnace was lowered and the sample quenched to room temperature. The system was then ventilated through tap 17 and the sample was taken out for further structural investigations i.e. X-ray powder pattern, electron microscopy.

3.2.3. The Horizontal Quench Furnace System

Applications of conventional microbalance techniques for quantitative measurements of solid-gas reactions at high temperatures (i.e. $T > 1300^{o}C$) are seriously limited by fundamental design inadequacies (1 and 2 below) and other disturbances (3-5 below):

(1) Conventional furnace designs are based on methods of heating such as resistance, induction and electron bombardment.

The induction method has been widely used in microbalance operations requiring high temperatures, but the presence of strong electromagnetic fields in close proximity to the microbalance can lead to errors in measurements (Walker, 1961; Steinheil, 1972).

In resistance furnaces such as platinum, Kanthal super, silicon carbide, molybdenum or tungsten elements, temperatures of about 1500°C can be achieved. The construction and vertical operation of such furnaces is not practical and permits little flexibility in microbalance experiments.

(2) Specimen support and suspension wires usually consist of platinum which melts at temperatures above 1770°C.

(3) Microbalance disturbances -- i.e. zero position shift and a high noise level (see above).

(4) Thermal diffusion effect -- i.e. segregation of mixed gases when a sharp temperature gradient is present in the system (see above).

(5) A probable, irreproducable and not measurable, weight loss due to fractional vapour transport of the sample from hot to cold zones of the furnace. This phenomenon, which hitherto has not been considered in the literature, could well be significant at higher temperatures when gas is passed over the sample.

The above problems are inherent in high-temperature microbalance operations and impair the accuracy of measurements in spite of the high sensitivity of the microbalance. For this reason, the Horizontal Quench Furnace system was designed and constructed by the present author to investigate

the phase equilibria in the system Ti-Nb-O at 1400°C. The furnace was designed in order to equilibrate titanium-niobium oxides -- i.e. $TiNb_2O_7$; $Ti_2Nb_{10}O_{29}$ and $TiNb_{24}O_{62}$ -- with various compositions of CO_2/CO at 1400°C, and to quench the equilibrated samples rapidly in a vacuum environment by transferring the sample from a hot to a cold zone of the furnace. In the next stage, the oxide compositions could chemically be analysed by re-oxidation in air at a relatively moderate temperature (i.e. 1000 - 1100°C) using the Cahn microbalance system (see above).

The Horizontal Quench Furnace system, schematically drawn in Fig. 8-B, consisted of the following components: Furnace (m); working tube (l); mercury manometer (h); rotary pump (g); mercury diffusion pump (f); gas bubbler (k).

The main components i.e. the working tube and the furnace are described below:

The working tube (Fig. 10)

The tube, which was integral with the furnace, consisted of two parts: 1) the reaction chamber and 2) the quench mechanism.

(1) The Reaction Chamber (f in Fig. 10), a 50 cm long impervious mullite tube (Morganite Refractory Ltd.) with an internal diameter of 30 mm, was sealed at both ends (e and g) to Pyrex glass tubes of the same diameter. The mullite-glass junctions were cooled during heating operations by air blowing from two electric fans. The reactive gas -- i.e. CO_2/CO mixture was admitted via inlet tube (c). At the same end of the working tube, a Pt vs Pt-13% Rh thermo-

FIGURE 10

FIGURE 10

Schematic diagram of the working tube of the Horizontal Quench Furnace System (Section 2.3.2.). The different components are:

a) Thermocouple leads (molybdenum-pyrex seals)

b) a Pt vs Pt - 13% Rh thermocouple

c) gas inlet tube

d) alumina refractory bed

e) pyrex-mullite seal

f) reaction chamber (mullite tube)

g) pyrex-mullite seal

h) alumina boat

i) gas outlet tube

j) the draw wire

k) the piston

l) metallic springs

m) the draw cylinder

n) vacuum chamber

o) the cylinder holder (1 cm long polythene tube)

p) standard ball and socket arrangement for gas supply/vacuum connections.

HORIZONTAL QUENCH FURNACE

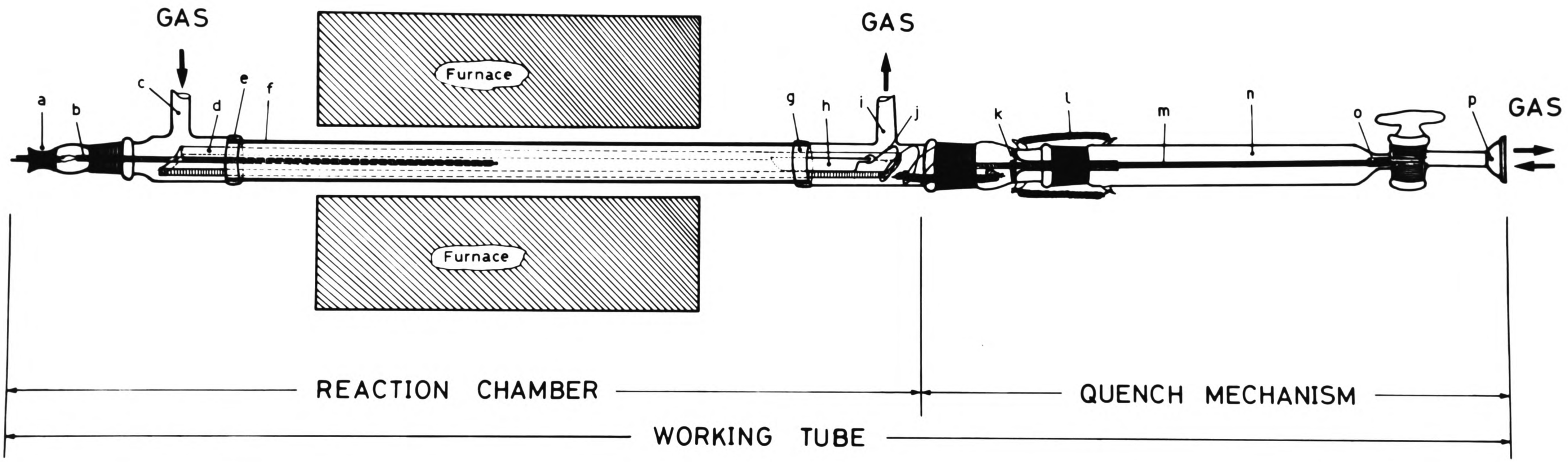

FIG. 10

couple (b) was incorporated in the reaction chamber to measure the sample temperatures. Thermocouple leads were brought out of the tube by means of molybdenum wire -- glass seals (a) arranged on a demountable cone and socket.

The reaction chamber was connected to both vacuum line and pressure control valve (i.e. Needle valve 23) via an outlet tube (i) and, at the same end, to the quench mechanism, via a further cone and socket.

To hold the specimen boat in the uniformly heated zone of the tube -- i.e. in the central axis of the heated part -- the lower half of the reaction chamber was furnished with an alumina refractory bed (d). The bed also provided a smooth gliding rail during specimen withdrawl and prevented a sudden thermal shock on the working tube during the quench process.

(2) The working of the quench mechanism was based on the pressure gradient imposed on the working tube at the end of the experiments. The mechanism consisted of three components: The piston (k); the draw cylinder (m) and the vacuum chamber (n).

Piston (k) was a Pyrex glass tube (inner diameter 3.5 mm; length 7 cm) oriented horizontally along the central axis of the working tube. The piston was attached 1) to the reaction chamber by a cone and socket arrangement and 2) with the vacuum chamber through another cone and socket connection.

The draw cylinder (m) was an alumina refractory rod (diameter 3 mm; length 31 cm) sliding freely through the piston and functioning as an arm to transfer the sample from the hot to the cold zone of the working tube. The rod

was linked to the sample container (an alumina refractory boat) by means of a 17 cm long platinum wire i.e. the draw wire (j). A 1 cm long polythene tube (o) was fitted around the free end of the piston in the vacuum chamber (below) to prevent the rod from shifting into the reaction chamber.

The vacuum chamber (n) was a Pyrex glass tube, functioning as a sheath to enclose the draw piston when the latter was in position for sample withdrawl. The tube was connected with the gas supply/vacuum line via a high vacuum tap and ball and socket arrangement (p).

The Furnace. An ordinary crusillite resistance furnace (30 cm long, 23 cm wide and 23 cm high) was used for prolonged operations at temperature up to 1400°C. The furnace, constructed of a ring of four silicon carbide elements held and insulated by Morgan M.I. 28 fire bricks, was housed in an aluminium case.

Power was supplied by a 10 amp. rotary Regvolt variable transformer. The furnace temperature was controlled and kept constant by an Ether Transitrol, type 991, temperature controller activated by a Pt vs Pt-13%Rh thermocouple located outside the working tube.

The EMFs generated from the sample thermocouple (b in Fig. 10) were fed to one pen of a Servoscribe potentiometric recorder with attenuated scales of 5, 10 and 50 mv. For accurate measurements, the signals could also be fed, via a switching board, to a Cambridge Vernier Potentiometer. The furnace had a uniform hot zone of approximately 10 cm. The temperature was recorded with an accuracy of $\pm$ 30°C.

Procedure of a complete run in the Horizontal Quench Furnace

A finely ground sample in a platinum container is placed in an alumina boat which is positioned in the hot, uniform, zone of the reaction chamber. The gas-tight quench mechanism is assembled using Appiezon "T" grease.

The system is evacuated, first via tap 21, keeping all other taps (i.e. 20, 22, and 24) closed to the gas supply and the vacuum line. At approximately 10^{-3} torr, taps 22, 24 and N 23 are also opened to the vacuum line. The mercury diffusion pump isswitched on.

After a high vacuum is obtained (approximately 10^{-5} torr), all taps to the vacuum line are closed. The diffusion pump isswitched off. A pre-set reducing gas mixture (see above) is admitted via tap 22, preventing displacement of the sample in the hot zone. At 1 atmosphere pressure indicated by a mercury manometer (h), tap 22 is closed and gas admission continued via tap 20. In the meantime, tap 24 is opened to the vacuum line and Needle valve 23 adjusted to permit an exist gas rate equal to the input rate. Exit gas is pumped (g) to the waste via a non-return valve (k).

At the attainment of equilibrium, the sample is quenched following a reverse procedure:

All taps connecting the system to the gas inlet and the vacuum line are closed. Next, the working tube is evacuated via tap 22. A sudden low pressure generated in the "vacuum chamber" (h in Fig. 10) sucks the draw cylinder into the vacuum chamber. As a result, the sample container is moved to the cold zone of the furnace where it cools down to room temperature attained by blowing cold air from

an electric fan. The quench rate is less than one minute. The furnace is ventilated via tap 20 and the sample is taken out for chemical analysis using the Cahn microbalance line.

Advantages of the Horizontal Quench Furnace System

From a practical point of view, the Horizontal Quench Furnace system offers the following advantages:

(1) The construction and maintenance of the system is less costly than that of the more complex designs of microweighing apparatus generally used for investigations of solid-gas systems at high temperatures.

(2) The system is simple to operate and versatile so that it can be used for various applications.

(3) The system can be designed in various capacities, allowing the preparation of different quantities of materials.

(4) A wide range of temperatures can readily be obtained by employing different kinds of heating furnaces -- e.g. resistance, conduction, etc. In addition, due to the horizontal operation of furnaces, high degree of precision can be obtained as far as sample temperature control is concerned.

(5) Certain experiments of long duration can satisfactorily be conducted in this unit. This is a definite advantage over microbalance experiments in which a short duration is essential in order to obtain a high degree of precision.

(6) The effect of thermal diffusion due to the horizontal flow of mixed gases -- i.e. CO_2/CO or CO_2/H_2 etc. -- in this system is reduced to a minimum. This, in combination, with the high precision of sample temperature measurements leads to a reliable atmosphere control.

(7) Rapid quenching of the samples in the vacuum environment minimizes undesirable effects of solid-gas contact during the cooling stage.

Suggestions for further improvements of the functioning of the Horizontal Quench Furnace System

(1) To obtain an increased rate of specimen quench, in the process of sample withdrawl from the hot zone, the cold zone of the furnace could be equipped with blades or shields (cooled by liquid nitrogen) mounted above and below the specimen.

(2) To minimize the effect of a small gas leak through the mullite tube at high temperatures, a double-walled construction of the reaction chamber -- i.e. the jacketing of the tube by an additional refractory tube -- is suggested here. The resulting intermediate chamber, in the process of the experiments, could then be evacuated.

Alternatively, an inert gas or an identical reactive gas might be circulated through the intermediate chamber to reduce the effect of the gas leak.

N.B. In the literature, a second design for a Horizontal quench mechanism has been described by Webster and Bright (1961) and Grey *et al.*, (1974).

CHAPTER IV

ELECTRON MICROSCOPY

In structural studies of crystalline materials, the application of conventional diffraction methods such as the X-ray technique provides only average statistical information covering a large number of unit cells and, ideally, is useful only in studies of perfectly ordered crystals. Real crystals however contain lattice defects which are coherently intergrown with the regular structure and are mainly due to:-

1) Intrinsic disorders i.e. thermodynamic equilibrium properties of solids, 2) Impurities and 3) Equilibrium disorders such as dislocations, micro-twins, frozen-in fluctuations etc. all of which are history-dependent. Such perturbations of the crystal structure are, at most, detectable in the X-ray diffraction patterns by the occurrence of diffuse reflections, extra lines or slight displacement of lines, or small intensity variations. It follows that the study of defects by X-ray diffraction may be ambiguous and can even lead to faulty conclusions (see Discussion, Chapter V, on the formation of M-Nb_2O_5).

Since their first application to structural studies of crystalline materials (Menter, 1956), electron diffraction and direct crystal lattice imaging have proven to be powerful techniques for dealing with the ultra-structure of materials and the unambiguous identification of the nature of their defects. The formation of crystal lattice images is basically due to the effect of the "phase contrast", arising at the level of the objective lens in the electron microscope from interference between the transmitted beam and Bragg scattered beam(s). Due to

aberrations in the objective lens, the number of beams contributing to the image has to be limited by the insertion of an objective aperture in the back focal plane. Details of phase contrast images have previously been described by Thon (1971).

Using the above technique, Menter (1956) obtained one-dimensional lattice images (formed by combination of a primary electron beam with second-order Bragg diffracted reflections from the specimen) from thin crystals of a copper and platinum phthalocyanine compound. The 12 Å periodicity of the lattice fringes was identified by Menter as corresponding to $(20\bar{1})$ planes of the crystal lattice; broken fringes were interpreted as dislocations. This method of lattice image analysis was also applied by several other investigators to studies of dislocation cores in metallic foils and other aspects of crystal chemistry (Phillips and Hugo, 1970; Parsons et al, 1970). Cockayne, Parsons and Hoelke (1971), however, on the basis of theoretical and experimental findings, discussed the validity of intuitive interpretations of lattice images which were showing bends and terminating fringes. These authors indicated that in the case of inclined screw dislocations and two-beam lattice images there was no direct one-to-one correlation between "lattice images" and the respective atomic planes.

In parallel to the above developments, electron diffraction and microscopy was applied in structural studies of some complex metal oxides, e.g. Nb-O; Ti-Nb-O; W-Nb-O systems (Allpress, Sanders and Wadsley, 1968, 1969; Allpress

and Wadsley, 1969; Allpress, 1969 a, b; Allpress, 1970; Allpress and Roth, 1970, 1971; Nimmo and Anderson, 1972). In these studies, images were recorded at a resolution limit of approximately 0.7 nm and the one-dimensional fringes were interpreted intuitively in terms of CS planes within the crystal structure of the oxide. Subsequent work on related compounds at a resolution of circa 0.5 nm (Hutchison and Anderson, 1972) and at a resolution of 0.35 nm (Iijima, 1971; 1973) confirmed that thin (< 100 Å) niobium oxide crystals approximate in their behaviour the phase object, provided that:

1) Images are recorded at the optimum de-focus in order to minimize the effect of instrumental aberrations (Scherzer, 1949).

2) The incident electron beam is parallel to the short 0.38 nm unit cell projection axis. According to Cowley and Iijima (1972), the crystal should be set within a 10^{-3} rad. of the exact orientation.

3) The number of Bragg diffracted beams contributing to the image contrast is selected carefully.

Lattice images obtained under these conditions represent an ideal projection of the charge density of the oxides. The distribution of charge density need not be periodic and it is possible to examine disorder materials and obtain information about their structure (Harburn, Taylor and Welberry, 1975).

A theoretical consideration of crystal lattice imaging has been given by Cowley and Moodie (1960), Grinton and Cowley (1971); Lynch and O'Keefe (1972); O'Keefe (1973),

Cowley and Iijima (1976), while recently a computer simulation of lattice images has been discussed by Skarnulis (1977); O'Keefe, Buseck and Iijima (1978).

As far as the classification of lattice images is concerned, Anderson and Hutchison (1975) in an electron optical study of the "long range order" in hexagonal barium ferrite layer structures discussed the effect of the crystallographic orientation of a specimen with respect to the incident electron beam. They classified crystal lattice images into two distinct categories:

1) The one-dimensional "systematic" orientation and
2) The two-dimension "zone-axis" setting.

In the systematic orientation, one-dimensional fringes are formed due to interference between the direct (undeviated) beam and at least one diffracted beam. The crystal is oriented in such a way that only one main row of reciprocal lattice reflections i.e. the (h00), (0k0) or (00l) sections are present. If the object is periodic, one might expect from the Abbe theory that in this method of imaging the image has the same periodicity as the object, hence, crystal lattice planes can be resolved.

In the zone-axis setting, the specimen is oriented in such a way that the incident electron beam of the microscope is parallel to a particular crystallographic direction - i.e. [u v w], giving rise to a diffraction pattern which leads to a two-dimensional lattice image in the microscopy mode. For the imaging of crystalline materials in the two-dimensional zone-axis setting, a specific

orientation retaining perfect order along the direction of the beam is required (Anderson, 1977). Complex binary and ternary oxides derived from niobium pentoxide are known to suit lattice imaging along the [010] crystallographic direction -- i.e. the b-axis of the crystals. These oxides, derived from an ReO_3 parent structure, have "blocks" or "columns" within their structures (Wadsley and Anderson, 1970), the nature of which is discussed below:

Basic structural groups -- i.e. (NbO_6) are linked through all their apices into three-dimensional open lattices. A subtle change of stoichiometry is achieved, while retaining a high degree of local order, by octahedra sharing edges along regular crystallographic shear (CS) planes in two orthogonal directions -- i.e. $(100)_R$ and $(010)_R$ planes. The CS planes demarcate columns of the ReO_3-type structure into an assembly of rectangular "columns" or "blocks" which extend along the [010] zone-axis. The blocks are (m x n) octahedra in cross section and have individual dimensions of octahedron diagonal ($\sim$ 0.4 nm) multiples. For example, in the H-Nb_2O_5 structure, blocks of (4 x 3) octahedra have dimensions of 12 x 8 Å and blocks of (5 x 3) measure 16 x 8 Å. A lattice image along the [010] zone-axis at a resolution limit of circa 0.3 nm can delineate individual "blocks" or "columns" and their internal details. A typical example is given in Plate 3-A which shows a two-dimensional lattice image of the compound H-Nb_2O_5 ($Nb_{28}O_{70}$). The image contains clearly outlined columns of the ReO_3-type structure with $(4 \times 3)_1$ and $(5 \times 3)_\infty$ octahedra in cross-section. Individual (NbO_6) octahedron

PLATE 3

PLATE 3

A) High resolution two-dimensional lattice image of a single crystal of H-Nb_2O_5 showing a structure of $[(4x3)_1 + (5x3)_\infty]$ blocks. The unit cell having a composition of $Nb_{28}O_{70}$ is outlined. Along (↑ T) WADSLEY DEFECTS are shown: A coherent intergrowth of 1:2 unit cell wide $(4x3)_2$ blocks of the neighbouring phase -- i.e. $Nb_{25}O_{62}$ -- into the host lattice. Wadsley defects represent a slight deviation from the ideal stoichiometry ($NbO_{2.500}$).

B) Idealized structure of H-Nb_2O_5 on the [010] projection. The darker and lighter squares represent octahedra of NbO_6, which form blocks of $(5x3)_\infty$ and (4x3) respectively. To the left in the model, a simplified representation of the rectangular blocks is given in which the unit cell in projection is outlined (a = 21.6 Å, b = 3.822 Å, c = 19.35 Å; $\beta = 119^\circ 50'$)

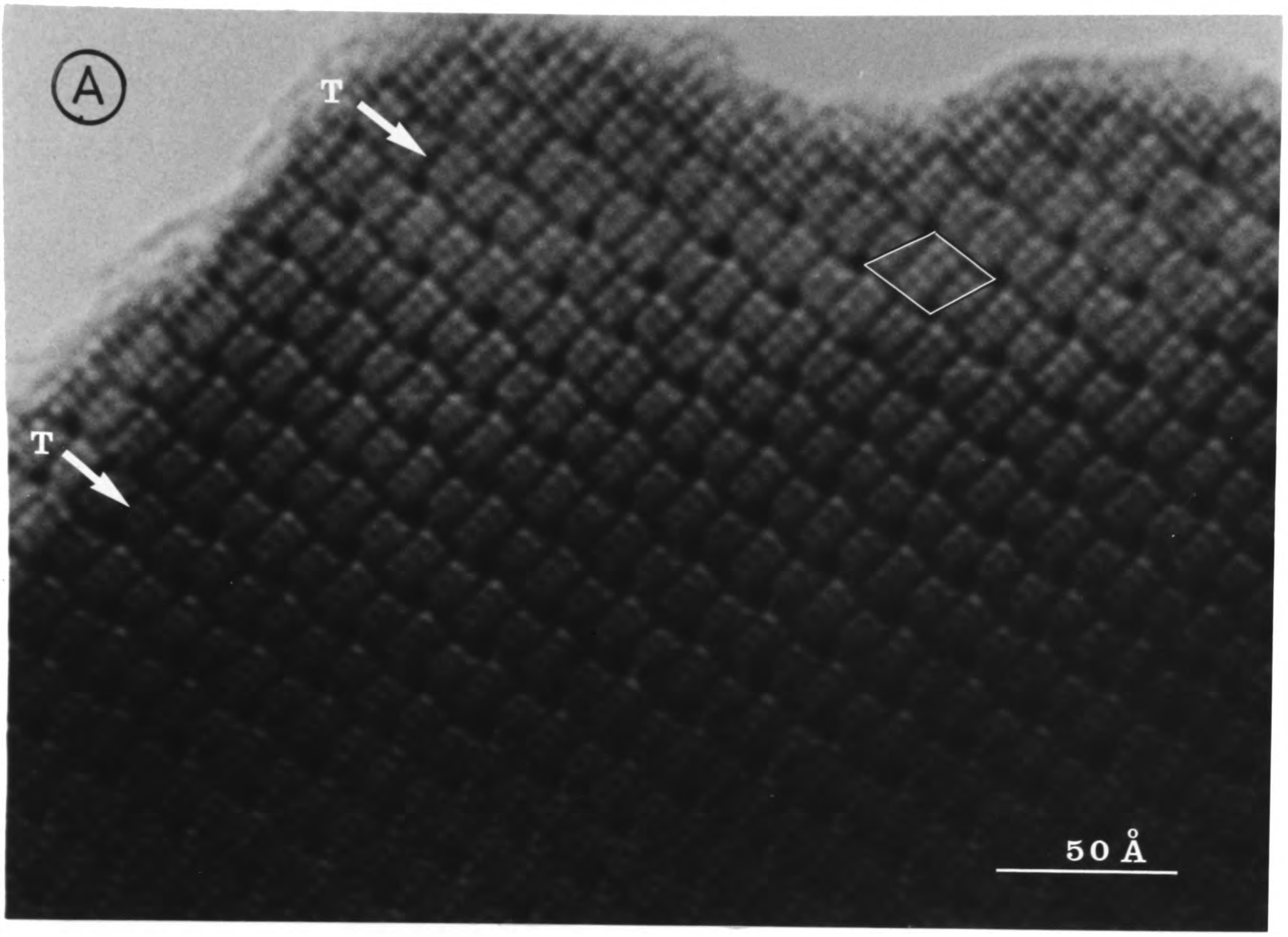

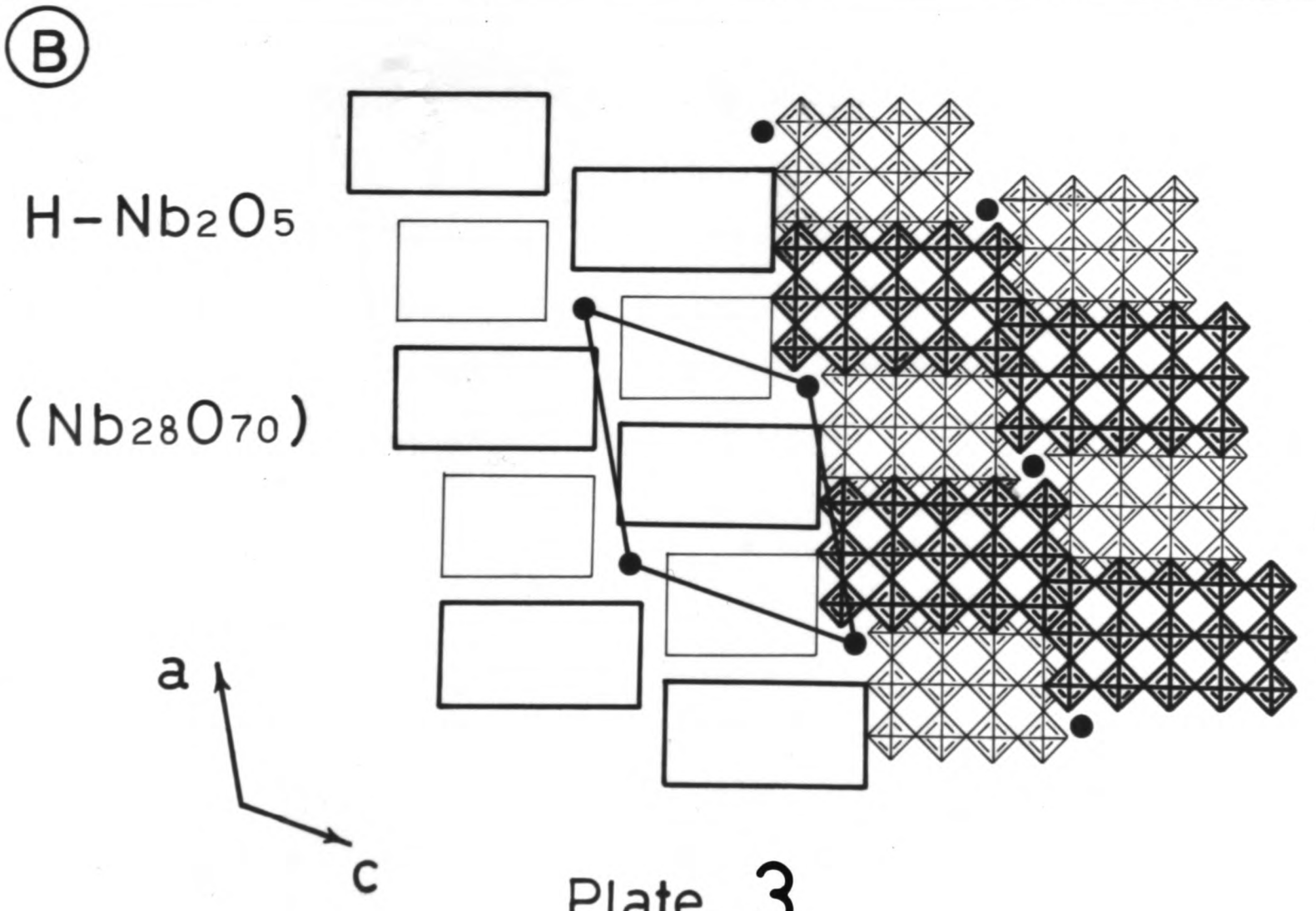

Plate 3

positions within each block (~ 0.4 nm apart) are clearly resolved and appear as dark-contrast dots. The empty square channels, 0.28 nm wide, between corner sharing (NbO_6) octahedra are imaged as white dots. At the interface between blocks where the octahedral groups overlap in projection (i.e. cations are about 0.2 nm apart) elongated dark lines are shown. Metal atoms are not resolved here. while the channels of tetrahedral sites appear as uniform, symmetrical, dark-contrast areas.

According to Iijima and Allpress (1974), the image contrast at the tetrahedral sites is sensitive to small changes in focus, to crystal thickness and to orientation. The image intensity at the tetrahedral positions is also affected by the number of contributing beams (O'Keefe, 1973).

The image further shows that along ↑T, columns of different structure have intergrown coherently with the matrix ($Nb_{28}O_{70}$). The impurity phase, which can be seen to contain $(4 \times 3)_2$ columns, is in fact a structural element of the compound $Nb_{25}O_{62}$. The implication is that the total anion/ cation ratio in this crystal fragment is less than 2.5 (i.e. $O/Nb < 28/70$) and that the small stoichiometric deviation has been adjusted in the form of planar defects. This effect cannot be detected by X-ray diffraction whereas the electron microscope reveals the local inhomogeneity.

In Plate 3-B, an <u>idealized model</u> of the H-Nb_2O_5 ($Nb_{28}O_{70}$) structure is given. In the model, ribbons of $(5 \times 3)_\infty$ at one level are combined with columns of $(4 \times 3)_1$ at the second level. The structure may be symbolized as $(5 \times 3)_\infty + (4 \times 3)_1$. The short-hand convention, introduced

by Allpress, Sanders and Wadsley (1969) is represented by rectangles which join the cation sites in the face of each column. Different thicknesses of lines in the diagram show the different levels (i.e. Z = 0 or Z = $\frac{1}{2}$b) of the respective cations. This method of structural representation has been employed in many diagrams in this thesis.

For ultrastructural work presented in this thesis, the electron microscope technique was employed -- at its resolution limit (circa 0.3 nm) -- to elucidate the mechanism by which oxides in the Nb-O and Ti-Nb-O systems are reduced under controlled oxygen potentials and high temperatures. The basic principles of the electron microscope technique concerning the design of the optical system, the diffraction geometry and the mechanism of image formation (i.e. contrast, focus etc.) have been discussed in several outstanding handbooks (see Hirsch et al, 1965; Glauert, 1972, 1974; Wenk, 1976) and need not be further explained here.

Below, the experimental conditions under which the reduced oxides were examined by electron microscopy are outlined:-

Specimens for electron microscopy were prepared by suspending fine crystals in chloroform by ultrasonic vibrations. A small drop, containing the dispersed crystals, was placed on a holey carbon supporting film on a copper grid and dried at room temperature.

The specimens were examined in a Siemens Elmiskop 102, operating at an accelerating voltage of 100 kV and equipped with a $\pm$ 45° double-tilt goniometer stage and a

mechanism for Z-axis adjustment.

Thin crystal fragments projecting over a hole in the supporting film were chosen and aligned with the goniometer stage to give a symmetrical (h0l) reciprocal lattice section. All beams up to about 3.3 nm^{-1} (i.e. corresponding to interplanar spacings down to about 0.3 nm) were included in the formation of the lattice images. Other beams were eliminated by using an objective aperture, diameter 40 μ.

CHAPTER V

THERMODYNAMICS AND STRUCTURAL ASPECTS OF B-Nb_2O_5 REDUCTION

PART A) Phase transformation of B-Nb_2O_5 into block-type structures

PART B) Phase equilibria in the system NbO_2-(B-Nb_2O_5)

5.1.

PART A: PHASE TRANSFORMATION OF B-Nb_2O_5 INTO BLOCK-TYPE STRUCTURES

5.1.1. INTRODUCTION

According to Schäfer et al (1966), B-Nb_2O_5 transforms endothermically above 900°C into the high temperature stable modification H-Nb_2O_5. They also point out that the rate of transformation is governed by several factors including environmental conditions, sample history and the presence of product nuclei. Detailed investigations on the relative stabilities of several Nb_2O_5 modifications have shown that H-Nb_2O_5 is the stable form above 760°C (Kodama et al., 1972). Recently, however, Yamawaki et al. (1974), in an oxidation study of Nb - 2.5 at % Mo alloy, reported that X-ray powder patterns taken from the surface of specimens oxidized for various lengths of time (3 - 2370 min.) at 835°C showed the following sequence of phase transformations: T-Nb_2O_5 formed initially, then transformed to B-Nb_2O_5 and subsequently changed to M-Nb_2O_5. They also investigated the effect of different temperatures on such transformation and found that within a temperature range of 735° - 985°, B-Nb_2O_5 is not a stable intermediate phase. Yamawaki et al. (1974), in addition, studied structural changes as a function of sample depth of the oxidized alloy at 835°C and found that the allotropic transformation of polymorphs of Nb_2O_5 is affected by the distance from the surface. In particular, the B- to M-Nb_2O_5 conversion appeared to proceed much faster below the surface, than in the outer part of the specimen.

Differences exist in the B-Nb_2O_5 preparation methods carried out by different investigators. Chemical vapour

transport technique and oxidation of NbO_2 in air at low temperature ~ 817°C were used by Schäfer et al (1966 and 1964, respectively), isothermal decomposition of Nb_3O_7Cl was adopted by Kodama et al (1972) and oxidation of Nb - 2.5 at % Mo alloy was used by Yamawaki et al (1974). In the present study, we have employed the vapour transport technique (see Chapter II).

Conflicting results on the stability range of the B-Nb_2O_5 structure have been reported by different investigators. For these reasons, the present study initially concentrated on a detailed investigation of the B-Nb_2O_5 phase transformation to block based structures. This was carried out by varying both the temperature and the oxygen partial pressure. Specific objectives of the study were:

a) To establish an optimum temperature for the reduction of B-Nb_2O_5 under controlled oxygen pressure generated from CO_2-CO or CO_2-H_2 gas mixtures.

b) To investigate the possible catalytic effect of nuclei of reduced B-Nb_2O_5 on the transformation of unreduced B- to block type structures.

5.1.2. MATERIALS AND METHODS

The B-Nb_2O_5 single crystals used in the present study were prepared by the chemical vapour transport technique (Chapter II) and were finely ground to powders in an agate mortar. Powder specimens afford a larger solid - gas interface for reduction experiments.

The platinum black powder which was used in a later part of the study was prepared by hydrogenation of pure platinum oxide, $PtO_2 . xH_2O$ (Johnson Matthey Chemicals Ltd.), in methanol.

Isothermal - isobaric reduction processes were carried out using the Cahn RG4 microbalance reduction line and also a horizontal quench furnace reduction line (Chapter III). The structures of materials obtained from the thermogravimetric experiments were studied by X-ray powder diffraction using a Guinier-Hägg focussing camera and Cuk α radiation. ThO_2, a_o = 5.600 (N.B.S. 1953) was used as an internal calibrant for the purpose of phase analysis. Selected area electron diffraction, and high resolution electron microscopy were also used as sensitive means of structural investigation (Chapter IV).

The results of the experiments (below) are presented in the order of descending temperature (i.e., at Isotherms of a) 950°C, b) 900°C, c) 880°C, d) 850°C and e) 750°C). After investigating the stability of B-Nb_2O_5 under oxidizing conditions (in air) at a selected isotherm, the isothermal - isobaric reductions were carried out in those cases where the structure of the starting material was found to be unchanged.

5.1.3. RESULTS

5.1.3.1. Thermodynamics:

a) Isotherm 950°C

A few milligrams B-Nb_2O_5 crystals were heated for 1 hour in a platinum boat at 950°C under atmospheric conditions.

TABLE 6

TABLE 6

Isotherm 900°C

Exp. no.	X-ray pattern Plate 4-A	$\frac{p_{CO_2}}{p_{H_2}}$	Duration of Exp.	p_{O_2}	Comment on the X-ray diffraction pattern
1	b	0.21	6 hr.	7.87×10^{-18}	Generated phases (weak and diffuse diffraction pattern) + predominantly B-Nb_2O_5
2	c	0.18	10 hr.	5.69×10^{-18}	Increase in intensity of the generated phase (sharp and diffuse lines) + predominantly B-Nb_2O_5
3	d	0.14	25 hr.	3.37×10^{-18}	Medium intensity of generated phases (sharp and diffuse pattern) + medium intensity of B-Nb_2O_5 lines
4	e	0.11	6 hr.	2.05×10^{-18}	Predominantly generated phases (sharp and diffuse pattern) + B-Nb_2O_5 pattern
5	f	0.09	12 hr.	1.68×10^{-18}	Predominantly generated phases, having both sharp and diffuse lines

The X-ray powder pattern of the product was diffuse, but suggested a change of the starting material to a block type structure. The very diffuse part of the X-ray pattern around 11.8° - 16.6° probably reflected the presence of extensively disordered H-Nb_2O_5. Since B-Nb_2O_5 is clearly unstable at this temperature, further studies were concentrated on lower temperatures.

b) Isotherm 900°C

The B-Nb_2O_5 crystals were heated for ten hours in a platinum container in air. X-ray diffraction patterns showed only lines of B-Nb_2O_5, indicating that under these conditions no phase transformation takes place. On the basis of this result, several preliminary qualitative isothermal - isobaric reduction experiments were carried out. CO_2-CO gas mixtures were used for the generation of the required oxygen pressures and the experiments were conducted in the high temperature reduction furnace. Thus, no quantitative measurements of weight loss could be recorded.

A summary of the results is given in Table 6. In Plate 4-A the Guinier X-ray pattern of the starting material B-Nb_2O_5 (indicated by a) is compared with the diffraction patterns of quenched samples from the experiments 1, 2, 3, 4 and 5 (labelled b, c, d, e and f, respectively). The results at 900°C and CO_2/H_2 = 0.21 show that a small fraction of B-Nb_2O_5 has undergone a phase change, most likely, to a block-type structure which co-exists with the starting material. Further reductions of the CO_2/H_2 ratio to 0.11 appeared to have a pronounced effect on the transformation

TABLE 7

TABLE 7

Guinier X-ray diffraction pattern analysis of transformed-reduced B-Nb_2O_5 at isotherm 900°C and $p_{O_2} = 5.69 \times 10^{-18}$ (Exp. 2, Table 6; Guinier pattern c, Plate 4-A)

I (obs.)	d(Cm)	$Sin^2\ \theta$ (obs.)	$Sin^2\ \theta$ (calc.) B-Nb_2O	hkl (B-Nb_2O_5)	$Sin^2\ \theta$ (calc.) H-Nb_2O_5	hkl (H-Nb_2O_5)
m	1.15	0.005157	———	———	0.005192	$20\bar{1}$
m	2.01	0.15699	0.01585	002	———	——
w	2.41	0.022517	———	——	0.02241	$40\bar{1}$
s	3.30	0.041939	———	——	0.041824	$40\bar{5}$
v.s.	3.41	0.044739	0.04475	$\bar{1}11$	0.0444619	$10\bar{5}$
s	3.47	0.046302	———	——	0.04663	111
s	3.55	0.048426	———	——	0.04851	$21\bar{2}$
w	3.70	0.052530	———	——	0.05264	005
s	4.77	0.054499	0.05463	111	0.05524 0.05392	$21\bar{3}$ 211
s	4.07	0.063323	0.06339	004	0.06184	$41\bar{2}$
s	4.18	0.066713	0.06657	$\bar{1}13$	0.06603	$\bar{1}06$
m	4.41	0.074065	———	——	0.07420	$70\bar{1}$
m	4.57	0.079387	0.07916	$\bar{2}02$	———	——
w	4.61	0.080744	———	——	0.08092	$21\bar{5}$
s	4.68	0.083144	0.08308	200	0.08336	$20\bar{7}$

of the starting material. The X-ray diffraction patterns c, d and e show a gradual increase in the intensity due to new phases and a decrease in the B-Nb_2O_5 intensities. This phenomenon could not be attributed to an unaccomplished reduction process since a prolonged experiment under identical conditions gave the same results (experiment 3 in Table 6 and X-ray diffraction pattern d in Plate 4-A).

At $CO_2/H_2 < 0.11$, the entire B-Nb_2O_5 sample underwent a complete phase change and became dark blue in colour; the relevant X-ray powder pattern did no longer show the B-Nb_2O_5 lines.

An entirely satisfactorily analysis of the X-ray diffraction patterns, taken from the above samples, could not be carried out as the transformed phase(s), unusually, gave rise to both sharp and diffuse lines. The sharp lines correspond to sub-stoichiometric H-Nb_2O_5; electron microscopy of a sample reduced at $p_{O_2} = 5.3008 \times 10^{-20}$ (see isotherm 850°C) suggested that the diffuse lines are due to the presence of heavily disordered block structures. In the X-ray diffraction pattern c in Plate 4-A the sharp lines can be indexed on the basis of literature data for B-Nb_2O_5 (Laves et al, 1964) and H-Nb_2O_5 (Holtzberg et al, 1957); the results are presented in Table 7.

The above experiment was repeated at 880°C and under controlled oxygen pressure generated by a CO_2-CO gas mixture. The Cahn RG4 microbalance reduction line was used in order to obtain quantitative data of the reduction process.

PLATE 4

PLATE 4

Guinier photographs (Cu-kα_1 radiation) showing the pathway of phase transformation of B-Nb_2O_5 into block-type structures (Section 5.1.3.1.).

A) X-ray powder diffraction patterns of the starting material B-Nb_2O_5 (a) and of transformed-reduced B-Nb_2O_5 (b-f) at isotherm 900°C and p_{O_2} = 7.87×10^{-18} - 1.68×10^{-18} (referred to in Table 6).

B) X-ray powder diffraction patterns of the starting material B-Nb_2O_5 (a) and of transformed-reduced B-Nb_2O_5 (b-e) at isotherm 880°C and p_{O_2} = 5.98×10^{-16} - 2.10×10^{-18} (referred to in Table 8).

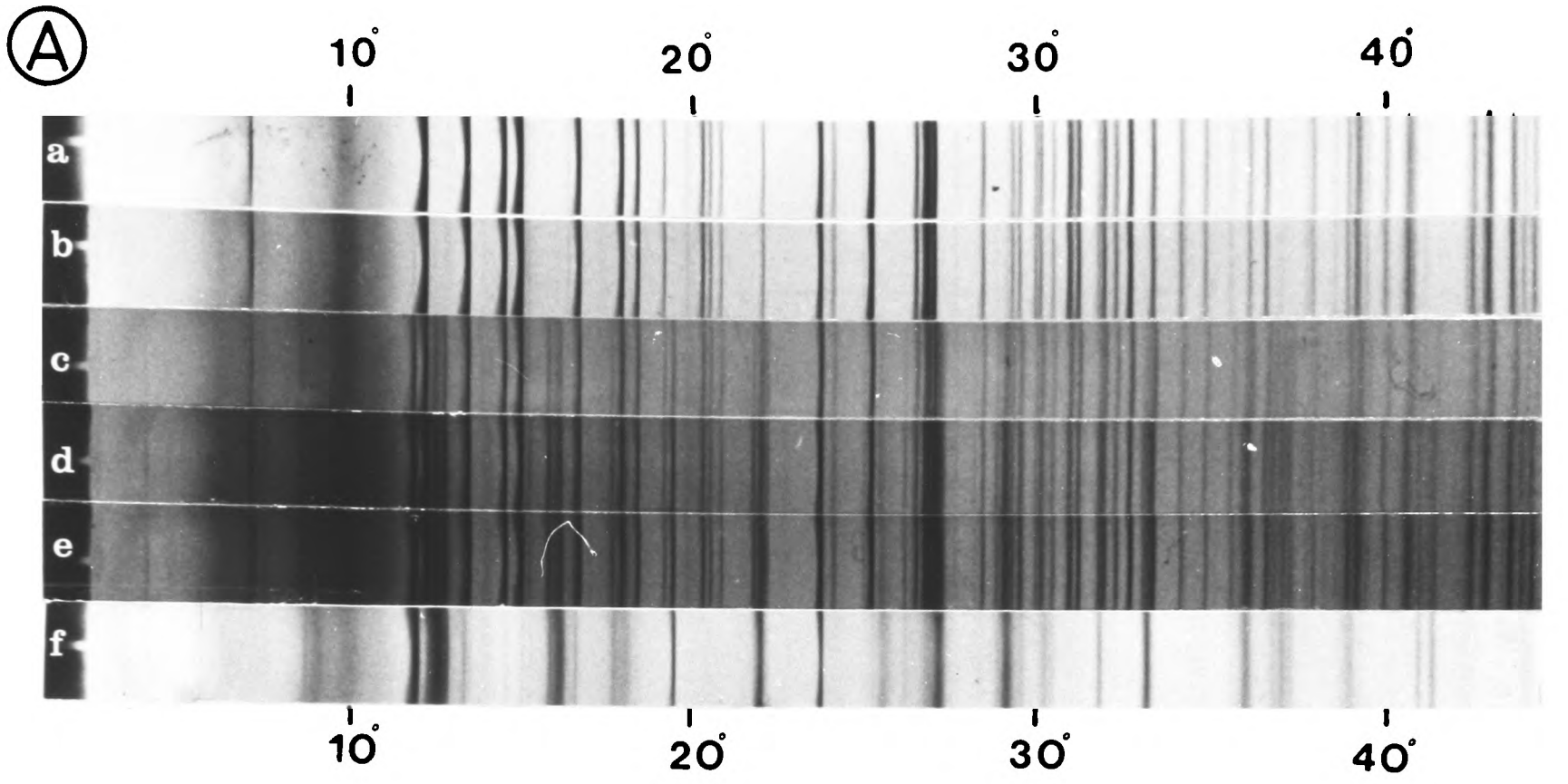

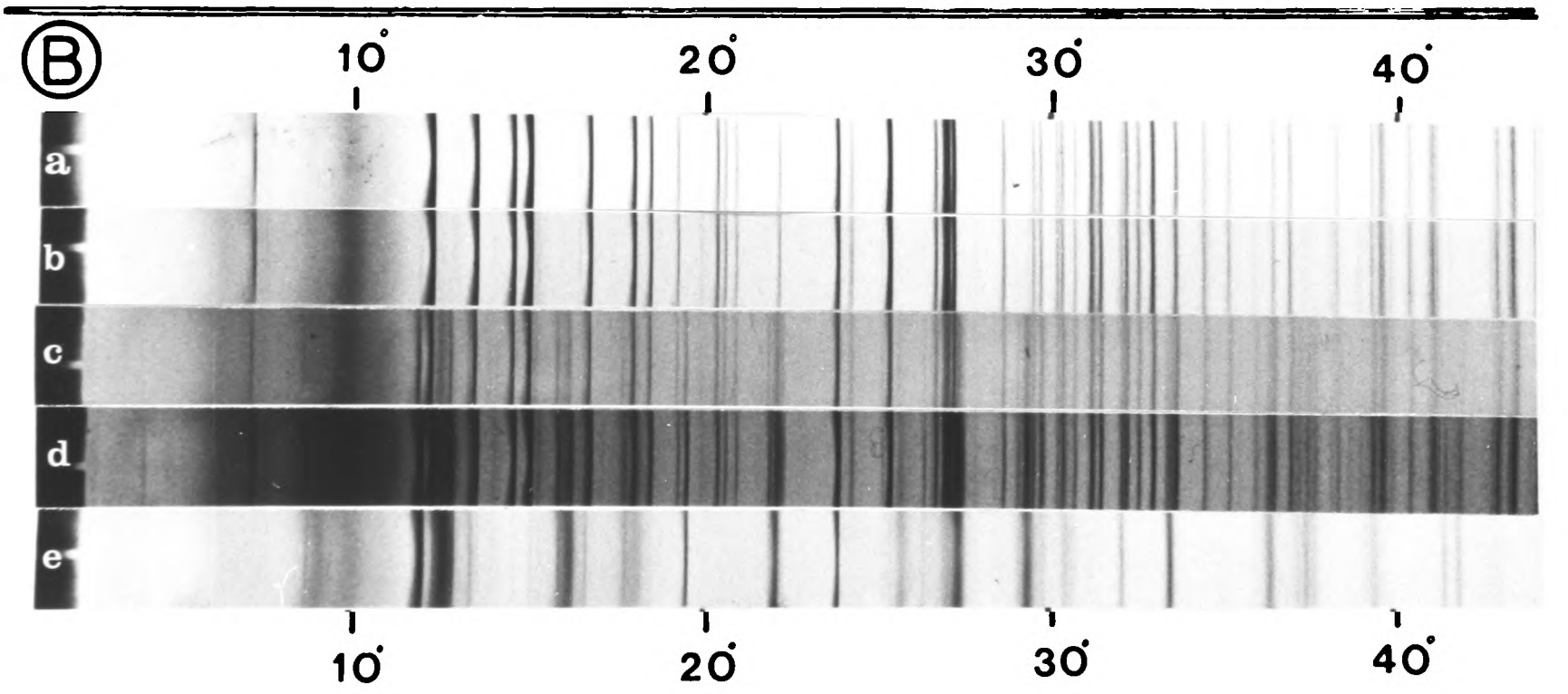

Plate 4

TABLE 8

TABLE 8

Isotherm 880°C

Exp. no.	X-ray pattern Plate 4-A	Duration of Exp.	$\frac{p_{CO_2}}{p_{CO}}$	p_{O_2}	Comment on the X-ray diffraction pattern
1	b	4 hr.	1.35	5.98×10^{-16}	Generated phases (weak and diffuse pattern) + predominantly B-Nb_2O_5 lines
2	c	16 hr.	0.61	1.22×10^{-16}	Increase in intensity of generated phases (sharp and diffuse lines) + B-Nb_2O_5 pattern
3	d	11 hr.	0.31	3.15×10^{-17}	Further increase in intensity of generated phases (sharp and diffuse pattern) + B-Nb_2O_5 lines
4	-	26 hr.	0.166	9.04×10^{-18}	X-ray diffraction pattern similar to that of d (exp. 3)
5	e	48 hr.	0.08	2.10×10^{-18}	Predominantly the transformed phases + trace of B-Nb_2O_5

c) Isotherm 880°C

This experiment was designed to investigate structural changes of about 50 mg B-Nb_2O_5 sample in the process of reduction. Oxygen partial pressures were altered stepwise from high to low. After establishing a solid-gas equilibrium condition at each isobar step and, before introducing the next oxygen partial pressure to the system, the experiment was interrupted and a small quantity of the sample removed. Care was taken to ensure that the remainder of the sample in the platinum bucket was not disturbed. Each fraction of the sample was examined by X-ray powder diffraction. The results are given in Table 8, while the relevant X-ray diffraction photographs are shown in Plate (4-B).

At CO_2/CO = 1.35 (exp. 1 Table 8), weight loss commenced with a parabolic curve and ended with a level plateau. Reduction proceeded with a weight loss of 10 μgr/hr during the first 5 hours and gradually slowed down until a constant weight was reached. The weight remained stable on this plateau for a further 12 hours and then the experiment was interrupted. Visual inspection of the product showed that the reduction had nucleated where the sample was in contact with the platinum bucket. A distinct thin coat of the dark blue reduced material could easily be distinguished from the grey-white unreduced upper part of the sample. An X-ray powder pattern of the sample, containing both reduced and unreduced parts showed a very faint and diffuse pattern similar to that obtained at 900°C but consisting predominantly of a B-Nb_2O_5 pattern (X-ray diffraction pattern b in Plate 4-B).

When the gas mixture was altered to $CO_2/CO = 0.61$ (exp. 2, Table 8), the microbalance detected an additional weight loss which progressed at a rate of 5 μgm/hr, for a period of 4 hours, then declined to a rate of 4 μgm/hr for another 2 hours and eventually curtailed to a rate of 1.5 μgm/hr. After 5 hours reduction at the latter rate, the experiment was interrupted and the appearance of the sample in the platinum bucket again examined. Both the reduced and unreduced regions, which were distinctly different in colour, could still be distinguished. The layer of the sample in contact with the platinum was now darker blue in colour and the upper part representing the untransformed B-Nb_2O_5 had remained grey-white. Therefore, the weight loss detected during the experiment could be attributed to a further reduction of the lower layer of the sample.

Continuation of the experiment at $CO_2/CO = 0.31$ (exp. 3, Table 8), was accompanied by a further weight loss. The kinetics of the reduction and appearance of the product in the platinum bucket (after simulating an equilibrium condition) in general were similar to the results of experiments 1 and 2. However, the thickness of the dark blue bottom layer was found to be increased, indicating an extension of the reduction of B-Nb_2O_5 further into the bulk. However, an unreduced layer of B-Nb_2O_5 still covered the upper surface part of the product. The X-ray diffraction pattern of a sample comprising the two regions showed the presence of the two phases, B-Nb_2O_5 and the transformed structure. The intensity of the X-ray lines due to reduced phases was greater than before.

Reduction of the sample at a lower oxygen pressure (exp. 4, Table 8) provided similar results as in experiments 1-3. However, a substantial decrease of the remaining B-Nb_2O_5 in the sample could be detected in the X-ray diffraction pattern, indicating a further conversion of B-Nb_2O_5 to block-based structure(s).

When the gas ratio was finally changed to CO_2/CO = 0.08, the microbalance detected a further weight loss. Gross study of the appearance of the sample after reaching an apparent equilibrium state showed that, though a substantial conversion of the starting material to a product had taken place, a very thin coat of white B-Nb_2O_5 could still be seen on the outer part of the sample. An X-ray diffraction pattern of this product revealed that a drastic phase change of the sample had occurred and only a trace of the B-Nb_2O_5 could be detected (X-ray diffraction pattern e, Plate 4-B). This pattern is strikingly similar to the one obtained under the most reducing conditions at 900°C (f in Plate 4-A).

As the transformed phases (exp. 1-5, Table 8) constituted only a fraction of the total sample, the metal-oxygen ratio of these phases could not be accurately determined by thermogravimetric measurements. Moreover, the frequent interruption of the experiments by sample taking for X-ray studies altered the original sample weight and disturbed the microbalance condition. For this reason, a separate thermogravimetric experiment, under the same reducing conditions as applied in experiment 5 (Table 8), was carried out. After attaining an equilibrium condition, the average composition of the product was found to be

$NbO_{2.4580}$. The X-ray powder pattern of this material was identical to that found in experiment 5, Table 8, (X-ray pattern e, Plate 4-B).

From the above observations it is clear that, under a reducing condition, the platinum surface of the sample container has a distinct effect on the acceleration of B-Nb_2O_5 phase transformation and reduction into block-type structures, whereas examination of the upper part of the sample showed that below 900°C, the structure of B-Nb_2O_5 is stable at $p_{O_2} > \sim 10^{-18}$ (Tables 6 and 8). This finding instigated an additional experiment to find the minimum temperature for the catalytic effect of the platinum surface; below this temperature we may then examine the equilibrium in the absence of catalysis.

d and e) <u>The catalytic effect of platinum at isotherms 750° and 850°C</u>

Approximately 25 mg of B-Nb_2O_5, contained in the platinum bucket, was loaded onto the microbalance. After eliminating the sample moisture and other impurities according to the method described in Chapter II, the reduction line was introduced to a constant CO_2/CO ratio of 0.16. The temperature was then varied stepwise from 750° to 850°C. At every isobaric step, the sample was equilibrated for several hours in order to detect any weight change. At 750°C ($p_{O_2} = 1.10 \times 10^{-22}$), after standing for 3 hours, the microbalance showed no weight loss, indicating that no phase change from B-Nb_2O_5 to block structures had taken place. This conclusion was confirmed by the X-ray

powder diffraction pattern which contained only B-Nb_2O_5 lines.

When the temperature was raised to 850°C (p_{O_2} = 5.30×10^{-20}), a distinct weight loss was detected which continued for 29 hours. The parabolic to level plateau feature of the sample reduction could be analysed into three different weight loss rates: Reduction started with an average rate of 8 μg/hr which continued for 2 hours, gradually declined to a rate of 4 μg/hr for 6 hours and eventually after 14 hours reduction at a rate of 2 μg/hr, the microbalance recorded a level plateau stage, indicating an apparent equilibrium state. After interrupting the experiment, the appearance of the product in the platinum bucket was examined and found to be similar to that of experiment 4 (Table 8). The average composition of the product (i.e. reduced and unreduced B-Nb_2O_5) from the microbalance was measured to be $NbO_{2.4647}$. The X-ray powder pattern of a sample part, comprising both reduced and unreduced materials, was found to be identical to pattern e in Plate 4-B. The product of this experiment was also studied by high resolution electron microscopy, the results of which are discussed in Section 5.1.3.2.

Effect of platinum black powder on the phase transformation of B-Nb_2O_5

The effect of the platinum surface on the transformation of B-Nb_2O_5 to block based structures was thought to be due to a catalytic action of platinum on the reduction reactions of niobium oxides. To confirm this idea, as well

as to elucidate the effect of environmental conditions such as oxidizing and reducing atmospheres on the observed phenomenon, the following experiment was carried out:

Approximately 5 mg of platinum black powder was thoroughly mixed with 20 mg B-Nb_2O_5. This sample, in the platinum bucket, was loaded onto the microbalance and subjected, in air, to 850°C for 5 hours. The X-ray powder pattern of the product, besides platinum + B-Nb_2O_5, showed no extra lines indicative of the existence of impurity phases.

Under reducing conditions, generated by a CO_2-CO gas mixture (CO_2/CO = 0.1, T = 850°C), the microbalance recorded a weight loss of the sample at a rate of 20 μgm/hr for 5 hours. Thereafter, it declined to a very slow weight loss and the experiment was interrupted and the structure of the product examined. A Guinier X-ray diffraction pattern of a sample fraction, containing the bottom part and upper layer, showed a weak and diffuse pattern in the background of predominantly sharp Pt + B-Nb_2O_5 lines. This observation which was consistent with results of experiments described in Tables 6 and 8, suggested that the surface of the platinum bucket might consist of a coat of activated platinum responsible for the catalytic action. As the platinum bucket, for several years, had been in continuous use for niobium oxide experiments, I assumed that the action of its surface was due to the formation of a coat of Pt-Nb-O ternary compounds [i.e. platinum (IV) hypothetically occupies an octahedral co-ordination in the niobium block-based structures and any compound formed as a result of the

platinum occupancy is likely to be an analogue of the Ti-Nb-oxides]. This coat could not be removed by the ordinary cleaning method applied in the present study. The above suggestion was further investigated in a thermo-gravimetric experiment in which the reactivity of platinum with Nb_2O_5 was examined.

A through mixture of platinum black powder and Nb_2O_5, with a stoichiometric ratio of 2/5 moles (equation 1 and 2 below) was pelleted and heated in air at 800°C in a silica crucible. After 40 days continuous heating, the sample was quenched and its weight measured by a precision balance.

$$2\,(Pt + O_2 = PtO_2) \qquad (1)$$

$$2PtO_2 + 5\,Nb_2O_5 = Pt_2Nb_{10}O_{29} \qquad (2)$$

Comparison of the initial and final weight of the sample revealed that no weight increase had taken place. Oxygen, thus, had not been taken up and the hypothetical compound of $Pt_2Nb_{10}O_{29}$ had not been formed. A small quantity of the product was examined by the X-ray powder diffraction method and no other phase other than Pt + H-Nb_2O_5 patterns were found.

The catalytic effect of the platinum surface on the reduction of B-Nb_2O_5 is supported by another observation made in an entirely different context: the localised reduction of mixed titanium-niobium oxides ($TiNb_2O_7$) in an area confined to surface contact with fresh - i.e. unused - platinum foil, under experimental conditions of high oxygen partial pressure generated in a molybdenum resistance furnace at 1400°C (see Plate 5 A and B). Preceding the description

of this particular observation. The construction of the molybdenum furnace employed in this study is briefly explained. Strips of molybdenum were wound on an impervious alumina refractory tube (Morganite Refractory Ltd.). The winding was coated with a cement consisting of pure alumina powder mixed with some organic binder (Morganite Refractory catalogue). The tube was insulated by a considerable thickness of calcined alumina powder and jacketed by a gas tight cylindrical steel case. The atmosphere used with the molybdenum furnace was pre-cracked ammonia (i.e. $2NH_3 \rightleftharpoons N_2 + 3H_2$), prepared by passing dry ammonia gas through a separate furnace packed with steel wool and heated at 850°C. In the course of the experiment both ends of the furnace were open, hence, air could circulate over the sample.

Approximately 5 gr. thoroughly mixed TiO_2 and Nb_2O_5 (Johnson Matthey Chemicals) in a 1:1 ratio was packed in a platinum boat (constructed of new platinum foil) which was placed in the hot zone of the furnace (1400°C) for a period of 48 hours. It was found that the oxide during this period was reduced only on the area of contact with the platinum container. This is evident from Plate 5 A and B which show a thin coat of dark blue colour --i.e. reduced oxide -- covering the unreduced (white colour) bulk of the sample.

The reducing atmosphere, most likely, stems from a high ratio of H_2O/H_2 gas buffer mixture in the environment of the sample. Here, hydrogen apparently diffuses through the alumina tube of the furnace and subsequently burns in air to produce a constant H_2O/H_2 ratio at 1400°C.

PLATE 5

PLATE 5

Possible catalytic effect of the platinum surface on the reduction of niobium oxides (Section 5.1.3.1.).

A and B) Polycrystalline $TiNb_2O_7$ sample, reduced (dark blue colour) in areas which have been in contact with the platinum container.

Note the unreduced inner part (white colour), exposed in A after removing the blue surface part. In B, the white part depicts the unreduced upper surface which had not been in contact with platinum. The reducing conditions were: 1400°C and a high oxygen partial pressure generated from continuous combustion of hydrogen.

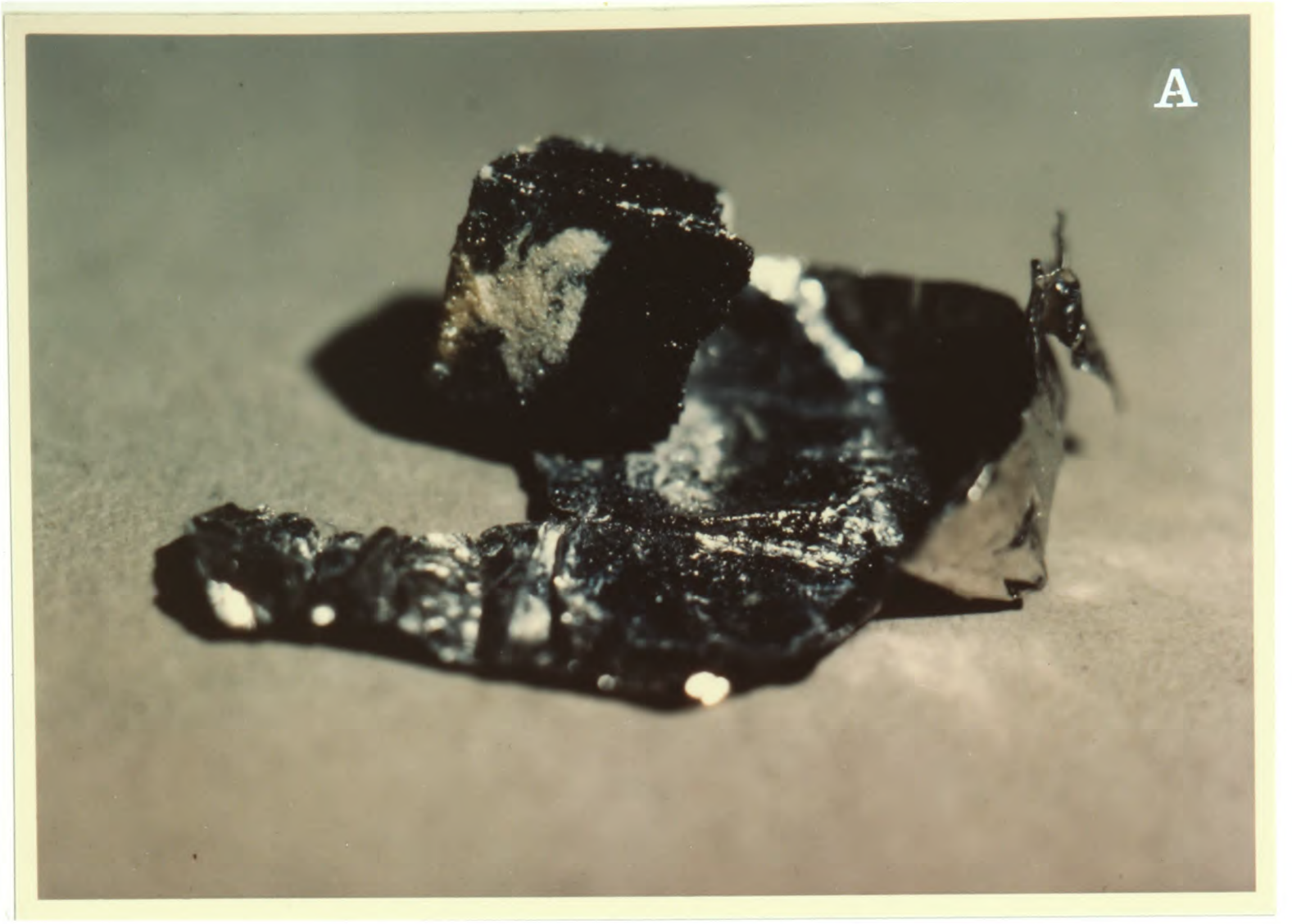



Plate 5

5.1.3.2. Structural studies (Electron microscopy)

Results of electron microscopy measurements carried out on the sample prepared at isotherm 850°C (see Section 5.1.3.1., d and e) could, in general, be classified into two distinct groups:

A) Crystals with extensively disordered block configurations,

B) Crystal fragments having well-ordered block structures.

A) Disordered Crystals

From a total of 15 crystal fragments examined by electron microscopy, approximately two-thirds showed structures with an extensively disordered block arrangement. Different individual blocks and in some cases abnormal sizes were identified in the crystallographic ac plane. The blocks are coherently packed and interconnected by edge sharing of MO_6 octahedra, and accomodate cations in tetrahedral sites. Plates 6, 7 and 8 show two-dimensional lattice images of three representative crystal fragments. Their respective electron diffraction patterns are shown in the inset. Idealized models of regions (X and Y) in Plate 6 are given in Figs. 11 and 12 respectively while an analysis of region (X) in Plate 7 is depicted in Fig. 13. The basic ReO_3 subcell orientation is unchanged in all the disordered crystals; the idealized models are drawn in such a way that the ReO_3 subcell direction is parallel to the photograph edges (see Fig. 11, 12 and 13).

The multiplicity and "jigsaw puzzle" fashion ordering of blocks indicates that the B-Nb_2O_5 single crystals in the

TABLE 9

TABLE 9

Calculated proportions of individual block constituents and chemical composition of crystal areas observed in Plates 6, 7 and 8

Plate	Area	% $(4 \times 3)_2$	% $(5 \times 3)_8$	% $(4 \times 4)_8$	% $(4 \times 3)_8$	% $(4 \times 3)_1$	% $(3 \times 3)_1$	% $(3 \times 3)_8$	% $(5 \times 4)_8$	% $(5 \times 2)_8$	% $(4 \times 4)_2$	% $(5 \times 3)_2$	% Nb (average)
6	X	40	21.6	25	5.3	5	0	0	0.8	0	0.4	2	$NbO_{2.4846}$
	Y(M)	26.7	40	13.3	0	16.7	0	3.3	0	0	0	0	$NbO_{2.4844}$
7	Z	48.3	25.8	19	5.2	0	1.44	0	0	0	0	0	$NbO_{2.4790}$
	Y	36.14	30	25.3	8.4	0	0	0	0	0	0	0	$NbO_{2.4770}$
	X	43.27	15.38	10.58	14.42	6.71	7.69	0	0.96	0.96	0	0	$NbO_{2.4649}$
8	X	48	12	8	28	0	0	0	0	0	0	0	$NbO_{2.4697}$

process of simultaneous phase transformation - reduction in most cases - contain blocks of different sizes. Plates 6, 7 and 8 show that crystals are often heavily disordered in the ac plane, but apparently perfectly ordered along the direction of the incident electron beam. It is therefore possible to determine the approximate chemical composition of disordered crystal fragments in which the structural details are adequately resolved. This was carried out by counting the total number of every individual block size and assuming that each column represents a definite cation - anion site ratio, and taking into account the manner in which the blocks are linked. The combination of the column sizes and the summation of their compositions represents the local stoichiometry of the crystal. The results, together with the proportions of individual block sizes constituting the crystal structure, are produced in Table 9. It is evident that the disordered structures contain a large proportion of (4 x 4) blocks (Table 9) which are segregated in isolated microdomains by forming an ordered N-Nb_2O_5 structure (labelled N in the region X of Plates 6 and 7 and in the idealized models Fig. 10 and 12). Similarly, microdomains of other lower oxides such as $Nb_{25}O_{62}$, $Nb_{53}O_{132}$, $Nb_{22}O_{54}$, $Nb_{15}O_{37}$, $Nb_{47}O_{116}$, $Nb_{12}O_{29}$ are also observed. These are coherently intergrown with the matrix of the disordered crystal. Consider region X in Plate 7 in which the ordered microdomains are formed as a result of irregular stacking of different structural elements, $Nb_{28}O_{70}$ (D-row), $Nb_{25}O_{62}$ (C-row) and $Nb_{22}O_{54}$ (J-row). Microdomains in which these three structures are stacked albeit irregularly are labelled

Q in Fig. 13. Further findings in the disordered crystals are:

a) Intergrowth of ordered and disordered structures,

b) Segregation of impurities,

c) Linear extended defects,

d) Point defect complexes,

which are discussed below:

a) Intergrowth of Ordered and Disordered Structures

Co-existence and coherent intergrowths of a large domain of an ordered phase with a heavily disordered block structure is depicted in Plate 6 in which area Z shows essentially an ordered $Nb_{25}O_{62}$ structure (↑C-row) containing occasional lamellae of $Nb_{28}O_{70}$ (H-Nb_2O_5) (↑D-row). The chemical composition of this area (i.e. Z) was estimated to be slightly higher than $NbO_{2.480}$. Region (Y) contains two distinct parts: in (P) the lamellae of D-rows and C-rows are stacked along the (100) direction of ReO_3 whereas in (M) the blocks are coherently packed without any distinct crystallographic relationship. Area (Y) is well resolved in the micrograph and an idealized model is shown in Fig. 12. Areas (M) and (P) are not intergrown along a specific crystallographic direction.

The metal-oxygen ratio of (M) has been estimated as $NbO_{2.484}$ (Table 9). This suggests that the composition of the crystal fragment is approximately the same in both ordered and disordered regions. This conclusion is also supported by a measurement of the metal-oxygen ratio in the other disordered region of the same crystal fragment

PLATE 6

PLATE 6

High resolution two-dimensional lattice image of an extensively disordered crystal fragment obtained from a transformed-reduced B-Nb_2O_5 sample prepared at isotherm 850°C and $p_{O_2} = 5.30 \times 10^{-20}$ (Section 5.1.3.1. d and e).

Simultaneous occurrence of ordered and disordered block structures (see Section 5.1.3.2.a).

Areas W and X have disordered block arrangements, whereas Z consists of an ordered $Nb_{25}O_{62}$ structure (↑ C), with occasional intergrowth of the $Nb_{28}O_{70}$ phase (↑ D).

Region Y shows the intergrowth boundary between ordered (P) and disordered (M) structures.

Chemical compositions of disordered regions in X and Y (M), as calculated from idealized models (Fig. 11 and 12), are $NbO_{2.4846}$ and $NbO_{2.4844}$, respectively (see Table 9), while the ordered side of the crystal (region Z) has a composition of $NbO_{2.480}$.

In region X, microdomains labelled N show N-Nb_2O_5 elements in the disordered region. Blocks labelled T indicate the presence of rectangular tunnels extending through the crystal in parallel to the incident electron beam (see Section 5.1.3.2.c). V indicates the presence of (5x4) blocks probably reflecting the segregation of impurity ions e.g. OH^- incorporated in the crystal structure (see Section 5.1.3.2.b).

Inset (B): Selected area (h0l) electron diffraction pattern of the crystal.

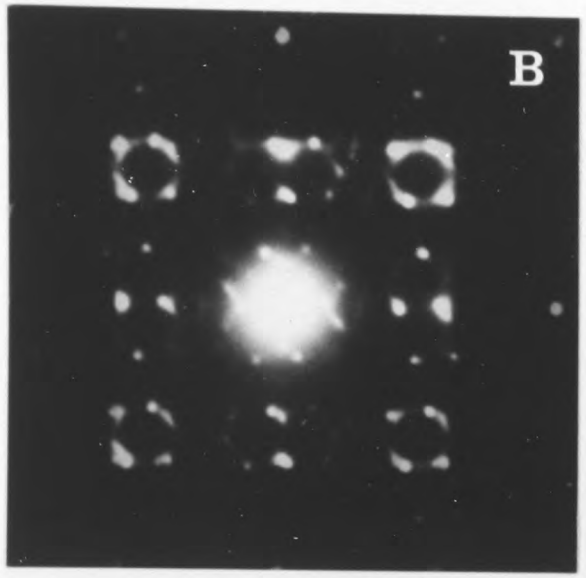

Plate 6

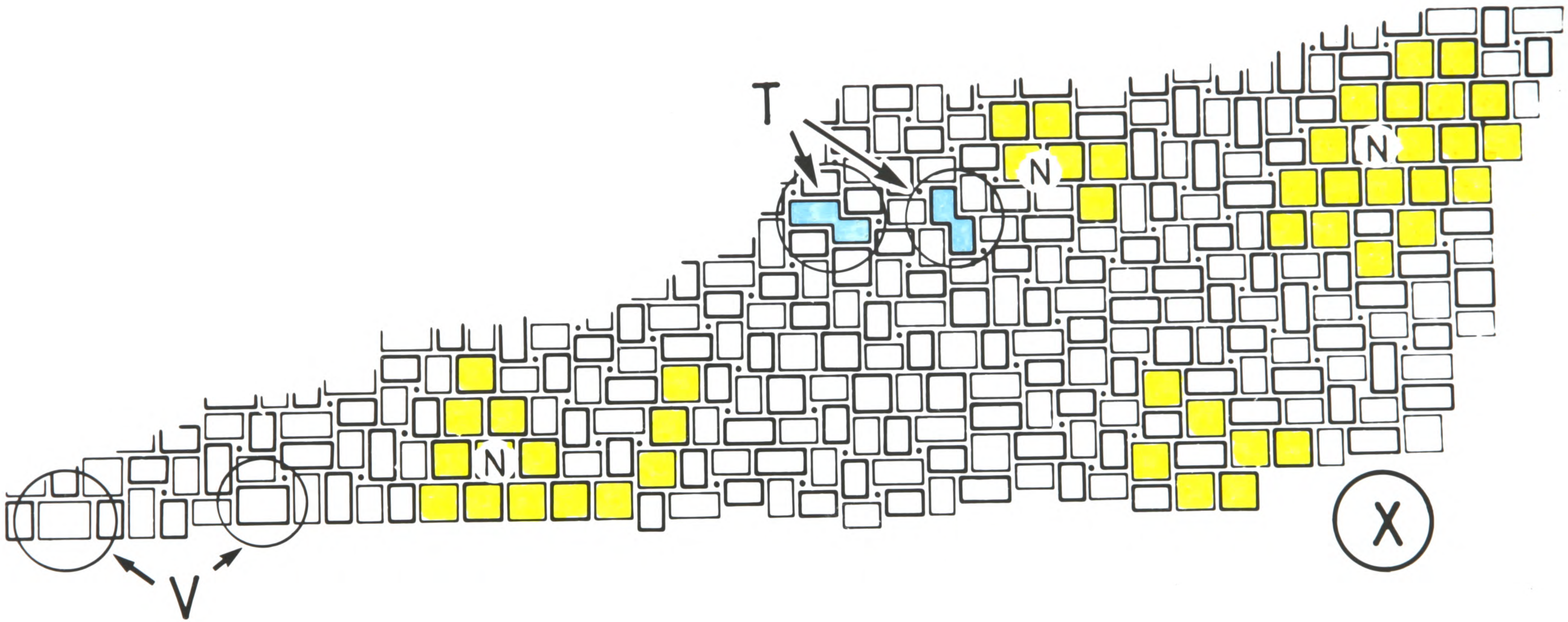

FIG. 11

Idealized model of region X as shown in Plate 6. The model shows a variety of defects which have been mentioned in Plate 6.

FIGURE 12

FIGURE 12

Idealized model of region (Y) in Plate 6. The model shows the simultaneous presence of ordered (P) and disordered (M) regions in one crystallite. No specific common intergrowth plane can be determined. The chemical composition of region M is $NbO_{2.4844}$ (Table 9), which approximates the composition in the ordered area P.

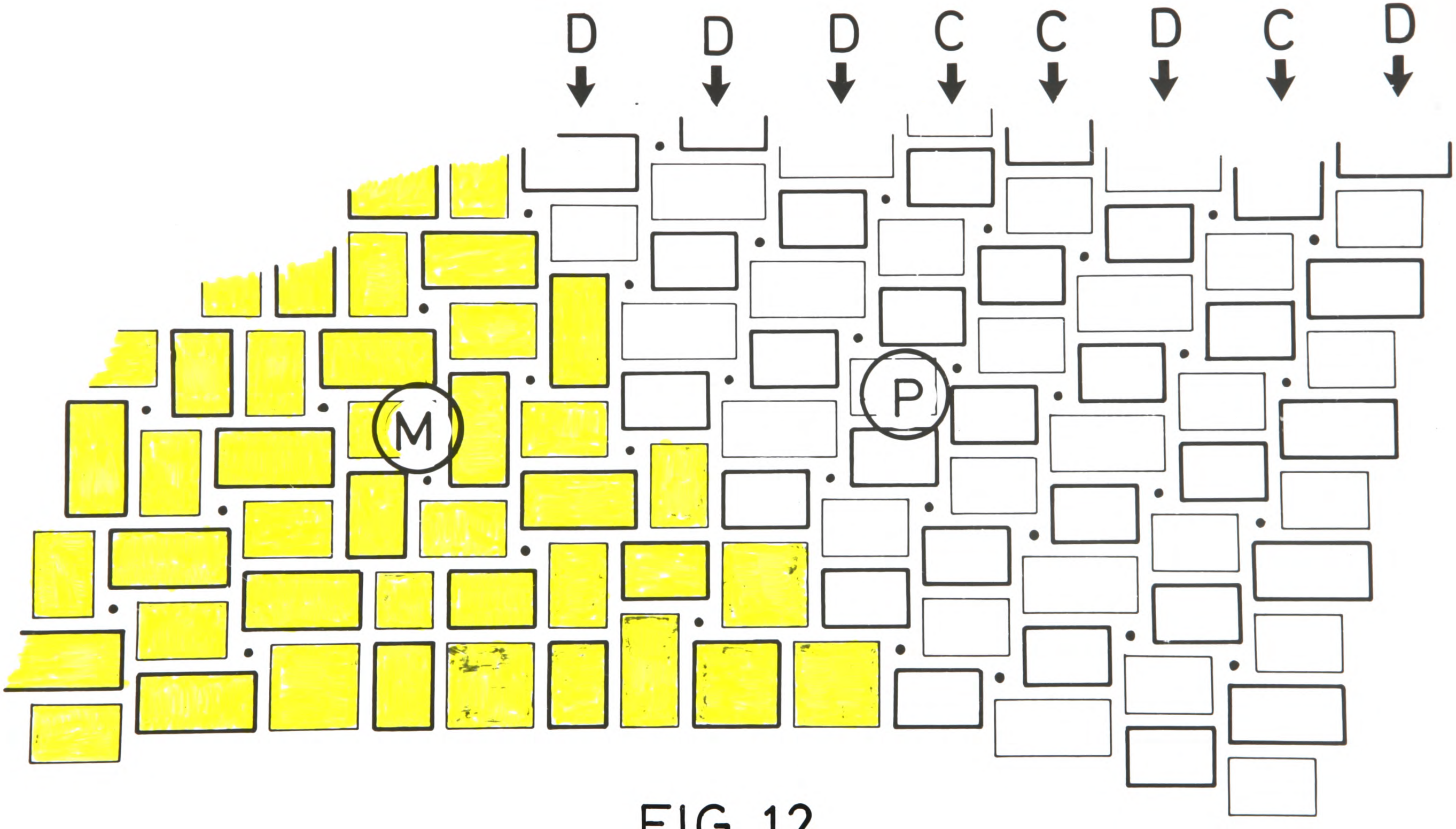

FIG. 12

(labelled X in Plate 6 -- idealized model Fig. 11). The composition of X is $NbO_{2.484}$ (Table 9).

b) Segregation of Impurities

Isolated larger blocks of sizes (5 x 4) and (6 x 3) are found in the matrix of the disordered block structures (indicated V and R in Plates 6, 7 and 8 respectively). The (5 x 4) block in Plate 7 and in idealized model Fig. 13 is fused in a "T" shape with another anomalous block size (5 x 2) having cations in the same level. (6 x 3) blocks (↑ R in Plate 8-b and c) represent the structural element of $Nb_{18}O_{45}$ which is a hypothetical modification of Nb_2O_5. This compound has not been reported in the literature and it appears to be beyond the stability range of the pure oxide system (Anderson and Tilley, 1974). However, a small domain of this structure containing (6 x 3) blocks has been observed in an electron microscopy study of the MgF_2-Nb_2O_5 system (Hutchison and Lincoln, 1973). The occurrence of larger block sizes reflects local stoichiometries with an oxygen-metal ratio in excess of 2.50. It is probable that impurity ions have been incorporated into these larger blocks. As has been explained earlier (Chapter II), the single crystal growth of B-Nb_2O_5 by the chemical vapour transport technique is promoted by the presence of H_2O dopant (as a source of $\bar{O}H$). It is therefore possible that the impurity ion in the larger blocks is $\bar{O}H$ which was incorporated, during the process of crystal growth, into the structure of B-Nb_2O_5. Where several larger blocks occur together (for example, regions N in Plates 6 and 7) the $\bar{O}H$ ions may have

concentrated during crystal growth to produce elements of a new structure with a different composition. This would presumably intergrow coherently with the B-Nb_2O_5 structure. This viewpoint, to be tested by direct observations of B-Nb_2O_5, remains to be investigated.

Finally, it may be pointed out that the effect described here has also been reported by Anderson et al (1972a) in an electron microscopy study of N-Nb_2O_5 and transformed M-Nb_2O_5 crystals.

c) Linear Extended Defects:

Under optimum focussing condition, as is the case in Plates 6 and 7, the white contrast streaking in the junctions of overlapping (4 x 3) blocks (↑ "T" in Plates 6 and 7) would indicate the presence of rectangular tunnels which are extending through the crystal parallel to the b-axis (and the electron beam). The geometrical dimensions of the tunnels are 5.6 x 2.8 $\mathring{A}^2$, as measured from the idealized model shown in Fig. 13 (↑ T).

The occurrence of extended linear defects has also been reported for the MgF_2-Nb_2O_5 system by Hutchison and Lincoln (1973), who discussed the relationship between linear defects and the distribution and ordering of Wadsley defects in block structures. Browne (1973), in an electron microscopy study of N-Nb_2O_5, found rectangular tunnels adjacent to larger blocks of $(5 \times 4)_\infty$. He postulated a mechanism which related the formation of linear defects at the time of crystallization and impurity segregation to the occurrence of unusually large block sizes.

PLATE 7

PLATE 7

High resolution two-dimensional lattice image of a disordered crystal fragment taken from a transformed-reduced B-Nb_2O_5 sample prepared at isotherm 850°C and $p_{O_2} = 5.30 \times 10^{-20}$ (Section 5.1.3.1. d and e).

The chemical compositions of the different domains X, Y and Z, as measured from idealized models, are $NbO_{2.4649}$, $NbO_{2.4770}$ and $NbO_{2.4790}$, respectively (Table 9).

In region X, the idealized model of which is given in Fig. 13, the following structures are visible: Ordered microdomains labelled Q composed of $Nb_{28}O_{70}$ (↑ D), $Nb_{25}O_{62}$ (↑ C) and $Nb_{22}O_{54}$ (↑ J). Microdomains labelled N, representing N-Nb_2O_5 structure intergrown in the disordered crystal (Section 5.1.3.2. b), and ↑ T showing the formation of rectangular tunnels extending through the crystal in parallel to the b-axis of the block structure (see Section 5.1.3.2. c). Anomalous blocks of (5x4) and (2x5) are indicated V (Section 5.1.3.2.b).

Inset (B): selected area (h01) electron diffraction pattern of the crystal fragment.

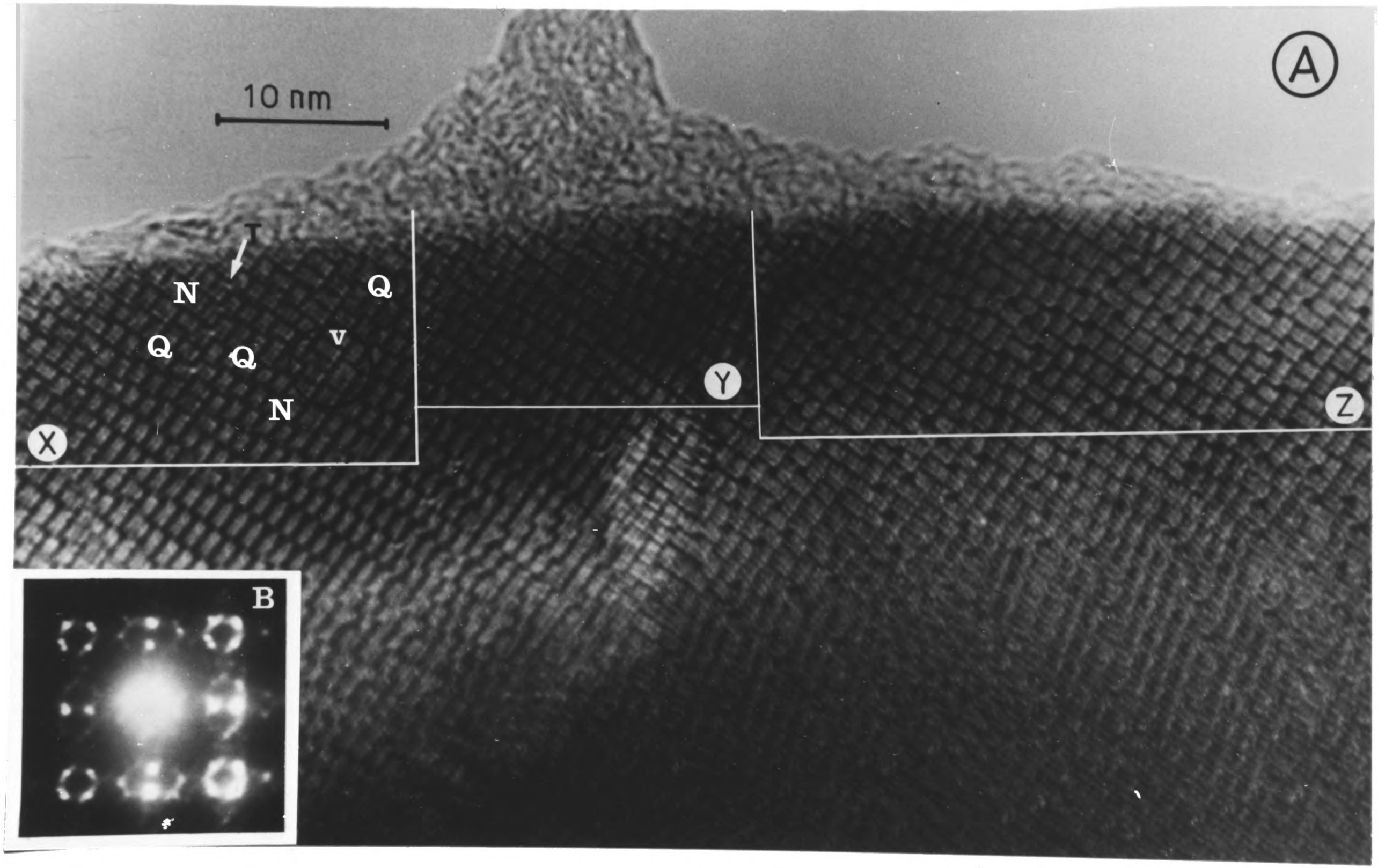

Plate 7

FIGURE 13

FIGURE 13

Idealized model of region X in Plate 7. The model illustrates details of the different microdomains mentioned in Plate 7.

Areas Q and N are given in blue and yellow, respectively.

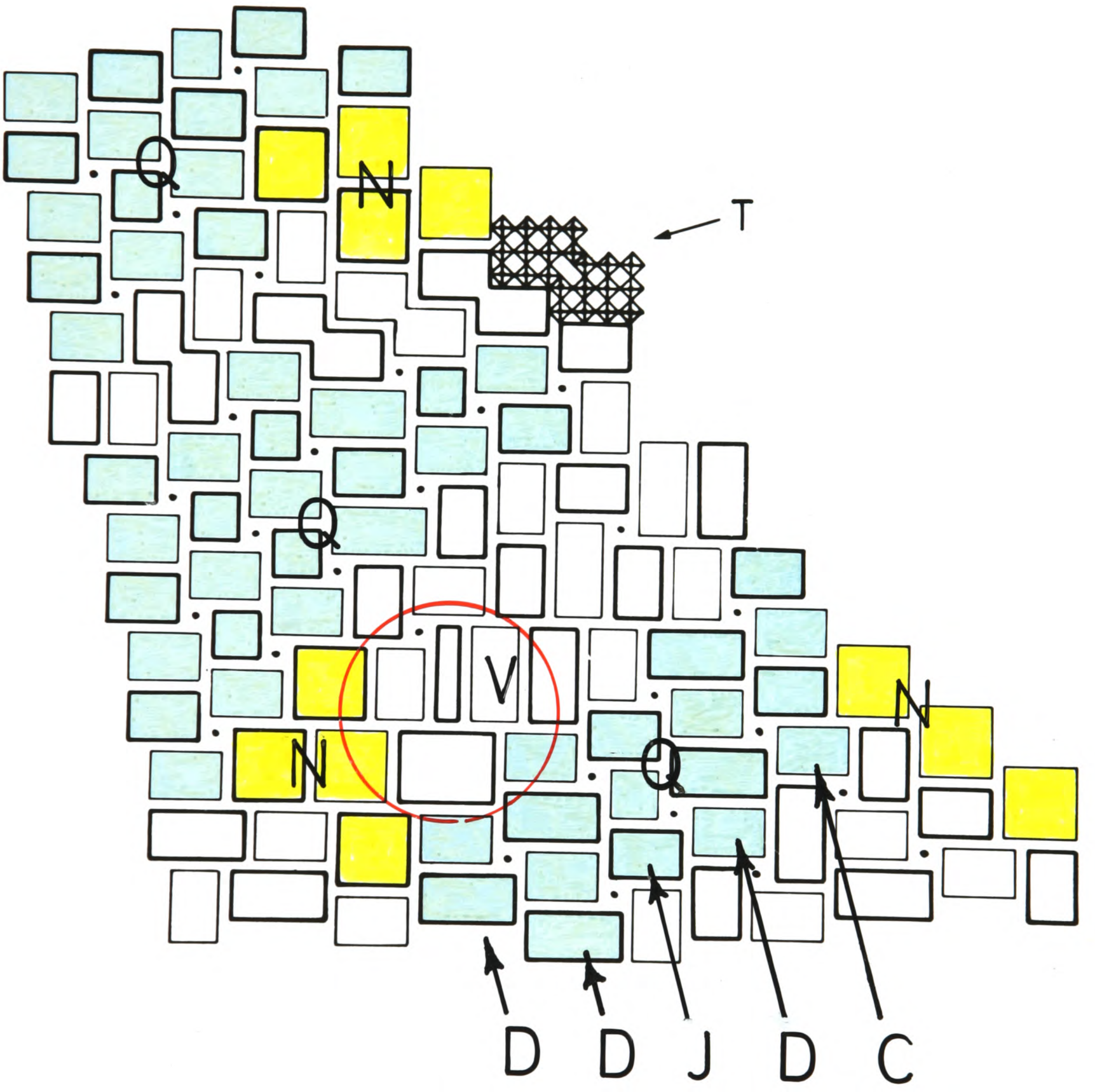

FIG. 13

PLATE 8

PLATE 8

A) High resolution two-dimensional lattice image of a disordered crystal fragment from a transformed-reduced B-Nb_2O_5 sample prepared at isotherm 850°C and $p_{O_2} = 5.30 \times 10^{-20}$ (Section 5.1.3.1. d and e). The chemical composition of domain X, as measured from an idealized model, is $NbO_{2.4697}$ (see Table 9). ↑R shows the formation of (6x3) blocks (Section 5.1.3.2.b).

Inset B) Selected area (h0l) electron diffraction pattern of the crystal fragment shown in (A).

C) Idealized model of area X in (A). (6x3) blocks are given in yellow.

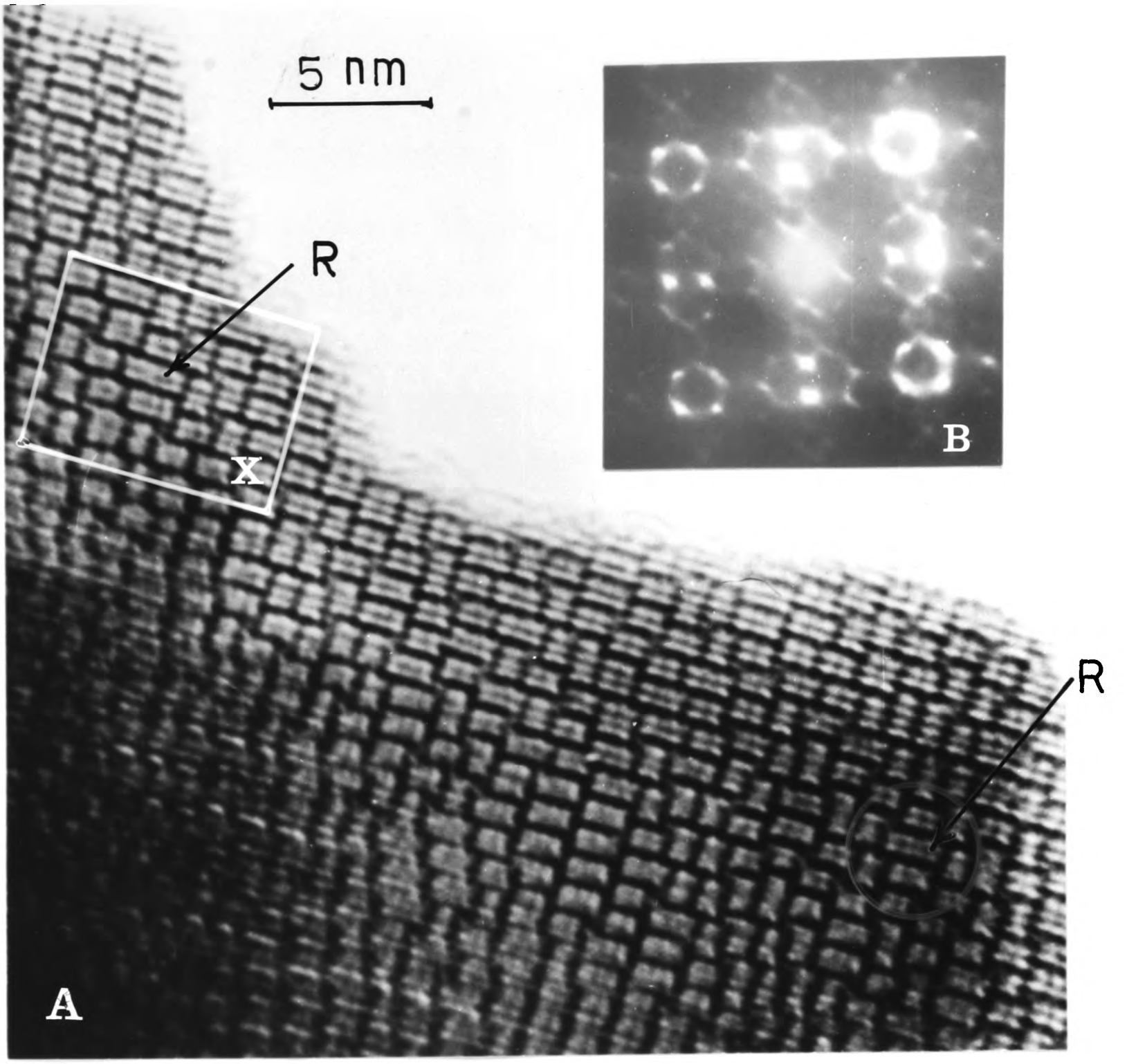

C

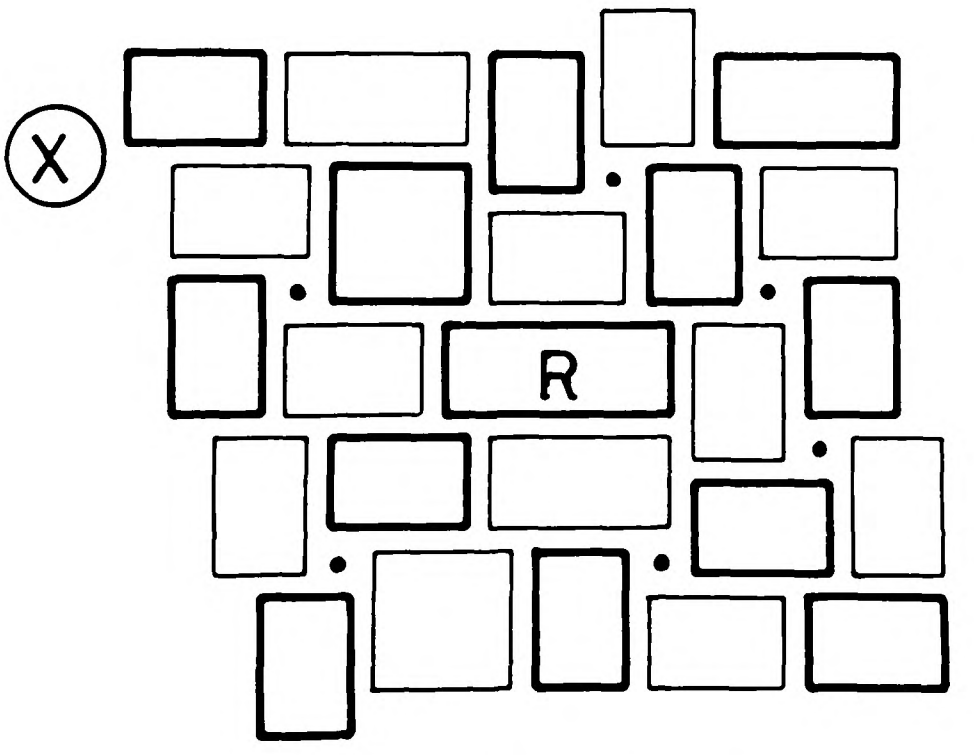

Plate 8

d) Point Defect Complexes

The monoclinic $Nb_{12}O_{29}$ structure shown in Plate 9 contains abundant point defects (↑ P) identical to those previously reported by Iijima (1973, 1975) and Iijima et al (1973). In their study of oxygen-excess $Nb_{12}O_{29}$ (Kimura's sample, 1973), a model was proposed in which the defects were formed by displacement of two specifically situated niobium atoms into interstitial positions of the host lattice (Plate 9-B). The metal atom, labelled a in Plate 9-B occupies empty tetragonal tunnels which run parallel to the b-axis of the matrix. In this way, tetrahedrally co-ordinated niobium atoms are formed, similar to those present in the higher oxide structures (e.g. $Nb_{25}O_{62}$). The second niobium atom (labelled b in Plate 9-B) is displaced to its new position and has retained the original octahedral co-ordination in which two extra oxygen atoms (open circles in Plate 9-B) are accommodated in the position of unshared apices. The point defects can be annihilated by intense electron beam irradiation (Iijima, 1973). A similar effect was noticed in the present work by comparison of two electron micrographs taken in succession with an interval of 6 seconds under weak electron beam irradiation. They revealed a considerable decrease in the density of the dark spots. The elimination of point defect complexes is thought to be due to the liberation of the two oxygen atoms (open circles Plate 9-B) from the environment of the displaced niobium atoms labelled a and b. This necessarily causes a reshuffling of the displaced metal atoms (a and b) to their original

PLATE 9

PLATE 9

A) $m\text{-}Nb_{12}O_{29}$ structure with abundant point defects (↑ P) found in a transformed-reduced $B\text{-}Nb_2O_5$ sample prepared at isotherm 850°C and $p_{O_2} = 5.30 \times 10^{-20}$ (Section 5.1.3.1. d and e).
Domain Y shows a superlattice structure composed of a coherent intergrowth of $Nb_{22}O_{54}$ and $m\text{-}Nb_{12}O_{29}$ on a plane running parallel to the c-axis of the matrix. The parameters of the monoclinic unit cell of the superlattice structure, as calculated from the idealized model, shown in (D), are a = 60 Å, b = 3.8 Å, c = 15.33 Å and $\beta = 121.5°$; the unit cell composition is $Nb_{46}O_{112}$. (↑ J) in domain Y indicates chains of tetrahedral atoms extending through the crystal in parallel to the b-axis of the block structure. These are probably reflecting the formation of the superlattice structure on the outer layer of $Nb_{22}O_{54}$.

B and C)(After Iijima, 1973). Idealized models for the formation (B) and annihilation (C) of point defect complexes (Section 5.1.3.2.d).

D) Idealized model of the superlattice structure shown in domain Y in (A).

Ⓐ

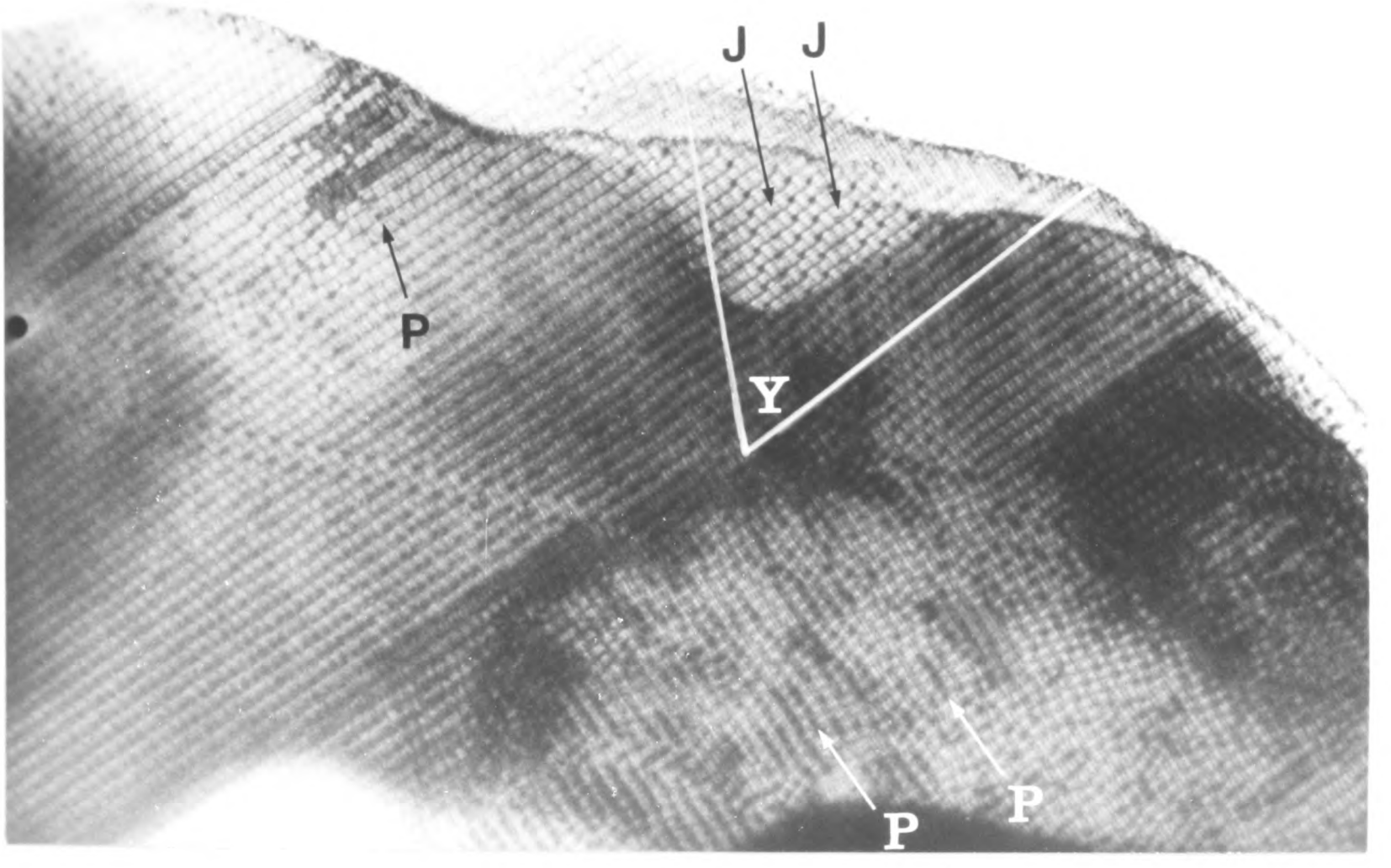

Ⓑ

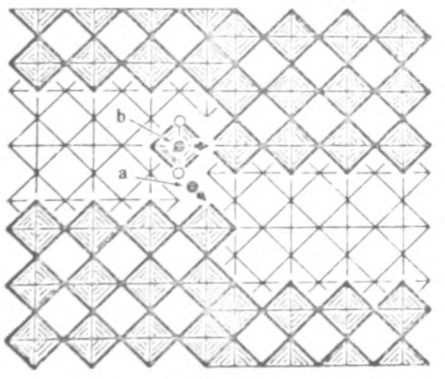

Ⓒ

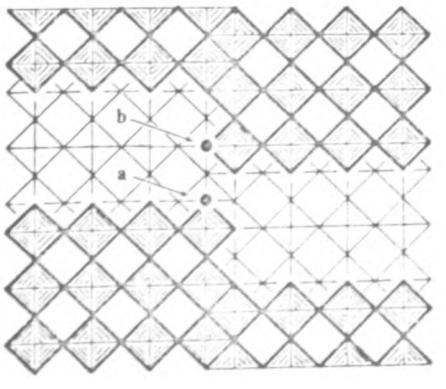

Ⓓ

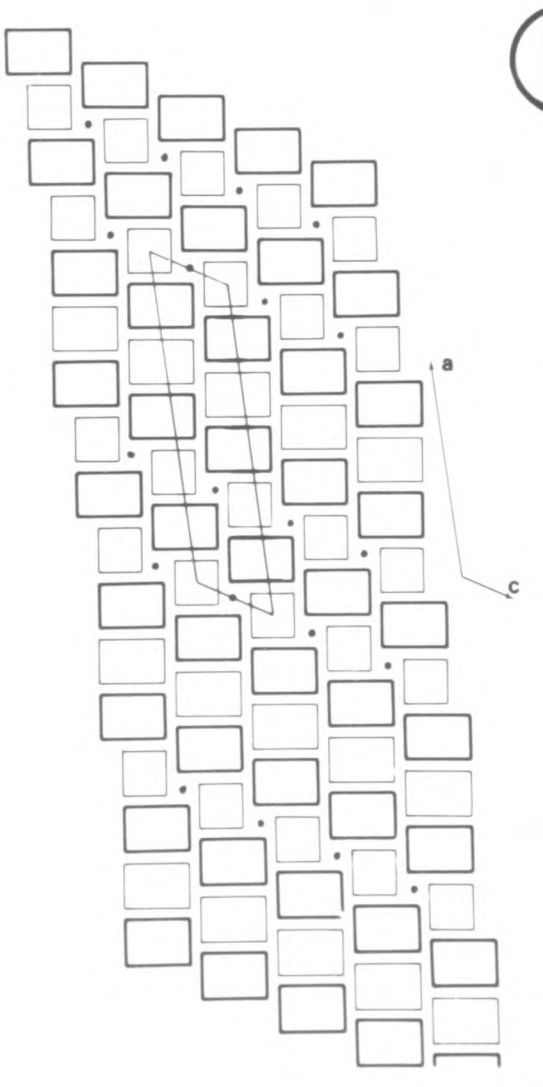

Plate 9

lattice sites to produce a perfect $Nb_{12}O_{29}$ structure (Plate 9-C).

Another finding in this micrograph (Plate 9-A) is a domain of superlattice structure (labelled Y) previously unreported in the literature. This structure is a coherent intergrowth of $Nb_{22}O_{54}$ and m-$Nb_{12}O_{29}$ on a plane running parallel to the c-axis of the matrix. The superlattice comprises regular stacking of (3 x 3) and (4 x 3) blocks in a proportion of 1:3 (Plate 9-D); this generates a monoclinic unit cell with lattice parameters of approximately a = 60 Å, b = 3.8 Å, c = 15.33 Å and $\beta = 121.5^{o}$ (derived from the idealized model Plate 9-D). The composition is $Nb_{46}O_{112}$.

Detailed inspection of the superlattice structure domain reveals arrays of black spots between the (4 x 3) blocks. Their location corresponds to the position of octahedral edge sharing of the middle layer $(4 \times 3)_{\infty}$ ribbons (↑J). The black spots run parallel to the c-axis of the matrix (m-$Nb_{12}O_{29}$) and may represent chains of tetrahedral atoms which extend through the crystal in the direction of the b-axis. One possibility is that two different structures, $Nb_{22}O_{54}$ and the $Nb_{46}O_{112}$, are superimposed upon each other and that growth of the superstructure has taken place on the $Nb_{22}O_{54}$ crystal surface. This would suggest that reduction of $Nb_{22}O_{54}$ to $Nb_{12}O_{29}$ takes place via intergrowths of $Nb_{12}O_{29}$ and $Nb_{22}O_{54}$. We observed one example ($Nb_{46}O_{112}$) while Iijima et al., has also observed $Nb_{34}O_{83}$.

B) Ordered Crystal Fragments

Out of several ordered crystal fragments which mostly

had $Nb_{12}O_{29}$ ($NbO_{2.417}$) structures, two were most informative. The findings are given below in the order:

I) Phase conversion within the H-Nb_2O_5-$Nb_{25}O_{62}$ system,

II) Defect properties of monoclinic $Nb_{12}O_{29}$ structure.

I) Phase conversion within the H-Nb_2O_5 - $Nb_{25}O_{62}$

Plates 10 and 11 represent a crystal fragment consisting of a well-ordered block arrangement in which three different structures labelled X, Y (and Y') and Z co-exist and are coherently intergrown with each other. Analysis of these micrographs provided information about the following:

1) Ordering of Wadsley defects in the reduced material under low temperature reduction conditions -- i.e. 850°C.

2) Formation of the $Nb_{43}O_{107}$ structure as an intermediate phase hitherto unknown in the chemistry of the niobium-oxygen system.

3) The structural relationship of the three intergrown phases -- i.e. H-Nb_2O_5 ($Nb_{28}O_{70}$), $Nb_{53}O_{132}$ and $Nb_{43}O_{107}$.

4) A possible mechanism for the conversion of $Nb_{53}O_{132}$ into $Nb_{43}O_{107}$, on the basis of the model proposed by Andersson and Wadsley (1966) -- see General Introduction, Chapter I.

(1) The regions (Y and Y') in Plate 10 show a well-ordered H-Nb_2O_5 structure. In area (Y), two isolated Wadsley defects are indicated (↑C and ↑F). Lamella (C) originates from the collapse of H-Nb_2O_5 along the (601) ReO_3 plane, in which the (5 x 3) blocks are cut up into (4 x 3) columns. They, in turn, are linked with neighbouring blocks forming a $(4 \times 3)_2$ strip with a local stoichiometry of

PLATE 10

PLATE 10

High resolution two-dimensional lattice image of an ordered crystal fragment taken from a transformed-reduced B-Nb_2O_5 sample prepared at isotherm 850°C and $p_{O_2} = 5.30 \times 10^{-20}$ (Section 5.1.3.1. d and e). The idealized model of the structure is shown in Fig. 14. Coherent intergrowth and co-existence of three structures are shown in the Plate: H-Nb_2O_5 ($Nb_{28}O_{70}$), $Nb_{53}O_{132}$ (1:1 intergrowth of H-Nb_2O_5 and $Nb_{25}O_{62}$, indicated by ↑ D and ↑ C, respectively) and $Nb_{43}O_{107}$. The three structures are labelled Y (and Y'), X and Z, respectively.

H-Nb_2O_5 and $Nb_{43}O_{107}$ structures are intergrown on the $(20\bar{9})_R$ plane, $Nb_{53}O_{132}$ and $Nb_{43}O_{107}$ structures on the $(101)_R$ plane and H-Nb_2O_5 and $Nb_{53}O_{132}$ phases on the $(601)_R$ plane.

$Nb_{43}O_{107}$ is a new structure having a monoclinic structure with lattice parameters: $a = 20.3$ Å, $b = 3.8$ Å, $c = 61.58$ Å and $\beta = 117°$.

↑ F and ↑ C in region Y indicate the occurrence of two Wadsley defects (i.e. $Nb_{15}O_{37}$ and $Nb_{25}O_{62}$, respectively) which terminate in the point of intersection (Section 5.1.3.2.B).

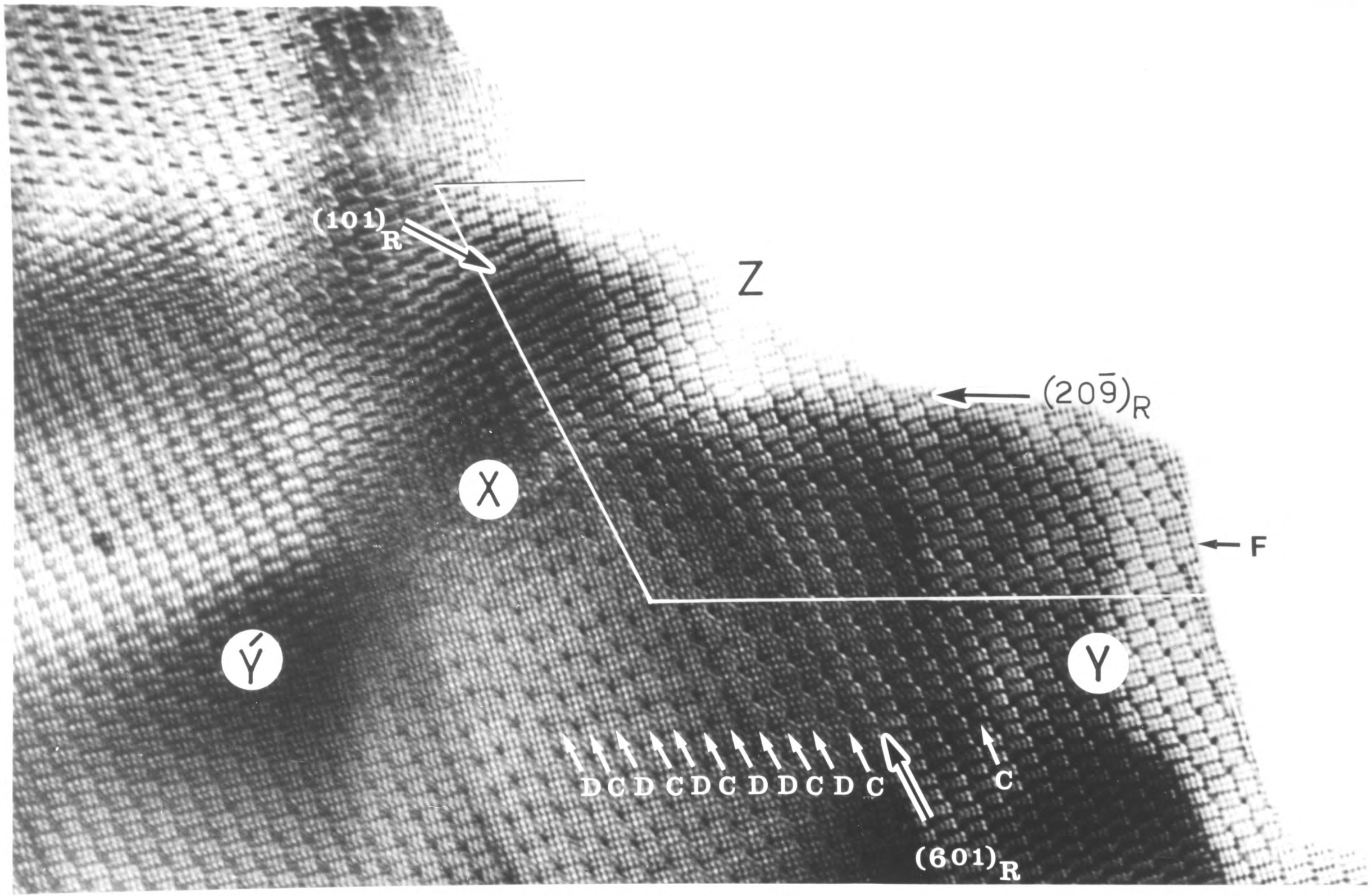

Plate 10

($NbO_{2.480}$). The extension of this fault into the bulk of the crystal is terminated at the intersection with a second planar defect running in the direction of the $(20\bar{9})$ ReO_3 plane. This second defect ($\uparrow$ F) stems from the incorporation of an additional ribbon of linked columns of (5 x 3) in place of $(4 \times 3)_1$ blocks of H-Nb_2O_5. As a result, a single ribbon of $Nb_{15}O_{37}$ structure, which has a local stoichiometry of $NbO_{2.4670}$, has been generated.

In region (X), the first reduction stage of H-Nb_2O_5 has taken place. Strips of $(4 \times 3)_2$, the structural element of $Nb_{25}O_{62}$ (C-row), are intergrown coherently in a regular 1:1 ratio with the matrix (D-row). Thus, the $Nb_{53}O_{132}$ ($NbO_{2.4906}$) structure has been formed in ribbons of two unit cells wide.

(2) In area (Z), a new structure has been generated which is composed of pairs of $(5 \times 3)_\infty$ ribbons with cations of each ribbon located at Y = 0 and Y = $\frac{1}{2}$, respectively. The $(5 \times 3)_\infty$ ribbons are joined together by edge sharing in the longitude of (5 x 3) blocks, forming pairs which are running parallel to the $(20\bar{9})$ plane of ReO_3. The pairs are stacked alternately with arrays of single (4 x 3), columns. These features are shown in Fig. 14 in which pairs of $(5 \times 3)_\infty$ ribbons are given in brown and (4 x 3) blocks in white. From the model, a monoclinic unit cell can be deduced which has lattice parameters of approximately:

a = 20.3 Å, b = 3.8 Å, c = 61.58 Å and $\beta = 117^\circ$

and a stoichiometry of $Nb_{43}O_{107}$ ($NbO_{2.4884}$). This structure represents the second intermediate compound in the region of $NbO_{2.5}$-$NbO_{2.00}$ of the (Nb-O) phase diagram.

FIGURE 14

FIGURE 14

Structural relationship between $Nb_{43}O_{107}$, $Nb_{53}O_{132}$ and H-Nb_2O_5 (Section 5.1.3.2.). The $Nb_{43}O_{107}$ and $Nb_{53}O_{132}$ ($Nb_{53}O_{132}$ = 1.1 intergrowth of H-Nb_2O_5 labelled $\underline{\uparrow D}$ and $Nb_{25}O_{62}$ labelled $\underline{\uparrow C}$) relationship involves the following: Each $(4 \times 3)_2$ strip ($\underline{\uparrow C}$) of $Nb_{53}O_{132}$ terminates when meeting a pair of $(5 \times 3)_\infty$ ribbons of $Nb_{43}O_{107}$. The two structures, i.e. $Nb_{53}O_{132}$ and H-Nb_2O_5 appear to have intergrown on the $(\bar{6}01)_R$ plane; intergrowth of $Nb_{43}O_{107}$ with H-Nb_2O_5 has taken place on the $(20\bar{9})_R$ plane.

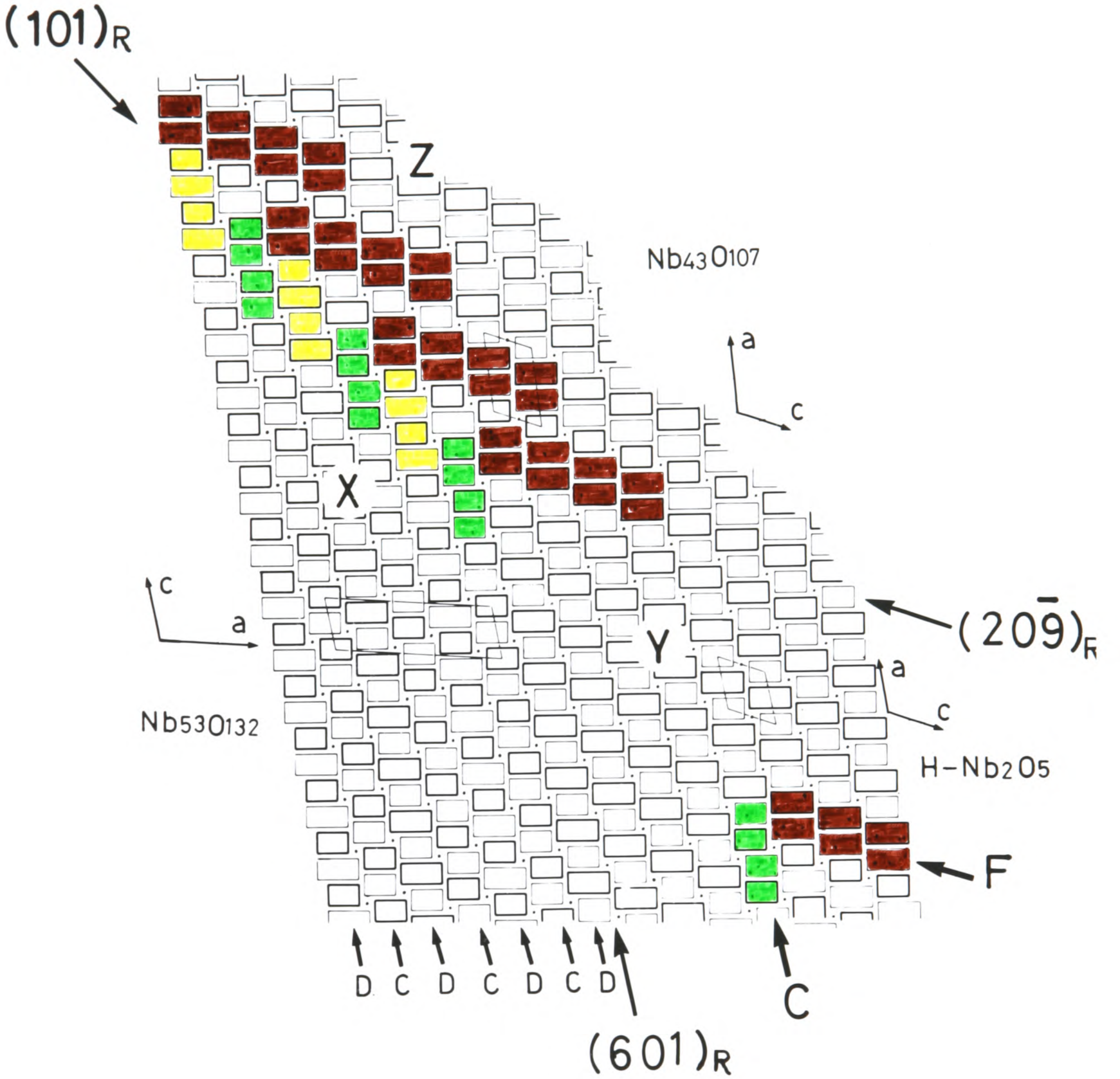
(101)R
Z
Nb43O107
a
c
X
c
a
Y
(20$\bar{9}$)R
Nb530132
a
c
H-Nb2O5
F
D C D C D C D
C
(601)R

FIG. 14

The block configuration of $Nb_{43}O_{107}$ can be tentatively regarded as a regular 1:1 intergrowth of $Nb_{15}O_{37}$ and $Nb_{28}O_{70}$ (H-Nb_2O_5) according to the equation:

$$Nb_{28}O_{70} + Nb_{15}O_{37} = Nb_{43}O_{107}$$

The $Nb_{15}O_{37}$ structure appears to be a distinct intermediate phase within the H-Nb_2O_5-NbO_2 system. This suggestion is supported by the frequent observation of (5 x 3) strips intergrown as Wadsley defects in the matrix of monoclinic $Nb_{12}O_{29}$ -- see defect properties of m-$Nb_{12}O_{29}$ in Section II (below).

(3) The compound $Nb_{43}O_{107}$ has a distinct geometrical relationship with the phases $Nb_{53}O_{132}$ and H-Nb_2O_5. This can be seen in Plate 10 and, more clearly, in Plate 11 which shows the intergrowth boundaries of the same crystal fragment in high magnification. The relationship with $Nb_{53}O_{132}$ can be described as follows:

Each $(4 \times 3)_2$ strip of $Nb_{53}O_{132}$ ($\uparrow$C in Plates 10 and 11) terminates when it meets a pair of $(5 \times 3)_\infty$ ribbons of the $Nb_{43}O_{107}$ structure. As this phenomenon is repeated consistently on the (101) (ReO_3) plane, the two structures appear to have intergrown on that plane. This is illustrated in the model shown in Fig. 14 in which the $(4 \times 3)_2$ strips ($\uparrow$C) are given in green, pair of $(5 \times 3)_\infty$ ribbons in brown and the H-Nb_2O_5 ($\uparrow$D) in yellow.

It can be noticed from Plates 10 and 11, as well as from Fig. 14, that intergrowth of $Nb_{43}O_{107}$ with H-Nb_2O_5 has taken place on the $(20\bar{9})$ (ReO_3) plane which is a common CS plane for the two structures.

PLATE 11

PLATE 11

High magnification of intergrowth boundaries of H-Nb_2O_5 (labelled Y), $Nb_{53}O_{132}$ (labelled X) and $Nb_{43}O_{107}$ (labelled Z).

The Plate reveals the structural relationship between $Nb_{53}O_{132}$ (1:1 intergrowth of H-Nb_2O_5 $\uparrow$D and $Nb_{25}O_{62}$ $\uparrow$C) and $Nb_{43}O_{107}$: Each $(4x3)_2$ strip ($\uparrow$C) of $Nb_{53}O_{132}$ terminates when meeting a pair of $(5x3)_\infty$ ribbons of $Nb_{43}O_{107}$. The two structures appear to have intergrown on the $(101)_R$ plane.

Intergrowth of $Nb_{43}O_{107}$ with H-Nb_2O_5 has taken place on the $(20\bar{9})_R$ plane, as also visible in Plate 10 and Fig. 14.

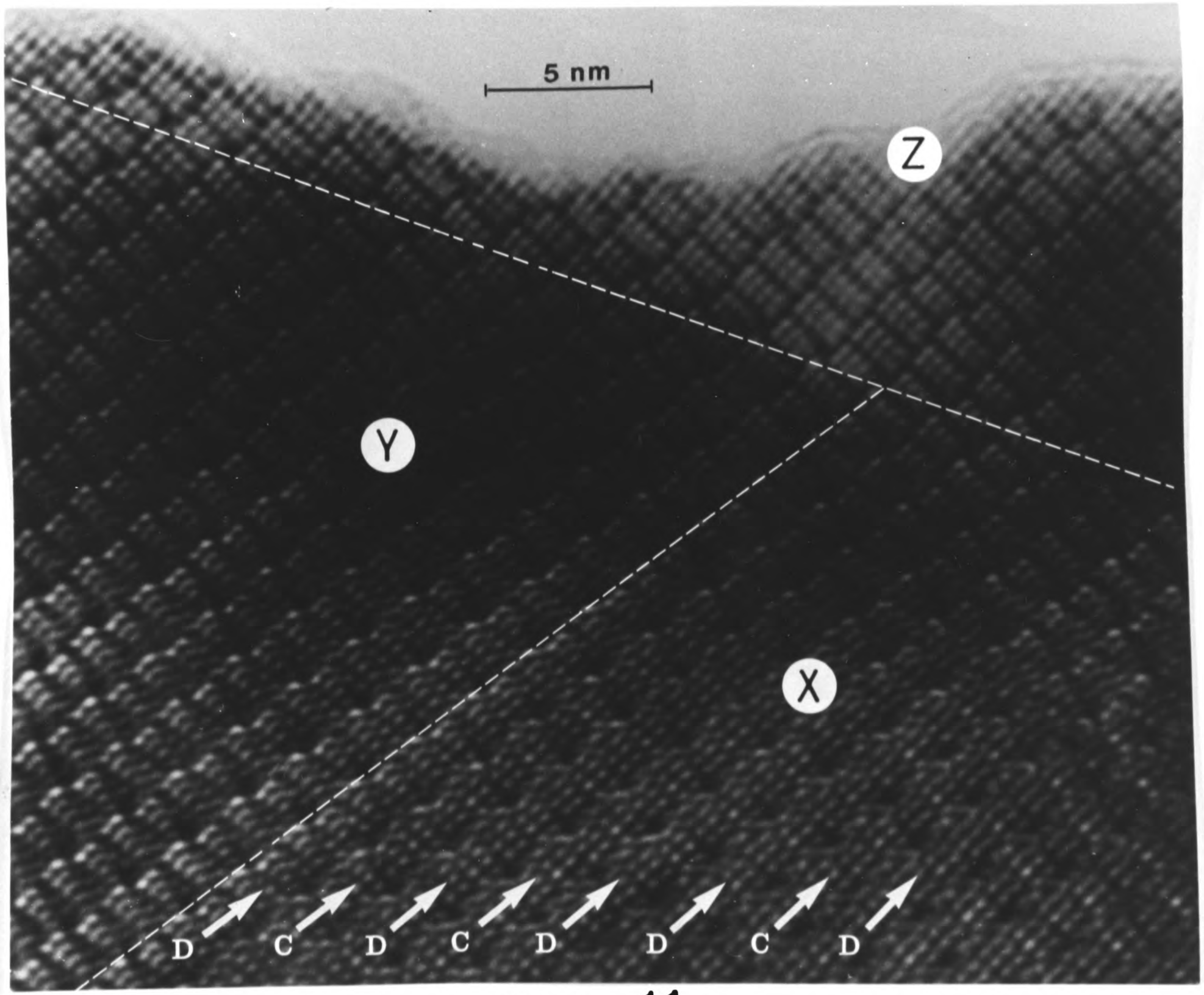

Plate 11

17 AUG 1978

(4) On the basis of structural relationships explained in (3), Plates 10 and 11 give direct evidence for a mechanism of the transformation of H-Nb_2O_5 ($Nb_{28}O_{70}$) → $Nb_{53}O_{132}$ → $Nb_{43}O_{107}$. Fig. 15 shows an idealized model for the second step; the two structures are drawn in a way to show the superposition of one upon the other. The $Nb_{53}O_{132}$ structure is drawn in black lines and $Nb_{43}O_{107}$ is depicted in yellow rectangules. The metal atom positions of both structures are given by small circles; full circles represent atoms situated in the Y = 0 level, open circles belong to the Y = $\frac{1}{2}$; arrows indicate the necessary co-operative movement which atoms should undergo in order to rearrange the $[(4 \times 3)_1 + (4 \times 3)_2 + (5 \times 3)]_\infty$ into $[(4 \times 3)_1 + 2(5 \times 3)]_\infty$ configuration. The mechanism is based on the principle that in low temperature phase conversion, unilateral atomic migrations should take place in single steps towards vacant sites in the immediate vicinity (Wadsley and Andersson, 1970).

The atomic reshuffling comprises three different components (1-3 below), which are indicated by arrows in the proposed model Fig. 15:

1) Displacement in the same level with preservation of the metal-atom octahedral co-ordination:

Along $(101)_R$ the entire $(010)_R$ string of ...-O-Nb-O-Nb-... displaces in unison through the octahedron edges ~ 2.90 Å to occupy an identical position in the adjacent tetrahedral channels. In this way, the octahedral co-ordination of cations is retained within the block structure of the new phase. The oblique arrows (↘), in the Figure, indicate

FIGURE 15

FIGURE 15

Idealized model for a possible mechanism involved in the transformation of $Nb_{53}O_{132}$ (drawn in black rectangles) into $Nb_{43}O_{107}$ (yellow rectangles) -- (Section 5.1.3.2.).

The metal atom positions of both structures are shown as small circles: full circles represent atoms situated in the y = 0 level, open circles represent atoms in the y = $\frac{1}{2}b$ level. Arrows indicate the necessary co-operative movements which atoms should undergo in order to rearrange $Nb_{53}O_{132}$ into $Nb_{43}O_{107}$. (P - S) shows the structural change at the interface of the two structures.

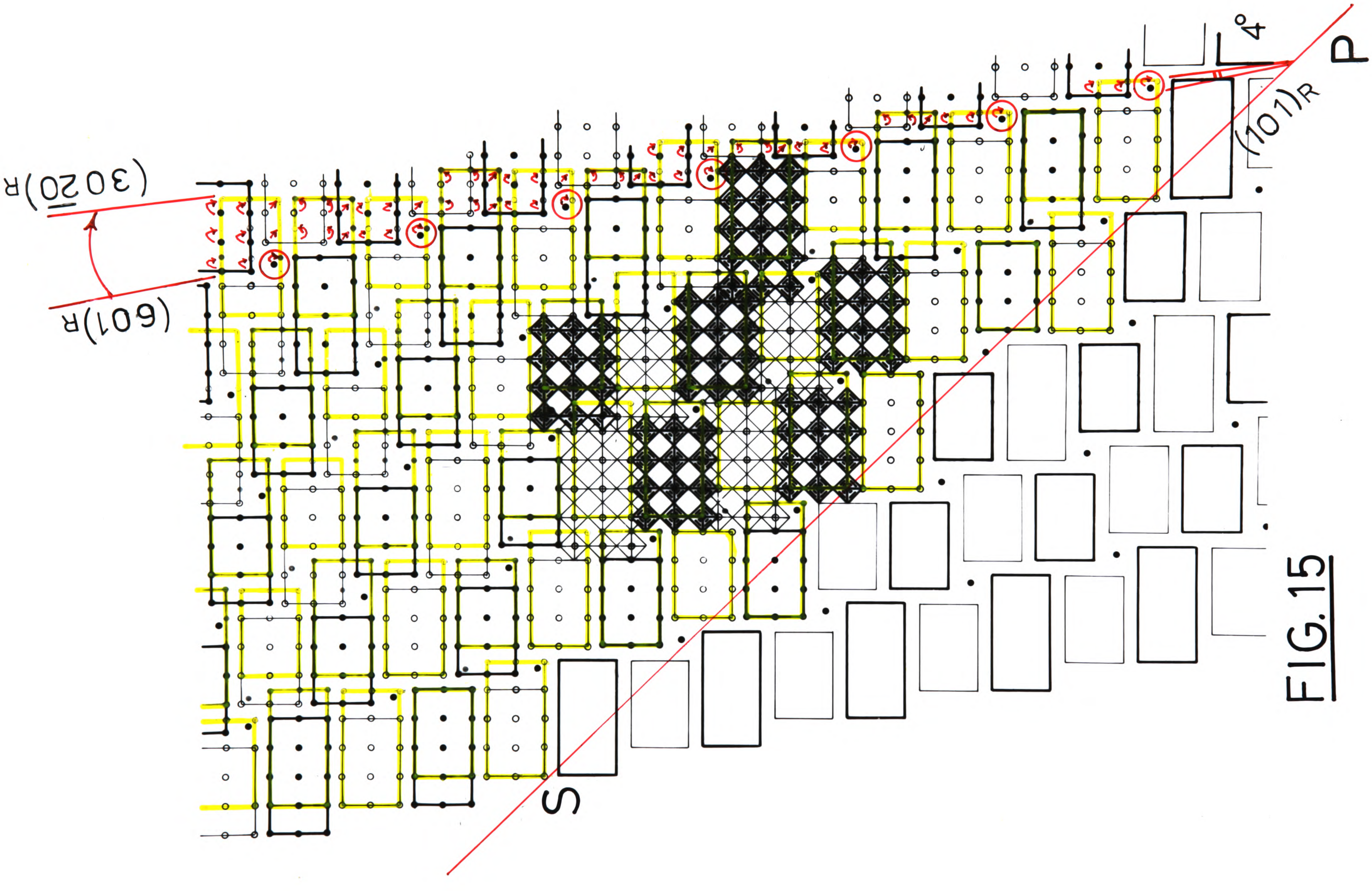

FIG. 15

such movements.

2) Displacement by change of site and level but retaining the octahedral co-ordination:

Localized migration of Nb-O atoms in the direction of $(120)_R$, through the octahedron edges $\sim$ 2.90 Å generates metal atoms in a new octahedral environment. The cation level changes from Y = 0 to Y = $\frac{1}{2}$. Such atomic motion is shown by arrows of the type (↘). The comparable migration from Y = $\frac{1}{2}$ to Y = 0, along the $(\bar{1}20)_R$ is indicated by arrows (↗).

3) Displacement accompanied by change of site, level and metal atom co-ordination number:

The new structure, i.e. $Nb_{43}O_{107}$, contains a lower proportion of tetrahedrally co-ordinated cations than $Nb_{53}O_{132}$. The calculated difference of 1.45% shows that tetrahedral sites have been eliminated and the remaining tetrahedral sites, as can be seen in the model, have moved in position. The former tetrahedral sites, as well as the newly created ones, are indicated by large circles in the model.

The elimination of tetrahedrally co-ordinated atoms takes place by a shift to the vacant octahedral positions in their immediate proximity. Hence, a single niobium atom alters its level from Y = $\frac{1}{4}$ to $\frac{1}{2}$ along $(111)_R$ or from Y = $\frac{1}{4}$ to Y = 0 in the direction of $(1\bar{1}\bar{1})_R$. In the creation of tetrahedral sites, niobium atoms move from the octahedron position to a newly formed tetrahedral environment, again along $(111)_R$ directions.

According to this mechanism, the stoichiometric change

in the process of phase transformation is adjusted by altering the proportion of (5 x 3) and (4 x 3) block sizes as well as the proportion of apex-sharing and edge-sharing octahedral co-ordination (i.e. decrease in the number of tetrahedral sites).

An essentially identical mechanism can be advanced for the direct transformation of H-Nb_2O_5 into $Nb_{43}O_{107}$. The situation shown in Fig. 16 indicates that three simultaneous reduction processes are taking place:

Along the interface R - U, the direct reduction of H-Nb_2O_5 to $Nb_{43}O_{107}$ is taking place. Along R - K, H-Nb_2O_5 is transforming into $Nb_{53}O_{132}$, which in turn is reducing to $Nb_{43}O_{107}$ along R - S. The mechanism for the reaction taking place along R - K has been discussed by Anderson (1974).

An interesting feature of the intergrowth shown in Fig. 16 is that the shear planes in the three phases are slightly misaligned with respect to each other. Thus the $(601)_R$ CS plane in H-Nb_2O_5 (indicated by R - K) is 4° out of alignment from the $(30\bar{2}\bar{0})_R$ plane (R-L in $Nb_{43}O_{107}$); the $(601)_R$ plane of $Nb_{53}O_{132}$ (M-O) is also 4° out of alignment with (O-N) in $Nb_{43}O_{107}$. As the interface between $Nb_{43}O_{107}$ and the other phases advances, the atoms in the new structure must progressively shift in order to accommodate this difference. At the interface itself, there will be a strain energy associated with the change in direction of the CS planes. By the time the S - R and U - R interfaces have reached S'-R' and U'-R', the $(30\bar{2}\bar{0})_R$ CS plane in $Nb_{43}O_{107}$ will have shuffled across to the line O'-N' and R'-L'

FIGURE 16

FIGURE 16

Idealized model showing features of three simultaneous reduction processes (Plates 10 and 11), namely, the conversion of H-Nb_2O_5 → $Nb_{43}O_{107}$, H-Nb_2O_5 → $Nb_{53}O_{132}$ and $Nb_{53}O_{132}$ → $Nb_{43}O_{107}$ along the respective interfaces R - U, R - K and R - S.

The rotation of shear planes through 4° on the intergrowth boundaries is indicated by (R - K, R - L) and (O - M, O - N), respectively. The interfaces R' - U' and R' - S' depict the advance of the reduction front in the crystal. Broken lines of O' - N' and R' - L' show the shuffling of shear planes during the reduction process (Section 5.1.3.2.).

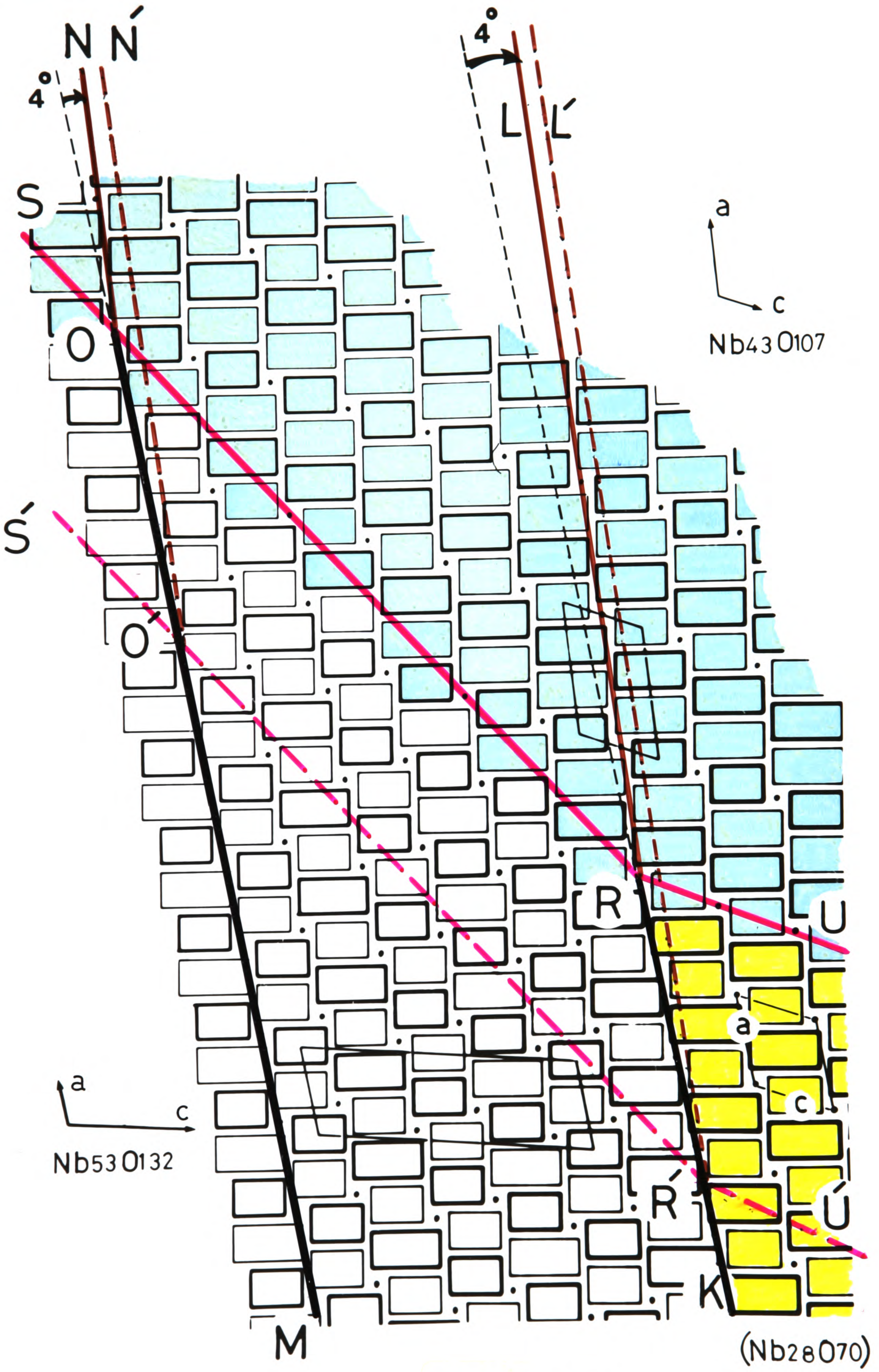

FIG. 16

respectively. There is of course no way of knowing which of the phases actually rotates, only the relative motions can be discussed.

In Fig. 15, the $Nb_{53}O_{107}$ plane is shown as black blocks and the new $Nb_{53}O_{107}$ plane as yellow blocks. The changes taking place at the interface (P-S) are shown, together with the history of changes that have taken place where the interface has already passed.

II Defect properties of monoclinic $Nb_{12}O_{29}$

Plate 12 shows an m-$Nb_{12}O_{29}$ structure, intergrown with (5 x 3) strips of Wadsley defects. The structure of the host consists of ribbons of (4 x 3) octahedra linked through by edge sharing. It is the lowest block structure oxide found in the reduction of H-Nb_2O_5. $Nb_{12}O_{29}$ represents the second member (n = 4) of the homologous series with the general formula of $M_{3n}O_{8n-3}$. Neither the lowest (n = 3) nor the higher members (n = 5 and 6) of the series have yet been reported in studies of the pure reduced oxide. Recently, however $MgNb_{14}O_{35}F_2$ was shown to have the structure of the member (n = 5) (Lundberg, 1970).

In the crystal fragment shown in Plate 12, the $Nb_{15}O_{37}$-type strips are randomly distributed and constitute a high density of Wadsley defects, intergrown on the (001) plane of the m-$Nb_{12}O_{29}$ (↑A in Plate 12). In the area (X) shown in Plate 12, the extension of (5 x 3) strips into the bulk of the crystal is interrupted by intersection with the $(10\bar{1})$ defect (↑J) as well as the occurrence of faulty

PLATE 12

PLATE 12

Two-dimensional lattice image of an ordered crystal fragment taken from a transformed-reduced B-Nb_2O_5 sample prepared at isotherm 850°C and p_{O_2} = 5.30×10^{-20} (Section 5.1.3.1. d and e).
The Plate shows the ordered structure of m-$Nb_{12}O_{29}$ with frequent occurrence of (5x3) strips of Wadsley defects (↑ A). Strips of (5x3) blocks represent local stoichiometry of $Nb_{15}O_{37}$. (↑ J) indicates a $(10\bar{1})$ $Nb_{12}O_{29}$ defect which intersects the (5x3) strips in the crystal. In the micro-domains labelled S and U, the (5x3) and (4x3) blocks are stacked in a zig-zag arrangement similar to the one (↑ S) present to the right in the Plate.
(↑ L) indicates incorporation of tetrahedral sites in the matrix.
(↑ N) shows occasional intergrowth of (4x4) blocks with m-$Nb_{12}O_{29}$. Strips of o-$Nb_{12}O_{29}$ intergrown with the matrix are indicated by (↑ B) (Section 5.1.3.2.).

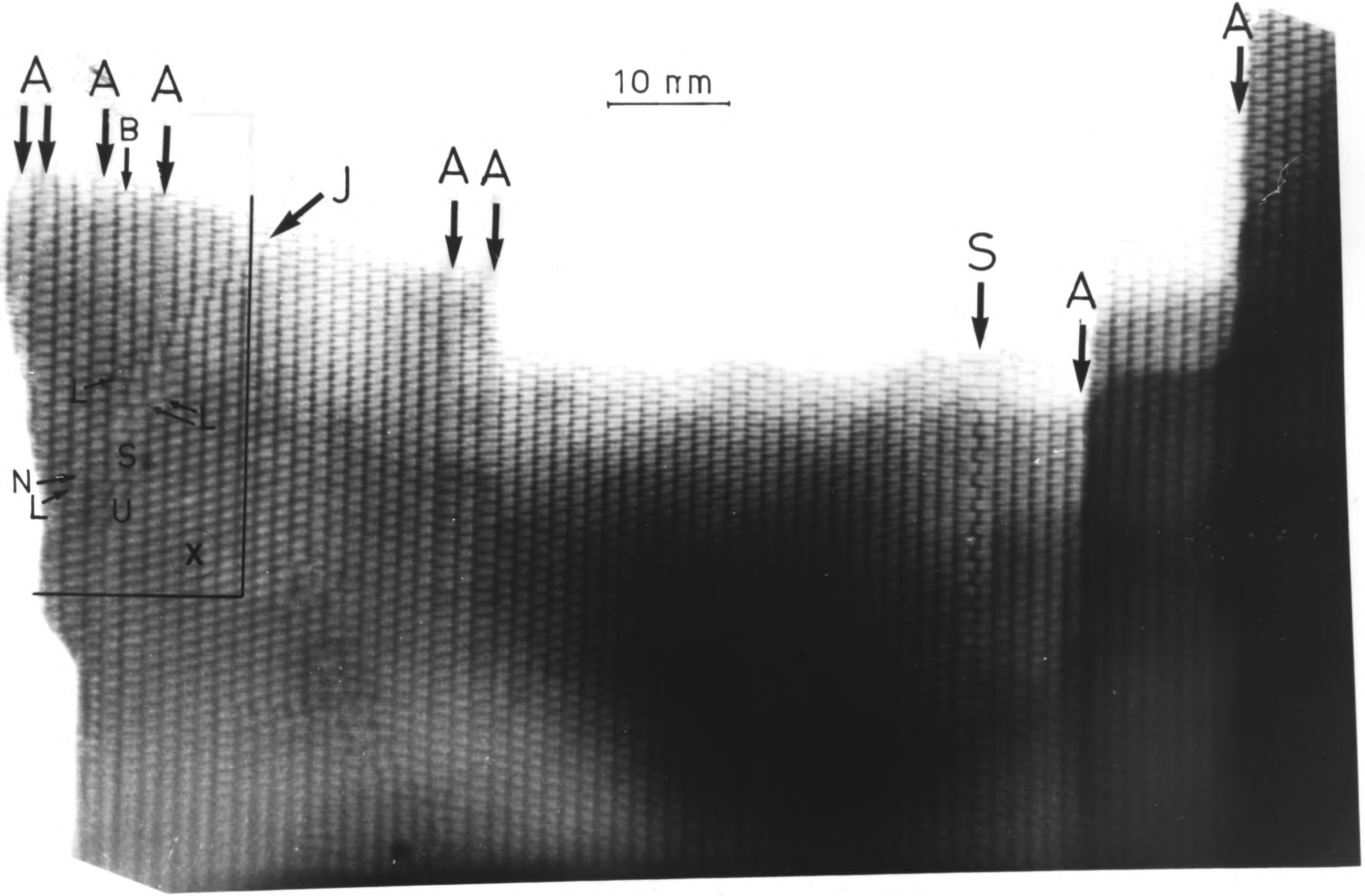

Plate 12

microdomains (labelled S and U in Plate 12 and Fig. 17). In the regions (S and U), the (5 x 3) and (4 x 3) blocks are stacked in a zig-zag arrangement, similar to the one to the right in Plate 12 (↑S); some tetrahedral sites (↑L) and an occasional intergrowth of (4 x 4) blocks (↑N) can also be found in the defective microdomains.

Defects associated with the stoichiometric change of m-$Nb_{12}O_{29}$ structure, previously reported in the literature (Browne, 1973), are also present in Plate 12.

Defect along the (001) plane: Parallel to (001) plane, the isolated strips of o-$Nb_{12}O_{29}$ modification have intergrown coherently with the matrix (↑B). The $(4 \times 3)_\infty$ ribbon stacking has been reversed at this interface.

Defect along the $(10\bar{1})$ plane: Along $(10\bar{1})$ of the matrix (↑J), the (4 x 3) blocks have rotated by 90°. As a result, the $(4 \times 3)_\infty$ ribbons have shifted laterally at this boundary.

5.1.4. DISCUSSION

Thermodynamic Consideration

Concerning the thermal behaviour of B-Nb_2O_5 in different temperature regions ($T > 900^\circ C$ and $750^\circ C < T < 900^\circ C$, respectively) the following can be stated:

The present observation that phase conversion of B-Nb_2O_5 to block based structures takes place readily above 900°C under atmospheric conditions is in accordance with Schäfer *et al*'s view (1966) that such conversion is monotropic

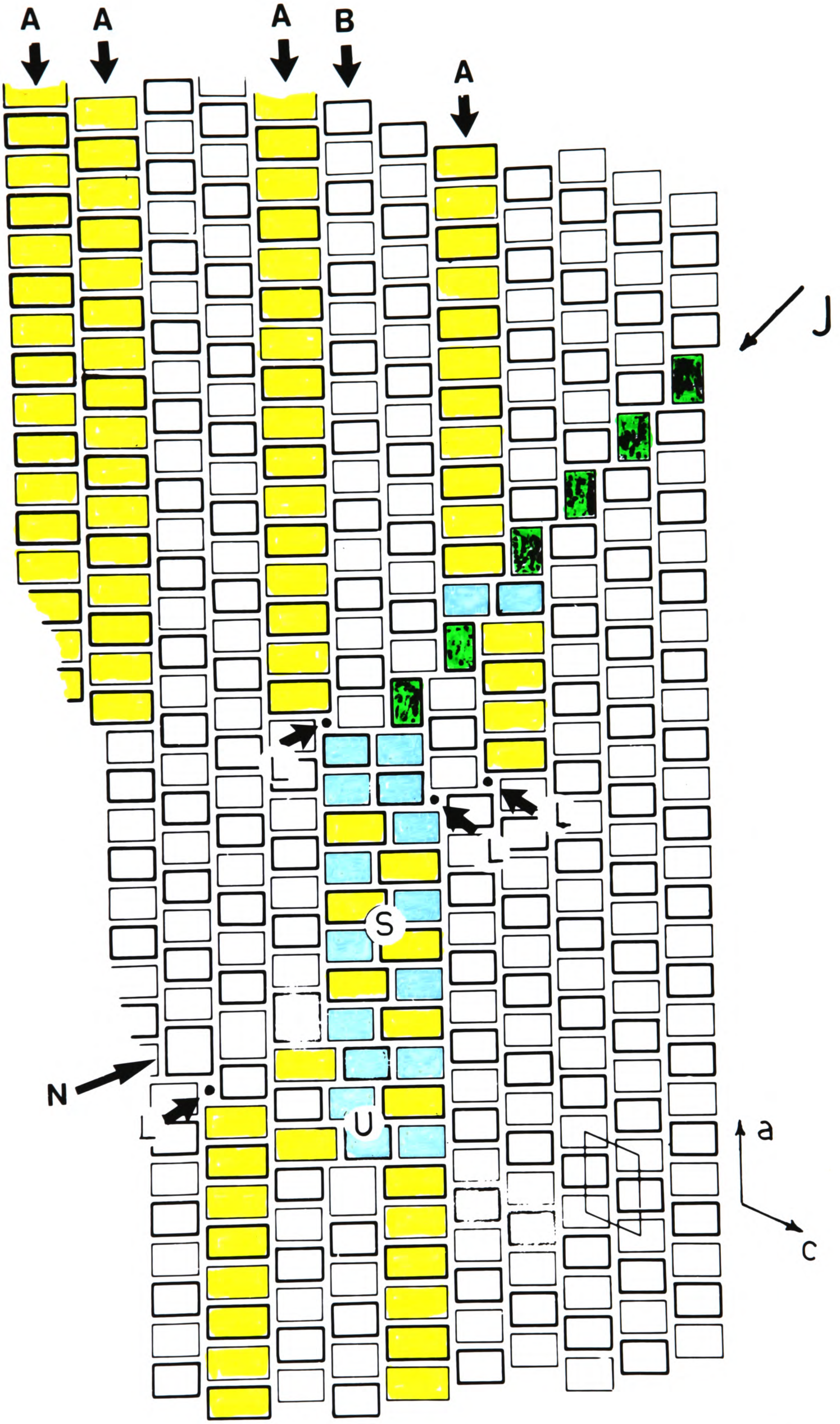

FIG.17 Idealized model of the area X outlined in Plate 12. The model shows details of the defect structure of m-$Nb_{12}O_{29}$ as has been mentioned in Plate 12.

and the transition temperature ($T > 900^{o}C$) is therefore kinetically controlled. In addition, Lapitskii et al (1952) have shown that the conversion of the B-Nb_2O_5 to H-Nb_2O_5 occurs slowly at about $900^{o}C$. (It should be emphasized that the present experiments and those of Schäfer and Lapitskii were carried out in the absence of seeding agents such as H-Nb_2O_5).

Within the thermal range of $750^{o} < T < 900^{o}C$, B-Nb_2O_5 was apparently stable under atmospheric conditions, but when a reducing atmosphere was introduced, the B- → block structure transformation and reduction was accelerated particularly where the sample was in contact with the surface of the platinum container. When the partial pressure of oxygen was reduced, the reaction was found to advance from the lowest layer of the sample towards the uppermost part (see isotherm $880^{o}C$, Section 5.3.1.3.). The effect of the platinum surface is assumed to be catalytic. However, no conversion was found when a mixture of platinum black powder and B-Nb_2O_5 sample was used under otherwise identical conditions. These conflicting results may be due to physical differences between the surfaces of the platinum powder and the platinum container.

The differences in behaviour of B-Nb_2O_5 under oxidizing and reducing conditions indicate: a) B-Nb_2O_5 is thermodynamically unstable above $750^{o}C$, even in air, and b) the transformation rate of B-Nb_2O_5 to block type structures in the temperature range $750^{o}C$ - $900^{o}C$ is so slow in air that B-Nb_2O_5 can be considered to be metastable in a super-heated state above its transition temperature. The

transformation appears to be accelerated by the presence of block structures which form more readily under reducing conditions at the environment of the platinum foil surface. The effect of seeding B-Nb_2O_5 with block structures has also been reported by Schäfer *et al* (1966) and Kodama *et al* (1972). According to them, isothermal heating of B- and H-Nb_2O_5 mixture at 750°C in an $NbOCl_3/Cl_2$ atmosphere results in the full conversion of B- into H-Nb_2O_5.

At 750°C, no conversion to block structure was detected, even under reducing conditions. Phase equilibria studies of B-Nb_2O_5 were therefore carried out at that particular isotherm.

Structural Consideration

The combination of X-ray powder diffraction, electron diffraction and electron microscopy applied in the structural study of the transformed B-Nb_2O_5 crystals above 750°C, shows that the phases generated, in most cases, are extremely disordered block structures (see Plates 6, 7 and 8). This disorder might be attributed to the slow rate of the ordering process. Yamawaki *et al*, (1974) in X-ray powder diffraction studies of oxidized Nb-2.5 at % Mo alloy specimens at 835°C, reported that the B- to H-Nb_2O_5 conversion takes place via the formation of M-Nb_2O_5. However, evidence presented in this study (Plates 6, 7 and 8) shows that M-Nb_2O_5 formation does not occur, even in the micro-domain scale. It is interesting to note that the diffuse characteristic of the X-ray powder patterns of the transformed B-Nb_2O_5 crystals (e.g. see *f* in Plate 4-A), as well as their measured d-values, are in close agreement with those

published for M-Nb_2O_5 (Schäfer et al, 1966; Mertin et al, 1970). Selected area electron diffraction patterns of the (h0l) sections of the disordered crystal fragments (insets in Plates 6, 7 and 8) also give the impression that the basic ReO_3-type subcell orientation is maintained and that the square grid array of reflections probably arises from a tetragonal structure. In an electron microscopy study of M-Nb_2O_5 single crystals, Browne (1973) has shown a similar diffraction pattern and has been able to index it on the basis of the M-Nb_2O_5 parameters reported by Mertin et al, (1970). Browne concluded that the steaked reflections at 45° to the grid axis were associated with the occurrence of disordered structures running parallel to the (100) and (010) directions of M-Nb_2O_5. However, in the present work, M-Nb_2O_5 was not found as an intermediate phase in the conversion process of B- into H-Nb_2O_5. The multiple orientations of different blocks with different sizes, coherently packed in a complex disordered manner, clearly results in a diffraction pattern with an artificially high symmetry. This phenomenon has also been observed by Iijima (1974) in an electron microscopy study of ferrous oxide.

In view of these observations, it is worthwhile reviewing the history of M-Nb_2O_5. This modification was first identified by Brauer (1941). According to Brauer, incremental heating of amorphous Nb_2O_5 resulted in a number of irreversible changes. At 500°C, T-Nb_2O_5 (low temperature phase) formed and at 1000°C the T-phase transformed into M-Nb_2O_5 (a middle temperature phase). Finally, at 1100°C, the M-Nb_2O_5 transformed to H-Nb_2O_5. Schäfer et al (1954;

1966) re-examined these Nb_2O_5 modifications and confirmed Brauer's findings. Holtzberg and Reisman (1957) examined the stability range of these Nb_2O_5 modifications by differential thermal analyses and reported that the β (M-form) is an imperfectly crystallized α phase (H-Nb_2O_5). Goldschmidt (1958), on the basis of *in situ* high temperature X-ray studies of Nb_2O_5, reported that β (M-form) and α (H-form) were probably the same phase. Schäfer *et al.*, (1966) gave a list of d-values for M-Nb_2O_5. They speculated that the M-modification was a less ordered precursor for H-Nb_2O_5. Recently, however, Mertin *et al.*, (1970) have reported a definitive structure for M-Nb_2O_5 based upon single crystal X-ray measurements. The structure apparently comprises $(4 \times 4)_\infty$ blocks with a tetragonal unit cell, having parameters of a = 20.44 Å and b = 3.832 Å. On the other hand, Kodama *et al.*, (1972) excluded M-Nb_2O_5 in their thermodynamic studies of niobium pentoxide polymorphs and reported that the stability of M-Nb_2O_5 depends largely on the presence of impurities. Browne (1973) studied M-Nb_2O_5 by both single crystal X-ray and electron diffraction. He concluded that M-Nb_2O_5 probably occurs in intergrowth with N- and H-Nb_2O_5.

The high resolution electron microscopy results presented in the present work strongly suggest that the M-modification of Nb_2O_5 does not exist as a discrete phase in that system.

It is shown, in this study, that the transformed B-Nb_2O_5 crystals comprise both ordered and disordered structures. The study of ordered crystals has given further

insight into the chemistry of the Nb-O system. Plate 10 shows the simultaneous occurrence of three ordered intermediate phases, namely $Nb_{28}O_{70}$ (H-Nb_2O_5), $Nb_{53}O_{132}$ and $Nb_{43}O_{107}$; these are coherently intergrown in one crystallite. The system might be considered in terms of Ubbelohde's hybrid crystal expression (1956) in which there is an additional contribution to the free energy from the strain at the interface between intergrowth structures. Under these circumstances, the classical Gibbs phase rule does not apply. Our results are therefore not inconsistent with thermodynamic measurements which reveal bivariant behaviour in this composition range (Nimmo and Anderson, 1972).

Nimmo and Anderson (1972), in a kinetic study of H-Nb_2O_5 reduction, concluded that the course of reaction is determined by two kinetically distinct type of processes: one is relatively easy and rapid at 1000°C and the other is a process of higher activation energy. At temperatures T < 1000°C, the co-operative ordering processes are very slow and intermediate intergrowth structures may only be observed at higher temperatures. According to Nimmo and Anderson, within the composition range of e.g. $NbO_{2.5}$ - $NbO_{2.48}$, phase conversion can be written as follows:

$$Nb_{28}O_{70}(\text{H-}Nb_2O_5) \dashrightarrow Nb_{25}O_{62} \text{ at } 1000^{\circ}C$$
$$[(5 \times 3)_{\infty} + (4 \times 3)_1] \quad (4 \times 3)_2$$
$$Nb_{28}O_{70} \rightarrow Nb_{53}O_{132} \rightarrow Nb_{25}O_{62} \text{ at } 1100^{\circ}C$$
$$\text{1:1 intergrowth}$$

However, the results of the present study indicate that the formation of intergrowth structures, as stable

entities, does take place at lower temperatures.

The $Nb_{43}O_{107}$ structure, found in this study (see Plate 10) is a new phase in the Nb-O system. The occurrence of this structure has not been reported in earlier works (Schäfer et al, 1969; Nimmo and Anderson, 1972; and Kimura, 1973) and, this probably, is due to the inadequacy of conventional X-ray diffraction methods applied previously in the phase analysis of complex systems of this type. According to the present results, the reaction sequence within the composition range of $NbO_{2.50}$-$NbO_{2.48}$ is as follows:

$Nb_{28}O_{70}$ (H-Nb_2O_5)

$[(5 \times 3)_\infty + (4 \times 3)_1]$

↓

$Nb_{53}O_{132}$

$[(5 \times 3)_\infty + (4 \times 3)_1 + (4 \times 3)_2]$

1:1 intergrowth of $Nb_{28}O_{70}$ and $Nb_{25}O_{62}$ structures

↓

$Nb_{43}O_{107}$

$[2\,(5 \times 3)_\infty + (4 \times 3)_1]$

↓

$Nb_{25}O_{62}$

$(4 \times 3)_2$

From this reaction pathway, it is evident that the intergrowth structure need not necessarily be constructed from the two adjacent compounds.

The nucleation of the reduction reaction probably takes place randomly and the initial lamellae of transformed

structure, which might be regarded as Wadsley defects, propagate into the bulk of crystal (see F↑ and C↑ in Plate 10). A similar effect has also been observed in Nb_2O_5 by Nimmo and Anderson (1972) and in TiO_2 by Anderson and Tilley (1970).

5.2.

PART B: PHASE EQUILIBRIA IN THE SYSTEM NbO_2-(B-Nb_2O_5)

TABLE 10

TABLE 10

		P_{O_2}	log P_{O_2}
CO_2/H_2 =	4.67	9.84×10^{-20}	-19.01
	3.10	4.54×10^{-20}	-19.34
	2.02	2.02×10^{-20}	-19.69
No reduction	1.83	1.69×10^{-20}	-19.77
	1.63	1.37×10^{-20}	-19.86
Reduction in slow rate	0.98	5.29×10^{-21}	-20.28
	0.93	4.86×10^{-21}	-20.31
	0.81	3.76×10^{-21}	-20.42
	0.71	2.91×10^{-21}	-20.54
	0.60	2.14×10^{-21}	-20.67
	0.55	1.85×10^{-21}	-20.73
Reduction in slow rate of weight loss	0.43	1.47×10^{-21}	-20.94
	0.39	9.93×10^{-22}	-21.00
	0.34	7.39×10^{-22}	-21.13
	0.31	6.17×10^{-22}	-21.21
	0.30	5.99×10^{-22}	-21.22
	0.26	4.59×10^{-22}	-21.34
	0.25	4.39×10^{-22}	-21.36
	0.22	3.42×10^{-22}	-21.47
	0.16	1.90×10^{-22}	-21.72
	0.16	1.75×10^{-22}	-21.76
	0.13	1.28×10^{-22}	-21.89
	0.13	1.24×10^{-22}	-21.90
Fast reduction	0.10	7.34×10^{-23}	-22.13
	0.10	7.06×10^{-23}	-22.15
	0.05	1.96×10^{-23}	-22.71

5.2.1. INTRODUCTION

B-Nb_2O_5 is derived from a PdF_3 parent structure. The B-modification consists of rutile-like ribbons of edge-shared octahedra, two octahedra wide, joined by octahedra corners (Andersson and Galy, 1970).

As B-Nb_2O_5 is thermodynamically stable below 750°C (see Discussion of Part A), reduction equilibria of this polymorph are here studied at that particular temperature.

5.2.2. MATERIALS AND METHODS

The B-Nb_2O_5 single crystals used were prepared by the chemical vapour transport method (see Chapter II).

Reduction experiments were carried out in the Cahn RG4 microbalance reduction line (see ChapterIII), using samples of 50 mg. The required oxygen partial pressures were generated by mixing CO_2 and H_2 gases in various ratios (see Chapter III). The different ratios were introduced into the microbalance system in a stepwise fashion, starting from the highest (i.e. CO_2/H_2 = 4.67, Table 10). At each isobaric step, the mixed gas stream was allowed to circulate in the system for at least 2 hours in order to remove previous gas mixtures, which were of a different ratio, from the system and to establish the required oxygen partial pressures around the sample.

The structure of the obtained products was studied by the Guinier X-ray powder diffraction method.

TABLE 11

TABLE 11

Exp. no.	CO_2/H_2	p_{O_2}	log p_{O_2}	W % of * reduced B-Nb_2O_5	Phases
1	1.80	1.64×10^{-20}	-19.78	Nil	B-Nb_2O_5
2	0.60	2.14×10^{-21}	-20.67	Nil	B-Nb_2O_5
3	0.26	4.59×10^{-22}	-21.34	5%	Predominantly B-Nb_2O_5 + NbO_2
4	0.16	1.75×10^{-22}	-21.76	13%	Predominantly B-Nb_2O_5 + NbO_2
5	0.10	7.06×10^{-23}	-22.15	36%	B-Nb_2O_5 + NbO_2
6	0.05	1.96×10^{-23}	-22.71	42%	B-Nb_2O_5 + NbO_2
7	0.05	1.96×10^{-23}	-22.71	78%	B-Nb_2O_5 + predominantly NbO_2

* Experiments were interrupted when the required degree of reduction was attained.

5.2.3. RESULTS

In the range of $CO_2/H_2 > 0.53$, no appreciable weight loss was detected, indicating that B-Nb_2O_5 is stable under those particular experimental conditions. At lower gas ratios, namely $0.13 < CO_2/H_2 < 0.53$, the microbalance recorded a slow and continuous sample weight loss, running at an average rate of 5 μgr/hr until reduction to NbO_2 had taken place. When the gas ratio was altered to $CO_2/H_2 < 0.13$, the reduction rate increased markedly and again no intermediate phases within the range $NbO_{2.5}$-$NbO_{2.00}$ were found. However, it is possible that the phase change from B-Nb_2O_5 to NbO_2 might pass through several transient stages which are not detected under these particular conditions. To investigate this possibility, several reduction experiments were carried out in order to prepare samples at different stages of reduction (Table 11).

The samples were examined by the Guinier X-ray method and the results indicated that in the process of reduction, the B-Nb_2O_5 does not pass through intermediate stages, but transforms directly to the NbO_2 phase. This is shown in Plate (13-A) in which the X-ray diffraction pattern (b) of the 42% reduced B-Nb_2O_5 has been compared with the starting material B-Nb_2O_5 (a) and the final product NbO_2 (c). The detailed phase analysis of the X-ray diffraction pattern (b) is given in Table 12.

The validity of the above conclusion was substantiated by repeating the experiments, now with a CO_2-CO gas buffer system. This was carried out in order to minimize the effect of changes in gas composition due to thermomolecular

PLATE 13

PLATE 13

A) Guinier X-ray powder diffraction patterns of:

a) B-Nb_2O_5 (starting material)

b) 42% reduced B-Nb_2O_5 at 750°C and p_{O_2} = 1.96×10^{-23}

c) NbO_2 (rutile structure)

B) B-Nb_2O_5 collapse along the $(100)_{PdF_3}$ plane resulting in the generation of the rutile phase (Section 5.2.3.).

(A)

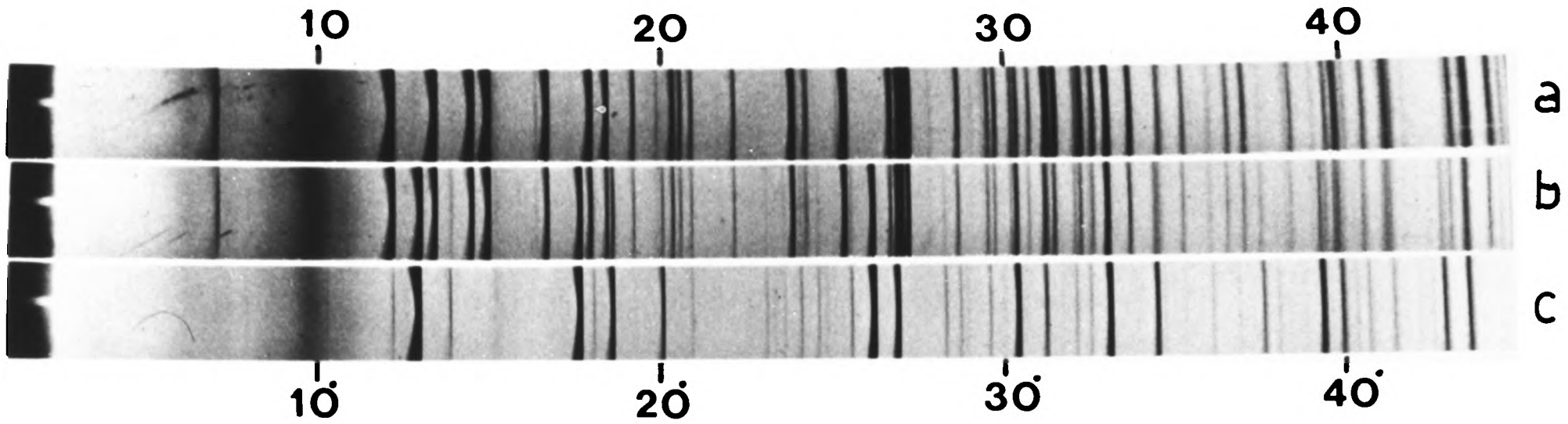

(B)

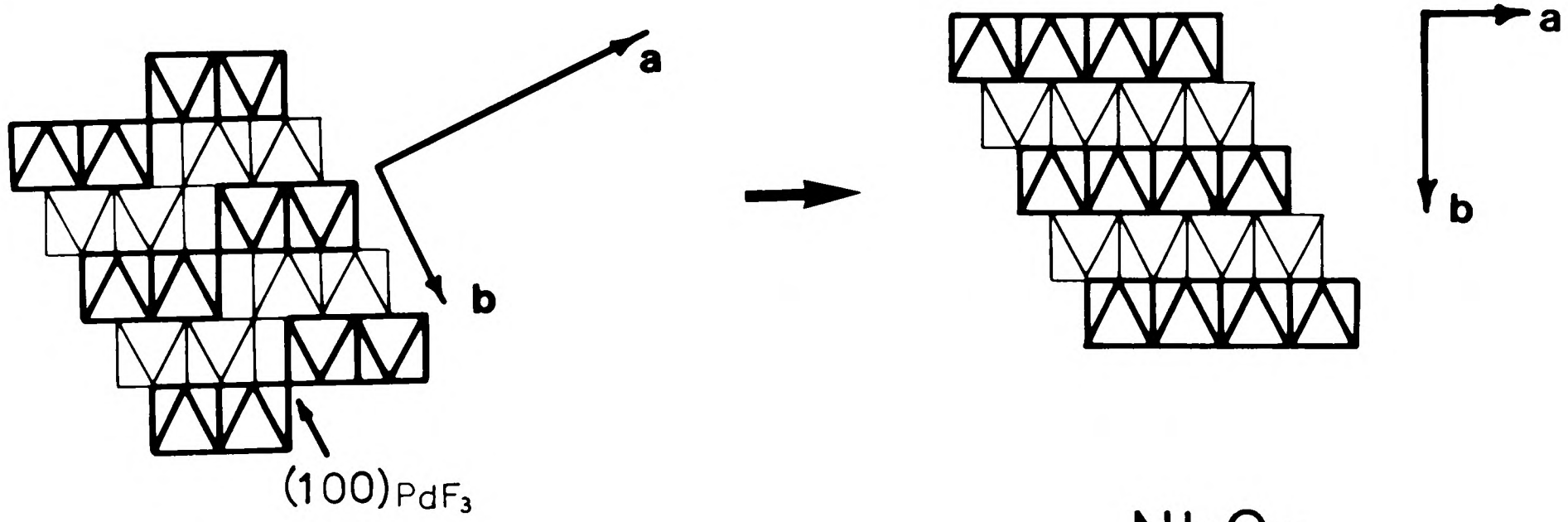

B-Nb_2O_5 NbO_2

Plate 13

TABLE 12

TABLE 12

Guinier X-ray diffraction pattern analysis of 42% reduced B-Nb_2O_5 at isotherm 750°C and $p_{O_2} = 1.96 \times 10^{-23}$ (Exp. 6, Table 11; Guinier pattern b in Plate 13-A)

I (obs.)	d (Cm)	$Sin^2\theta$ (obs.)	$Sin^2\theta$ (calc.) B-Nb_2O_5	hkl (B-Nb_2O_5)	$Sin^2\theta$ (calc.) NbO_2	hkl (NbO_2)
s	2.01	0.015699	0.01585	002	———	———
v.s.	3.41	0.044739	0.04475	$\bar{1}11$	0.04508	301
v.s.	3.63	0.050595	———	———	0.05066	400
v.s.	3.77	0.054499	0.05463	111	———	———
w	3.89	0.057954	———	———	0.05774	231 321
v.s.	4.07	0.063323	0.06339	004	———	———
v.s.	4.18	0.066713	0.06657	$\bar{1}13$	———	———
w	4.57	0.079387	0.07916	$\bar{2}02$	———	———
v.s.	4.68	0.083144	0.08308	200	———	———
v.s.	4.92	0.091613	———	———	0.09165	222 431
v.s.	5.03	0.095618	0.09621	113	0.09574	341 501
s	5.14	0.099700	0.09985	020	———	———
s	5.19	0.101580	———	———	0.10132	440

m	5.36	0.108089	0.10695	$\bar{2}04$	0.10840	521 251
v.w.	5.55	0.115573	0.11569	022	———	———
m	5.59	0.117177	———	———	0.11698	402
m	5.68	0.120819	0.12061	120	———	———
m	5.75	0.123685	0.12401	015	———	———
m	5.82	0.126580	0.12658	$\bar{1}22$	0.12665	260 620
m	6.20	0.142789	0.14263	006	———	———
v.v.w.	6.29	0.146748	———	———	0.14640	541 451
v.v.w.	6.42	0.152544	———	———	0.15238	103
v.v.w.	6.57	0.159347	———	———	0.15906	361
v.s.	0.65	0.163024	0.16324	024	———	———

flow around the reduction zone.

5.2.4. DISCUSSION

The formation of the rutile structure of NbO_2 as the only product of the B-Nb_2O_5 reduction probably takes place through the abstraction of the apical oxygen layers parallel to the (100) PdF_3 planes (Plate 13-B). As a result, the two halves collapse and shear to form the rutile structure. In this manner, the first member of the M_nO_{3n-1} homologous series is generated from the reduction of the second one.

Of all Nb_2O_5 modifications, only B-Nb_2O_5 single crystals, prepared in an oxidizing atmosphere (see Chapter II) occur occasionally in a bluish tint (Gruehn et al, 1964; Schäfer et al, 1966; Emmeneger et al, 1968; Browne, 1973; this study, Chapter II). Schäfer et al (1966) suggested that the bluish colour of the B-form might arise from additional incorporation of Nb atoms in unoccupied sites of the B-Nb_2O_5 structure. Emmeneger and Robinson (1968) reported that in B-Nb_2O_5 grown above 1000°K, the bluish tint coincides with the presence of 250 to 900 ppm of SiO_2 which probably had been transported to the growing crystal by trace quantities of water in the silica transport ampoule. Such bluish Nb_2O_5 crystals, according to the above and the present authors, can be made colourless by annealing them for several hours at 800°C in air or oxygen. However, in some crystals the blue colour does not disappear even under prolonged annealing. Yamawaki et al (1974), on the basis of structural principles of B-Nb_2O_5 described by Laves et al

(1964), attributes this to the fact that B-Nb_2O_5 constitutes an effective barrier against the diffusion of oxygen. However, in view of the results of the present study it is tentatively suggested here that the observed bluish tint is probably due to occasional intergrowth of the rutile-based shear structure of B-Nb_2O_5 with NbO_2, giving rise to Wadsley defects which cannot be detected by conventional X-ray measurements.

CHAPTER VI

THERMODYNAMICS AND STRUCTURAL ASPECTS OF P-Nb_2O_5 PHASE TRANSFORMATION

Part A) Phase transformation of P-Nb_2O_5 into H-Nb_2O_5

Part B) Phase equilibria in the system NbO_2- (P-Nb_2O_5)

6.1. INTRODUCTION

Single crystals of P-Nb_2O_5 were synthesized for the first time by Schäfer *et al* (1964) by chemical vapour transport reactions. Almost concurrently, P-Nb_2O_5 was obtained in an independent study by Petter and Laves (1965). They detected the new polymorph, which was designated by them as η -Nb_2O_5, in hot to cold iodine transport experiments.

The crystal structure of the η -phase (Schäfer's P-phase) was determined by Petter and Laves (1965). They indexed single crystal films on the basis of a "tetragonal" unit cell with a = 3.896 Å and c = 25.43 Å and reported that the optical data of the crystal indicated a bi-axial characteristic which might have been due to sub-microscopic twinning of the structure. Wadsley and Andersson (1970), in their comprehensive review, state that the structure of P-Nb_2O_5 is based on the ReO_3 sub cell and can be described in terms of (CS) planes as is illustrated in their figure (see B in Plate 14). There are two kinds of shear planes in P-Nb_2O_5; the first one is derived from the ReO_3 parent by a shear of half a lattice vector in the direction $[\bar{1}\bar{1}0]$ and the second one can be described as a shear operation whose vector is $a/2\,[0\bar{1}\bar{1}]$. The two (CS) planes alternate in parallel to the (010) ReO_3, dividing the structure into slabs ($2 \times \infty \times \infty$) octahedra wide (see Plate 14-B).

Another modification of Nb_2O_5, grown also by a vapour transport method using either halogen or a halogen-water mixture, was characterized by Gruehn (1966). He designated this compound as R-Nb_2O_5 and showed that it had a monoclinic

structure with lattice parameters of a = 3.98 Å, b = 3.82 Å, c = 12.791 Å and β = 90° 45'. This phase is structurally comparable to a distorted idealised V_2O_5 structure, (Bachmann, et al., 1961; Andersson, 1965). There is also a close similarity between P- and R-Nb_2O_5, as both contain only shear planes parallel to the (010) plane of ReO_3. The structure of the R-form is less complicated and contains only one kind of shear plane which is generated by the operation of shear whose c vector is also a/2 $[0\bar{1}\bar{1}]$ (Wadsley and Andersson, 1970). Both compounds (i.e. P- and R-Nb_2O_5) represent members (n = 2) of a homologous series of phase M_nX_{3n-1}, but as differences exist in the shear planes of their structures, ideally, each should be classified in a different series.

Gruehn (1966) reported that R-Nb_2O_5 transforms into the P-form at 760°C. This suggests that R- is less stable than the P-modification. Browne (1973) studied P-Nb_2O_5 by electron microscopy and found "streaking" along the c* direction of the (h0l) section of an electron diffraction pattern. He suggested that the fault might be due to a structural intergrowth of P- and R-Nb_2O_5 which can occur in parallel to the (001) ReO_3.

P-Nb_2O_5 transforms into H-Nb_2O_5 at 900°C (Petter and Laves, 1965). Schäfer et al., (1964) reported that P-Nb_2O_5 also transforms monotropically into H-Nb_2O_5 at 850°C. However, they indicated that with isothermal heating of a P- and B-Nb_2O_5 mixture under conditions of [750°C, p ($NbOCl_3$) = 5 atm. and p (Cl_2) = 3.5 atm.], direct conversion of P-

into B-Nb_2O_5 takes place. A detailed investigation of the relative thermal stability of different polymorphs of Nb_2O_5 (P-, B-, T- and H-Nb_2O_5) was carried out by Kodama et al, (1972). They concluded that the relative stabilities increase in the order of T → H → P → B at 800°C. The P-, B- and H- forms of Nb_2O_5, therefore, were regarded as stable modifications under atmospheric pressure at low, medium and high temperature ranges, respectively.

In the present study, attention was focussed on two basic aspects of P-Nb_2O_5 reactions:

a) Phase transformation of P- into H-Nb_2O_5 using a hot-stage Philips EM 300 electron microscope (Part A).

b) Phase equilibria in the system NbO_2- (P-Nb_2O_5) using CO_2-H_2 gas buffer mixtures at isotherm 750°C - i.e. within its thermal stability range (Petter and Laves, 1965; Schäfer et al, 1964; Kodama et al, 1972; and this study, Part A.). Reduction products were structurally studied by the X-ray powder diffraction method as well as by electron diffraction and electron microscopy (Part B.).

6.2. MATERIALS AND METHODS

6.2.1. Materials

Single crystals of P-Nb_2O_5 were prepared by the chemical vapour transport technique (see Chapter II). From the crystals obtained, thin ones were selected for the investigation of the P- → H-Nb_2O_5 reaction (see Results "Part A"). The remaining crystals were crushed and ground into a very fine powder in an agate mortar for the solid-gas

TABLE 13

TABLE 13

X-ray powder diffraction pattern of P-Nb_2O_5 a = 3.896 Å, c = 25.43 Å (Petter and Laves, 1965).

$I_{(obs)}$	$Sin^2\ \theta_{(obs)}$	$Sin^2\theta_{(calc)}$	hkl
m	0.01477	0.01467	004
vs	0.03995	0.03999	101
m	0.04744	0.04732	103
s	0.05877	0.05869	008
s	0.06210	0.06200	105
w	0.07859	0.07814	110
m-	0.08190	0.08181	112
m+	0.08407	0.08401	107
m-	0.11121	0.11116	116
w	0.11341	0.11335	109
m+	0.13201	0.13206	0012
m	0.15620	0.15628	200
w-	0.17096	0.17096	204
w+	0.19403	0.19406	1013
m-	0.19624	0.196271	121
w+	0.21496	0.21498	208

reaction involving the use of the microbalance (see Results "Part B"). Prior to every microbalance run, impurities (such as $NbOCl_3$ and moisture) contaminating the sample were removed by procedures described in Chapter II, Section 2.3.2. The oxide used in the reduction experiments, described below, was assumed to be pure, having a composition of $NbO_{2.5}$. The purity of P-Nb_2O_5 was assessed by the X-ray powder diffraction method and all the reflections were indexed on the basis of data given by Petter and Laves (1965). No impurity lines were found (see Plate 16-A and Table 13). Electron diffraction patterns taken from a (hk0) and (h0l) reciprocal lattice section as well as direct lattice imaging of a (h0l) section of P-Nb_2O_5 crystals largely confirmed the X-ray diffraction finding of the purity of the starting material (see Plate 14).

For the process of chemical reduction of P-Nb_2O_5, the requisite chemical potential of oxygen was obtained by using CO_2-H_2 mixtures. The impurity levels of the gases and their effects on the oxygen partial pressures generated from fixed CO_2/H_2 ratios have been discussed in Chapter III.

6.2.2. Methods

For Part A of this Chapter, the phase conversion of P-Nb_2O_5 into H-Nb_2O_5 was studied in a Philips EM 300 electron microscope operating at 100kV and equipped with a single tilt axis heating holder. Electron diffraction patterns were photographed using Ilford plates type EM 4 with an exposure time of approximately 2 seconds, thus minimizing

PLATE 14

PLATE 14

A) Direct (h0l) lattice image of a P-Nb_2O_5 single crystal showing shear planes (dark lines) with 12.7 Å spacing. Stacking faults (↑ S) occur in parallel to the b-axis. Edge dislocation faults (Section 5.3.1.1.) are shown in regions x, and are enlarged in the inset (X).

B) Idealized model of P-Nb_2O_5 containing two kinds of $(010)_{ReO_3}$ CS planes (Section 6.3.). Shear vectors are indicated: $\frac{a}{2}\ [1\bar{1}0]_{ReO_3}$ and $\frac{a}{2}\ [0\bar{1}\bar{1}]_{ReO_3}$

C) Electron diffraction pattern (h0l reciprocal lattice section) of the same area as shown in A.

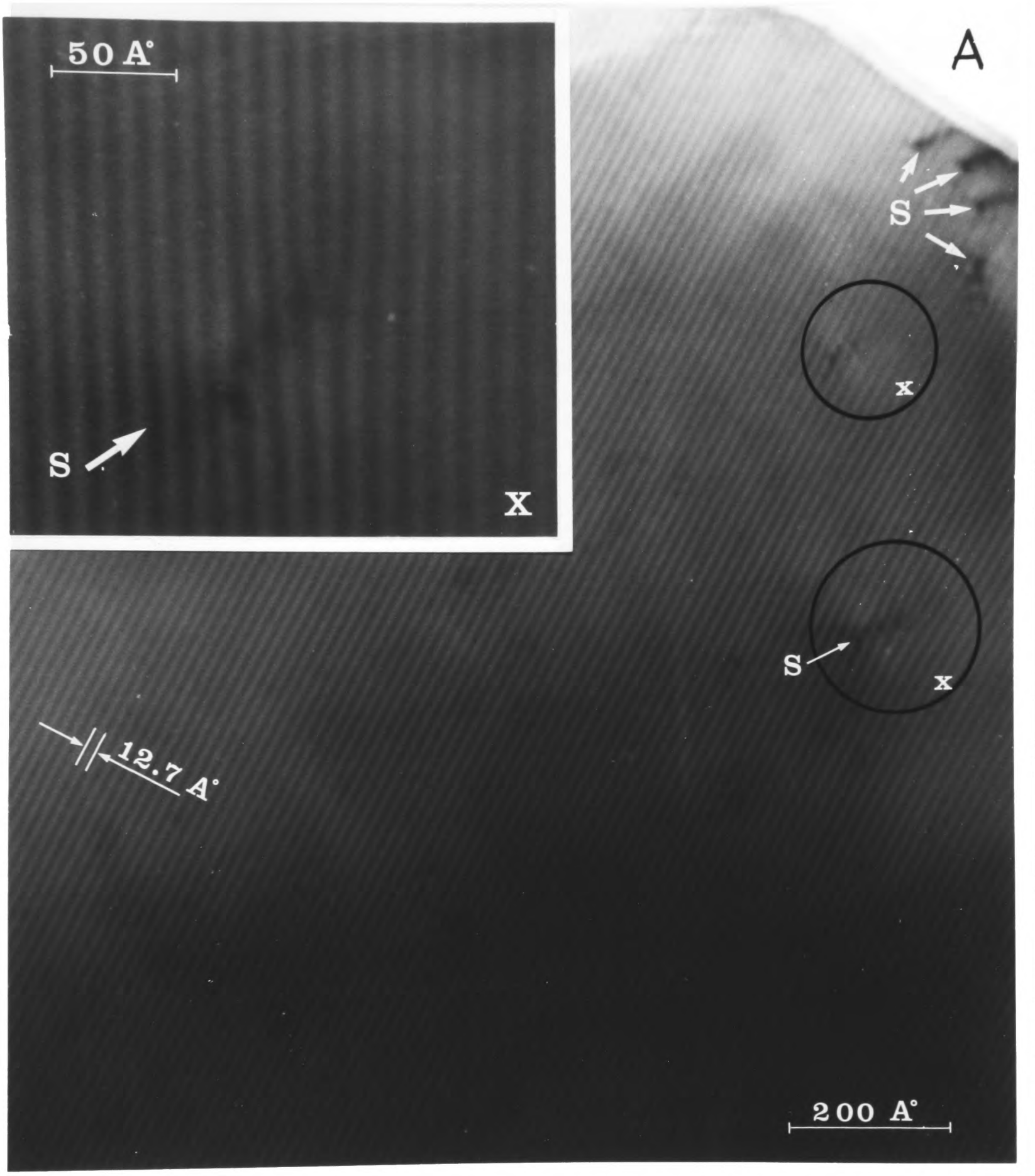
A
50 A°
S
X
S
x
S
x
12.7 A°
200 A°

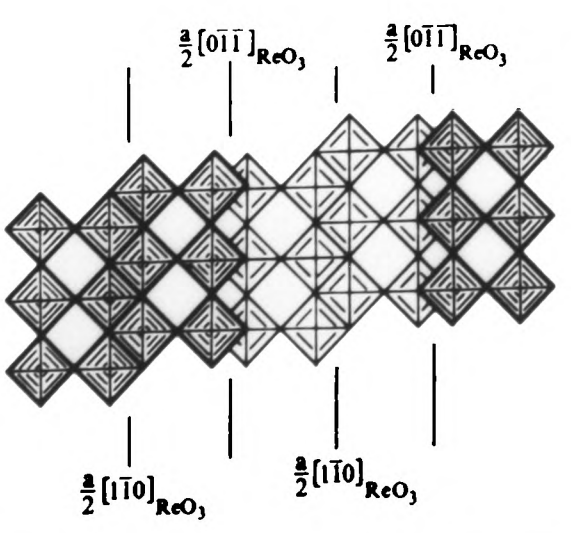
B
$\frac{a}{2}[0\bar{1}\bar{1}]_{ReO_3}$
$\frac{a}{2}[0\bar{1}\bar{1}]_{ReO_3}$
$\frac{a}{2}[1\bar{1}0]_{ReO_3}$
$\frac{a}{2}[1\bar{1}0]_{ReO_3}$

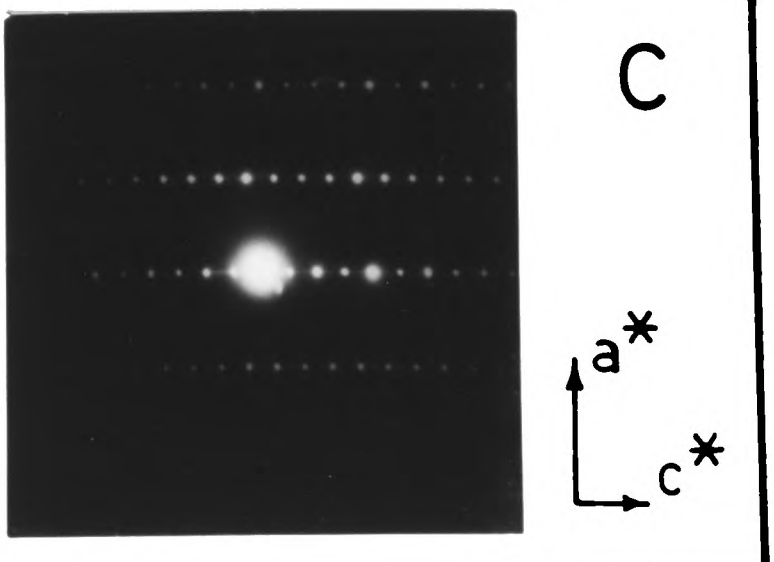
C
a*
c*

Plate 14

effects of specimen drift. The specimen in the microscope holder was heated by raising the temperature stepwise by 20°C at a time. After each step of temperature increase the specimen was allowed, during 5-10 minutes, to stabilize till the point was reached that no further thermal drift occurred and the specimen could be photographed. The temperature ranged from that of heat generated by the electron beam to 950°C and was recorded with an accuracy of $\pm$ 10°C (Philips EM 300 manual).

For Part B of this Chapter, phase equilibria studies of the system NbO_2 - (P-Nb_2O_5), were carried out using a Cahn RG4 microbalance reduction line (see Chapter III). For each experiment, approximately 50 mg of the finely ground sample was used. Oxygen partial pressure in the system was lowered stepwise, using various CO_2-H_2 gas buffer ratios at isotherm 750°C. At each CO_2/H_2 fixed ratio (gas flow rate circa 30 ml/min) the experiment was run for at least three hours in order to ensure a complete removal of the previous gas composition and to establish the new one in the system. When the reduction of the oxide was found to proceed at a slow rate (max. $\sim 5\mu g$/hr) the gas ratio was altered to the next lower value.

The reduced oxides, dark blue in colour, were first studied by the X-ray powder diffraction method using a diffractometer with Cu-Kα radiation (wavelength = 1.5405 Å). Diffraction lines were measured from a slow scanned powder pattern (0.5°/min) using pure silicon powder as an internal standard. Next, reduced oxides were examined, structurally,

in a Siemens Elmiscop 102 electron microscope following the procedure described in Chapter IV.

6.3. RESULTS

6.3.1. PART A

Phase transformation of P-Nb_2O_5 into H-Nb_2O_5

Single crystals of P-Nb_2O_5 may be regarded as rectangular platelets (see Chapter II) in which the long axis of the crystal (c = 25.43 Å) is perpendicular to the large surface of the platelets (Petter and Laves, 1965). This favourable relation of the crystal shape with its internal structure was utilized in an attempt to determine the orientation relationship between P-Nb_2O_5 and its high temperature stable modification (H-Nb_2O_5).

In principle, during the heating process in the electron microscope, individual electron diffraction patterns of oriented P-Nb_2O_5 and H-Nb_2O_5 can be recorded from a single crystal fragment when a tetragonal → monoclinic reaction takes place at the inversion isotherm. From the electron diffraction patterns it ought to be possible to define the structural relationship between the two phases, by determining the zone axes of both P- and the generated H-Nb_2O_5 patterns.

In practice, thin flakes of P-Nb_2O_5, sandwiched between folded golden grids, were clamped firmly onto the heater of the single tilt holder of the microscope. The incident electron beam was parallel to the c-axis of the P-Nb_2O_5 crystal, therefore, an electron diffraction pattern from a (hk0) section of the reciprocal lattice could readily

be obtained (see Plate 15-A). While the crystal was kept in this particular orientation, its temperature was increased stepwise at intervals of 5-10 minutes with 20°C at each step. It was noticed that, during the process of heating, thermal drift of the crystal, possibly caused by gradual expansion of both the supporting grid and the specimen holder of the microscope, resulted in a slight crystal disorientation with respect to the incident electron beam. As long as the P-Nb_2O_5 structure had not yet been transformed, the slight disorientation of the crystal could be corrected by a small degree of specimen tilt. However, at the conversion temperature where the P-phase changed into the H-form, the disorientation of the crystal due to the thermal drift could no longer be corrected; for this reason, a precise determination of the orientation relationship between the P-Nb_2O_5 and the generated H-Nb_2O_5 could not be carried out satisfactorily.

However, despite the difficulties encountered in the heating experiment, the following information could be obtained after isothermal heating of several P-Nb_2O_5 single crystals:

P-Nb_2O_5 appeared to transform directly and very rapidly into H-Nb_2O_5 becoming a polycrystalline product. This is evident from the superimposed composite electron diffraction patterns taken from the generated H-Nb_2O_5 (see Plate 15-B and C). The conversion temperature for the individual crystals, used in the experiment, varied from the heat generated solely by the incident electron beam in the microscope with-

PLATE 15

PLATE 15

Electron diffraction patterns of oriented P-Nb_2O_5 (A) and H-Nb_2O_5 (B and C), suggesting (Section 6.3.1.) an orientation relationship of

$$[001]_{P\text{-}Nb_2O_5} \parallel [100]_{H\text{-}Nb_2O_5}$$

A) A (hk0) reciprocal section of a P-Nb_2O_5 single crystal platelet.

B) H-Nb_2O_5 pattern generated at 850°C.

C) id. transformed at 920°C.

Plate 15

P_Nb2O5

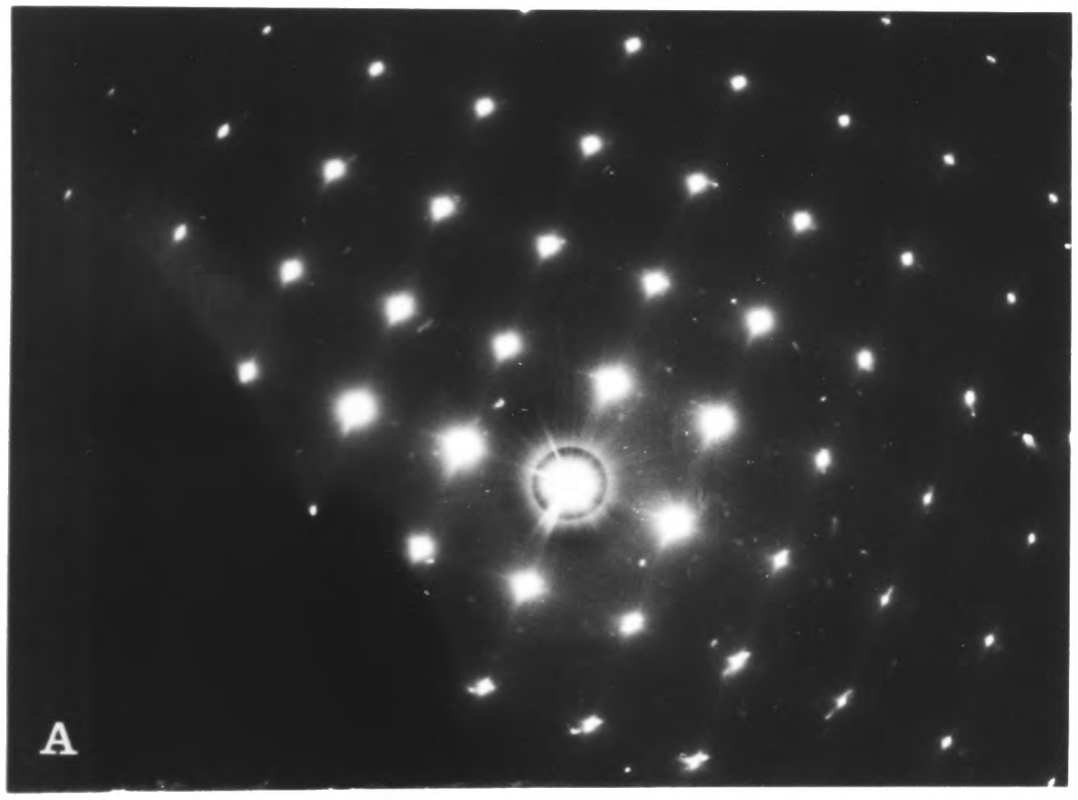

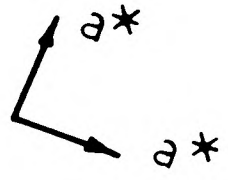

H-Nb2O5

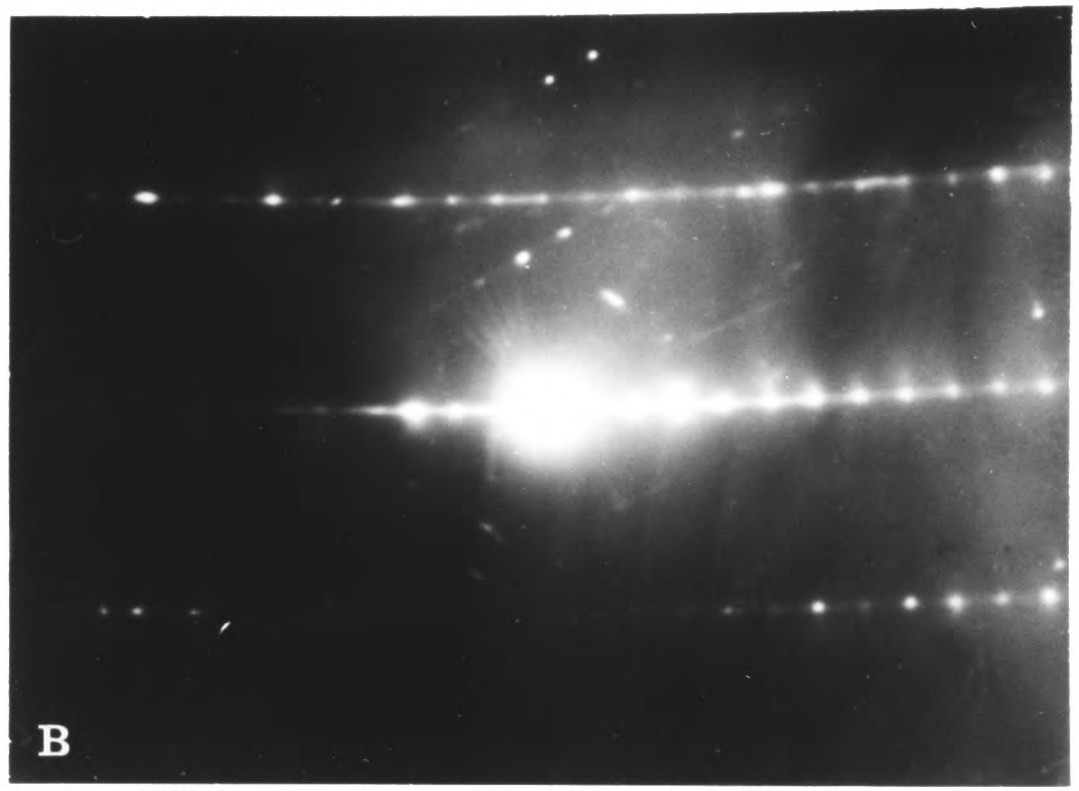

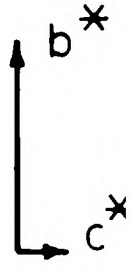

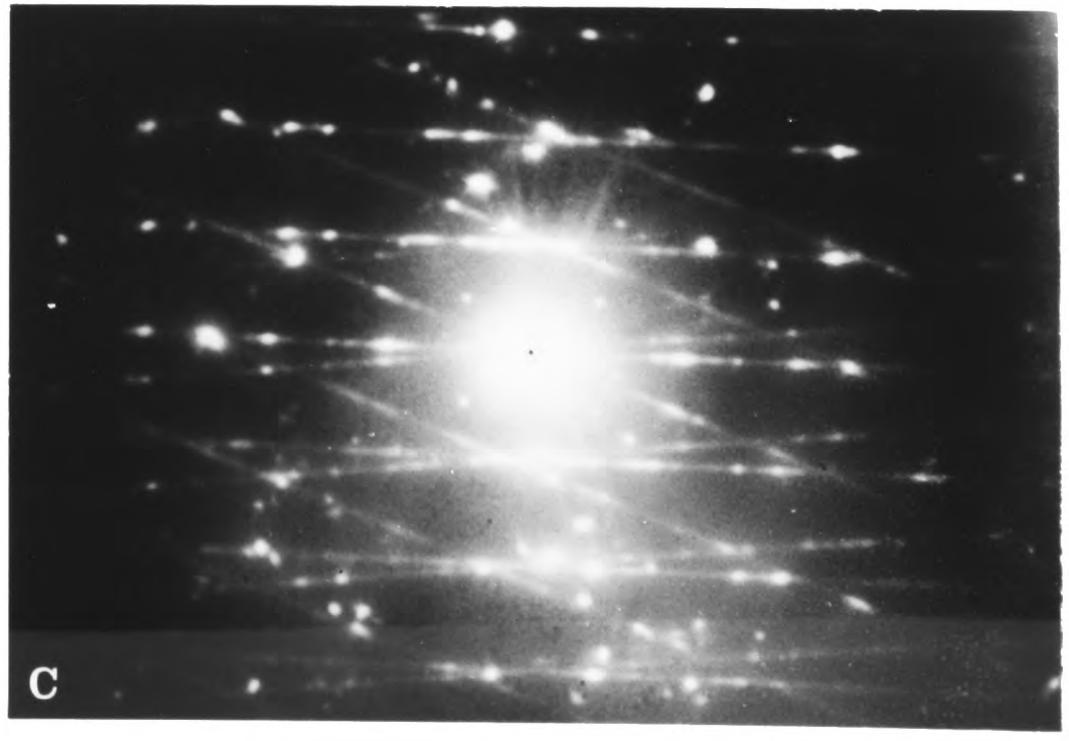

out any heating of the stage, (We estimate the temperature of the crystals to be approximately 500°C) to 950°C, obtained after stage heating. However, the majority of the crystals transformed at temperatures around 850°C. The low temperature ~500°C phase change of some crystals might be due to the presence of, metastable, defective domains in the matrix.

The most frequent types of defects found in the P-Nb_2O_5 structure are: 1) a partial edge dislocation and 2) a stacking disorder along the b-axis of the crystals. These are labelled S and x in Plate 14, respectively.

The dislocation regions (labelled x, Plate 14) are probably formed and retained during a dendritic process of crystal growth. The additional disorder found close to the dislocation lines (↑ S in the regions x, Plate 14; for details see the higher magnification of the areas x in the inset X) might indicate the presence of an appreciable amount of segregated impurities incorporated during the crystal growth (see Chapter II).

The electron diffraction patterns recorded both from the oriented P- and H-Nb_2O_5, suggest that during the inversion reaction the following orientation relationship between P- and H-Nb_2O_5 is probably present.

$$[001]_{P\text{-}Nb_2O_5} \parallel [100]_{H\text{-}Nb_2O_5}$$

This relationship is shown in Plate 15-A, B and C. Patterns B and C represent the uniform results obtained from two subsequent experiments. The H-Nb_2O_5 pattern (B) is

TABLE 14

TABLE 14

Oxygen partial pressures in equilibrium with P-Nb_2O_5 at isotherm 750°C

p_{CO_2}/p_{H_2}		p_{O_2}	$\log p_{O_2}$
25.1	slow reduction rate	2.59×10^{-18}	-17.59
22.4		2.07×10^{-18}	-17.68
14.0		8.24×10^{-19}	-18.08
9.0		3.54×10^{-19}	18.45
6.2		1.69×10^{-19}	-18.77
4.6		9.84×10^{-20}	-19.01
4.0		7.49×10^{-20}	-19.13
3.5		5.95×10^{-20}	-19.23
2.6		3.44×10^{-20}	-19.46
2.0		2.02×10^{-20}	-19.69
1.5		1.19×10^{-20}	-19.92
1.2		8.30×10^{-21}	-20.08
1.0		6.08×10^{-21}	-20.22
0.9		5.02×10^{-21}	-20.30
0.8	fast reduction	4.10×10^{-21}	-20.39
0.7		2.91×10^{-21}	-20.54

generated at 850°C and the one labelled C has been transformed at 920°C. Both patterns (i.e. B and C) show heavy streaking along the c* axis. This would indicate the occurrence of an extensive disorder in the structure of H-Nb_2O_5.

6.3.2. PART B

6.3.2.1. Phase equilibria in the system NbO_2- (P-Nb_2O_5)

Isothermal-isobaric reduction experiments of P-Nb_2O_5 were carried out at 750°C in which CO_2-H_2 gas buffer ratios were lowered stepwise from CO_2/H_2 = 25.1 to 0.8 (see Table 14). Microbalance recordings showed that in the higher oxygen partial pressures (CO_2/H_2 > 0.8) the reduction of P-Nb_2O_5 proceeded very slowly. At CO_2/H_2 = 0.8 a considerable increase in reduction rate was recorded. Hence, from the very moment that fast reduction was detected (i.e. CO_2/H_2 = 0.8) the mixed gas composition was no longer varied and the experiment was run until, after 76 hours, the oxide composition approached an almost constant value of $NbO_{2.419}$. At this point the composition still continued to drift slightly even after an extension of the experiment for another five hours. This gave the impression that the reduced oxide, $NbO_{2.419}$, at 750°C and p_{O_2} = 4.10 x 10^{-21} had still not reached equilibrium. To check whether this was the case, the oxygen partial pressure was again varied to a new value of p_{O_2} = 2.91 x 10^{-21}. As no further significant weight loss of the oxide could be detected, the experiment was terminated and the sample removed for structural

PLATE 16

PLATE 16

X-ray powder diffraction patterns (diffractometer charts) of:

A) The starting material P-Nb_2O_5 (Table 13).

B) Incompletely reduced P-Nb_2O_5 at 750°C and $p_{O_2} = 4.10 \times 10^{-21}$ (Section 6.3.2.2.).

C) Completely reduced P-Nb_2O_5 at 750°C and $p_{O_2} = 4.10 \times 10^{-21}$ (Section 6.3.2.1.).

Plate 16

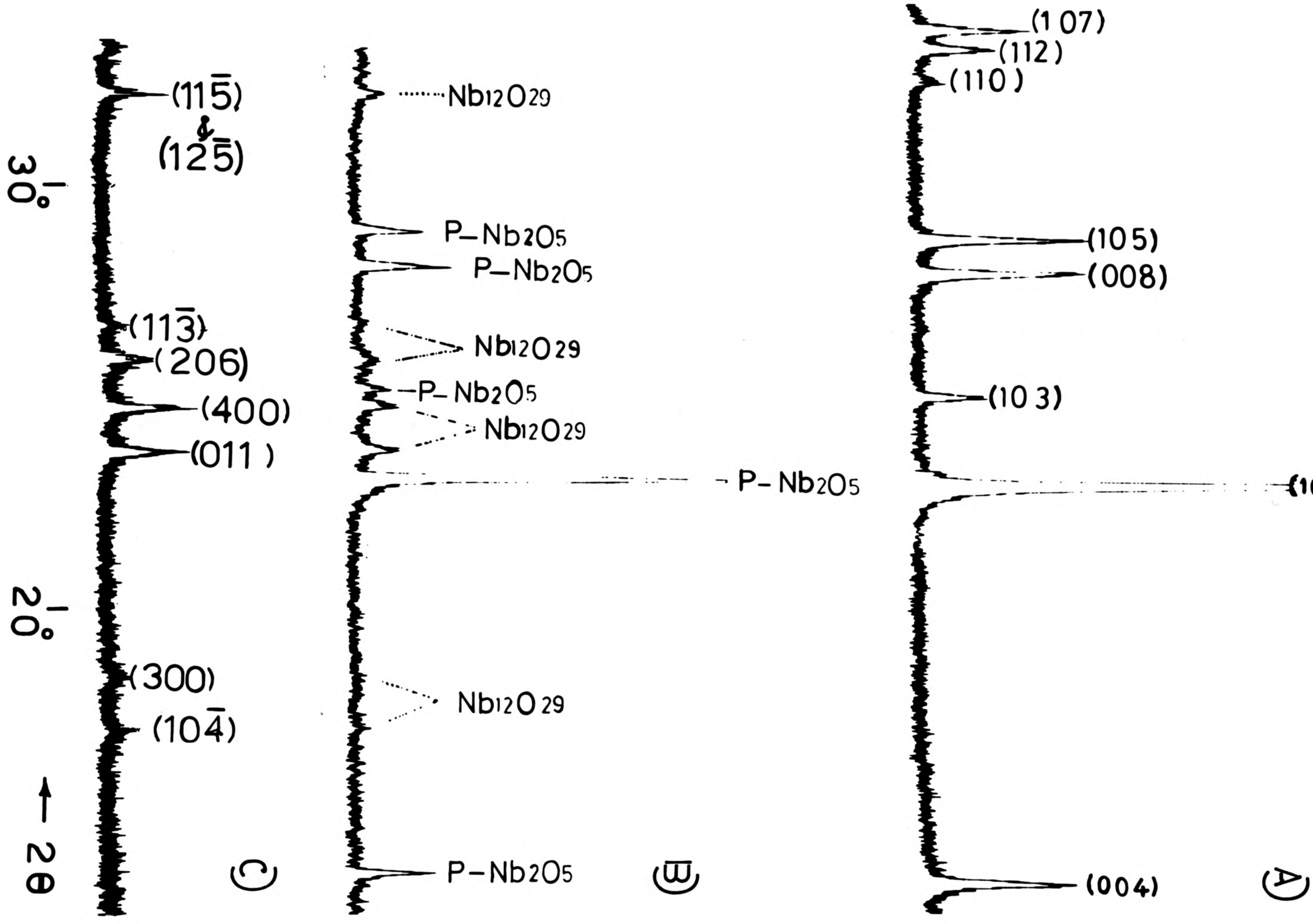
30°
(11$\bar{5}$)
&
(12$\bar{5}$)
(11$\bar{3}$)
(206)
(400)
(011)
20°
(300)
(10$\bar{4}$)
2θ
C
Nb12O29
P–Nb2O5
P–Nb2O5
Nb12O29
P–Nb2O5
Nb12O29
P–Nb2O5
Nb12O29
P–Nb2O5
B
(107)
(112)
(110)
(105)
(008)
(103)
(101)
(004)
A

28-3-78

identification.

6.3.2.2. Structural Studies

An X-ray powder diffraction pattern taken from the product shows the occurrence of broad lines (see Plate 16-C) which could indicate the presence of extensive disorder in the structure. As the composition of the reduced oxide ($NbO_{2.419}$) is very similar to that of the $Nb_{12}O_{29}$ phase ($NbO_{2.417}$), the maxima of the broad lines were roughly indexed on the basis of data obtained for the monoclinic $Nb_{12}O_{29}$ structure (Norin, 1966), to ascertain whether the structure of the oxide was m-$Nb_{12}O_{29}$. The specimen was further studied by electron diffraction and electron microscopy.

Electron diffraction patterns and direct lattice images obtained from several single crystal fragments of the specimen showed that the reduction product of P-Nb_2O_5 is indeed m-$Nb_{12}O_{29}$. The crystals had, in most cases, a heavily disordered $Nb_{12}O_{29}$ structure. This finding is consistent with the results of the X-ray powder diffraction study. In Plate 17-A, a high resolution lattice image of a (h01) section of a single crystal taken from the reduced specimen is shown. The picture indicates that the crystal has a composition near to $Nb_{12}O_{29}$ ($NbO_{2.417}$) and contains regions of disordered block arrangements which give rise to stoichiometric defects. For example, in the area labelled X, Plate 17-A, two stoichiometric defects are present which are indicated (001) ↑ and $(10\bar{1})$ ↑ . The (001) defect is

generated from a change in the $(4 \times 3)_\infty$ ribbon stacking. The fault, in principle, represents half a unit cell of an orthorhombic modification of the $Nb_{12}O_{29}$ structure. The defect along the $(10\bar{1})$ direction shows that alternate columns of (4 x 3) octahedra have rotated by 90° and have kinked the remaining $(4 \times 3)_\infty$ ribbon stacking. An idealized model representing the structure of the crystal in the area X is shown in Plate 17-B. In the model, each 4 x 3 octahedral column is represented by a rectanguler square, joining the corner metal atoms in the column. The lighter and darker squares are being centered on parallel planes 1.9 Å apart. The lighter columns represent $z = \frac{1}{2}b$ and the darker ones $z = 0$ levels. The columns, in the same level, are spliced together across their faces by edge sharing between their respective octahedra. The columns extend through the crystal along the b-axis. The crystal structure has a monoclinic symmetry locally with lattice dimensions of a = 20.50 Å, b = 3.814 Å, c = 15.37 Å and $\beta = 114^\circ$. In the model, the occurrence of (001) and $(10\bar{1})$ defects is again indicated by arrows.

Plate 17-C is an electron diffraction pattern of a (h0l) reciprocal lattice section of the same area of the crystal. The pattern indicates the occurrence of a substantial structural disorder in the bulk of the crystal and indeed has a 4-fold symmetry which probably reflects the microtwinning of $Nb_{12}O_{29}$ blocks in orthogonal directions.

Combination of the results of phase equilibria and structural studies of reduced P-Nb_2O_5, under controlled

PLATE 17

PLATE 17

A) Two-dimensional (h0l) lattice image of a disordered m-$Nb_{12}O_{29}$ structure taken from a reduced P-Nb_2O_5 sample (p_{O_2} = 4.10 x 10^{-21}, T = 750°C). The area labelled x shows two stoichiometric defects of (001)↑ and (10$\bar{1}$)↑.

B) Analysis of the column structure within area (x) in (A). The model shows the presence of (001)↑ and (10$\bar{1}$)↑ defects (Section 6.3.2.2.).

C) Electron diffraction pattern (h0l reciprocal section) of the crystal shown in (A).

Plate 17

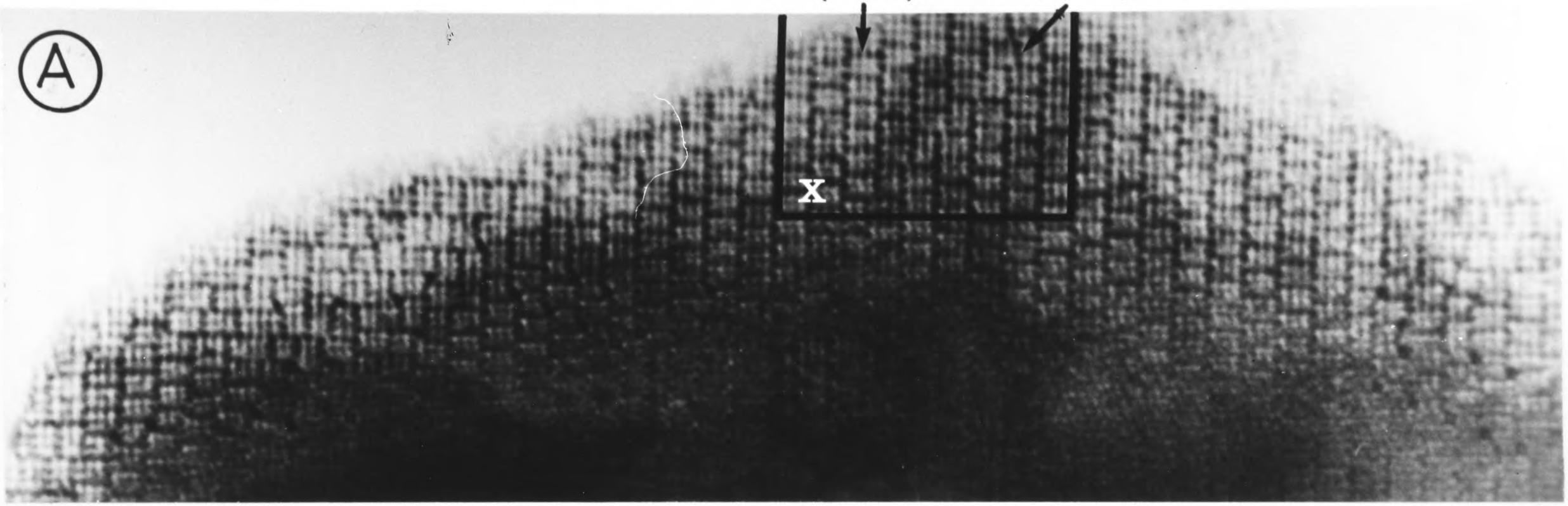

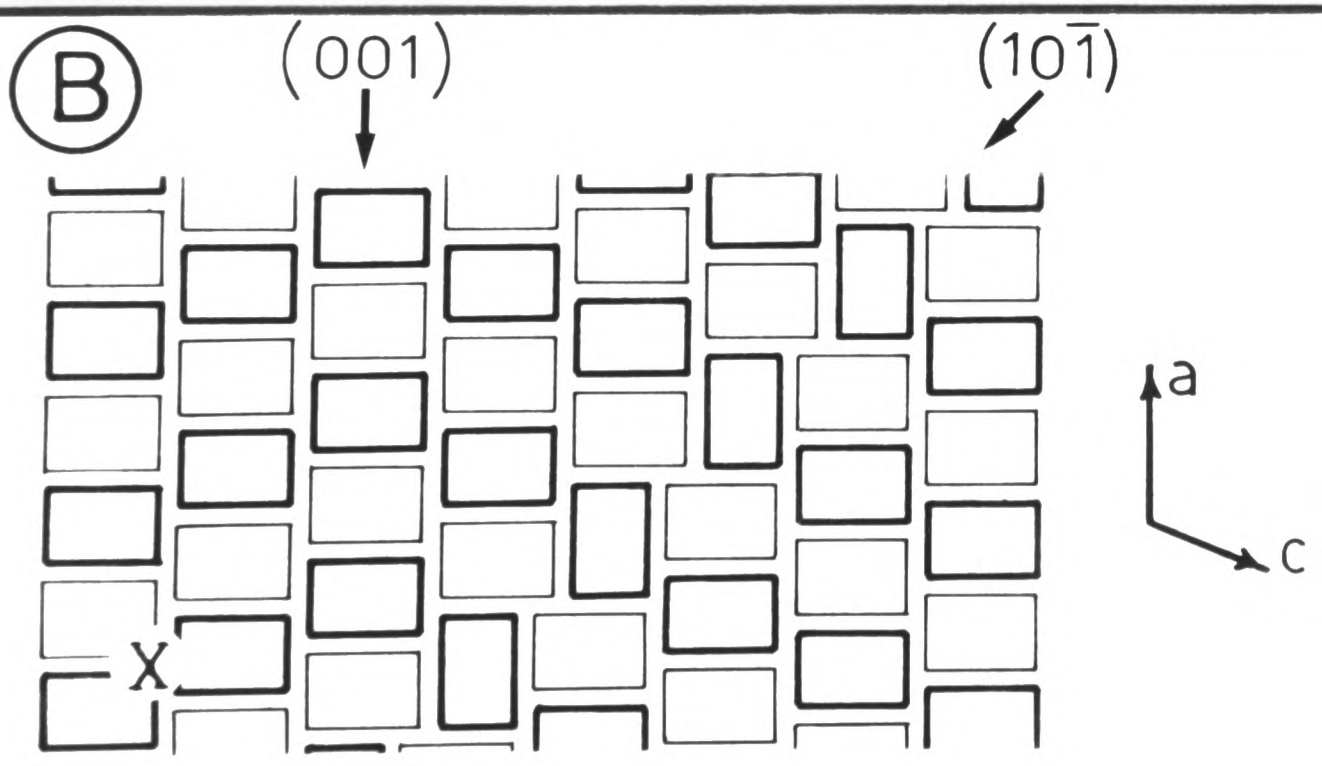

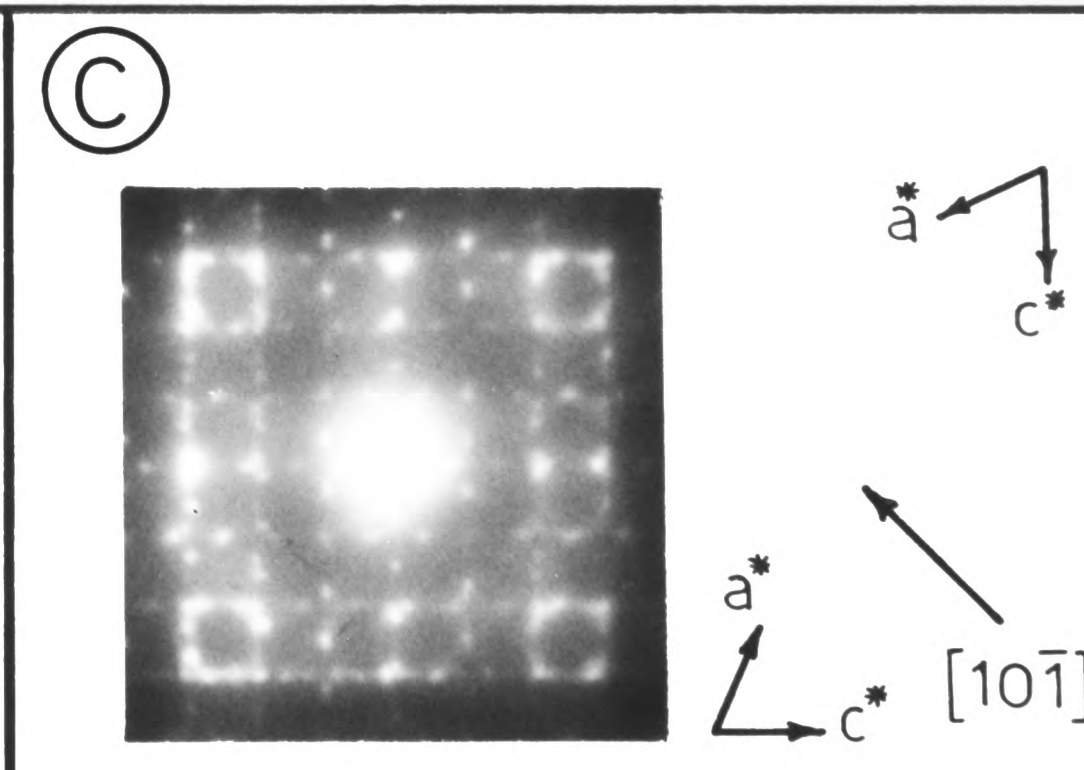

oxygen potentials, can be interpreted in two different ways:

a) P-Nb_2O_5, at the studied isotherm (750°C) and under controlled reducing atmospheres transforms directly into a disordered m-$Nb_{12}O_{29}$ phase which is the only intermediate phase in the system NbO_2-(P-Nb_2O_5), or

b) P-Nb_2O_5, under conditions described in (a), undergoes an initial structural rearrangement forming a metastable transient phase which subsequently reduces into m-$Nb_{12}O_{29}$. The transient phase might be either a disordered block-type structure, the so-called "M-Nb_2O_5", or an R-Nb_2O_5 based structure. Such a transient phase could arise due to a catalytic effect either of the low oxygen partial pressure or a nucleus of reduced P-Nb_2O_5.

To distinguish between these two possibilities and to study the significance of either the reducing atmosphere or the presence of reduced oxide nuclei, an additional experiment was carried out. In this experiment, a fixed CO_2/H_2 ratio of 0.8 was applied and the reductions of P-Nb_2O_5 was run at 750°C. The experiment was interrupted after 8.3% reduction of the sample was obtained (a 100% weight loss is assumed to occur in the case of a complete reduction of Nb_2O_5 into NbO_2). The incompletely reduced oxide, which had an average composition of $NbO_{2.4585}$ (i.e. intermediate between $NbO_{2.5}$ and $NbO_{2.417}$) was studied by the X-ray powder diffraction method. The pattern recorded shows the exclusive presence of mixed phases of P-Nb_2O_5 and $Nb_{12}O_{29}$. This is clear from Plate 16-B in which the pattern obtained is compared with those of the starting material - i.e. P-Nb_2O_5

(A) - and reduced P-Nb_2O_5 (C) under identical condition (Section 6.3.2.1.). N.B. the low intensities of the X-ray powder reflections depicted in Plate 16B and C are due to the small quantities of the samples, approximately 50 mg, used in the diffractometer.

6.4. DISCUSSION

Phase transformation of P-Nb_2O_5 into H-Nb_2O_5

The present study of the relationship between P-Nb_2O_5 and its high temperature stable modification, H-Nb_2O_5, has revealed several points of interest:

1) P-Nb_2O_5 transforms sharply at a certain temperature into the H-form. It was noticed that, while the majority of the crystals transformed at approximately 850°C, several single crystals did so at lower temperatures i.e. in heat generated by the incident electron beam as well as at the higher temperatures (900-950°C). Such differences in conversion temperature may be based on the presence of disordered regions and incorporated impurities in the structure of the matrix which have arisen during the process of crystal growth (see Chapter II, Section 2.3.2.). Concerning the disordered regions (partial edge dislocation and stacking faults perpendicular to the b-axis of the crystal), it is possible that under high temperature conditions a strain field arises locally, leading to a premature transformation of the structure at a lower temperature than is the case for a well-ordered structure.

The final conclusion of the above findings is that it

appears to be difficult to define the thermodynamic stability of these compounds unless a detailed history of the sample, including its impurity level and defect structure, is exactly known.

2) A single crystal of P-Nb_2O_5 taken through a transition point at the conversion temperature breaks up into a random assembly of one or more crystals of the H-phase. This phenomenon is probably due to a symmetry change of the crystal from tetragonal into monoclinic.

3) The transformation of the P- into the H-form is fast and irreversible and appears not to proceed via the formation of hybrid crystals.

Similar observations have been made by Browne (1973) in studies on the transformation of N-Nb_2O_5 into the H-form. He states that the transformation takes place rapidly and gives rise to polycrystalline H-Nb_2O_5. Electron microscopy of the end product revealed, according to him, no simultaneous occurrence of N- and H-Nb_2O_5 domains - i.e. no hybrid structures within the single crystals.

4) Electron diffraction patterns recorded before and after the P-Nb_2O_5 phase change (Plate 15, patterns A, B and C, respectively) suggest the existence of the following structural orientation relationship between P- and H-Nb_2O_5:

$$[001]_{P\text{-}Nb_2O_5} \parallel [100]_{H\text{-}Nb_2O_5}$$

A critical note should be made here. Due to experimental limitations caused by specimen drift during the heating process in the electron microscope the above observations need to be supplemented by other methods, in

particular, the application of a high voltage electron microscope equipped with a double tilt heating holder enabling direct observations of transformation in the larger and thicker P-Nb_2O_5 flakes and ensuring a proper correction of slight disorientation of the specimen due to thermal drift.

Phase equilibria in the system NbO_2 - (P-Nb_2O_5

Reduction of P-Nb_2O_5 under controlled oxygen partial pressures (generated from CO_2-H_2 gas buffer mixtures) was carried out at 750°C. The monovariant behaviour of the $(p, x)_T$ scan, recorded in the cahn RG4 microbalance reduction line (Section 6.3.2.1.) clearly demonstrated that a $Nb_{12}O_{29}$ compound occurred as the only intermediate stable phase in the composition range of NbO_2 to P-Nb_2O_5. The findings of the exclusive occurrence of $Nb_{12}O_{29}$ was confirmed by structural studies of the reduced oxides (Section 6.3.2.2.) using X-ray powder diffraction, electron diffraction and electron microscopy. No hybrid crystals, such as described by Ubbelohde (1956), were detected indicating that the conversion of P-Nb_2O_5 into a $Nb_{12}O_{29}$ phase occurs abruptly and, thus, the system conforms to the classical Gibbs phase assembly.

The slow kinetics of the P-Nb_2O_5 reduction process and the slight drift of the oxide composition at the equilibrium point may be due to the low temperature (750°C) of the reaction.

Similar slow kinetics, in other metal-oxygen phase equilibria systems at comparable low temperatures, have been

observed by other investigators (e.g. Nimmo and Anderson, 1972; Merritt and Hyde, 1973). Nimmo and Anderson studied the NbO_2 - (H-Nb_2O_5) system at 950-1050°C and reported that "A very slow drift of the compositions attained indicates that it is not a true equilibrium". (their paper, p. 2333). Merritt and Hyde investigated the (p, x) isotherm of TiO_x ($1.67 < x < 1.98$) at 1030°C and introduced the "steady mass" criterion for the obtained equilibrium. A steady mass, according to them, is "..... a rate (of weight change, K.F.) of not more than 0.55 ngs^{-1} (2 $\mu g h^{-1}$) ....." (their paper, p. 636) at constant chemical potential of oxygen.

In the present study, the slight drift of the oxide composition at the equilibrium point and the oxygen excess composition ($NbO_{2.419}$) of the obtained $Nb_{12}O_{29}$ phase may arise from two conditions, as follows:

a) Incomplete reduction of very occasional crystal fragments which have escaped the fine grinding process and thus have a larger grain size, requiring a longer reduction time.

b) The probable occurrence of very occasional H-Nb_2O_5 crystallites arisen from the transformation of P-Nb_2O_5 at 750°C (see Part A). These crystals follow an entirely different reduction pathway (see Nimmo and Anderson, 1972) and may still continue to reduce at the equilibrium point.

Mechanisms of (CS) plane generation

The structure of P-Nb_2O_5 is topologically different from that of H-Nb_2O_5 and $Nb_{12}O_{29}$ where two sets of $\{100\}_{ReO_3}$ (CS) planes intersect each other at right angles. The

mechanism underlying the generation of the second (CS) plane and the subsequent reorganization of the structure, in the process of phase change of P- → H-Nb_2O_5 and reduction of P-Nb_2O_5 to $Nb_{12}O_{29}$, at present, is not clear. However, for the generation of one-dimensional crystallographic shear structures (Magneli phases) three different mechanisms have been proposed in the past (Gado, 1965; Anderson and Hyde, 1965, 1967; Anderson[s] and Wadsley, 1966. These mechanisms have been discussed in Chapter I and are briefly summarised below:

Model 1 (Gado, 1965):

This model envisages the initial generation of a relatively high concentration of anion vacancies on the crystal surface. The structure subsequently undergoes superlattice ordering along a plane which is identical to the ultimately formed (CS) plane. The crystal then collapses, the vacant sites are annihilated and a (CS) plane is generated. This model can be applied to any transformation process, involving the formation of a (CS) structure, when as an intermediate stage a super-structure ordering similar to the one in Gado's model is present.

Model 2 (Anderson and Hyde, 1965, 1967):

Loss of oxygen from the surface sites of the crystal produces anion vacancies (point defects) in the lattice. Adjacent anion vacancies aggregate into a vacancy disc which collapses and forms a nucleus of crystallographic shear

structures bound by a dislocation loop. The dislocation loop can climb through the lattice acting as a sink in which the immediately surrounding vacancies are drained into and, next, are eliminated by the climbing dislocation.

The chemical potential of oxygen at lattice sites in the dislocation region of the crystal will probably rise, by strain energy, and the distorted region may therefore be subject to preferential chemical attack (i.e. reduction).

Model 3 (Andersson and Wadsley, 1966):

Loss of a layer of oxygen atoms from lattice sites on the crystal surface is followed by displacement of a sheet of cations co-operatively into adjacent interstitial sites to form a (CS) plane at the surface. During progressive reduction, the generated shear plane on the crystal surface migrates inwards into the crystal bulk. By this mechanism, the shear plane can move unilaterally to form an ordered series of parallel shear planes within the crystal.

Andersson and Wadsley's model, thus, can explain the interconversion of block-type structures such as have presently been found in the conversion of $Nb_{53}O_{132}$ into $Nb_{43}O_{107}$ (see Chapter V).

Whether one or several of the above mechanisms (1-3) applies to the formation of block-based structures resulting from the transformation of P-Nb_2O_5 into H-Nb_2O_5 and $Nb_{12}O_{29}$ remains to be seen. To elucidate these possibilities or the envolvement of alternate mechanisms, single crystal platelets

of P-Nb_2O_5 would need to be examined in a high voltage electron microscope equipped with an environment-controlled stage enabling a direct observation of the reduction processes in the microscope.

CHAPTER VII

PHASE EQUILIBRIA IN THE SYSTEM Ti-Nb-O AT 1400°C

PART A : $(Ti,Nb)O_2$-$TiNb_2O_7$

PART B : $(Ti,Nb)O_2$-$Ti_2Nb_{10}O_{29}$

PART C : $(Ti,Nb)O_2$-$TiNb_{24}O_{62}$

7.1. Introduction

Phase equilibrium reactions in the system TiO_2-Nb_2O_5 were studied for the first time by Roth and Coughanour (1955). They reported the presence of two distinct compounds with compositions of $TiO_2.3Nb_2O_5$ and $TiO_2.Nb_2O_5$, respectively.

The crystal structure of $TiO_2.Nb_2O_5$ was determined by Dyson (1957) and, later, by Wadsley (1961a). Their findings were at variance in that the value given for the c-axis by Wadsley was twice that given by Dyson.

The structure of $TiO_2.3Nb_2O_5$ was also identified by Wadsley (1961b). He showed that the compound was in fact $Ti_2Nb_{10}O_{29}$ ($TiO_2.5Nb_2O_5$), and that both phases i.e. $TiNb_2O_7$ and $Ti_2Nb_{10}O_{29}$ are closely related and can be regarded as members n = 3 and 4 of a homologous series of oxides with the general formula $Me_{3n}O_{8n-3}$ (Me = metal atom). Of this series, Nb_3O_7F represents the parent compound (Andersson, 1964). Wadsley (1961b) attempted to prepare an additional, higher, member of the homologous series, namely, $TiO_2.7Nb_2O_5$ or $TiNb_{14}O_{37}$ (n = 5), conceived to contain (3 x 5) blocks. Whereas Wadsley could not identify this compound in his original X-ray study, Iijima and Allpress (1974) have detected domains of a (5 x 3) structure corresponding to $TiNb_{14}O_{37}$ by electron microscopy.

A new compound in the TiO_2-Nb_2O_5 system with the empirical composition of $(Ti,Nb)O_{2.482}$ was reported by Gruehn and Schäfer (1963). Roth, Wadsley and Gatehouse (1964), however, found that the material was $TiNb_{24}O_{62}$ ($TiO_2.12Nb_2O_5$), occurring in that particular region of the equilibrium phase

diagram previously described as Nb_2O_5 solid solution by Roth and Coughanour (1955). The compound was shown to represent a definite phase in the $TiO_2.Nb_2O_5$ system with a formula corresponding to that of a member (n = 8) of the homologous series $Me_{3n+1}O_{8n-2}$. Its structure was found to be basically different from that of two other members (n = 7 and n = 9) known in the binary Nb-O system - i.e. $Nb_{22}O_{54}$ and H-Nb_2O_5 ($Nb_{28}O_{70}$), respectively (Gatehouse and Wadsley, 1964).

With regard to the ordering process of the different cations (Ti^{4+} and Nb^{5+}) in the titanium-niobium oxides, different data have been reported in the literature. Wadsley (1961 a and b), on the basis of single crystal X-ray diffraction studies of $TiNb_2O_7$ and $Ti_2Nb_{10}O_{29}$, concluded that altervalent cations fill the octahedral sites in a completely random way. Von Dreele and Cheetham (1974), who examined the crystal structure of $TiNb_2O_7$ and $Ti_2Nb_{10}O_{29}$ by the neutron diffraction method, showed that there is substantial ordering of Ti^{4+} cations in the corner and edge sites of the blocks, the distribution being consistent with the sequence of the calculated site potentials. The structural determinations of the latter authors also showed that the displacement vector of the crystallographic shear is not an exact lattice vector, and that edge-shared octahedra are distorted, considerably increasing the cation-cation distances at the interface.

The liquidus curve of the TiO_2-Nb_2O_5 system was studied by Jongejan and Wilkins (1969) who reported three distinct phases having compositions $2TiO_2.5Nb_2O_5$, $2TiO_2.3Nb_2O_5$

TABLE 15

TABLE 15

Guinier X-ray diffraction pattern of $Ti_{0.5}Nb_{0.5}O_2$: Rutile, a = 4.719 Å, c = 2.997 Å (Marinder, et al 1962)

I (obs.)	d (Cm)	$Sin^2 \theta$ (obs.)	$Sin^2 \theta$ (calc.)	hkl
v.s.	3.72	0.053089	0.053249	110
v.s.	4.95	0.092698	0.092634	101
m+	5.32	0.106542	0.106498	200
m+	5.65	0.119600	0.119259	111
m-	5.985	0.133305	0.133123	210
v.s.	7.41	0.199582	0.199132	211
m+	7.68	0.213240	0.212996	220
s	8.64	0.264336	0.264039	002
s	8.68	0.266544	0.266245	310
s	9.37	0.305500	0.305630	301
s	9.58	0.317657	0.317288	112
v.w.	9.83	0.3332292	0.332255	311
m	10.43	0.371075	0.370537	202
s	11.16	0.412554	0.412128	321

and $TiO_2.Nb_2O_5$. The structures of the $2TiO_2.5Nb_2O_5$ and $TiO_2.Nb_2O_5$ compounds were reported to be consistent with earlier determinations but the existence of the previously unreported $2TiO_2.3Nb_2O_5$ appeared to be limited to temperatures higher than 1424°C.

The present study aimed at the investigation of the reduction equilibria of three compounds i.e. $TiNb_2O_7$, $Ti_2Nb_{10}O_{29}$ and $TiNb_{24}O_{62}$. These compounds can be prepared in large quantities (Wadsley, 1961 a and b; Roth and Wadsley Gatehouse, 1964) and they melt congruently at 1498°, and 1488°C and ~1500°C respectively (Jongejan and Wilkins, 1969). The reduction equilibria were investigated at 1400°C (below the melting points of the compounds). The main objectives of the study were:

a) to correlate the thermodynamic behaviour with the structural modification during the reduction

b) to elucidate the role of the foreign ion (Ti^{4+}) in the process of the reduction and to suggest possible pathways for the reduction.

c) to determine a ternary phase diagram for the system Ti-Nb-O at the isotherm 1400°C.

7.2. Materials and Method

7.2.1. Materials

$TiNb_2O_7$, $Ti_2Nb_{10}O_{29}$ and $TiNb_{24}O_{62}$ were prepared in large quantities sufficient for a 20 g sample of each. High purity niobium pentoxide and titanium dioxide (Johnson Matthey specpure Chemicals) were weighed with a precision

balance in mole ratios of 1:1, 2:5 and 1:12, respectively. Each sample was mixed initially by grinding it in an agate mortar and later in an agate ball mill to ensure thorough mixing. The mixtures were pelleted, placed in platinum crucibles and reacted in air at 1400°C for ten periods of 24 hours using a muffle furnace. After each 24 hour heat treatment, the samples were quenched to room temperature and the discs ground in an agate mortar. The mixing and heating process was repeated until well-ordered and homogenous samples were obtained. The purity of the materials was studied by X-ray powder diffraction, electron diffraction and electron microscopy. The results are given in Sections 7.3.1.1., 7.3.2.1. and 7.3.3.1.

A mixed TiO_2-NbO_2 oxide with a composition of $Ti_{0.5}Nb_{0.5}O_2$ was also prepared from an intimate mixture of high purity titanium and niobium dioxides with mole ratio of 1:1. The mixture was pelleted, sealed in an evacuated silica tube and heated at $\sim$ 1100°C for three periods of 24 hours. After each heating process, the sample was cooled and then ground in an agate ball mill to ensure thorough mixing. An X-ray powder diffraction pattern of the microcrystalline product was indexed according to lattice parameters given by Marinder et al, (1962). Results are given in Table 15.

The polycrystalline sample of NbO_2 used in the preparation of $Ti_{0.5}Nb_{0.5}O_2$ was obtained by hydrogen reduction of specpure Nb_2O_5 (Johnson Matthey Chemicals) at 1400°C for 10 hours. Its oxygen content was analysed as $NbO_{2.00}$ by gravimetric oxidation to Nb_2O_5 at 1000°C using a Cahn microbalance line.

7.2.2. Experimental Method

The phase equilibrium diagram in the system Ti-Nb-O was determined at the isotherm 1400°C by equilibrating samples of $TiNb_2O_7$, $Ti_2Nb_{10}O_{29}$ and $TiNb_{24}O_{62}$ with CO_2-CO gas buffer mixtures as described in Chapter III.

Approximately 400 milligrams of each oxide was held in a platinum boat and reduced to the equilibrium state in a Horizontal Quench Furnace (see Chapter III). The oxides were then quenched to room temperature in vacuum.

The oxygen content of the reduced oxides was determined gravimetrically by measuring the weight gain of the sample after reoxidation, in air, at 1000°C. The measurements were carried out in a Cahn RG4 microbalance line (see Chapter III) using ~100 mg samples. A constant flow of (~ 10 ml/min) oxygen was maintained during each run.

The re-oxidation reaction took place rapidly and a constant weight was attained in less than one hour. However to ensure a complete re-oxidation of the oxides, the experiments were extended for a further three hours.

7.3. Results

To determine the minimum time in which a solid-gas system in a perfect equilibrium state could be obtained, reduction experiments of varying duration were carried out. It was found that a solid-gas equilibrium state was already attained in less than one hour. However, knowing that the magnitude of the driving force behind structural ordering of the generated phases is small (Anderson, 1974) a minimum

duration of 10 hours was employed for each experiment in the three systems.

Presentation of data in Tables and in phase equilibria diagrams

The phase equilibria data obtained for the systems $TiNb_2O_7$, $Ti_2Nb_{10}O_{29}$ and $TiNb_{24}O_{62}$ are arranged in Tables 17, 20 and 23 respectively in the columns of which the following information is presented:

1) The number of each experiment (or specimen),
2) CO_2-CO gas buffer ratios in equilibrium with the respective oxide compositions,
3) The oxygen partial pressures, at isotherm 1400°C, in log p_{O_2} (atm.),
4) Compositions of the equilibrated oxides in atom oxygen per atom metal (O/Ti,Nb),
5) Structural studies.

In the phase equilibrium diagrams of $TiNb_2O_7$, $Ti_2Nb_{10}O_{29}$ and $TiNb_{24}O_{62}$ (Figures 18, 19 and 20, respectively), the composition of the oxides is plotted against the oxygen partial pressure (atm) on a logarithmic scale.

An extensive discussion of phase equilibria data obtained is given below in Sections 7.3.1., 2. & 3.

7.3.1. PART "A"

PHASE EQUILIBRIA IN THE SYSTEM $(Ti,Nb)O_2$-$TiNb_2O_7$

AT ISOTHERM 1400°C

TABLE 16

TABLE 16

Guinier X-ray powder diffraction pattern of $TiNb_2O_7$; monoclinic, a = 20.44 Å, b = 3.81 Å, c = 11.93 Å, $\beta = 120.2^{\circ}$ (Wadsley, 1961a)

I (obs.)	d (Cm)	$Sin^2 \theta$ (obs.)	$Sin^2 \theta$ (calc.)	hkl
m-	1.19	0.005521	0.00558	(001)
m+	1.31	0.006689	0.00663	($\bar{2}$01)
m-	1.40	0.007637	0.00760	($\bar{2}$02)
s	2.40	0.022332	0.02231	(002)
s	2.43	0.022889	0.02288	($\bar{4}$01)
w-	2.62	0.026575	0.02651	($\bar{4}$02)
w+	2.81	0.030528	0.03040	(400)
s+	3.34	0.042947	0.04275 0.04302	(110) ($\bar{2}$02)
s	3.43	0.045257	0.04506	($\bar{1}$11)
w+	3.58	0.049234	0.04908	(401)
s	3.62	0.050322	0.05020	(003)
s	3.66	0.051420	0.05142 0.05161	($\bar{6}$02) ($\bar{1}$11)
m+	3.75	0.053933	0.05371	($\bar{3}$11)
m-	3.77	0.054499	0.05434	($\bar{6}$01)
v.v.w.	3.91	0.058540	0.05852	($\bar{1}$12)
w	3.975	0.060611	0.06062	($\bar{3}$12)
w	4.205	0.067332	0.06725	($\bar{4}$04)
m+	4.345	0.071790	0.07162	(112)
s	4.515	0.077371	0.07746 0.07756 0.07792	($\bar{2}$03) ($\bar{5}$11) ($\bar{5}$12)
s	4.55	0.078713	0.07868 0.07892	($\bar{3}$13) (402)
m+	4.56	0.079050	0.07905	($\bar{6}$04)
s	4.68	0.083144	0.08313	($\bar{1}$13)
w	4.85	0.089105	0.08925	(004)
w	4.86	0.089461	0.08943	($\bar{5}$13)
w	4.92	0.091613	0.09152	(802)
m+	4.98	0.093788	0.09364	($\bar{6}$01)
w	5.17	0.100826	0.10099	(801)
v.v.w.	5.22	0.102716	0.10278	($\bar{1}$13)
w	5.26	0.104239	0.10435	($\bar{4}$05)
v.v.w.	5.40	0.109647	0.10960	($\bar{6}$05)
m-	5.42	0.110429	0.11032 0.11042	($\bar{5}$11) ($\bar{7}$12)
m+	5.46	0.112001	0.11210	($\bar{5}$14)
m	5.51	0.113979	0.11430	($\bar{2}$05)
v.v.w.	5.58	0.116775	0.11662	($\bar{7}$11)
w	5.74	0.123274	0.12162 0.12306	(800) ($\bar{2}$04)
w-	5.94	0.131610	0.13151	($\bar{7}$14)
v.w.	6.12	0.139309	0.13946	(005)
s	6.18	0.141916	0.14197	(1003)
s	6.21	0.143227	0.14343	(512)

7.3.1.1. Assessment of the purity of the starting material ($TiNb_2O_7$)

To ensure the purity of the starting material prior to phase equilibria studies, an X-ray powder diffraction pattern was taken. All the lines in the Guinier powder pattern were indexed on the basis of the lattice parameters reported by Wadsley (1961a). Results are given in Table 16.

The sample was also checked by electron diffraction and electron microscopy. Examination of several single crystals showed that the starting material was pure and structurally homogeneous. In Plate 18, a two dimensional lattice image of a $TiNb_2O_7$ crystal, which is representative of the sample, is shown. The idealized model for this structure, in its simple representation, is depicted in Plate (18-B). In the model, blocks of (3 x 3) octahedra are linked into finite ribbons by further octahedra edge sharing. The block structure of $TiNb_2O_7$ can therefore be symbolized as $(3 \times 3)_\infty$. The unit cell is outlined in Plate 18-B and measures a = 20.44 Å, b = 3.80 Å, c = 11.93 Å and $\beta = 120^\circ 10'$. In Plate 18-C an electron diffraction pattern of the (h0l) reciprocal lattice section of the same region of the crystal is shown. Defective crystals other than occasional twin structures of $TiNb_2O_7$ were not encountered.

7.3.1.2. Thermodynamics

Results of phase equilibrium studies in the system $(Ti,Nb)O_2$-$TiNb_2O_7$ are given in Table 17 and presented diagramatically in Figure 18.

PLATE 18

PLATE 18

A) A two-dimensional lattice image of a well-ordered $TiNb_2O_7$ single crystal.

B) Idealized model of $TiNb_2O_7$.

C) (h0l) electron diffraction pattern of the crystal fragment shown in (A) (Section 7.3.1.1.).

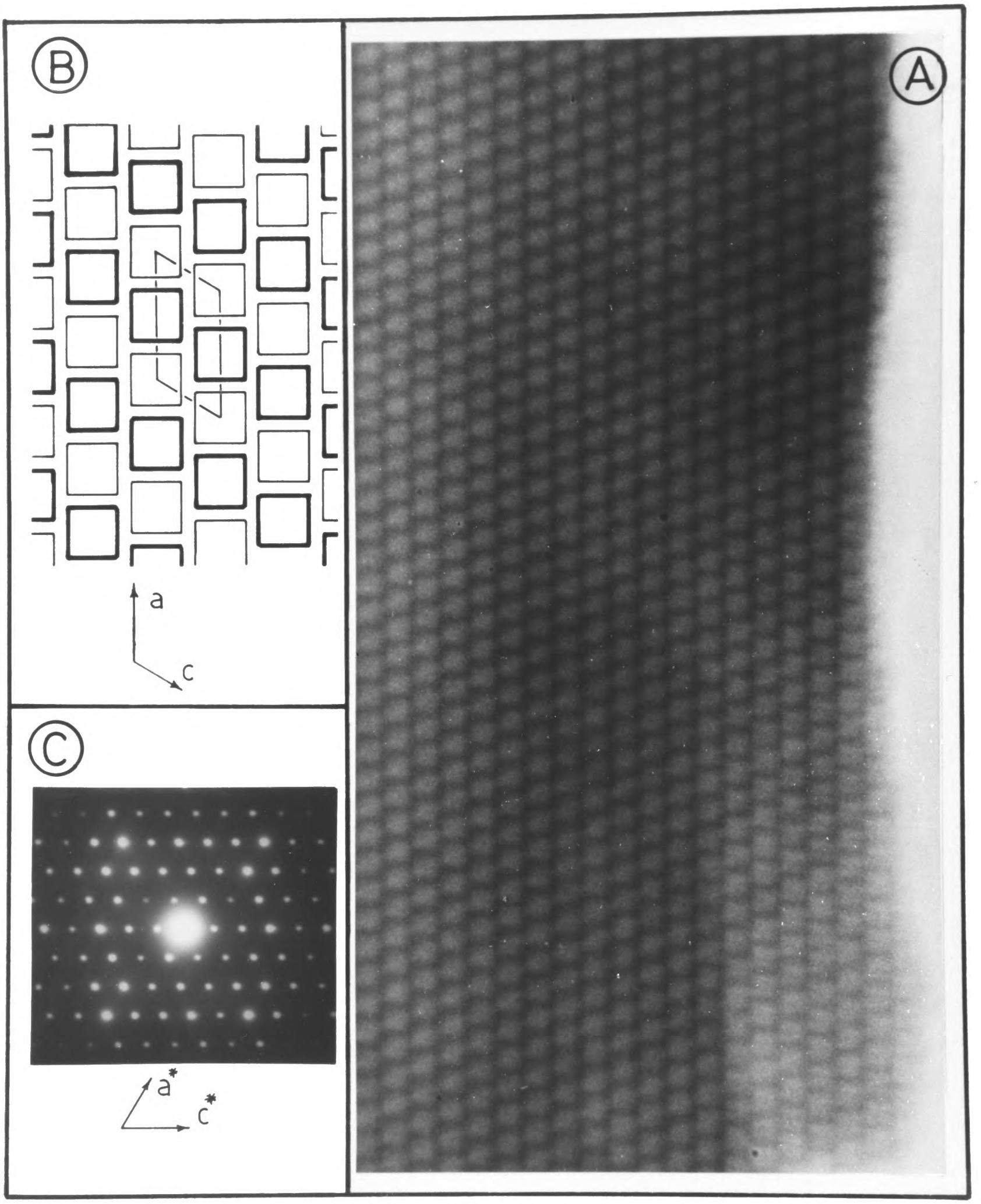

Plate 18

TABLE 17

TABLE 17

System $(Ti,Nb)O_2$ - $TiNb_2O_7$ Equilibrium Results at 1400°C

Specimen no.	CO_2/CO	$\log p_{O_2}$	Composition $(Ti,Nb)O_x$	Structural studies (see Section 7.3.1)
1	0.09	-10.64	1.9996	
2	0.09	-10.67	2.0000	
3	0.10	-10.53	2.0223	
4	0.10	-10.55	2.0281	
5	0.13	-10.35	2.0547	
6	0.19	-10.01	2.1376	
7	0.24	-9.81	2.1435	
8	0.24	-9.82	2.1740	
9	0.26	-9.73	2.1527	
10	0.30	-9.62	2.1778	
11	0.41	-9.34	2.2005	
12	0.60	-9.02	2.2245	
13	0.69	-8.90	2.2463	
14	1.19	-8.43	2.2726	
15	1.45	-8.25	2.2806	
16	1.51	-8.22	2.2814	
17	1.63	-8.15	2.2792	
18	2.52	-7.77	2.3139	
19	4.37	-7.30	2.3219	
20	5.05	-7.17	2.3206	
21	5.47	-7.10	2.3218	
22	7.13	-6.87	2.3230	
23	7.20	-6.86	2.3238	
24	7.62	-6.87	2.3239	
25	13.80	-6.30	2.3248	
26	13.84	-6.29	2.3250	
27	15.03	-6.22	2.3235	
28	15.25	-6.21	2.3241	

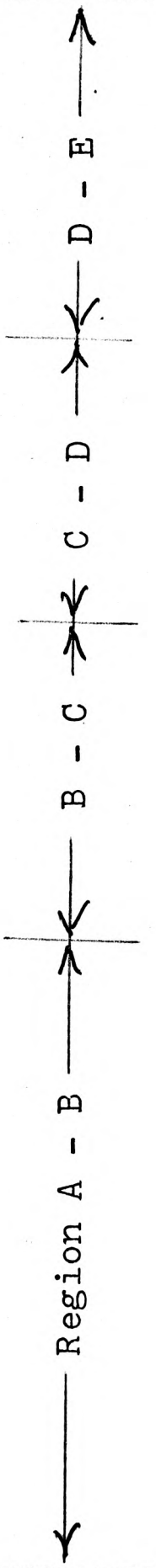

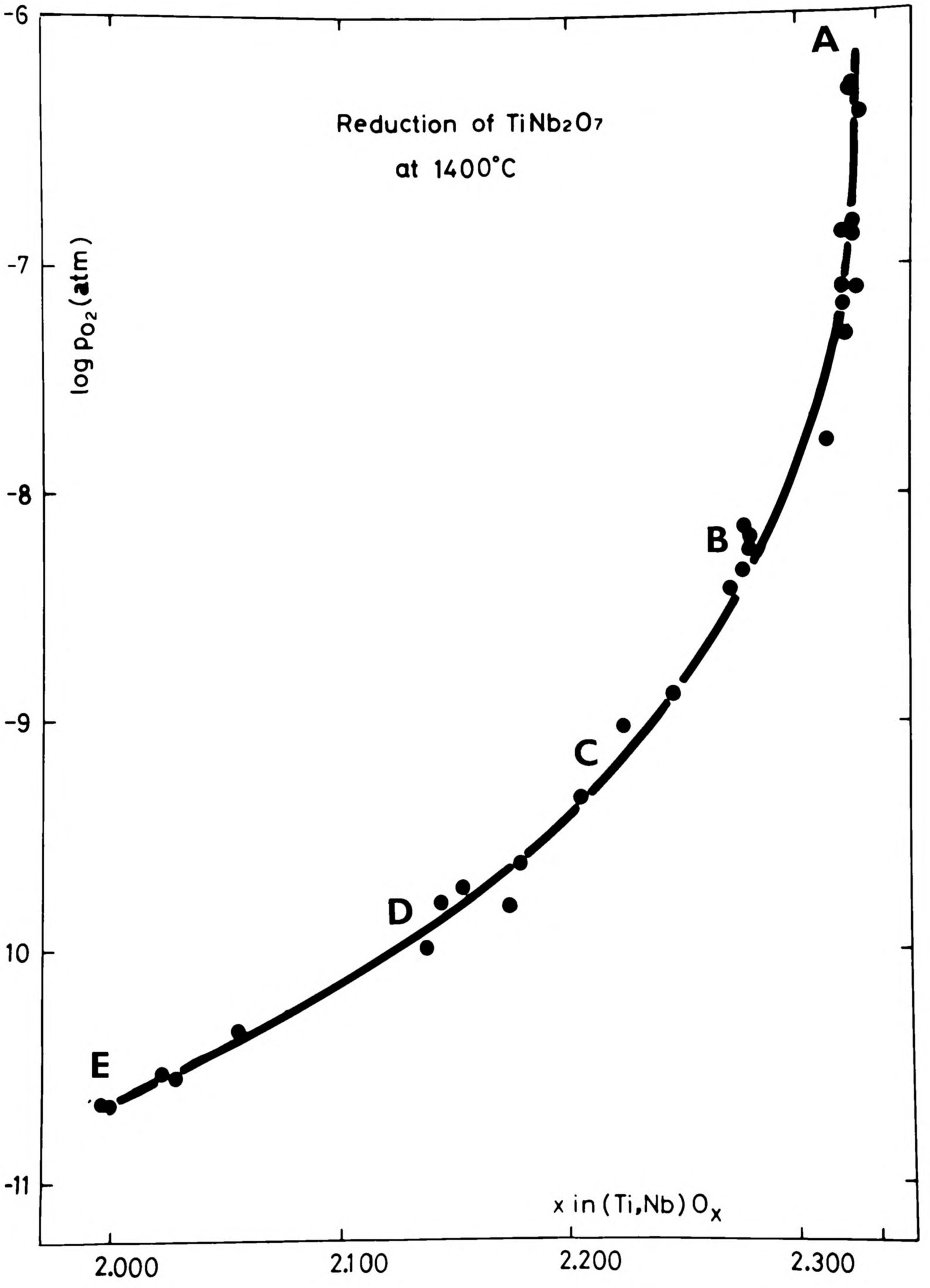
Reduction of TiNb2O7
at 1400°C
log Po2 (atm)
-6
-7
-8
-9
10
-11
A
B
C
D
E
x in (Ti,Nb) Ox
2.000
2.100
2.200
2.300

FIG. 18

Figure 18 shows that the composition of all the samples in the range of $(Ti,Nb)C_{2.000}$-$(Ti,Nb)O_{2.333}$, which are in equilibrium with their respective oxygen partial pressures, lie very close to a smooth and continuous parabolic curve. No singularities which would be indicative of the formation of discrete intermediate phases can be detected. In terms of classical thermodynamics, the diagram appears to reflect the presence of a single solid phase with a wide range of non-stoichiometry.

7.3.1.3. Structural studies

The reduced oxides, dark blue in colour, were studied by X-ray powder diffraction, electron diffraction and electron microscopy.

7.3.1.3.1. X-ray powder diffraction studies

A detailed analysis of the X-ray powder patterns of the oxides indicates that $TiNb_2O_7$ under reducing atmospheres rejects a rutile phase, $Ti_xNb_{1-x}O_2$, from the matrix and itself transforms to a $Me_{12}O_{29}$ (Me = Ti,Nb) compound.

The composition (i.e. Ti/Nb ratio) of the rutile phase is found to be dependent on the equilibrium oxygen partial pressure. At higher pressures, the rutile phase appears to be richer in titanium than at lower oxygen potentials. With regard to the rutile phase composition, thereduced oxides are classified into four different regions, marked A-B, B-C, C-D and D-E in the diagram (Fig. 18). The composition range of each region and its corresponding

partial pressures at the highest and lowest points of the region boundaries are listed in Table 17. Findings of each region are discussed below:

Region A-B

In this region, the diffraction patterns show the presence of the starting material ($TiNb_2O_7$) and some impurity lines. The impurity lines are consistent with the formation of rutile phases, $Ti_xNb_{1-x}O_2$, with $x > 0.5$.

Region B-C

Powder patterns of oxides in this region show the occurrence of both block-structure and rutile phases. The rutile phase, in all the oxides, appears to have the composition $Ti_{0.5}Nb_{0.5}O_2$.

In the higher composition range (i.e. MeO_x; $2.26 \lesssim x \lesssim 2.28$), the reflections of the block-structure phase indicate the presence of $TiNb_2O_7$ structure; in the lower composition range (i.e. MeO_x; $2.20 \lesssim x \lesssim 2.26$), $Ti_2Nb_{10}O_{29}$ (orthorhombic) lines are observed (Plates 19 and 20). In Plate 19, the Guinier powder patterns of oxides $MeO_{2.2806}$ (labelled B) and $MeO_{2.2463}$ (C) are compared with patterns of the starting material, $TiNb_2O_7$ (A) and the standard $Ti_{0.5}Nb_{0.5}O_2$ (D).

In Plate 20, a Guinier powder pattern of $MeO_{2.2008}$ (B) has been compared with powder patterns of o-$Ti_2Nb_{10}O_{29}$ (A) and $Ti_{0.5}Nb_{0.5}O_2$ (E).

Region C-D

Powder patterns of all the oxides in this region comprised both rutile phase with the composition of $Ti_{0.5}Nb_{0.5}O_2$ and o-$Me_{12}O_{29}$ reflections. This is shown in Plate 20 in

PLATE 19

PLATE 19

Guinier X-ray powder diffraction patterns (Section 7.3.1.3.1.) of:

A) The starting material $TiNb_2O_7$.

B) A reduced $TiNb_2O_7$ sample having the composition $(Ti,Nb)O_{2.2806}$.

C) A reduced $TiNb_2O_7$ sample having the composition $(Ti,Nb)O_{2.2463}$.

D) A standard $Ti_{0.5}Nb_{0.5}O_2$ compound.

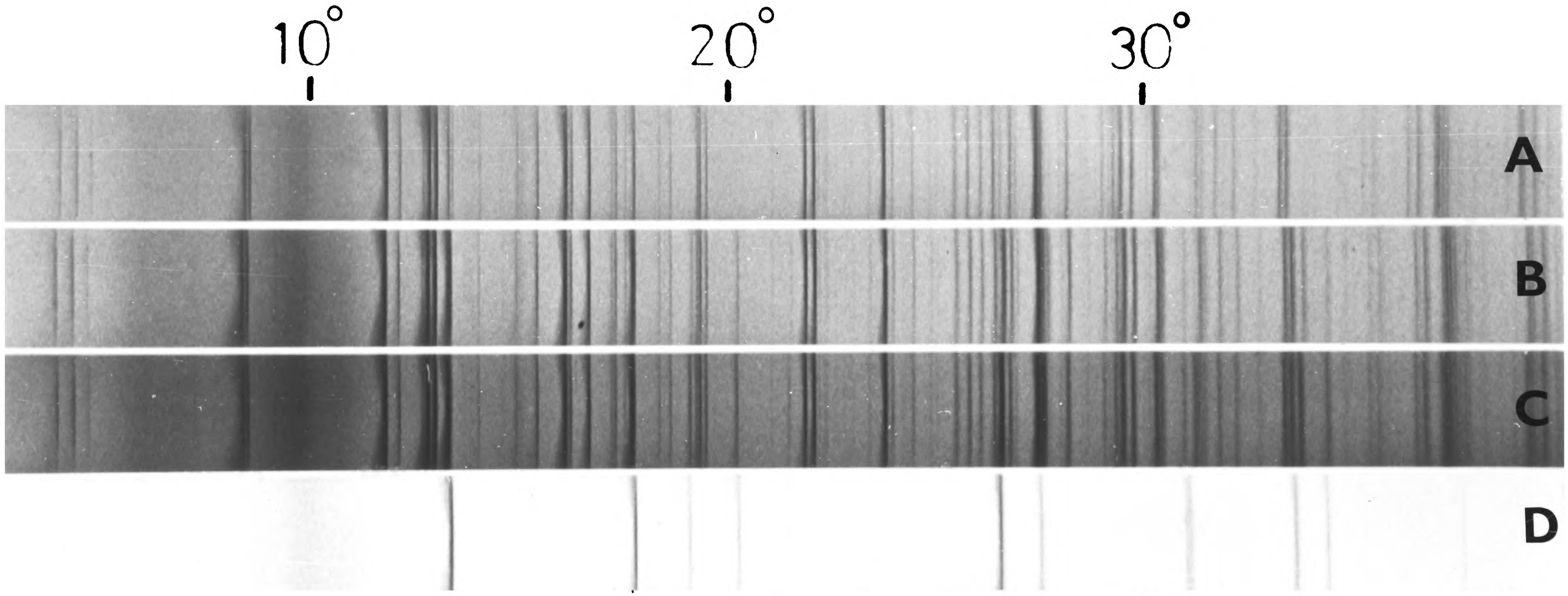

Plate 19

PLATE 20

PLATE 20

Guinier X-ray powder diffraction patterns (Section 7.3.1.3.1.) of:

A) Standard o-$Ti_2Nb_{10}O_{29}$.

B) A reduced $TiNb_2O_7$ sample having the composition $(Ti,Nb)O_{2.2005}$.

C) A reduced $TiNb_2O_7$ sample with composition $(Ti,Nb)O_{2.1740}$.

D) A reduced $TiNb_2O_7$ sample with composition $(Ti,Nb)O_{2.1435}$.

E) A standard $Ti_{0.5}Nb_{0.5}O_2$ compound.

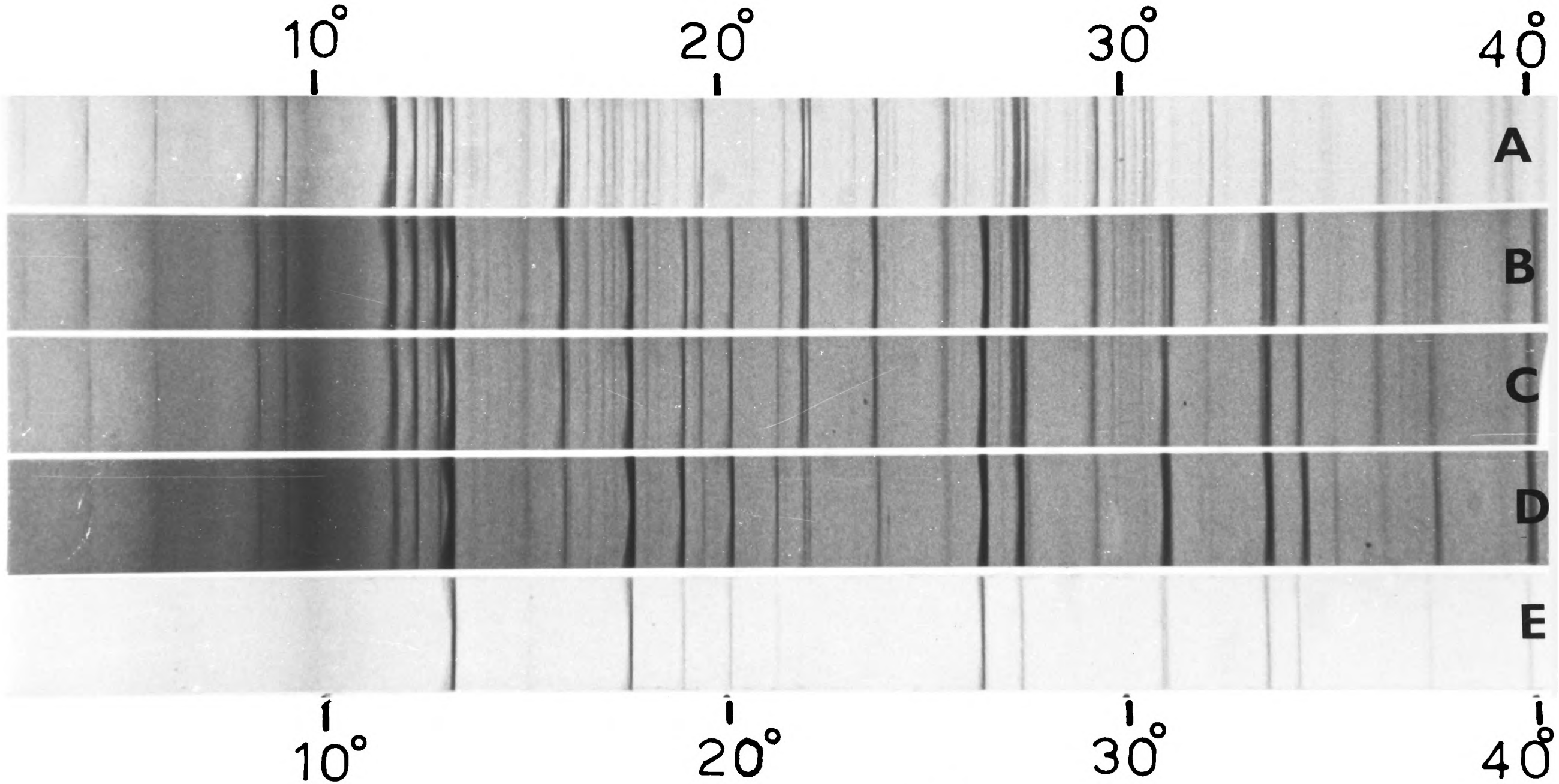

Plate 20

which Guinier patterns of $MeO_{2.2005}$ (B), $MeO_{2.1740}$ (C) and $MeO_{2.1435}$ (D) are compared with o-$Ti_2Nb_{10}O_{29}$ (A) and $Ti_{0.5}Nb_{0.5}O_2$ (E) patterns.

Region D-E

In this region, X-ray powder patterns contain o-$Me_{12}O_{29}$ and rutile phase reflections. The gradual displacement of rutile lines towards the final composition of $TiNb_2O_6$ suggests that a progressive enrichment of niobium in the rutile phase ($Ti_xNb_{1-x}O_2$) takes place as the reduction proceeds at lower oxygen partial pressures.

7.3.1.3.2. Electron microscopy studies

Electron diffraction and electron microscopy were applied to study the ultrastructure of the intermediate block-based oxides. The results are presented below following the same classification as in the X-ray powder studies.

Region A-B

Electron optical studies of the oxides in this region showed the exclusive presence of the starting material - i.e. single crystals having block-structures of $(3 \times 3)_\infty$. This finding, which is consistent with the X-ray study, may indicate that the reduction of $TiNb_2O_7$ in this composition range takes place via a partial formation of an isomorphous Nb_3O_7 compound which occurs in solid solution with the starting material. The existence of Nb_3O_7 as a distinct phase in the NbO_2-Nb_2O_5 system has not been reported in the literature - e.g. see Nimmo and Anderson (1972). However, a tentative indication of its partial generation in the present ternary system is given in a proposed phase diagram

PLATE 21

PLATE 21

a) High resolution two-dimensional lattice image of a crystal fragment taken from a reduced $TiNb_2O_7$ sample ($MeO_{2.2245}$). The generated phase, i.e. monoclinic $Me_{12}O_{29}$ contains remnants (↑ A) of the initial phase $TiNb_2O_7$. (Section 7.3.1.3.2.).

b) Idealized model of the outlined area x in (a), showing a monoclinic $Me_{12}O_{29}$ structure, the unit cell of which is indicated. Coherent intergrowth of (3 x 3) blocks of $TiNb_2O_7$ are labelled ↑ A.

c) (h0l) reciprocal section of the same crystal as shown in (a).

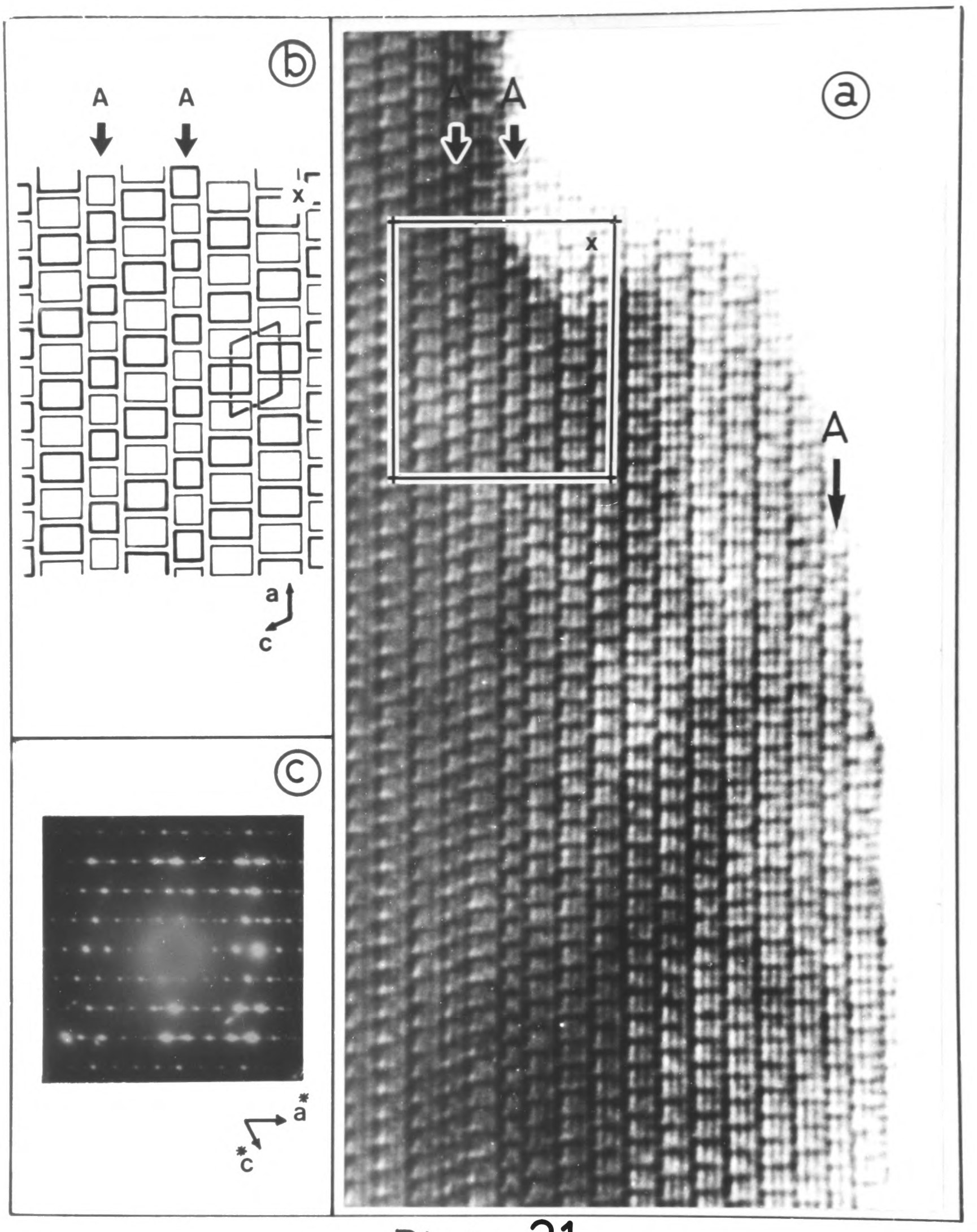

Plate 21

(Figure 22).

Region B-C

In oxides having compositions of $MeO_{2.2463}$ and $MeO_{2.2245}$, all the single crystals contained strips and domains of the starting material in a matrix of $Me_{12}O_{29}$. The density of the remaining elements of the initial phase in the crystals of sample $MeO_{2.2245}$ was lower than that in the oxide $MeO_{2.2463}$. This finding is significant since it explains clearly the reason for the bivariant appearance of the equilibrium diagram (Figure 18). It follows that the phase change from $TiNb_2O_7$ into an $Me_{12}O_{29}$ structure, under controlled oxygen potentials, takes place in a continuous and coherent manner.

Plate 21-a depicts a high resolution lattice image (h0l section) of a single crystal fragment taken from sample $MeO_{2.2245}$. The micrograph shows the simultaneous occurrence of the initial phase ($TiNb_2O_7$) and the intermediate phase ($Me_{12}O_{29}$). The initial phase, represented by strips of (3 x 3) blocks (↑ A), is coherently intergrown with the m-$Me_{12}O_{29}$ structure along the (001) ReO_3 plane.

The monoclinic form of $Me_{12}O_{29}$ is known to be a low temperature phase which transforms into an orthorhombic polymorph at higher temperatures (Norin, 1963; Wadsley, 1961b) such as presently applied (1400°C). The present observations suggest that the transformation of $TiNb_2O_7$ into o-$Me_{12}O_{29}$ takes place via formation of an m-$Me_{12}O_{29}$ precursor.

In Plate (21-b), a projection along the b-axis of an idealized model for the area labelled (x) is shown. The

regions of m-$Me_{12}O_{29}$ are interrrupted by lamellae of (3 x 3) blocks (indicated ↑ A). The unit cell of m-$Me_{12}O_{29}$ is outlined; its lattice parameters are a = 20.50 Å, b = 3.80 Å, c = 15.37 Å and β = 114°.

In Plate (21-c) the electron diffraction pattern of the same crystal fragment is given; the pattern shows the (h0l) reciprocal lattice section.

Regions C-D and D-E

Three oxides, having compositions of $MeO_{2.2005}$, $MeO_{2.1775}$ and $MeO_{2.1435}$, were studied by electron microscopy.

In sample $MeO_{2.2005}$ the majority of the crystals have a perfect o-$Me_{12}O_{29}$ structure, but a few crystals show occasional Wadsley defects consisting of strips of (3 x 3) blocks of octahedra.

Samples $MeO_{2.1778}$ and $MeO_{2.1435}$ consist exclusively of an o-$Me_{12}O_{29}$ phase suggesting that a complete transformation of $TiNb_2O_7$ into a solid solution of o-$Ti_2Nb_{10}O_{29}$ and $Nb_{12}O_{29}$ has taken place.

The above results are consistent with the X-ray powder diffraction findings of o-$Me_{12}O_{29}$ reflections reported above. Both findings indicate that the bivariant feature of regions C-D and D-E in the equilibrium diagram (Fig. 18) is due to a progressive reduction of the o-$Ti_2Nb_{10}O_{29}$ into an o-$Nb_{12}O_{29}$ phase. The two phases in the intermediate oxides of regions C-D and D-E, thus, occur in solid solution.

In contrast to the above finding of a continuous phase change from $TiNb_2O_7 \rightarrow Ti_2Nb_{10}O_{29} \rightarrow Nb_{12}O_{29} \rightarrow TiNb_2O_6$, one single crystal out of several examined by electron microscopy of sample $MeO_{2.2005}$ had a different

PLATE 22

PLATE 22

A) High resolution two-dimensional lattice image of a crystal fragment taken from a reduced $TiNb_2O_7$ sample having a composition $MeO_{2.2005}$. The crystal structure reveals anomalous 6 Å wide dark contrast bands running into the crystal in parallel to the $(001)_{ReO_3}$ plane. White contrast dots occur on these bands in a regular periodicity.

B) (h0l) electron diffraction pattern of the same crystal fragment as shown in (A). The pattern suggests the presence of a well-ordered o-$Me_{12}O_{29}$ structure and this is in direct conflict with the crystal lattice image shown in (A).

A possible explanation for this anomaly is given in Section 7.3.1.3.2. and is illustrated in Plate 23.

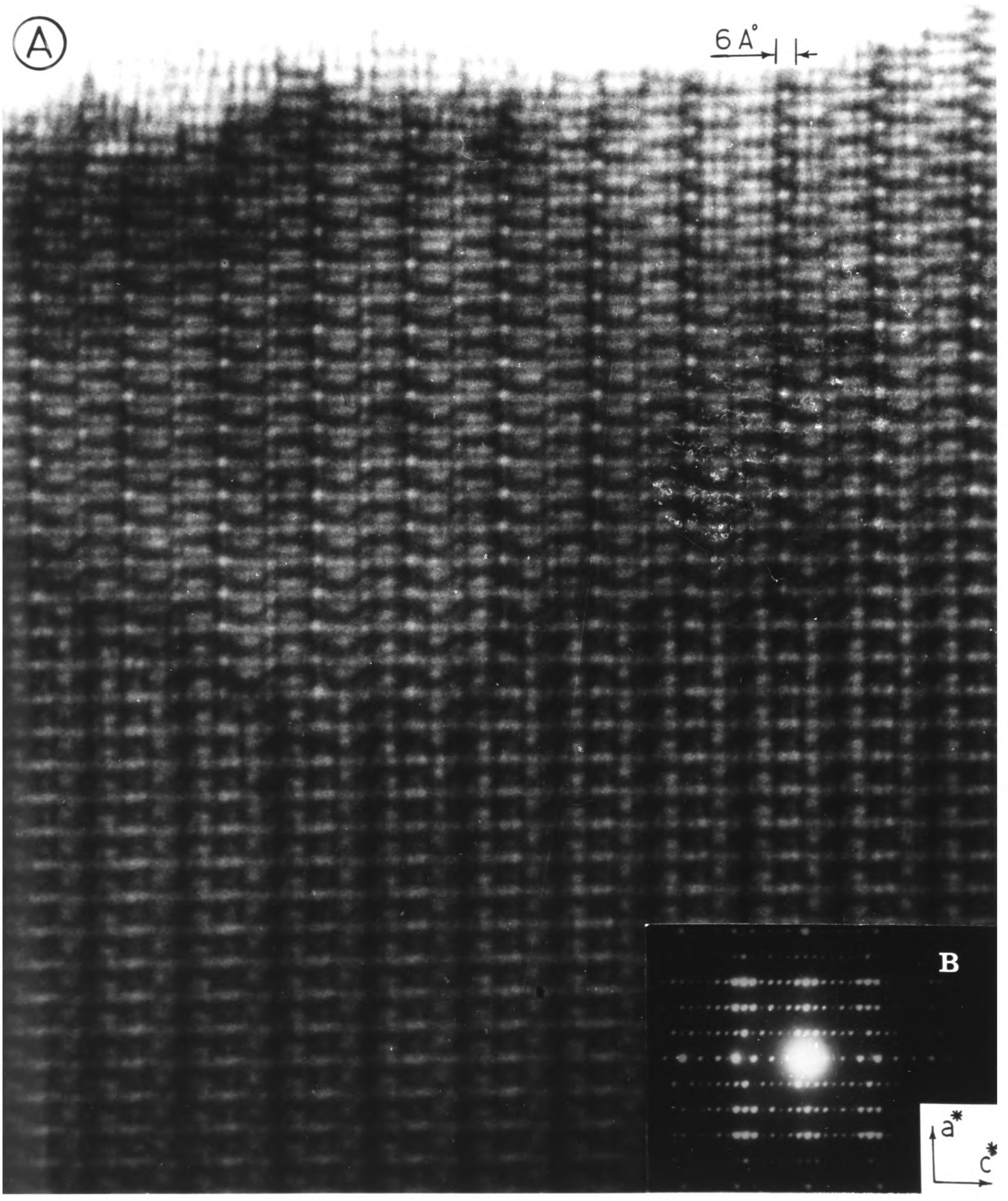

Plate 22

structure which suggested an alternative reduction pathway - i.e. an abrupt and discontinuous phase change. Evidence for this is given below:

Plate 22-A shows a (h0l) lattice image of this particular crystal which appears to be in contradiction with its corresponding (h0l) electron diffraction pattern (Plate 22-B). The pattern indicates the occurrence of a well ordered o-$Me_{12}O_{29}$ phase whereas the electron micrograph suggests the existence of an entirely different structure. In Plate 23, the tentative contrast diagram (C) based upon the lattice image (D), shows a perfect projection through a set of (3 x 3) and (4 x 3) arrays on either side of the usual 2 Å wide cation rows (an ordinary shear plane). The sets of (3 x 3) and (4 x 3) blocks are separated by bands 6 Å wide. The contrast in these bands is distinctly heavier than in the remainder of the crystal. The repetitive occurrence of white spots with a regular periodicity of 10 Å, along the dark bands represents an overlap contrast of the blocks on either side of the band.

The idealized models, shown in (A) and (B) of Plate 23, depict a plausible structure for this crystal. The structure consists of alternative arrays of (5 x 3) and (4 x 3) octahedral blocks. The (5 x 3) and (4 x 3) columns, at the same level, overlap at every other common intergrowth plane, thus, giving rise to the formation of rectangular tunnels with dimensions of 5.6 x 2.8 $Å^2$. The tunnels extend through the crystal in parallel to the [010] direction and have repeat distances of 10 Å and 22 Å along the a and the c axis of the crystal, respectively. In the overlap region

PLATE 23

PLATE 23

A and B) Plausible structure suggested for the crystal image shown in Plate 22 and given, in higher magnification in D.

C) A tentative contrast diagram based on the lattice image shown in D.

D) A high magnification of the same crystal structure as shown in Plate 22.

The unit cell of the crystal is outlined, both, in the lattice image in (D), and in the proposed model of the structure in (A). The unit cell parameters are almost identical with those of o-$Me_{12}O_{29}$. The unit cell composition is $Me_{25}O_{60}$.

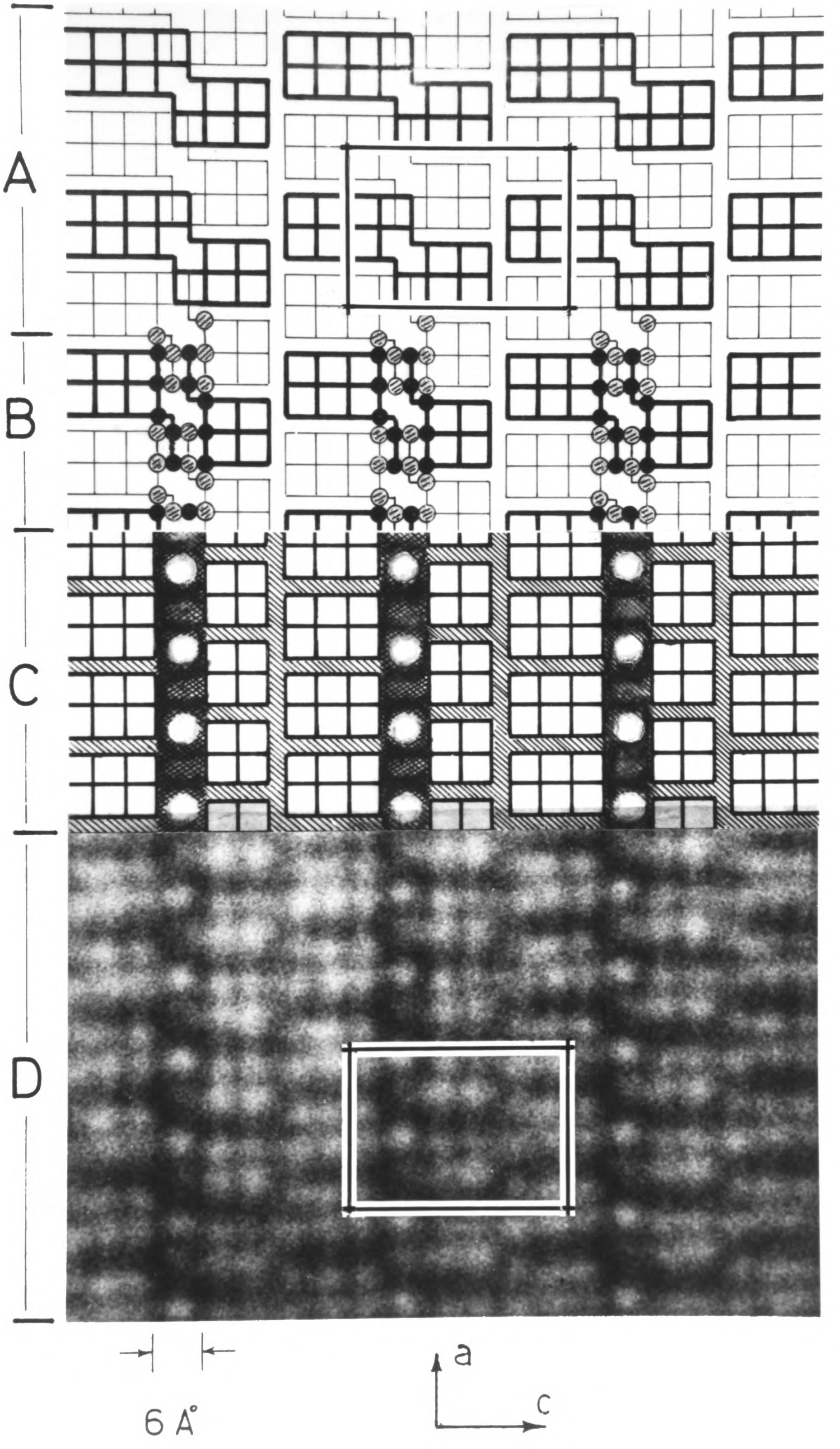

Plate 23

PLATE 24

PLATE 24

A proposed mechanism for an abrupt and discontinuous reduction of $TiNb_2O_7 \rightarrow Me_{25}O_{60} \rightarrow$ o-$Me_{12}O_{29}$.

A) a two-dimensional lattice image of the same crystal fragment as shown in Plates 22 and 23.
6 Å wide dark contrast bands continue into 2 Å wide dark lines (an ordinary CS plane) suggesting that the two structures of $Me_{25}O_{60}$ (Region M) and o-$Me_{12}O_{29}$ (Region N) are intergrown on the $(001)_{ReO_3}$ plane.

B) An idealized model for the intergrowth of $Me_{25}O_{60}$ (M) and o-$Me_{12}O_{29}$ (N) is depicted.

C) An atomic reshuffling is suggested to be associated with the transformation of $Me_{25}O_{60}$ into o-$Me_{12}O_{29}$ and rutile phase (Section 7.4.).

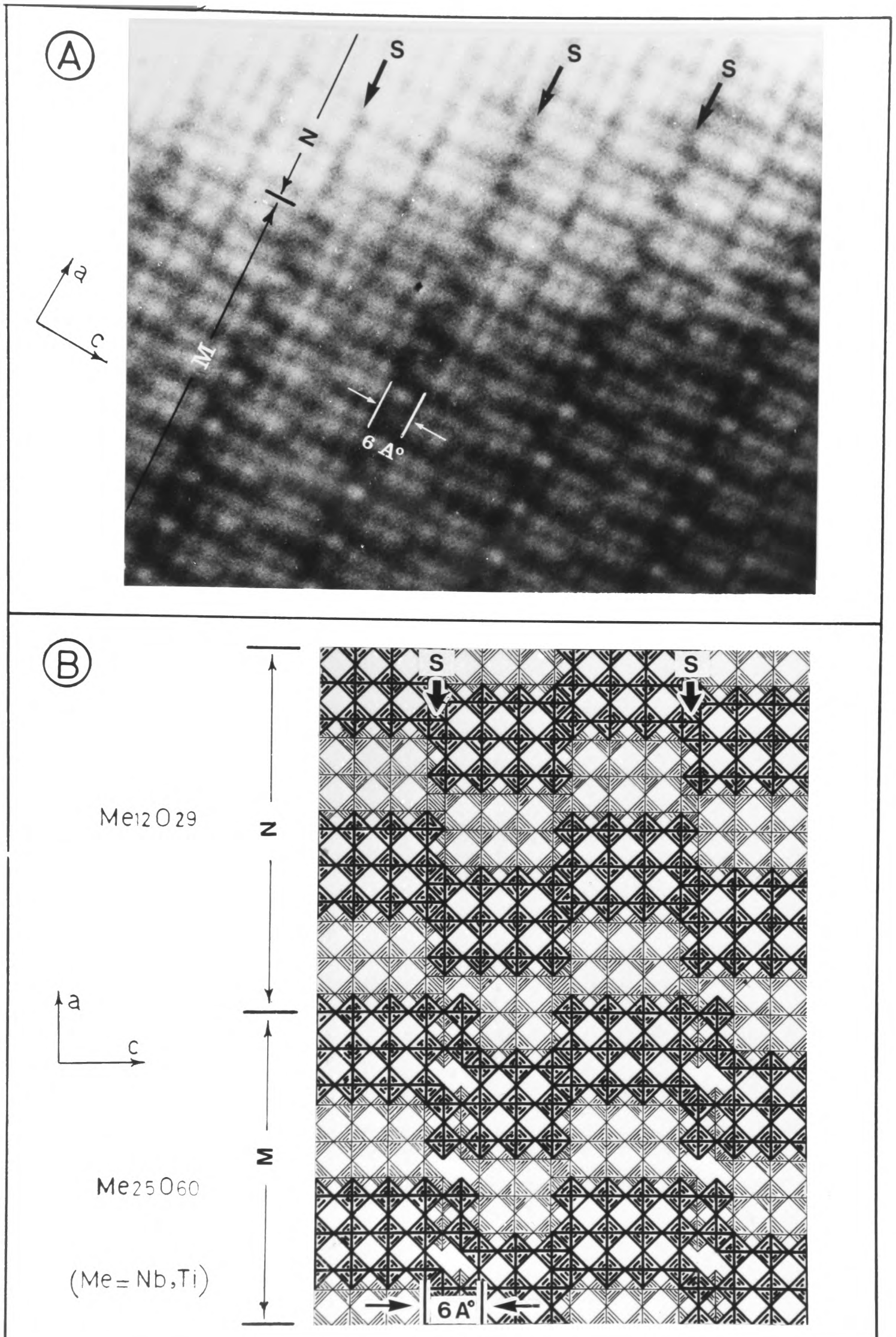
A
S
S
S
N
a
c
M
6 A°
B
Me12O29
N
S
S
a
c
M
Me25O60
(Me = Nb, Ti)
6A°
C
1
2
3
a
b
e
f
g
+MeO2

Plate 24

of the blocks (- i.e. the 6 Å wide band) the metal atom density has clearly increased and this probably is the reason for the very distinct contrast observed in the lattice image (D).

The unit cell of the crystal, outlined in both (A) and (D), shows an orthorhombic symmetry with lattice parameters of a = 28.50 Å, b = 3.8 Å, c = 20.51 Å. These dimensions are almost identical to those reported for o-$Ti_2Nb_{10}O_{29}$ (Wadsley, 1961b) and this similarity explains the appearance of the corresponding selected area electron diffraction pattern (Plate 22-B).

As calculated from the idealized model (Plate 23-A), the unit cell composition is $Me_{25}O_{60}$ ($MeO_{2.400}$). This is a new compound, hitherto not reported in the literature.

7.3.1.4. Summary

Phase equilibria measurements in the system (Ti,Nb)O_2-$TiNb_2O_7$ were carried out thermogravimetrically at 1400°C. Oxygen partial pressures in equilibrium with the oxides were generated by using CO_2 - CO gas buffer mixtures.

The phase equilibrium diagram exhibits a continuous and parabolic shape which suggests, in terms of classical thermodynamics, the presence of a solid phase with a wide range of non-stoichiometry. Structural studies (X-ray powder diffraction, electron diffraction and electron microscopy), however, have shown the presence of distinct intermediate phases such as $Me_{25}O_{60}$, m-$Ti_2Nb_{10}O_{29}$, m-$Nb_{12}O_{29}$, o-$Ti_2Nb_{10}O_{29}$, o-$Nb_{12}O_{29}$ and $Ti_xNb_{1-x}O_2$. In the majority of the crystals

TABLE 18

TABLE 18

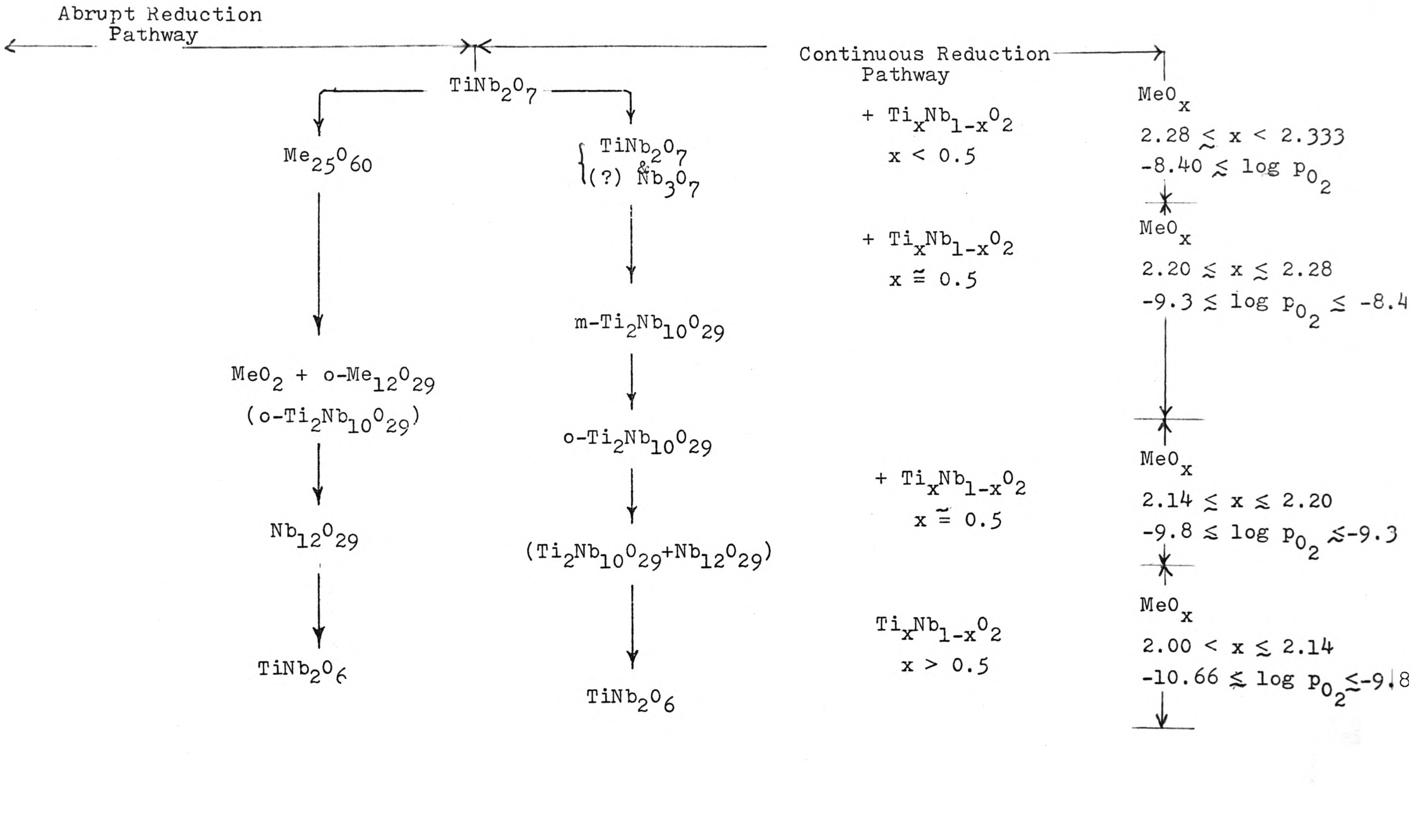
Abrupt Reduction Pathway
Continuous Reduction Pathway
TiNb2O7
Me25O60
{ TiNb2O7 &(?) Nb3O7
MeO2 + o-Me12O29
(o-Ti2Nb10O29)
Nb12O29
TiNb2O6
m-Ti2Nb10O29
o-Ti2Nb10O29
(Ti2Nb10O29+Nb12O29)
TiNb2O6
+ TixNb1-xO2
x < 0.5
+ TixNb1-xO2
x ≅ 0.5
+ TixNb1-xO2
x ≅ 0.5
TixNb1-xO2
x > 0.5
MeOx
2.28 ≲ x < 2.333
-8.40 ≲ log pO2
MeOx
2.20 ≲ x ≲ 2.28
-9.3 ≲ log pO2 ≲ -8.4
MeOx
2.14 ≲ x ≲ 2.20
-9.8 ≲ log pO2 ≲-9.3
MeOx
2.00 < x ≲ 2.14
-10.66 ≲ log pO2 ≲-9.8

studied by electron microscopy, the neighbouring phases were found to be intergrown coherently as lamellae or domains suggesting that the reduction proceeds in a continuous and coherent manner. Associated with these structural transformations, a rutile phase, $Ti_xNb_{1-x}O_2$, is rejected from the matrix. The composition of the rutile phase is dependent on the oxygen partial pressure - i.e. at higher oxygen potentials the rutile phase is richer in titanium than the one obtained at lower oxygen potentials. These structural observations are consistent with the bivariance of the equilibrium diagram.

Structural data obtained from one crystal fragment suggest that $TiNb_2O_7$ may also transform in an abrupt process during which a metastable transient phase occurs.

The two possible reduction pathways are summarized in Table 18.

7.3.2. PART "B"

PHASE EQUILIBRIA IN THE SYSTEM $(Ti,Nb)O_2$-O-$Ti_2Nb_{10}O_{29}$ AT THE ISOTHERM 1400°C

TABLE 19

TABLE 19

Guinier X-ray diffraction pattern of o-$Ti_2Nb_{10}O_{29}$:

a = 28.50 Å, c = 20.51 Å (Wadsley, 1961b)

I (obs.)	d (Cm)	$Sin^2\theta$ (obs.)	$Sin^2\theta$ (calc.)	hkl
w	1.20	0.005614	0.00564	002
m+	1.28	0.006386	0.00637	102
m	1.73	0.011646	0.01168	400
v.v.w.	2.11	0.017290	0.01732	402
s	2.41	0.022517	0.02256	004
m	2.48	0.023833	0.02389	502
m	2.61	0.026375	0.02628	600
v.s.	3.32	0.04244	0.04237	011
v.s.	3.35	0.043201	0.04310	111
v.s.	3.49	0.046829	0.04673	800
m	3.57	0.048964	0.04894	311
v.s.	3.66	0.051420	0.05148	106
v.s.	3.69	0.052252	0.05237	802
m+	3.74	0.053651	0.05367	206
w	3.77	0.054499	0.05438	113
w-	3.87	0.057371	0.05732	306
w-	3.91	0.05854	0.05833	704
w+	3.98	0.060611	0.06063	511
w	4.14	0.065471	0.06533	413
w	4.26	0.06923	0.06929	804
w+	4.38	0.073086	0.07301	1000
v.s.	4.51	0.077376	0.07704	606
s	4.56	0.079050	0.07913	215
v.w.	4.64	0.081769	0.08170	904
m	4.67	0.082799	0.08278	315
m+	4.81	0.087685	0.08789	415
m+	4.88	0.090176	0.09023	008
w	4.90	0.090893	0.09096	108
m+	5.03	0.095618	0.09557	1004
m+	5.08	0.094464	0.09748	806
m	5.19	0.10158	0.10151	911
m	5.29	0.105387	0.10514	1200
m	5.43	0.110821	0.11078	1202
s	5.48	0.112790	0.11279	913
v.v.w.	5.76	0.124097	0.12377	1006
w	5.82	0.126580	0.12666	1013
m	6.05	0.136293	0.13633	617
s	6.18	0.141916	0.14171 0.14200	10 10 1113
s	6.22	0.143665	0.14390	2010
w	6.43	0.152994	0.15266	40 10
m	6.54	0.157977	0.15808	219
s	6.71	0.165803	0.16566 0.16577	1404 1311
m	6.78	0.169070	0.16918	917
m	6.85	0.172363	0.17241	222
m	6.98	0.178543	0.17857	1108
m	7.17	0.187728	0.18771 0.18774	80 10 522

7.3.2.1. Assessment of the purity and structural homogeneity of the starting material ($o\text{-}Ti_2Nb_{10}O_{29}$)

To investigate the purity of the starting material, an X-ray powder diffraction pattern was taken. The results (listed in Table 19) showed that the pattern was consistent with the lattice parameters of $o\text{-}Ti_2Nb_{10}O_{29}$ given by Wadsley (1961b). No extraneous lines were present, indicating that the material was pure and homogeneous.

The sample was also studied by electron microscopy. In Plate 25-A, a high resolution (h0l) lattice image of a thin crystal fragment, representative of the sample, is shown. In Plate 25-B, a b-axis projection of an idealized model of the crystal structure is given. In the model, columns of (4 x 3) octahedra are linked in a zig-zag fashion by octahedra sharing edges. Alternate blocks in the b-axis direction give an axial length of b = 3.80 $\mathring{A}$. The projection of the unit cell is indicated by dashed lines which measure a = 28.5 $\mathring{A}$ and c = 20.5 $\mathring{A}$. From the same region as shown in (25-A), an electron diffraction pattern of the crystal is depicted (Plate 25-C). The pattern confirms the structural homogeneity of the crystal.

7.3.2.2. Thermodynamics

The system $(Ti,Nb)O_2\text{-}Ti_2Nb_{10}O_{29}$ was investigated thermogravimetrically at 1400°C over a range of oxygen potentials established by using CO_2-CO gas buffer mixtures. The results are given in Table 20.

The variation of the oxide composition with the oxygen

PLATE 25

PLATE 25

A) A two-dimensional lattice image of an o-$Ti_2Nb_{10}O_{29}$ crystal (Section 7.3.2.1.).

B) An idealized model of the $(4 \times 3)_\infty$ blocks of o-$Ti_2Nb_{10}O_{29}$ shown in (A). The unit cell of the crystal structure is outlined.

C) h0l reciprocal lattice section of the same crystal as shown in (A).

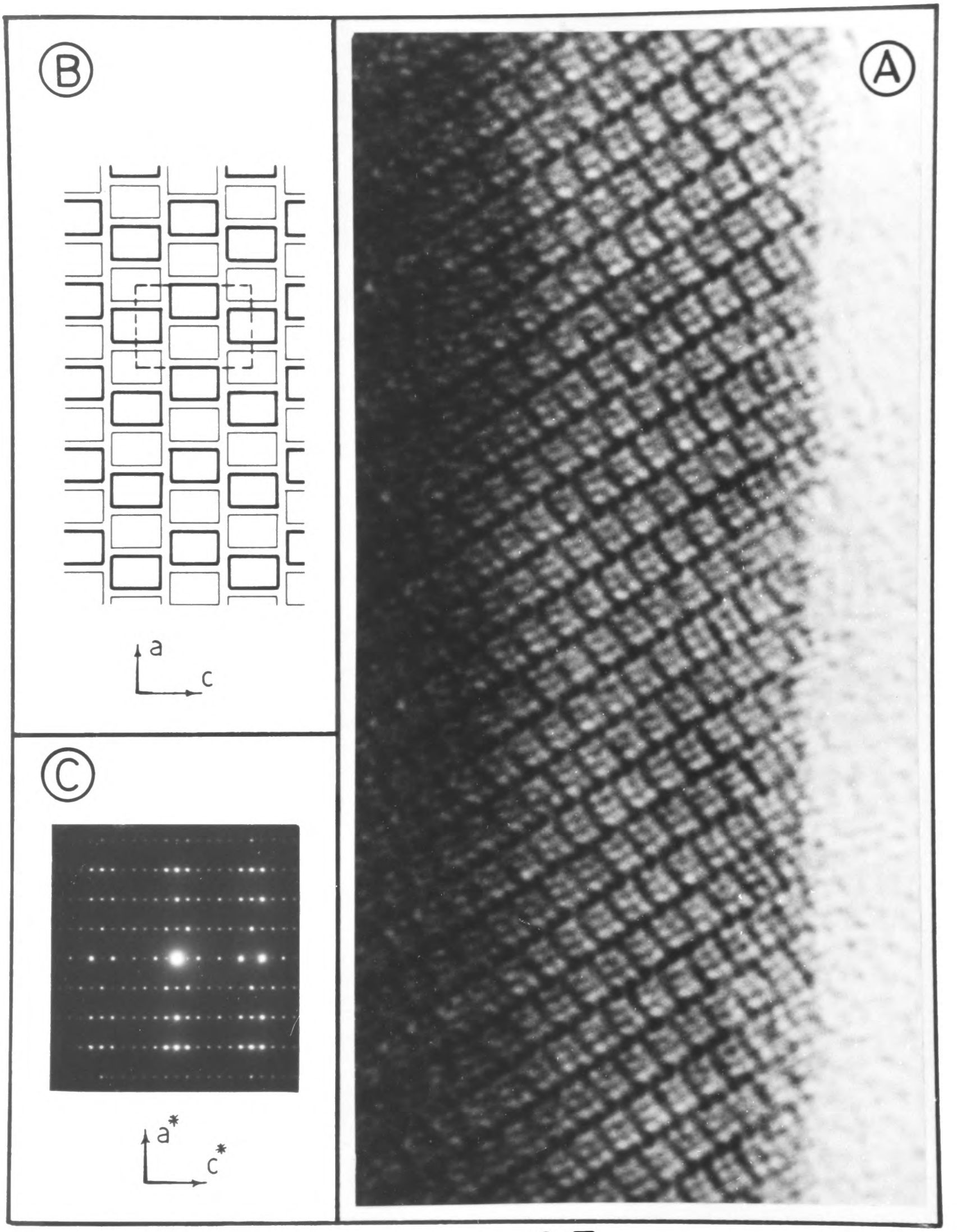

Plate 25

partial pressure is represented in a diagram (Fig. 19) which shows a smooth and continuous relationship between the oxide composition and its corresponding oxygen partial pressure, similar to that found in the system $(Ti,Nb)O_2$-$TiNb_2O_7$ (see Section 7.3.1.). No discrete steps, suggestive of biphasic behaviour, can be detected. In terms of the classical Gibbs phase rule, the diagram implies a single phase with a wide range of non-stoichiometry. In this particular case, the pseudobivariant characteristic found in the diagram may suggest that the interconversion of oxides in this system takes place through a continuous intergrowth of rows or domains of neighbouring phases in the host structure.

The diagram further shows that the composition variation of oxides in the region MeO_x; $2.38 \lesssim x < 2.417$; (labelled A-B in Fig. 19) is achieved with large changes in oxygen potential. By contrast, in the region MeO_x; (labelled B-C in Fig. 19); $(2.29 \lesssim x \lesssim 2.38)$, a marked increase in the degree of reduction occurs with small changes of oxygen partial pressures, and is reflected in the parabolic shape of curve. At still lower oxygen potentials (MeO_x; $2.00 < x \lesssim 2.29$), a drastic change in oxide composition with a small variation in oxygen pressure takes place (segment C-D in Fig. 19).

7.3.2.3. Structural studies

X-ray powder diffraction patterns for all the reduced oxides in the composition range of $(Ti,Nb)O_2$-$Ti_2Nb_{10}O_{29}$ indicate the presence of an orthorhombic $Me_{12}O_{29}$ phase (Me = Ti,Nb) and a rutile phase ($Ti_xNb_{1-x}O_2$). The rutile

TABLE 20

TABLE 20

System $(Ti,Nb)O_2$ - $Ti_2Nb_{10}O_{29}$. Equilibrium Results at 1400°C

Specimen no.	CO_2/CO	log p_{O_2}	Composition $(Ti,Nb)O_x$	Structural studies (see Section 7.3.2.)
1	0.05	-11.17	2.005	
2	0.08	-10.77	2.0203	
3	0.10	-10.55	2.1718	
4	0.11	-10.49	2.2158	
5	0.12	-10.38	2.1851	
6	0.14	-10.28	2.2382	
7	0.18	-10.06	2.2937	
8	0.19	-10.02	2.3085	
9	0.24	-9.81	2.3461	
10	0.26	-9.74	2.3444	
11	0.30	-9.62	2.3619	
12	0.30	-9.62	2.3649	
13	0.33	-9.53	2.3582	
14	0.43	-9.31	2.3760	
15	0.44	-9.28	2.3754	
16	0.52	-9.14	2.3841	
17	0.59	-9.03	2.3855	
18	0.71	-8.87	2.3868	
19	1.01	-8.56	2.3949	
20	1.05	-8.53	2.3949	
21	1.19	-8.42	2.3948	
22	1.19	-8.42	2.3967	
23	1.31	-8.34	2.3946	
24	1.36	-8.30	2.3975	
25	1.50	-8.22	2.3973	
26	1.82	-8.05	2.4070	
27	1.89	-8.02	2.4034	
28	2.48	-7.78	2.4021	
29	3.75	-7.42	2.4064	
30	4.69	-7.23	2.4081	
31	10.8	-6.50	2.4112	
32	13.8	-6.29	2.4125	



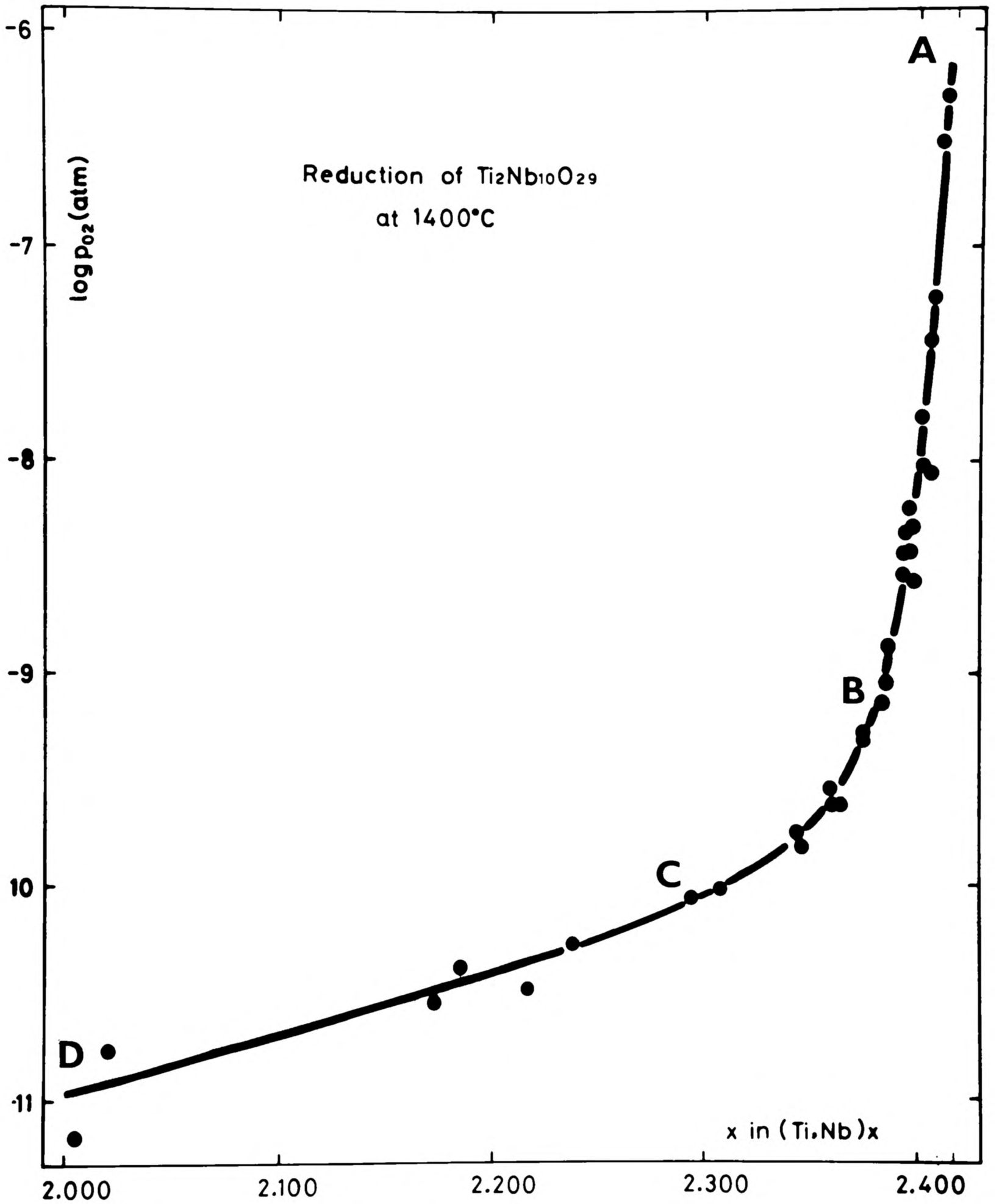
Reduction of $Ti_2Nb_{10}O_{29}$
at 1400°C
log p_{O_2}(atm)
-6
-7
-8
-9
10
·11
A
B
C
D
x in (Ti,Nb)x
2.000
2.100
2.200
2.300
2.400

FIG. 19

phase can be identified following data given by Marinder et al, (1962); in intermediate reduced oxides equilibrated at high oxygen partial pressures the titanium content of the rutile phase is higher than in oxides obtained at lower oxygen potentials. This finding instigated a classification ofintermediate oxides in two regions (labelled A-C and C-D in Fig. 19 and Table 20).

Region (A-C): In this region, the rutile phase has a fixed composition of $Ti_{0.5}Nb_{0.5}O_2$. This is illustrated in Plate 26 in which Guinier X-ray powder diffraction patterns of the oxides $MeO_{2.3444}$ and $MeO_{2.2937}$ are shown (labelled B and C, respectively). Also depicted in Plate 26 are Guinier X-ray powder patterns of the starting material o-$Ti_2Nb_{10}O_{29}$ (A) and $Ti_{0.5}Nb_{0.5}O_2$ (D).

Region (C-D): In this region, X-ray powder diffraction patterns show that (compared with a rutile phase of composition $Ti_{0.5}Nb_{0.5}O_2$) the rutile reflections have shifted towards the powder pattern of the final oxide composition, $Ti_2Nb_{10}O_{24}$. Reduction of the oxides in this region may take place by oxygen dissociation from $Nb_{12}O_{29}$ which is present in solid solution with $Ti_2Nb_{10}O_{29}$.

Examination of several single crystals of samples $MeO_{2.3949}$, $MeO_{2.3444}$ and $MeO_{2.2153}$, by electron diffraction and microscopy, show the exclusive occurrence of an o-$Me_{12}O_{29}$ phase, comparable to the starting material presented in Plate 25. This confirms the results obtained by X-ray powder diffraction.

In addition, occasional crystal fragments were

PLATE 26

PLATE 26

Guinier X-ray powder diffraction patterns (Section 7.3.2.3.). of:

A) The starting material o-$Ti_2Nb_{10}O_{29}$.

B) A reduced o-$Ti_2Nb_{10}O_{29}$ sample with composition (Ti, Nb)$O_{2.3444}$.

C) A reduced o-$Ti_2Nb_{10}O_{29}$ sample with composition (Ti,Nb)$O_{2.2937}$.

D) A standard $Ti_{0.5}Nb_{0.5}O_2$ compound.

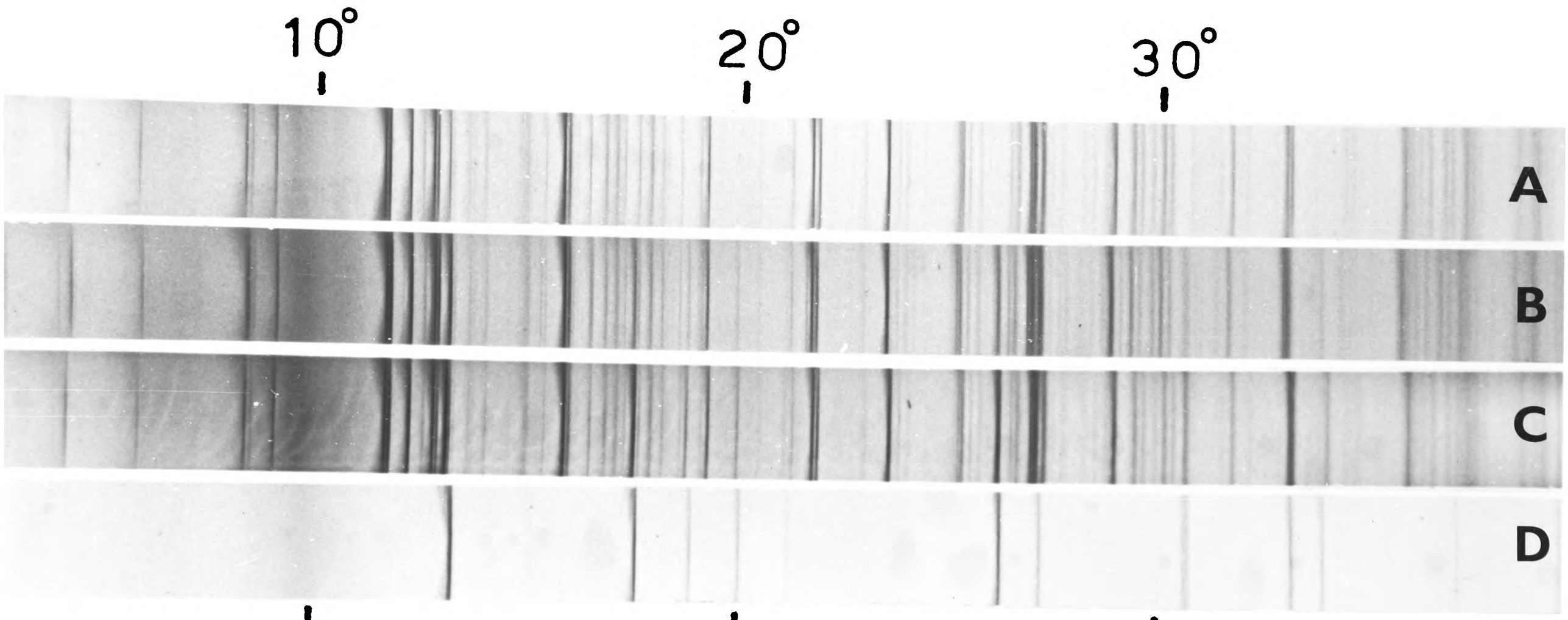

Plate 26

encountered which contained a well-ordered monoclinic $Me_{12}O_{29}$ structure. As the monoclinic $Me_{12}O_{29}$ structure is a metastable modification at this temperature (1400°C), its occurrence in the samples suggests the presence of an intermediate, metastable, stage preceding the final change into o-$Me_{12}O_{29}$.

7.3.2.4. Summary and Discussion

Phase equilibria studies in the system $(Ti,Nb)O_2$-$TiNb_2O_7$ were carried out thermogravimetrically at 1400°C. After plotting the oxide composition versus the oxygen partial pressure, a diagram was obtained which showed bivariant characteristics of the oxides throughout the system. According to the classical phase rule, the diagram suggests the occurrence of a single phase with a wide range of non-stoichiometry.

Structural studies revealed that the o-$Ti_2Nb_{10}O_{29}$ compound, in the course of reduction under controlled atmospheres, transforms progressively into a $Nb_{12}O_{29}$ phase by rejecting a rutile phase - i.e. $Ti_xNb_{1-x}O_2$ from the host lattice. The findings that the rutile phase is richer in titanium at high oxygen potentials than at lower oxygen potentials suggests the following model for the mechanism of the reduction process:

At high oxygen partial pressures, the small value of oxide weight loss in response to a large change in oxygen partial pressure (i.e. a big step decrease in p_{O_2}) in equilibrium with solid (see Section 7.3.2.2.) may reflect a progressive

outward diffusion of the altervalent cation (i.e. Ti^{4+}) from the matrix. At lower oxygen partial pressures, however, a large degree of weight loss with a small excursion from equilibrium oxygen partial pressure may arise from facile oxygen dissociation from $Nb_{12}O_{29}$ occurring in high proportion in solid solution with $Ti_2Nb_{10}O_{29}$.

The route proposed for the phase change is shown in Table 21 below:-

TABLE 21

o-$Ti_2Nb_{10}O_{29}$		
		MeO_x
		$2.29 \lesssim x < 2.417$
V		
m-$Ti_2Nb_{10}O_{29}$	$Ti_xNb_{1-x}O_2$	
	+ ($x = 0.5$)	
&		
m-$Nb_{12}O_{29}$		
V		(Me = Ti,Nb)
o-$Nb_{12}O_{29}$		
	$Ti_xNb_{1-x}O_2$	
	+	MeO_x
	$0.17 \lesssim x \lesssim 0.5$	$2 < x \lesssim 2.29$
V		
$Ti_{0.17}Nb_{0.83}O_2$		

7.3.3. PART "C"

PHASE EQUILIBRIA IN THE SYSTEM $(Ti,Nb)O_2$-$TiNb_{24}O_{62}$ AT ISOTHERM 1400°C

(Results and Discussion)

TABLE 22

TABLE 22

Guinier X-ray diffraction pattern of $TiNb_{24}O_{62}$: monoclinic, $a = 29.78\ \text{Å}$, $b = 3.821\ \text{Å}$, $c = 21.12\ \text{Å}$, $\beta = 94.9^{\circ}$

I (obs.)	d (Cm)	$\sin^2\theta$ (obs.)	$\sin^2\theta$ (calc.)	hkl
v.w.	1.06	0.004383	0.00435	201
s	1.17	0.005338	0.00531	002
w	1.37	0.007314	0.00736	202
v.w.	1.68	0.010985	0.01078	400
v.v.w.	1.72	0.011512	0.01146	401
w	1.81	0.012743	0.01275	401
v.w.	1.88	0.013743	0.01368	203
m	2.34	0.021237	0.02125	004
v.s.	2.42	0.022703	0.02265	204
m	2.62	0.026575	0.02655	601
m	2.67	0.027590	0.02762	602
v.v.w.	2.76	0.029462	0.02944	404
v.w.	2.94	0.033386	0.03320 0.03329	005 603
v.v.w.	3.19	0.039226	0.03911	603
v.w.	3.25	0.040695	0.04075	405
w	3.27	0.041191	0.04129	110
w	3.29	0.04168	0.04162	604
v.s.	3.32	0.042442	0.04246	111
s	3.33	0.042694	0.04278	111
v.w.			0.04311 0.04315	800 801
v.s.	3.45	0.045778	0.04584	802
v.s.	3.48	0.046565	0.04668	310
m	3.52	0.047624	0.04753 0.04781	311 006
m	3.55	0.048426	0.04850	311
w	3.56	0.048695	0.04856	206
v.s.	3.59	0.049505	0.04938	604
m	3.70	0.052530	0.05244 0.05260	206 605
v.w.	3.71	0.052809	0.05276 0.05296	113 312
s	3.74	0.053651	0.05373	113
w	3.78	0.054783	0.05471	406
m	3.92	0.058834	0.05894	803
v.w.	3.93	0.059128	0.05919	804
w	3.95	0.059719	0.05960	511
v.w.	3.96	0.060016	0.06009	313
v.w.	4.00	0.061209	0.06116	512
m	4.07	0.063323	0.06319	114
w	4.14	0.065471	0.06550	207
dif.w.	4.27	0.069547	0.06944 0.06953 0.06985	1002 804 805
w	4.33	0.071467	0.07133 0.07184	407 513
v.s.	4.45	0.075379	0.07530	115
w	4.47	0.076041	0.07609	711
w	4.49	0.076705	0.07668	712
v.s.	4.525	0.077700	0.07788	606
v.w.	4.59	0.080064	0.08037	407
v.s.	4.67	0.082799	0.08278	805
w	4.68	0.083144	0.08316	806
w	4.71	0.084182	0.08416	1003
w	4.79	0.086980	0.08662	515
w	4.82	0.088039	0.08813	116
w	4.88	0.090176	0.09007	116
w	4.92	0.091613	0.09158	316
w	4.94	0.092336	0.09248	1005
s	5.01	0.094884	0.09470	515

7.3.3.1. Assessment of the purity of the starting material ($TiNb_{24}O_{62}$)

$TiNb_{24}O_{62}$ samples were prepared according to the procedure described in Section 7.2.1. The sample was characterized by X-ray powder diffraction, electron diffraction and electron microscopy methods. The X-ray powder diffraction pattern was indexed on the basis of data given by Roth and Wadsley (1965) and showed no impurity lines. Results are given in Table 22.

Electron diffraction patterns and lattice images of several single crystals were in complete agreement with the X-ray diffraction findings. In Plate (27-a), a two-dimensional lattice image of a typical $TiNb_{24}O_{62}$ crystal is shown. The image is viewed down the short b-axis and displays a contrast distribution similar to the a-c plane projection of the idealised crystal structure as given in Plate 23-b. The (4 x 3) blocks are infinite along the b-axis and are joined at the same level in pairs. The junctions at the corner and (001) face of the unit cell contain tetrahedrally co-ordinated metal atoms; these are indicated by dark dots in the model. The unit cell of the crystal, in the projection, is outlined by heavy dashed-lines and has dimensions of: a = 29.8 Å, b = 3.8 Å, c - 21.1 Å and $\beta = 94.9^{\circ}$. Plate 27-C is an (h01) electron diffraction pattern obtained from the same region of the crystal.

7.3.3.2. Thermodynamics

Phase equilibria in the system $(Ti,Nb)O_2$-$TiNb_{24}O_{62}$ were studied thermogravimetrically at 1400°C using CO_2-CO

PLATE 27

PLATE 27

a) A two-dimensional lattice image of a $TiNb_{24}O_{62}$ crystal fragment. (Section 7.3.3.1.).

b) An idealized model of the $TiNb_2O_7$ crystal structure as shown in (a). The monoclinic unit cell of the structure is outlined.

c) h0l reciprocal lattice section of the same crystal as shown in (a).

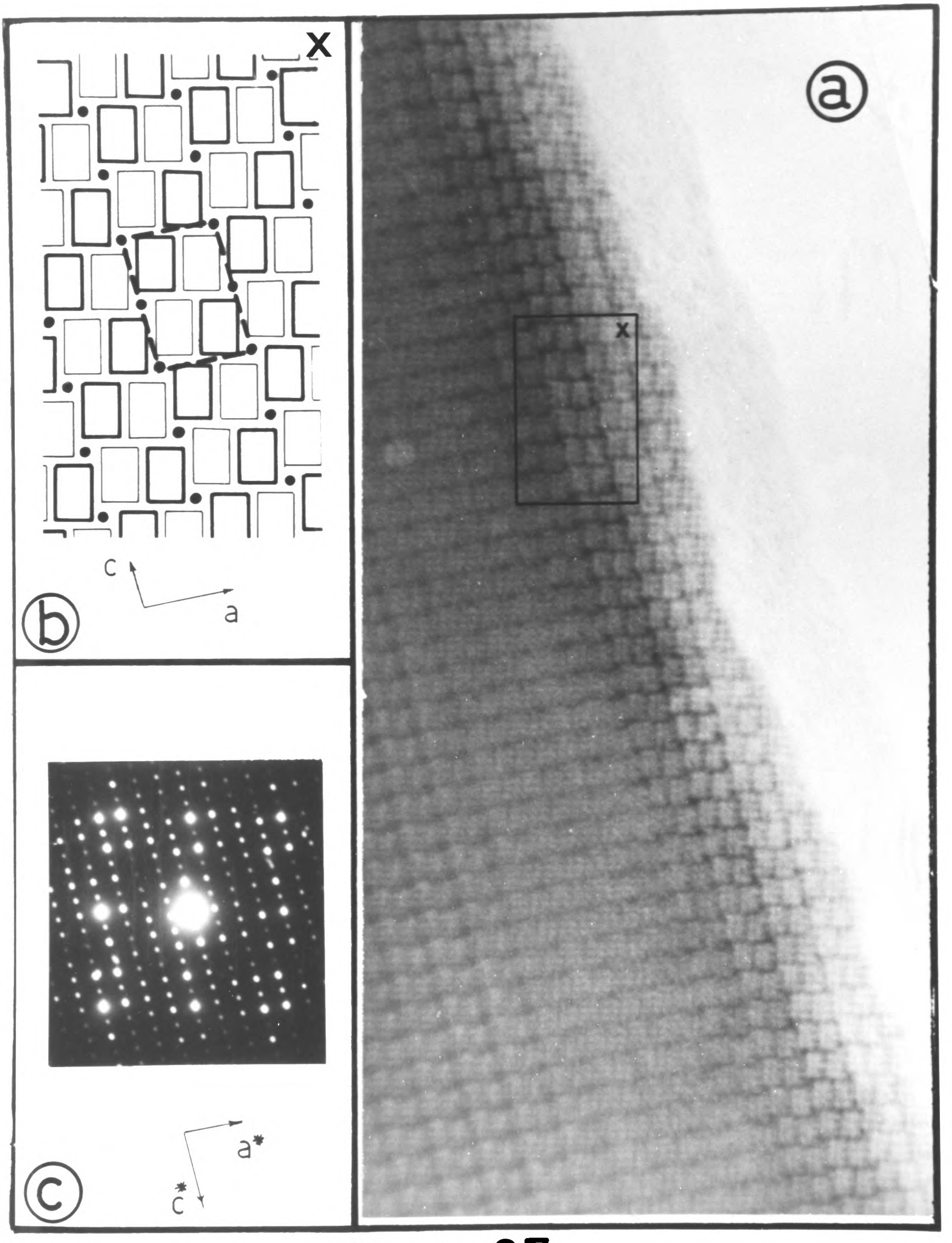

Plate 27

gas buffer mixtures (see Section 3.2.1.). The data obtained are given in Table 23. In Figure 20, the composition of the oxides (O/Ti,Nb) is plotted against the oxygen partial pressure (log p_{O_2}).

The smooth and continuous shape of the projection of experimental points in Figure 20 shows that the response of the oxide composition to a change in oxygen partial pressure simulates bivariant behaviour over the complete composition range. Closer examination of the (p, x) isotherm reveals the presence of four relatively linear regions (A-B, C-D, E-F and F-G). These sections embrace a significant proportion of the curve and are linked by regions (B-C and D-E) in which the slope transforms from one limiting value to another in a smooth and continuous manner. The minimum and maximum points of each region are indicated in Table 23.

Comparison with literature findings shows that the bivariant feature of Figure 20 is very similar to that found in the NbO_2-(H-Nb_2O_5) system, in which extreme hysteresis is involved in the adjustment of neighbouring structures (Nimmo and Anderson, 1972). For mixed oxides of titanium and niobium, Allpress (1969*a*) and Wadsley (1961 a and b) have also shown that there is a close analogy between titanium-niobium oxides and the intermediate phases in the binary Nb-O system. In these systems (i.e. reduced $TiNb_{24}O_{62}$ and H-Nb_2O_5) there are large numbers of intermediate phases with very close structural relationships. The energetic differences between the successive intermediate phases are small, thus, a reduced crystal can accomodate domains of different structures in a coherent manner. It follows that the usual

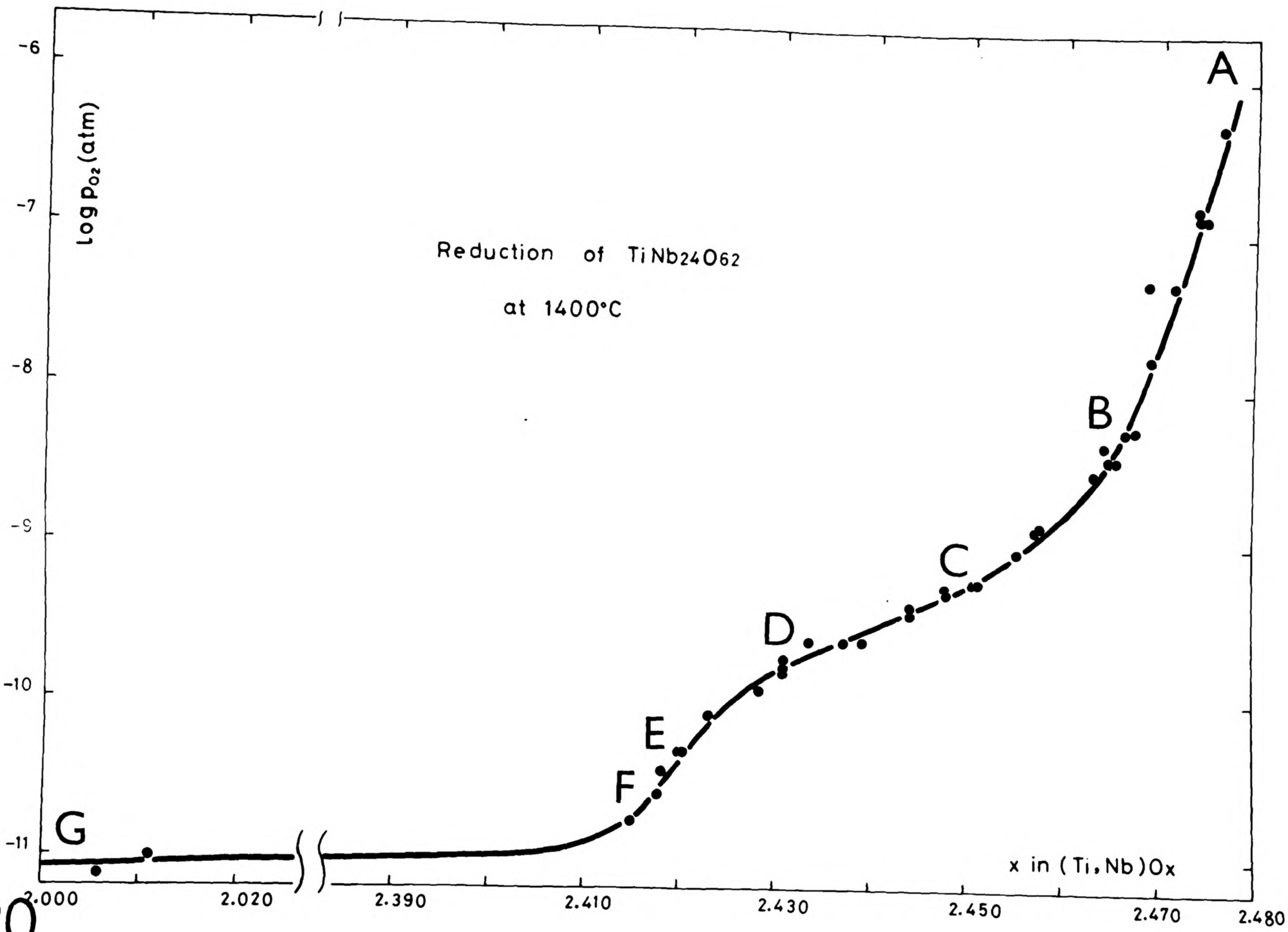
Reduction of TiNb24O62
at 1400°C
Log Po2 (atm)
-6
-7
-8
-9
-10
-11
A
B
C
D
E
F
G
x in (Ti, Nb)Ox
2.000
2.020
2.390
2.410
2.430
2.450
2.470
2.480

FIG. 20

TABLE 23

TABLE 23

System $(Ti,Nb)O_2$ - $TiNb_{24}O_{62}$ Equilibrium Results at 1400°C

Specimen no.	CO_2/CO	log p_{O_2}	Composition $(Ti,Nb)O_x$	Structural studies (see Section 7.3.3.)
1	0.05	-11.17	2.0061	
2	0.06	-11.02	2.0115	
3	0.08	-10.77	2.4148	
4	0.09	-10.60	2.4174	
5	0.10	-10.55	2.4182	
6	0.13	-10.32	2.4196	
7	0.13	-10.32	2.4200	
8	0.17	-10.09	2.4230	
9	0.21	-9.93	2.4282	
10	0.24	-9.80	2.4306	
11	0.24	-9.81	2.4309	
12	0.26	-9.73	2.4307	
13	0.30	-9.62	2.4335	
14	0.30	-9.62	2.4372	
15	0.30	-9.62	2.4391	
16	0.37	-9.44	2.4442	
17	0.39	-9.39	2.4443	
18	0.43	-9.30	2.4480	
19	0.44	-9.28	2.4479	
20	0.48	-9.21	2.4508	
21	0.52	-9.14	2.4513	
22	0.59	-9.03	2.4554	
23	0.69	-8.89	2.4571	
24	0.71	-8.87	2.4576	
25	1.05	-8.53	2.4634	
26	1.19	-8.42	2.4648	
27	1.19	-8.42	2.4657	
28	1.31	-8.33	2.4643	
29	1.45	-8.25	2.4667	
30	1.47	-8.24	2.4676	
31	2.48	-7.78	2.4691	
32	4.36	-7.30	2.4715	
33	4.38	-7.29	2.4687	
34	7.13	-6.87	2.4740	
35	7.13	-6.87	2.4747	
36	7.62	-6.81	2.4739	
37	13.8	-6.29	2.4764	

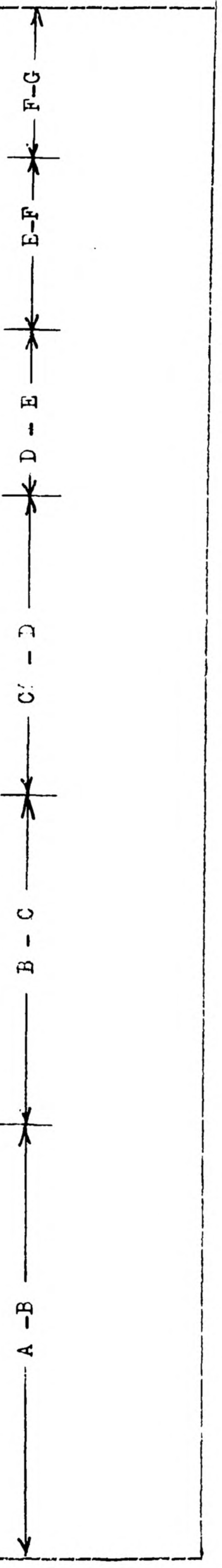

Gibbs phase rule is not applicable here and the system may be recognized in terms of classical thermodynamic operations, as a single phase with regions of different structures.

7.3.3.3. Structural aspects

7.3.3.3.1. Composition range $(Ti,Nb)O_{2.417}$-$(Ti,Nb)O_{2.480}$

Detailed examination of the X-ray powder diffraction patterns of the oxides in this range reveals the absence of any rutile phase. This finding, unlike observations in the two other systems, suggests that titanium remains in the crystal lattice and that reduction is confined to an oxygen dissociation reaction. Thus, the system follows a similar reduction pathway to that described for NbO_2-(H-Nb_2O_5). For this reason, it is justified to compare the structures of successive intermediate phases generated in the reduction of $TiNb_{24}O_{62}$ with those identified in the NbO_2-(H-Nb_2O_5) system (Schäfer *et al*, 1969; Nimmo and Anderson, 1972; Kimura, 1973). The two systems are compared in a composite equilibrium diagram shown in Fig. 21.

Region A-B. The rapid change of oxide composition with oxygen partial pressure in this region suggests that this is an area of $TiNb_{24}O_{62}$ non-stoichiometry (oxygen deficiency).

Structural results obtained in the $TiNb_2O_7$ and $Ti_2Nb_{10}O_{29}$ systems have shown that Wadsley defects are the main source of non-stoichiometry (see Sections 7.3.1.3. and 7.3.2.3. respectively). Thus, it is suggested here that deviations from the ideal composition in the present system

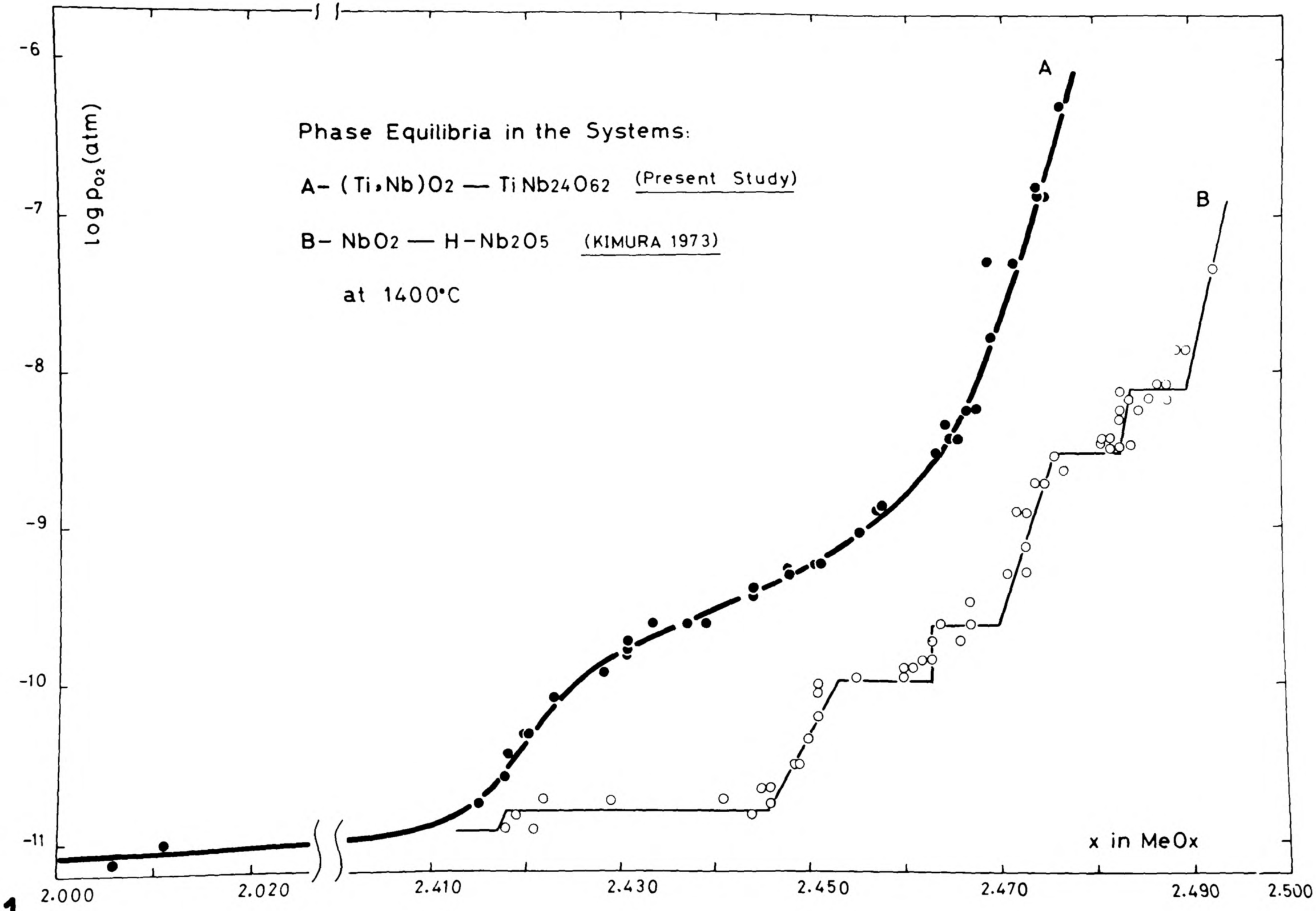
Phase Equilibria in the Systems:
A- (Ti,Nb)O2 — TiNb24O62 (Present Study)
B- NbO2 — H-Nb2O5 (KIMURA 1973)
at 1400°C
A
B
log Po2 (atm)
-6
-7
-8
-9
-10
-11
2.000
2.020
2.410
2.430
2.450
2.470
2.490
2.500
x in MeOx

FIG. 21

arise from coherent intergrowth of strips or domains of a lower composition oxide in the host structure. The lower composition oxide in this particular region is likely to be $Me_{22}O_{54}$.

In the binary Nb-O system, several investigators have reported an oxygen deficient non-stoichiometric range for the $Nb_{25}O_{62}$ compound. Schäfer *et al.* (1969), reported that the oxygen deficiency in the $Nb_{25}O_{62}$ phase extended over the range $NbO_{2.472}$ - $NbO_{2.478}$. In their diagram, univariant behaviour is shown in the range $NbO_{2.467}$ - $NbO_{2.472}$, suggesting a mixed phase region for $Nb_{25}O_{62}$ and $Nb_{47}O_{116}$. [$Nb_{47}O_{116}$ is a 1:1 intergrowth of $Nb_{25}O_{62}$ and $Nb_{22}O_{54}$ structures which was identified by Gruehn and Norine (1968)].

Similarly, Kimura (1973) reported that a non-stoichiometric range $NbO_{2.470}$ - $NbO_{2.476}$ existed for $Nb_{25}O_{62}$. In his phase equilibrium diagram (Figure 21-B), the composition range of $NbO_{2.4630}$ - $NbO_{2.470}$ also shows a univariant step, again suggesting the occurrence of a mixed phase region for $Nb_{25}O_{62}$ and $Nb_{47}O_{116}$.

Whilst the above authors confined their phase identifications to X-ray powder diffraction pattern analysis, Nimmo and Anderson (1972) utilized electron optical methods. After reacting $Nb_{12}O_{29}$ and $Nb_{25}O_{62}$ in different ratios in vacuum (10^{-6} Torr) and at 1200-1300°C in an induction furnace, electron microscopy showed that the significant oxygen deficiency observed in $Nb_{25}O_{62}$ was in fact due to a coherent intergrowth of $Nb_{22}O_{54}$ lamellae with the matrix (i.e. $Nb_{25}O_{62}$). In lower oxides of the non-stoichiometric region, such intergrowths tended to generate an intermediate phase having

a regular 1:1 intergrowth structure based on the reaction:

$$Nb_{25}O_{62} + Nb_{22}O_{54} = Nb_{47}O_{116}$$

The bivariant characteristic of the present equilibrium diagram (Figure 20) appears to be consistent with Nimmo and Anderson's observations. For this reason it is assumed that at around log p_{O_2} = - 8.25 where the oxide composition approaches x = 2.464 (B in Fig. 20), the number and spatial density of Wadsley defects increase to such an extent that they give rise to the formation of an ordered 1:1 intergrowth structure of $Me_{47}O_{116}$. This compound is probably a solid solution of $Nb_{47}O_{116}$ with a hypothetical ternary oxide having a composition of $Ti_3Nb_{44}O_{116}$; the latter is generated as follows:

$$TiNb_{24}O_{62} + Ti_2Nb_{20}O_{54} \longrightarrow Ti_3Nb_{44}O_{116}$$

$$(4 \times 3)_2\ [(4 \times 3)_\infty + (3 \times 3)_1]\ \{(3 \times 4)_2 + [(3 \times 4)_\infty + (3 \times 3)_1]\}$$

It should be noted that, besides the predominant occurrence of Wadsley defects in the non-stoichiometry of $TiNb_{24}O_{62}$, metal-excess point defects may also contribute to oxygen deficiency. Metal-excess point defects have been described in a study of GeO_2-$9Nb_2O_5$ by Anderson et al, (1975). They found that oxygen deficiency in oxides having tetrahedral sites in their structure could be due to the incorporation of some extra metal atoms in interstitial positions within tetrahedral columns.

Region B-C. The very marked curvature in this region (Fig. 20) may reflect a considerable acceleration in the degree of reduction during which a transformation of $Me_{47}O_{116}$

into $Me_{22}O_{54}$ takes place progressively:

$$(Nb_{47}O_{116} + Ti_3Nb_{44}O_{116}) \longrightarrow (Nb_{22}O_{54} + Ti_2Nb_{20}O_{54})$$

$$\{(3 \times 4)_2 + (3 \times 4)_\infty + (3 \times 3)_1\} \quad [(3 \times 4)_\infty + (3 \times 3)_1]$$

Several other compounds have also been reported in this composition range.

1) Iijima and Allpress (1973), in quenched $TiO_2.7Nb_2O_5$, found a few unit cells of $TiNb_{14}O_{37}$ - i.e. $(Ti,Nb)O_{2.4667}$. [The $TiO_2.7Nb_2O_5$ sample was originally prepared by Wadsley in 1961 in an attempt to investigate the possible occurrence of $TiNb_{14}O_{37}$]. $TiNb_{14}O_{37}$ has a $(5 \times 3)_\infty$ block structure and is a member n = 5 of a homologous series of $Me_{3n}O_{8n-3}$.

In the binary (Nb-O) system, the occurrence of $Nb_{15}O_{37}$, isomorphous with $TiNb_{14}O_{37}$, has not been reported in the literature. However, intergrowth of (5 x 3) lamellae as Wadsley defects in the structure of m-$Nb_{12}O_{29}$ has been observed frequently in the present work (see Section 5.3.2.).

2) Allpress (1969a) has reported the formation of a series of structurally related oxides between $TiNb_{24}O_{62}$ and $Ti_2Nb_{10}O_{29}$. The microdomains of $Ti_3Nb_{34}O_{91}$ $[(Ti,Nb)O_{2.459}]$ and $Ti_5Nb_{44}O_{120}$ $[(Ti,Nb)O_{2.449}]$ formed in disordered crystal fragments were regarded as 1:1 and 1:2 regular intergrowth structures of $TiNb_{24}O_{62}$ and $Ti_2Nb_{10}O_{29}$. Anderson (1969b) proposed a general formula of $(4 \times 3)_n$ for compounds in this homologous series.

Allpress's findings would suggest that $TiNb_{24}O_{62}$, under controlled oxygen partial pressures, may transform directly into $Ti_2Nb_{10}O_{29}$ through the formation of a series of intermediate intergrowth structures. However, considering

the close similarity between phase equilibrium curves given for the present study and for the NbO_2 - ($H\text{-}Nb_2O_5$) system (Kimura, 1973), it appears that the formation of discrete intermediate phases, isomorphous with those in the binary system, is more likely to take place.

In the binary (Nb-O) system, Schäfer *et al*, (1969) and Kimura (1973) have reported a mixed phase region (i.e. $Nb_{22}O_{54}$ and $Nb_{47}O_{116}$) for the composition ranges of $NbO_{2.453}$-$NbO_{2.464}$ and $NbO_{2.453}$-$NbO_{2.463}$.

Region (C-D). At (C) in Figure 20, the overall composition of the oxide corresponds to an $Me_{22}O_{54}$ phase (a probable solid solution of $Nb_{22}O_{54}$ with $Ti_2Nb_{20}O_{54}$). As the oxygen partial pressure in equilibrium with the oxide decreases, the oxide composition traverses along the bivariant segment C-D. Area C-D represents a non-stoichiometric (oxygen deficiency) region for the $Me_{22}O_{54}$ compound which may arise from a progressive intergrowth of elements of the next lower oxide phase (i.e. $Me_{12}O_{29}$) in the matrix.

Comparison with literature findings shows that Kimura (1973) has described the presence of an oxygen deficiency range ($NbO_{2.446}$-$NbO_{2.453}$) for $Nb_{22}O_{54}$. This region of his diagram was later studied by Iijima *et al* (1974) applying high resolution electron microscopy. Their results show that the observed non-stoichiometry may largely be due to both the intergrowth of $Nb_{12}O_{29}$ strips into the matrix (i.e. $Nb_{22}O_{54}$) and the occurrence of point defects. The point defects, according to these authors, were of two kinds: for one type Iijima *et al*, proposed a model which consisted of two displaced metal atoms and two extra interstitial oxygen

atoms within the blocks. This kind of defect has also been observed by the present author, studying the ultrastructure of pure niobium oxides (see Section 5.3.2.). For the other point defect, Iijima et al assumed that one metal atom and three oxygen atoms were missing from a tetrahedral site. They concluded, therefore, that non-stoichiometry of $Nb_{22}O_{54-x}$ results from the net effect of extended defects as well as from point defects.

Region (D-E). A smooth and continuous change in the slope of the reduction curve in this region may reflect a gradual transition of oxides predominantly with an $Me_{22}O_{54}$ structure into an $Me_{12}O_{29}$ phase. In addition, a series of intermediate regular intergrowth structures may occur between $Me_{22}O_{54}$ and $Me_{12}O_{29}$ in this region. For these intermediate (hypothetical) compounds, the general formula $Me_{12n + 22}O_{29n + 54}$ and the structure of $[(n + 1)\ (4 \times 3)_{\infty} + (3 \times 3)_1]$ are suggested here. The intergrowth structures, ideally, are solid solutions of oxides in the ternary system having a general formula of $Ti_{2n + 2}Nb_{10n + 20}O_{29n + 54}$ with an isomorphous compound in the binary system - i.e. $Nb_{12n + 22}O_{29n + 54}$. In the diagram (Fig. 20), oxides in the upper (D) and lower limits (E) of the region have compositions of $MeO_{2.431}$ and $MeO_{2.423}$ which correspond to $Me_{58}O_{141}$ (n = 3) and $Me_{130}O_{315}$ (n = 9) of the series, respectively. The oxides are speculated to be solid solutions of ($Ti_8Nb_{50}O_{141}$, $Nb_{58}O_{141}$) and ($Ti_{20}Nb_{110}O_{315}$, $Nb_{130}O_{315}$).

In the binary (Nb-O) system, a domain of $Nb_{46}O_{112}$ (member n = 2 of the series) by electron microscopy is observed, in the reduction of transformed B-Nb_2O_5 (see

Section 5.1.3.2.). Iijima et al, (1974) in structural studies of Kimura's (1973) samples has detected a domain structure of $Nb_{34}O_{83}$ (n = 1) of the homologous series. The occurrence of an intermediate phase having composition $NbO_{2.432}$ has also been indicated by Burdeze et al (1969) and Abbatista et al (1968).

Region E-F

Analysis of X-ray powder diffraction patterns of oxides in this region indicate the exclusive presence of o-$Me_{12}O_{29}$ reflections. Thus, the obvious bivariance of the diagram (showing a wide range of oxygen-excess non-stoichiometry for $Me_{12}O_{29}$ probably stems from: a) Wadsley defects (i.e. coherent intergrowth of remaining elements of $Me_{22}O_{54}$ in the matrix) and b) the involvement of oxygen-excess point defects.

In the binary (Nb-O) system, Schäfer's (1969) diagram shows a complete univariant region (i.e. the occurrence of mixed phases of $Nb_{22}O_{54}$ and $Nb_{12}O_{29}$) in the composition range of $NbO_{2.417}$-$NbO_{2.453}$. Similarly, in Kimura's curve (1973), a step discontinuity in the composition range of $NbO_{2.418}$-$NbO_{2.453}$ is reported (see Fig. 21-B), and he also interprets his data to show a bivariant region in the composition range of $NbO_{2.417}$-$NbO_{2.418}$ suggesting the presence of a non-stoichiometric region (oxygen-excess) for the $Nb_{12}O_{29}$ phase. Iijima (1973), investigating Kimura's samples by high resolution electron microscopy, has published micrographs which show the presence of $Nb_{22}O_{54}$ strips together with large numbers of oxygen excess point defects. Results of the present study are consistent with Iijima's findings.

7.3.3.3.2. Composition range: $(Ti,Nb)O_{2.000}$-$(Ti,Nb)O_{2.417}$ (Region F-G)

Our observations indicate a bivariant characteristic for this composition range. Examination of X-ray powder diffraction patterns of the intermediate oxides $MeO_{2.4148}$, $MeO_{2.0115}$, $MeO_{2.0061}$, show the presence of very weak o-$Me_{12}O_{29}$ reflections besides rutile phase ($Ti_xNb_{1-x}O_2$) lines. The rutile phase was identified to have compositions of $x < 0.5$. Thus, the reduction of $TiNb_{24}O_{62}$ in this region of the diagram (Fig. 21) most likely follows a similar pathway to that discussed in the $Ti_2Nb_{10}O_{29}$ reduction system.

7.3.3.4. Summary

Phase equilibrium measurements in the system $(Ti,Nb)O_2$-$TiNb_{24}O_{62}$ were carried out thermogravimetrically at the isotherm 1400°C. The oxygen partial pressure, in equilibrium with the oxide, was varied in the range of 10^{-6}- 10^{-12} (atm) using CO_2-CO gas buffer mixtures.

X-ray powder diffraction patterns of the intermediate oxides indicated the absence of a rutile phase, $Ti_xNb_{1-x}O_2$, in the range $(Ti,Nb)O_{2.417}$-$(Ti,Nb)O_{2.480}$, whereas rutile lines - i.e. $Ti_xNb_{1-x}O_2$ ($x < 0.5$) -- and o-$Me_{12}O_{29}$ reflections were detected in the range $(Ti,Nb)O_{2.000}$-$(Ti,Nb)O_{2.417}$. The oxide reduction in the system $(Ti,Nb)O_{2.417}$-$(Ti,Nb)O_{2.480}$, thus, is confined to an oxygen disscciation reaction. In the range $(Ti,Nb)O_{2.000}$-$(Ti,Nb)O_{2.417}$ an identical reduction pathway to $Ti_2Nb_{10}O_{29}$, probably, takes place. With regard to a close parallel between oxides in the ternary (Ti-Nb-O) system and isomorphous oxides in the binary (Nb-O) system,

the formation of several discrete intermediate phases in the present system - i.e. $(Ti,Nb)O_2$-$TiNb_{24}O_{62}$ -- is suggested here. The proposed reduction route showing intermediate phases is given in Table 24.

7.3.4. Phase relations in the system (TiO_2-Nb_2O_5-NbO_2)

A Gibbs triangle representation of phase relations in the system (TiO_2-Nb_2O_5-NbO_2) at the isotherm 1400°C is given in Figure 22. The ternary diagram, which summarizes all the equilibrium relationships determined in this Chapter, is constructed of:

1) Lines of equal partial pressures of oxygen (dash-dot-dash curves) depicting the composition of gas phase in equilibrium with its respective condensed phases.

2) Heavy lines which represent the boundaries between various one- or two-phase areas. In contrast to the classical phase rule, the boundary lines do not represent abrupt transformations but indicate smeared and continuous phase changes.

3) The position of the $Me_{25}O_{60}$ phase (see Section 7.3.1.3.2.) is labelled (C). $Me_{25}O_{60}$ is a metastable transient phase which subsequently transforms into o-$Me_{12}O_{29}$ (o-$Ti_2Nb_{10}O_{29}$) and a rutile phase (MeO_2). Its phase relations with $Ti_2Nb_{10}O_{29}$, $Nb_{12}O_{29}$ and ($TiNb_2O_7$/Nb_3O_7) are depicted by heavy dashed-lines.

4) The position of a postulated solid solution of Nb_3O_7 in $TiNb_3O_7$ is labelled (D). Nb_3O_7 is probably generated in the reduction of $TiNb_2O_7$. The value indicated in the diagram for the partial generation of this phase is speculative.

TABLE 24

Labelled in Diagram (Fig.20)	Reduction Pathway	Composition
(A)	$TiNb_{24}O_{62}$	($MeO_{2.480}$)
	↓	
	$(Ti_3Nb_{44}O_{116})$*	
(B)	&	($MeO_{2.464}$)
	$Nb_{47}O_{116}$	
	↓	
	$(Ti_2Nb_{20}O_{54})$*	
(C)	&	($MeO_{2.455}$)
	$Nb_{22}O_{54}$	
	↓	
	$Ti_8Nb_{50}O_{141}$ *	
(D)	&	($MeO_{2.431}$)
	$Nb_{58}O_{141}$	
	↓	
	$Ti_{20}Nb_{110}O_{315}$ *	
(E)	&	($MeO_{2.423}$)
	$Nb_{130}O_{315}$	
	↓	
	$Ti_2Nb_{10}O_{29}$	
(F)	&	($MeO_{2.417}$)
	$Nb_{12}O_{29}$	
	↓	
(G)	$TiNb_{24}O_{50}$	($MeO_{2.000}$)

* Hypothetical compound

TABLE 25

No.	Assemblage
i	$H\text{-}Nb_2O_5$ ($Nb_{28}O_{70}$) $Nb_{53}O_{132}$, $TiNb_{52}O_{132}$; $Nb_{43}O_{107}$, $TiNb_{42}O_{107}$; $TiNb_{38}O_{97}$
ii	$Nb_{25}O_{62}$, $TiNb_{24}O_{62}$; $Nb_{47}O_{116}$, $(Ti_3Nb_{44}O_{116})$*; $Ti_3Nb_{34}O_{91}$; $Nb_{22}O_{54}$, $(Ti_2Nb_{20}O_{54})$*; $Ti_5Nb_{44}O_{120}$; $(Nb_{130}O_{315}$ $Ti_{20}Nb_{110}O_{315})$*
iii	$Ti_2Nb_{10}O_{29}$; $TiNb_2O_7$, Me_3O_7
iv	$TiNb_2O_7$, Me_3O_7; $Ti_xNb_{1-x}O_2$ $(0.5 < x < 1)$
v	$Ti_2Nb_{10}O_{29}$; $(TNb_2O_7$, $?Nb_3O_7)$; $Ti_9Nb_{41}O_{120}$; $Ti_{0.5}Nb_{0.5}O_2$
vi	$Ti_2Nb_{10}O_{29}$, $Nb_{12}O_{29}$; $Ti_9Nb_{41}O_{120}$; $Ti_{0.5}Nb_{0.5}O_2$
vii	$Nb_{12}O_{29}$; $Ti_xNb_{1-x}O_2$ $(0.5 < x < 0)$

* a speculative compound

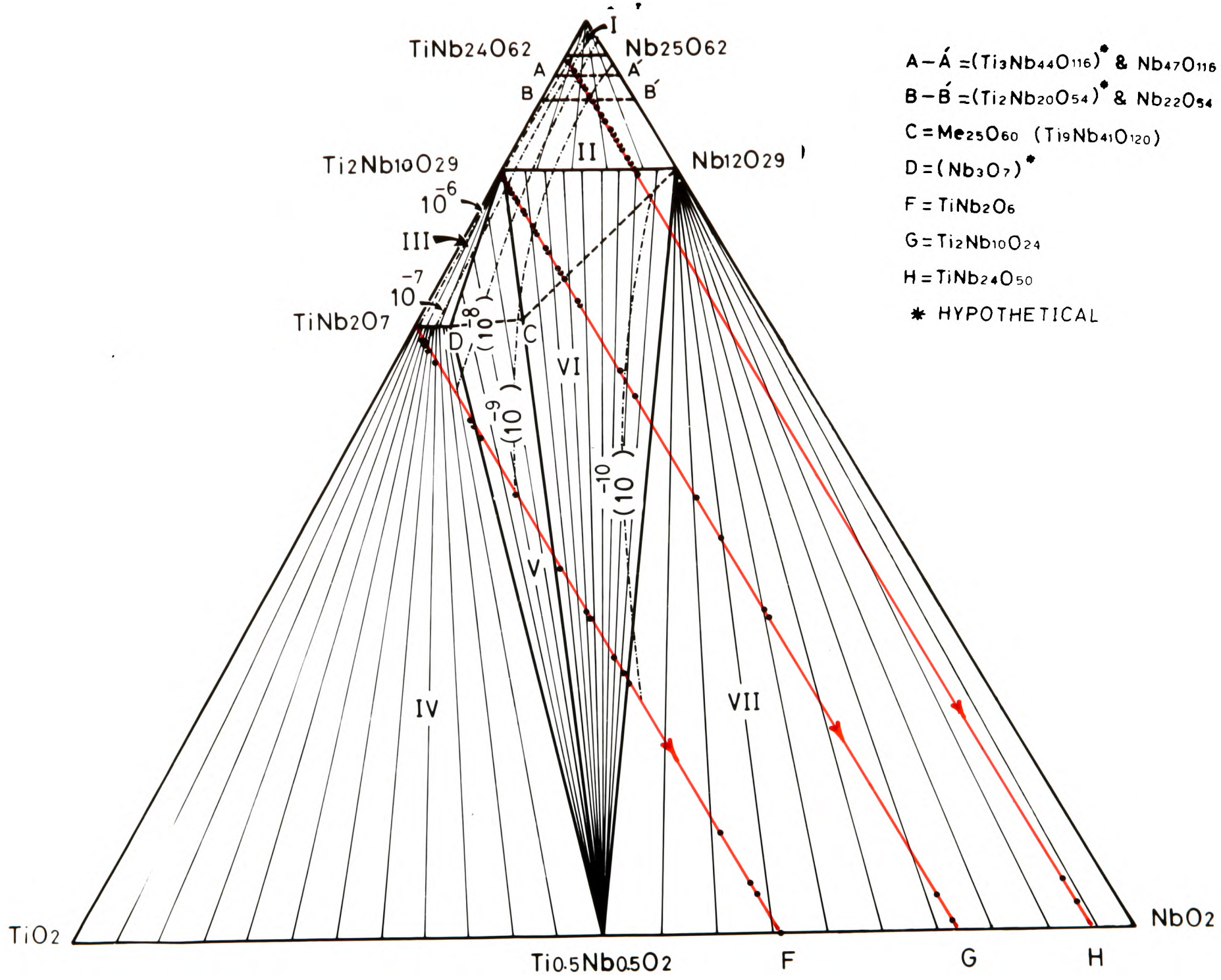
TiNb24O62
Nb25O62
I
A
A´
B
B´
II
Ti2Nb10O29
Nb12O29
10-6
III
10-7
TiNb2O7
D
(10-8)
C
VI
(10-9)
V
(10-10)
IV
VII
TiO2
Ti0.5Nb0.5O2
F
G
H
NbO2
A–Á =(Ti3Nb44O116)* & Nb47O116
B–B́ =(Ti2Nb20O54)* & Nb22O54
C = Me25O60 (Ti9Nb41O120)
D = (Nb3O7)*
F = TiNb2O6
G = Ti2Nb10O24
H = TiNb24O50
* HYPOTHETICAL

FIG. 22

5) Heavy dashed-lines labelled A-A' and B-B' in region II depict a probable solid solution of $Nb_{47}O_{116}$ and $Nb_{22}O_{54}$ with their respective isomorphous compounds in the ternary system -- i.e. $Ti_3Nb_{44}O_{116}$ and $Ti_2Nb_{20}O_{54}$. The compounds in the ternary system are hypothetical.

6) The tie-lines in the regions represent compositions of two condensed phases in equilibrium with each other. The tie-lines also indicate the relative proportions of each phase existing under equilibrium conditions.

7) Solid-circles represent the compositions of reduced oxides as determined by chemical analysis following the equilibrium runs (see Tables 17, 20 and 23 respectively). The data are lying on reduction path-lines (indicated by arrows) showing the course along which the oxide composition changes during reduction.

8) Phase assemblages, in the diagram, are labelled with Roman numerals. The assemblages are listed in Table 25.

7.4. Discussion

Literature findings (summarized in Chapter I) on thermodynamic aspects of block-based oxides (of which H-Nb_2O_5 is a representative) show that data obtained for the NbO_2 - (H-Nb_2O_5) system are contradictory and, in general, support one of two theories:

a) A stepwise phase equilibrium diagram which suggests the formation of discrete intermediate phases (Abbattista et al, 1968; Burdeze et al, 1969; Schäfer et al, 1969; Kimura, 1973; Marucco, 1974).

b) A continuous and coherent phase equilibria diagram

such as reported by Nimmo and Anderson (1972).

Research reported in the present Chapter of this Thesis, in part, has a direct bearing upon the above controversy. The present results are therefore compared below with findings in the three most relevant papers, namely those of Schäfer et al (1969); Kimura (1973) and Nimmo and Anderson (1972). Preceding this particular discussion, the character of Wadsley defects, and the duration of each reduction run are briefly discussed:

During the equilibration of mixed titanium-niobium oxides with CO_2/CO gas buffer mixtures at 1400°C, it was found that, at a given oxygen activity, a stationary composition was operationally obtainable in less than one hour. This indicates that a perfect internal adjustment in the solid-gas equilibration process takes place with great mobility.

Structural studies of the reduced oxides show that the reduction process involves both the dissociation of a rutile phase ($Ti_xNb_{1-x}O_2$) from the matrix, as well as changes in the density and orientation of shear planes. The frequent occurrence of rows or domains of a variant structure - i.e. neighbouring phases - suggest that Wadsley defects are in all probability thermodynamically stable species which represent a state of minimum free energy in the solid (obtained under fixed environmental conditions).

This finding is supported by several other workers:

Allpress and Roth (1971), in studies of tungsten - niobium mixed oxides, found that Wadsley defects which occurred in stoichiometric oxides disappeared after prolonged annealing (780 hr, at about 1350°C) while defects found in

non-stoichiometric compounds could never entirely be removed from the matrix.

Allpress (1969a,1970), in investigations of defect structures of a series of compounds in the system TiO_2-Nb_2O_5 by electron microscopy, suggested that the deviation from crystallographically expected values may be attributed to Wadsley intergrowth defects, or to microdomain intergrowths of neighbouring phases.

Nimmo and Anderson (1972), in studies of phase equilibria in the system NbO_2-Nb_2O_5 at 1300°C, reported that Wadsley defects of adjacent phases occurred frequently in the host structure.

Iijima, Kimura and Goto (1974), investigating Kimura's (1973) samples by high resolution electron microscopy, also observed some Wadsley defects. They suggested that even well-equilibrated samples are allowed to incorporate neighbouring phases of the host structure as Wadsley defects. This would imply that Wadsley defects are an inherent equilibrium property of the block-structure oxides.

Earlier, Schäfer et al (1969) had reported that a long duration of reduction was needed to attain a perfect solid gas equilibrium. Kimura (1973), confirming Schäfer et al's results, indicated that a sample with composition near $Nb_{53}O_{132}$ could not be obtained in perfect equilibrium, even after 75 hr. heating at 1300-1400°C.

It should be emphasized that Schäfer et al (1969) and Kimura (1973) applied only the X-ray powder diffraction method for the phase analysis of their reduced oxides. It is known that this technique is inadequate to reveal

structural details of block-structure oxides (Anderson, 1972b; Wadsley and Andersson, 1970) because the structures are interrelated and the patterns dominated by the ReO_3-type sub-cell. Moreover, the true unit-cells are large and have similar but complex diffraction patterns. Also, the non-stoichiometric faults (point defects, defect complexes, extended defects or domain intergrowth) cannot be detected satisfactorily by X-ray diffraction because the effect of such structural inhomogeneities would only be reflected by slight shifts or broadening of the diffraction lines.

As far as the <u>duration</u> of each of the present experiments is concerned, the following should be noted: while the high-temperature ($T \gtrsim 1300^{\circ}C$) reduction equilibrium is a kinetically rapid process, data available in the literature suggest that, at lower temperatures ($T < 1300^{\circ}C$), attainment of a true solid-gas equilibrium is not accessible (see Nimmo and Anderson, 1972; Merritt and Hyde, 1973). In addition, the attainment of structural uniformity and ordering of the new CS planes (or annihilation of the existing ones) is greatly dependent upon extensive co-operative movements of atoms in the crystal lattice. Such lateral migration and ordering of (CS) planes is kinetically hindered at lower temperatures (Anderson, 1974) and this may lead to a sluggish approach to equilibrium as well as to hysteresis phenomena (Merritt and Hyde, 1973; Nimmo and Anderson, 1972; Marucco, 1974). For this reason, in the present study, a minimum duration of 10 hours was applied for each

isothermal-isobaric reduction.

Phase equilibrium diagrams obtained in the three systems $TiNb_2O_7$, $Ti_2Nb_{10}O_{29}$ and $TiNb_{24}O_{62}$ all showed complete bivariance over the composition range of $(Ti,Nb)O_2$-$TiNb_2O_7$; $(Ti,Nb)O_2$-$Ti_2Nb_{10}O_{29}$ and $(Ti,Nb)O_2$-$TiNb_{24}O_{62}$. When the usual Gibbs phase rule is applied to the diagrams, only monophasic non-stoichiometric oxides appear to be present. Structural studies of the reduced oxides, however, reveal that the systems consist of several successive intermediate phases which are generated at different oxygen activities. The individual systems are discussed below:

System $(Ti,Nb)O_2$-$TiNb_2O_7$

$TiNb_2O_7$ transforms under controlled oxygen activities into $Me_{12}O_{29}$ by rejecting a rutile phase from the matrix. The generated $Me_{12}O_{29}$ compound is probably $Ti_2Nb_{10}O_{29}$ which transforms subsequently into $Nb_{12}O_{29}$. The phase change from $TiNb_2O_7$ into $Ti_2Nb_{10}O_{29}$ seems to proceed via two different pathways:

1. a coherent and continuous process,
2. an abrupt or discontinuous phase change.

Following the first pathway, $TiNb_2O_7$ initially rejects a rutile phase and generates a partial quantity of Nb_3O_7 compound. Formation of pure Nb_3O_7, which is isostructural with the matrix has not been reported in the literature. This phase is speculated here to occur in solid solution with the starting material. At lower oxygen partial pressures, however, $TiNb_2O_7$ crystals reject a rutile

phase ($Ti_xNb_{1-x}O_2$) and, subsequently, transform into a $Ti_2Nb_{10}O_{29}$ structure. The interconversion of one phase into the other takes place through continuous and coherent incorporation of the neighbouring phase in the host structure. As the reduction of the oxide advances at lower oxygen activities, the density of $Me_{12}O_{29}$ in the matrix increases until it becomes the predominant structure. This process of phase change involves the formation of "hybrid" crystals; hence Ubbelohde's (1966 and references therein) interpretation of "continuity" in solid state phase transformations may be relevant here. According to Ubbelohde, the hybrid crystals, due to some degree of structural mismatch, build up strain and interfacial surface energy at common intergrowth boundaries. Although a chemical equilibrium is attained with the gas phase at each appropriate composition and temperature, the crystal does not possess mechanical equilibrium because of the strain resulting from the microdomain texture of the oxide. In terms of thermodynamics, the Gibbs phase rule must be modified to include an additional degree of freedom. Thus, the two-phase system is no longer univariant and hysteresis effects may be expected.

Anderson (1969a,b; 1970) has discussed the link between thermodynamic properties and crystal structure in solid-state phase transformations. With regard to (CS) and block-structure oxides, in which several ordered intermediate (line) phases of definite composition occur, he states: ": ... In a very closely spaced phase succession, such as exists in these titanium oxides or the block-structure niobium oxides, this relation between the free energy minima

of the line phases means that the phase coexistence tangents differ very little in slope from one phase pair to the next, and merge into an almost continuous envelope. This is a source of possible experimental confusion in measurements of $\bar{G}_{O_2}$ unless the precision and density of experimental data is high. The $\bar{G}$-x relation can simulate a continuous dependence on x: the system acts as a pseudo-bivariant one" p. 12, Anderson,1970).

The coexistence of microdomains of several phases in single crystals may also arise in part from thermal fluctuations within the crystals when treated at high-temperatures or quenched to low-temperatures. Consequently, local free energy and structural fluctuations within a crystal may take place. This will lead to local unmixing of the adjacent line phases and the (p, x) isotherm will again exhibit a smeared-out behaviour (Anderson, 1969a)

The theoretical ideas advanced by Ubbelohde and Anderson would appear to be in full accordance with the experimental results of the present study and to agree with the conclusion that thermodynamic measurements of block-structure oxides cannot be used for the specification of the intensive thermodynamic properties of any intermediate phases. Moreover, the exact definition of "phase" in these systems, needs reconsideration since, in the block-based oxides, the structures are interrelated and single crystals contain domains of intergrowth structures. The question of the definition of "phase" has been raised by several authors [see the General Discussion in "The chemistry of extended defects in non-metallic solids (1970), eds Eyring, L. and

O'Keeffe, M.] but, so far, only two clear views have been expressed: Wadsley (1964) suggested that "phase" should be defined on the basis of the wave length of the radiation used in the sample examination as well as on the sample volume. The disadvantage of this proposal is that "single phase" material, identified by X-ray diffraction, might turn out to be "multiphasic" by electron microscopy. Recently, however, Nimmo and Anderson (1972) in structural studies of reduced H-Nb_2O_5, using electron microscopy, have introduced the term "structure" instead of "phase" in (CS) and block-based systems.

The composition of the <u>rutile phase</u>, rejected from the matrix in the process of solid-gas equilibration, is found to be dependent on the equilibrium oxygen activity -- i.e. at higher oxygen potentials the rutile phase is richer in titanium than when generated at lower oxygen partial pressures. However, the rutile phase in oxides obtained in the range $-9.8 \lesssim \log p_{O_2} \lesssim -8.4$ appears to have a composition $Ti_{0.5}Nb_{0.5}O_2$ and this gives the impression that $Ti_{0.5}Nb_{0.5}O_2$ is a discrete phase in the TiO_2-NbO_2 system. According to literature data, TiO_2 and NbO_2 form a continuous solid solution in which the normal rutile phase is retained in the composition range up to 75% NbO_2 (Rudorff and Lungińsland, 1964) or 85% NbO_2 (Sakata, 1969). In view of the present results, however, we speculate here that short range ordering of titanium and niobium atoms probably, takes place in $Ti_{0.5}Nb_{0.5}O_2$ leading to a minimum in the free energy of mixing at this composition.

The second pathway of reduction is by way of an abrupt phase change from $TiNb_2O_7$ into o-$Me_{12}O_{29}$. The process involves the formation of an intermediate transient stage having a composition of $Me_{25}O_{60}$ which transforms subsequently into o-$Me_{12}O_{29}$ by rejecting a rutile phase from its structure. A possible mechanism underlying the latter transformation process -- i.e. $Me_{25}O_{60} \rightarrow MeO_2$ + o-$Me_{12}O_{29}$ is postulated below:

A possible mechanism for an abrupt phase change

$Me_{25}O_{60}$ is suggested here to represent a metastable transient phase, generated during the direct transformation of $TiNb_2O_7$ into o-$Me_{12}O_{29}$. No direct evidence was obtained for the structural rearrangement of $TiNb_2O_7$ into $Me_{25}O_{60}$, but with regard to the phase change of $Me_{25}O_{60}$ into o-$Me_{12}O_{29}$ the following structural evidence was present.

In Plate 24-A, which shows a clearly recognizable two-dimensional image of the crystal studied, the two structures $Me_{25}O_{60}$ and o-$Me_{12}O_{29}$ (labelled M and N, respectively) co-exist and are coherently intergrown on a plane parallel to (001) ReO_3. This is evident from a change of 6 Å wide dark contrast band (the overlap region) into an ordinary 2 Å spacing shear plane (↑ S). An idealized model of the intergrowth area is given in Plate 24-B in which rectangular columns of corner sharing (MO_6) octahedra (i.e. the ReO_3 type) are spliced together at two levels -- i.e. $z = 0$ and $z = \frac{1}{2}$ b.

The model suggests that the conversion of $Me_{25}O_{60}$ into o-$Me_{12}O_{29}$ would require the dissociation of MeO_2 units (the rutile phase) from the crystal lattice according to

the following equation:

$$Me_{25}O_{60} = 2Me_{12}O_{29} + MeO_2$$

The outward diffusion of the rutile phase is, in all probability, a kinetically difficult process which may involve the dissociation of oxygen and metal atoms in their original lattice site and diffusion of these atoms from the crystal. On the crystal surface, the atoms recombine to form the discrete rutile phase.

The mechanisms underlying the diffusion process of the rutile phase and the formation of orthorhombic $Me_{12}O_{29}$ are shown in an idealized model in Plate 24-C. In model (e), the structural element of $Me_{25}O_{60}$ is depicted; (f) and (g) represent subsequent atomic reshufflings leading to the generation of o-$Me_{12}O_{29}$ and rutile phases. The locus of the reaction, according to this mechanism, is effectively confined. In model c, a (010) string of atoms (-O-Me-O-Me-O etc.) labelled b, in a co-operative displacement by a_R through a short diffusion path [i.e. a_R (101)R], occupies the vacant position in the rectangular tunnel in its vicinity (labelled 3). Concurrently, the adjacent metal atom (labelled a) together with two free oxygen atoms, located in the apex of the octahedra (a in Model f), diffuses out of the crystal through the 0.38 nm diagonal channels of the ReO_3 structure (1 or 2 in Model e). The channels extend without interruption down the b-axis. Diffusion, normal to the b-direction (i.e. through the channels within each block of ReO_3 structure), is impeded by changes of level at the interfaces between the columns. Moreover, such diffusion across an interface would be a highly activated

process and is likely to be slow. The proposed diffusion process parallel to the b-axis is supported by findings of Shearsby and Cox (1968) who reported that the chemical diffusion of oxygen in H-Nb_2O_5 at high temperatures is highly anisotropic and 100 times faster in parallel than normal to the b-axis.

The above mechanism for the transformation of $Me_{25}O_{60}$ into $Me_{12}O_{29}$ also suggests that altervalent cations (i.e. Ti^{4+} and Nb^{4+}, generated in the process of the reduction) are segregated preferentially in the corners of the blocks. This observation is in full agreement with results of Von Dreele and Cheetham (1974). They redetermined the crystal structures of $TiNb_2O_7$ and $Ti_2Nb_{10}O_{29}$ by the neutron diffraction method and found that the lower valence cation (i.e. Ti^{4+}) occupies mainly the block corners and the edge sites. The occupancy number was estimated to be 64.5% for corner sites of $TiNb_2O_7$ and 40.0% in corner positions of the o-$Ti_2Nb_{10}O_{29}$ compound.

Based on this structural relationship it is speculated that the $Me_{25}O_{60}$ structure is probably generated according to the following reaction:

$$32\ TiNb_2O_7 \longrightarrow Ti_9Nb_{41}O_{120} + 23\ TiNbO_4 + 60_2 \quad \text{(Eq. 1)}$$

The composition of solid phase obtained in this reaction is $MeO_{2.208}$ which is close to the one measured by chemical analysis of the sample ($MeO_{2.2005}$).

Generation of $TiNbO_4$ in Eq. 1 is also consistent with the experimental observations where $Ti_{0.5}Nb_{0.5}O_2$ occurs as a distinct phase in this composition range.

In the second stage of the reduction, the $Ti_9Nb_{41}O_{120}$

($Me_{25}O_{60}$), rejects $TiNbO_4$ and transforms into a perfect o-$Ti_2Nb_{10}O_{29}$ compound following the reaction:

$$Ti_9Nb_{41}O_{120} \longrightarrow 4Ti_2Nb_{10}O_{29} + TiNbO_4 \quad \text{(Eq. 2)}$$

A similar reduction process, involving the rejection of a foreign ion from the mixed oxide structure, has also been reported by Hutchison and Anderson (1977) for the system Ga-Nb-O. These authors traced the decomposition path of $GaNbO_4$ by electron microscopy and found that the intense electron beam radiation and the vacuum environment of the microscope removed Ga_2O_3 from the system. The reaction was highly localized and proceeded through a succession of metastable intermediate phases.

The abrupt mechanism for the phase transformation of $TiNb_2O_7$ into o-$Ti_2Nb_{10}O_{29}$ via the formation of a transient phase ($Ti_9Nb_{41}O_{120}$) is not consistent with the bivariant characteristics of the phase equilibrium diagram. For this reason, we conclude that a coherent and continuous reduction pathway takes place in the great majority of the crystals; the abrupt route, by contrast, occurs much less frequently.

The discussion given above for the continuity and coherence of phase transformations in the reduced $TiNb_2O_7$ system is also applicable to observations made on the two remaining systems, namely reduced $Ti_2Nb_{10}O_{29}$ and $TiNb_{24}O_{62}$.

In the $(Ti,Nb)O_2$ - $Ti_2Nb_{10}O_{29}$ system both the observed bivariant feature of the phase equilibria diagram and structural results suggest that $Ti_2Nb_{10}O_{29}$, under controlled oxygen partial pressures, transforms progressively into the isomorphous compound in the binary Nb-O system (i.e. $Nb_{12}O_{29}$).

In the process of reduction, a rutile phase $Ti_xNb_{1-x}O_2$ is rejected from the matrix. The composition of the rutile phase (and the degree of $Nb_{12}O_{29}$ formation) is dependent on the oxygen activity in equilibrium with the solid phase -- i.e. at higher oxygen partial pressures the rutile phase is richer in titanium (or the block-structure phase is richer in $Ti_2Nb_{10}O_{29}$) than the one generated at lower oxygen partial pressure.

The bivariant behaviour of the phase equilibria diagram in the system $(Ti,Nb)O_2$-$TiNb_{24}O_{62}$ has already been discussed and compared with the isomorphous Nb-O system (see section 7.3.3.). The $TiNb_{24}O_{62}$ system fully conforms with the conclusion given in the discussion of reduced $TiNb_2O_7$ and shows, in addition, that the stepwise interpretation of the phase equilibria diagram, such as given by Schafer et al (1969) and Kimura (1973) in studies of the NbO_2-(H-Nb_2O_5) system, must be regarded as an oversimplification.

A comparison of the Nb-O phase equilibria system studied by Kimura (1973) with the results obtained in the present study of $(Ti,Nb)O_2$-$TiNb_{24}O_{62}$ (see Fig. 21, diagrams B and A, respectively) show that the equilibrium oxygen partial pressures of the oxides in the two systems do not follow the classical thermodynamic laws of dilute solutions i.e. we observed that the mixed metal oxides are more readily reduced than the binary oxides. The reason for this anomaly remains obscure.

REFERENCES

1 Abbatistta, F., Chiantaretto, G. and Tkachenko, E.V. (1968) Acad. Sci. Torino, 102, 866.

2 Addison, W.E. (1961) Structural Principles in Inorganic Compounds. (Longmans, London).

3 Allpress, J.G. (1969a) J. Solid State Chem. 1, 66.

4 Allpress, J.G. (1969b) Mat. Res. Bull. 4, 707.

5 Allpress, J.G. (1970) J. Solid State Chem. 2, 78.

6 Allpress, J.G. and Roth, R.S. (1970) J. Solid State Chem. 2, 366.

7 Allpress, J.G. and Roth, R.S. (1971) J. Solid State Chem. 3, 209.

8 Allpress, J.G. and Wadsley, A.D. (1969) J. Solid State Chem. 1, 28.

9 Allpress, J.G., Sanders, J.V. and Wadsley, A.D. (1968) Phys. St., Solid. 25, 541.

10 Allpress, J.G. Sanders, J.V. and Wadsley, A.D. (1969) Acta. Cryst. B25, 1156.

11 Allpress, J.M., Tilley, R.J.D. and Sienko, M.J. (1971) J. Solid State Chem. 3, 440.

12 Anderson, J.S. (1969a) in: Problems in non stoichiometry, ed. A. Rabenau[a] (North-Holland, Amsterdam).

13 Anderson, J.S. (1969b), Bull-Soc. Chim. France, 2203.

14 Anderson, J.S. (1970) in: The Chemistry of Extended Defects in Non-Metallic Solids. eds. Eyring, L. and O'Keefe, M.L. (North Holland, Amsterdam).

15 Anderson, J.S. (1972a) N.B.S. Special Publication, 364, Solid State Chemistry.

16 Anderson, J.S. (1972b) in: "The Surface and Defect Properties of Solids" Vol. 1, Specialist Periodical Reports, The Chemical Society, eds. Roberts, M.W. and Thomas J.M. (London).

17 Anderson, J.S. (1974) Paper presented at a meeting on "Kinetics and Reactions in Hetrogeneous Systems". Societe de Chimie Physique Dijon.

18 Anderson, J.S. (1977) Chemistry in Britain, 13, No. 5.

19 Anderson, J.S., Bevan, D.J.M., Cheetham, A.K., Von Dreele, R.B., Hutchison, J.L. and Strahle, J. (1975) Proc. Roy. Soc. 19346, 139-156.

20 Anderson, J.S., Browne, J.M. and Hutchison, J.L. (1972a) J. of Solid State Chem. 5, 419.

21 Anderson, J.S., Browne, J.M. and Hutchison, J.L. (1972b) Nature, Vol. 237, No. 5351, p. 151.

22 Anderson, J.S. and Hutchison, J.L. (1975) Cont. Phys. Vol. 16, No. 5, 443.

23 Anderson, J.S. and Hyde, B.G. (1965) Bull. Soc. Chem. France, 1215.

24 Anderson, J.S. and Hyde, B.G. (1967) J. Phys. Chem. Solids. 28, 1393.

25 Anderson, J.S. and Tilley, R.J.D. (1970) J. Solid State Chem. 2, 472.

26 Anderson, J.S. and Tilley, R.J.D. (1974) in: "Surface and Defect Properties of Solids", Vol. 3, Specialist Periodical Reports, The Chemical Society, eds. Roberts, M.W. and Thomas, J.M. (London).

27 Andersson, S. (1964) Acta Chem. Scand.

28 Andersson, S. (1965) Bull. Soc. Chem. France, 1088.

29 Andersson, S. (1967) Z. Anorg. Allgem. Chem. 351, 106.

30 Andersson, S. and Galy, J. (1970) J. Solid State Chem. 1, 576.

31 Andersson, S., Mumme, W.G. and Wadsley, A.D. (1966) Acta Cryst. 21, 802.

32 Andersson, S. and Wadsley, A.D. (1966) Nature, 211, 581.

33 Anthony, A.M., Anderson, J.S. and Hutchison, J.L. (1977) J. of Solid State Chem. 21, 233.

34 Ariya, S.M. and Morozova, M.P. (1958) J. Gen. Chem. (U.S.S.R.) 28, 2647.

35 Ariya, S.M. and Popov, Y.G. (1962) J. Gen. Chem. (U.S.S.R.) 32, 2077

36 Astrom, A. (1966) Acta Chem. Scand. 20, 969.

37 Bachmann, H.G., Ahmed, F.R. and Barnes, W.H. (1961) Z. Kristallogr. Kristallgeometr. Kristallphysik, Kristall Chim. 115, 110.

38 Barr, G. (1934) J. Sci. Instrum. 11, 324.

39 Bevan, D.J.M. (1973) "Non-stoichiometric Compounds" Chapter 49 in: "Comprehensive Inorganic Chemistry" Pergamon Press, New York.

40 Bevan, D.J.M., Baker, W.W. and Martin, R.L. (1965) in: "Rare Earch Research" Vol. 3, p. 441. Gordon & Breach, N.Y.

41 Blumenthal, J.B., Mason, J.B. and Whitmore, D.H. (1965) J. Amer. Ceram. Soc. 48, 620.

42 Boggs, W.E. (1961) in: Vacuum Microbalance Technique" ed. Katz, M.J. (Planum Press, Inc., New York). p. 145.

43 Brack, D.W. (1964) J. Chem. Educ. 41, 678.

44 Brauer, G. (1941) Z. Anorg. Allgem. Chem. 248, 1.

45 Browne, J.M. (1973) D. Phil. Thesis, Oxford.

46 Browne, J.M. and Anderson, J.S. (1974), Proc. Roy. Soc. (London), A339, 463.

47 Browne, J.M., Hutchison, J.L. and Anderson, J.S. (1972) in: Reactivity of Solids, eds. J.S. Anderson, M.W. Roberts and F.S. Stone (Chapman Hall, London).

48 Burdeze, A., Tkachenko, E.V. and Abbatista, F. (1969) Inorganic Materials, 5, 1666.

49 Bursill, L.A. (1969) Proc. Roy. Soc. (London), A311, 267.

50 Bursill, L.A. and Hyde, B.G. (1969) Phil. Mag. 20, 657.

51 Bursill, L.A., Hyde, B.G. and Philp, D.K. (1971) Phil. Mag. 23, 1501.

52 Cahn, L. and Schuttz, H.R. (1963) in: Vacuum Microbalance Techniques. Vol. 3 p. 29. Plenum Press, New York.

53 Cheetham, A.K. (1971) D.Phil. Thesis, Oxford.

54 Cheetham, A.K., Fender, B.E.F. and Taylor, R.I. (1971) J. Phys. C. 4, 2160.

55 Chisholm, J.E. (1975) in: Surface and Defect Properties of Solids Vol. 4. ed. M.W. Roberts and J.M. Thomas (Specialist Periodical Reports). The Chemical Society, London.

56 Cockayne, D.J.H., Parsons, J.R. and Hoelke, C.W. (1971) Phil. Mag. 24, 139.

57 Cowley, J.M. and Iijima, S. (1972) Zeit. Naturforsch. 27A, 445.

58 Cowley, J.M. and Iijima, S. (1976) in: "Electron Microscopy in Mineralogy" ed. H-R. Wenk; Springer-Verlag, New York.

59 Cowley, J.M. and Moodie, A.F. (1960) Proc. Phys. Soc. 76, 378.

60 Czanderna, A.W. (1961) in: Vacuum Microbalance Techniques, Vol. 1, p. 129, ed. M.J. Katz, Plenum Press, New York.

61 Darken, L.S. and Gurry, R.W. (1945), J. Am. Chem. Soc. 67, 1398.

62 Dyson, P. (1957) Acta Cryst. 10, 140.

63 Ekström, T. (1971) Acta Chem. Scand. 25, 2591.

64 Elliott, R.P. (1960) Trans. Amer. Soc. Metals, 52, 990.

65 Emmenegger, F.P. and Robinson, M.L. (1968) J. Phys. Chem. Solids. 29, 1673.

66 Etsell, T.H. and Flengas, S.N. (1970) Chem. Rev. 70, 339.

67 Evans, B. and White, T.E. (1967) in: Vacuum Microbalance Techniques, ed. A.W. Cazanderna, Vol. 6, p. 157. Plenum Press, New York.

68 Eyring, L. and Tai, L.-T. (1973) in: Treatise on Solid State Chemistry, Vol. 3. ed. N.B. Hannay (Plenum Press - New York).

69 Fairbrother, F. (1967) "The Chemistry of Niobium and Tantalum", Elsevier Publishing Company.

70 Faktor, M.M. and Garrett, I. (1974) "Growth of Crystals from the Vapour", Chapman Hall, London.

71 Fender, B.E.F. (1972) in: "Solid State Chemistry". ed. L.E.J. Roberts [MTP Internat. Review of Sci.] Inorganic Chem., Ser. 1, Vol. 10, Butterworth, Oxford.

72 Fender, B.E.F. and Riley, F.D. (1970) in: "The Chemistry of Extended Defects in Non-Metallic Solids" ed. L. Eyring and M. O'Keefe, North-Holland, Amsterdam.

73 Fieser, L.F. and Fieser, M. (1967) in: "Reagents for Organic Synthesis" Vol. 1, Wiley, New York.

74 Forland, K.S. (1964) Acta Chem. Scand. 18, 1267.

75 Gado, P. (1965) Acta Phys. Hung. 18, 111.

76 Galy, J. and Andersson, S. (1968) Acta Cryst. B24, 1027.

77 Gatehouse, B.M. and Wadsley, A.D. (1964) Acta Cryst. 17, 1545.

78 Glauert, A.M. (1972 and 1974) "Practical Methods in Electron Microscopy" Vols. 1 and 2 respectively, North-Holland, Amsterdam.

79 Goldschmidt, H.J. (1958) J. Inst. Metals, 87.

80 Goldschmidt, H.J. (1960) Metallurgia, 62, 373.

81 Grey, I.E., Li, C. and Reid, A.F. (1974) J. of Solid State Chem. 11, 120.

82 Grinton, G.R. and Cowley, J.M. (1971) Optik, 34, 221.

83 Gruehn, R. (1966) J. Less Common Metals, 11, 119.

84 Gruehn, R. (1967) Naturwiss. 54, 645.

85 Gruehn, R. (1972) N.B.S. Spec. Pub. 364, Solid State Chemistry, 63 (eds. R.S. Roth and S.J. Schneider) Washington: Nat. Bur. Stand.

86 Gruehn, R. and Norin, R. (1967) Z. Anorg. Allg. Chem. 355, 176.

87 Gruehn, R. and Norin, R. (1968) Z. Anorg. Allg. Chem. 367, 209.

88 Gruehn, R. and Schäfer, H. (1963) Naturwiss. 50, 642.

89 Harburn, G., Taylor, C.A. and Welberry, T.R. (1975) Atlas of optical transforms: London, Bell.

90 Hirsch, P.B., Howie, A., Nicholson, R.B., Pashley, D.W. and Whelan, M.J. (1965) "Electron Microscopy of Thin Crystals", Butterworths.

91 Holtzberg, F. and Reisman, A., Berry, M. and Berkenblit, M. (1957) J. Amer. Chem. Soc. 79, 2039.

92 Hutchison, J.L. and Anderson, J.S. (1972) Phys. Status Solidi. 9, 207.

93 Hutchison, J.L. and Anderson, J.S. (1977) J. Solid State Chem. 22, 135.

94 Hutchison, J.L. and Lincoln, F.J. (1973) Phys. Stat. Sol. (A), 17, 169.

95 Hyde, B.G. and Bursill, L.A. (1970) Proc. Roy. Soc. A320, 147.

96 Hyde, B.G. and Eyring, L. (1965) in: Rare-earth Research, Vol. 3 (ed. L. Eyring) p. 623. Gordon & Breach, New York.

97 Hyde, B.G., Bevan, D.J.M. and Eyring, L. (1966) Phil. trans. 259A, 583.

98 Iguchi, E. and Tilley, R.J.D. (1978a) J. Solid State Chem. 24, 121.

99 Iguchi, E. and Tilley, R.J.D. (1978b) J. Solid State Chem. 24, 131.

100 Iijima, S. (1971) J. Appl. Phys. 42, 5891.

101 Iijima, S. (1973) Acta Cryst. A29, 18.

102 Iijima, S. (1974) Proc. of Conference on the diffraction of Real Atoms and Real Crystals, Melbourne, Australia.

103 Iijima, S. (1975) Acta Cryst. A31, 784.

104 Iijima, S. and Allpress, J.G. (1973) Acta Cryst. A30, 29.

105 Iijima, S., Kimura, S. and Goto, M. (1973) Acta Cryst. A29, 632.

106 Iijima, S., Kimura, S. and Goto, M. (1974) Acta Cryst. A30, 251.

107 Isvealsson, M. and Kihlborg, L. (1968) Arkiv Kemi 30, 129.

108 JANAF Tables of thermochemical data (1968) Dow Chemical Company, Midland, Michigan, including supplement No. 30.

109 Jongejan, A. and Wilkins, A.L. (1969) J. Less Common Metals. 19, 203.

110 Khan, A.S. (1968) D. Phil Thesis, Oxford.

111 Kikuchi, T. and Goto, M. (1976) J. Solid State Chem. 16, 363.

112 Kimura, S. (1973) J. Solid State Chem. 6, 438.

113 Kiukkola, K. and Wagner, C. (1957) J. Electrochem. Soc. 104, 379.

114 Knudsen, M. (1909) Ann. Phys. 28, 78. Ibid, (1909) 29, 179.

115 Koch, F. and Cohen, J.B. (1969) Acta Cryst. B25, 275.

116 Kodama, H., Kikuchi, T. and Goto, M. (1972) J. Less-Common Metals. 29, 415.

117 Kofstad, P.J. (1962) Phys. Chem. Solids. 23, 1579.

118 Kofstad, P. and Anderson, P.B. (1961) J. Phys. Chem. Solids. 21, 280.

119 Komark, K.L. and Silver, M. (1962) Proc. I.A.E.A. Sympos. in: "Thermodynamics of Nuclear Materials" (Vienna). p. 749.

120 Kovba, L.M., Trunov, V.K. and Pol'schikova, Z.Y. (1967) Inorg. Materials. 3, 354.

121 Kubaschewski, O., Evans, E.L.L. and Alcock, C.B. (1967) "Metallurgical Thermochemistry". Pergamon Press Ltd.

122 Kubaschewski, O. and Slough, W. (1969) in: "Progress in Material Science" Vol. 14, eds. Bruce Chalmers and W. Hume-Rothery, Pergamon-Press.

123 Langmuir, I. (1913) Phys. Rev. (2). 2, 329.

124 Lapitskii, A.J., Simanov, Yu. P. and Yarembasch, E.I. (1952) Zh. fig. Khim. 26, 56.

125 Laves, F., Petter, W. and Wulf, H. (1964) Naturwiss. 51, 633.

126 Lavrent'ev, V.I., Gerasimov, Y.I. and Rezukhina, T.N. (1961) Proc. Acad. Sciences U.S.S.R. (Physical Chem.) 136, 201.

127 Levin, H.L. and Roth, R.S. (1970) J. Solid State Chem. 2, 250.

128 Levy, A. (1964) J. Sci. Instrum. 41, 449.

129 Lundberg, M. (1970) J. Solid State Chem. 1, 463.

130 Lynch, D.F. and O'Keefe, M.A. (1972) Acta Cryst. A28, 536.

131 Magneli, A. (1948) Acta Chem. Scand. 2, 501.

132 Magneli, A. (1950) Arkiv Kemi. 1, 513.

133 Magneli, A. (1953) Acta Cryst. 6, 495.

134 Marinder, B., Dorm, E. and Seleborg, M. (1962) Acta Chem. Scand. 16, 293.

135 Marucco, J.F. (1974) J. Solid State Chem. 10, 211.

136 Massiani, Y., Crousier, J.P. and Streiff, R. (1978) J. Solid State Chem. 24, 85.

137 Menter, J.W. (1956) Proc. Roy. Soc. A236, 119.

138 Merten, U. (1959) J. Phys. Chem. 63, 443.

139 Mertin, W., Andersson, S. and Gruehn, R. (1970) J. Solid State Chem. 1, 419.

140 Mertin, W., Gruehn, R. and Schäfer, H. (1970) J. Solid State Chem. 1, 425.

141 Merritt, R.R., Hyde, B.G., Bursill, L.A. and Philp, D.K. (1973) Phil. Trans. A274, 627.

142 Millazo, G. (1956) Ann. Chim (Rome), 46, 1105.

143 Muan, A. (1958) Am. J. Sci. 256, 171.

144 N.B.S. Standard X-ray diffraction Powder Patterns (1953) Vol. 1, p. 57.

145 Nat. Bur. Stand. Tables - see Rossini et al., 1945.

146 Nimmo, K.M. (1971) D. Phil Thesis, Oxford.

147 Nimmo, K.M. and Anderson, J.S. (1972) J. Chem. Soc. Dalton. 18, 2328.

148 Nitsche, R. (1960) J. Phys. Chem. Solids. 17, 163.

149 Nitsche, R., Bolsterli, H.U. and Lichtensteiger, M.J. (1961) Phys. Chem. Solids. 21, 199.

150 Norin, R. and Magneli, A. (1960) Naturwiss. 47, 354.

151 Norin, R. (1963) Acta Chem. Scand. 17, 1391.

152 Norin, R. (1966) Acta Chem. Scand. 20, 871.

153 Norin, R. (1969) Acta Chem. Scand. 23, 1210.

154 Norin, R. (1971) Acta Chem. Scand. 25, 347.

155 Norin, R. and Dahlen, B. (1969) Acta Chem. Scand. 23, 1826.

156 Norin, R. and Magneli, A. (1960) Naturwiss. 47, 1354.

157 Norin, R. and Rappinger, B. (1971) Acta Chem. Scand. 25, 3484.

158 Norin, R., Arbin, C.-G. and Nolander, B. (1972) Acta Chem. Scand. 26, 3389.

159 Norin, D., Carlsson, M. and Elgquist, B. (1966) Acta Chem. Scand. 20, 2892.

160 O'Keefe, M.A. (1973) Acta Cryst. A29, 389.

161 O'Keefe, M.A., Buseck, P.R. and Iijima, S. (1978) Nature. 274, 322.

162 Parks, T.C., Thornber, M.R. and Bevan, D.J.M. (1970) J. Solid State Chem. 1, 536.

163 Parsons, J.R. and Halke, C.W. (1970) Phil. Mag. 22, 1071.

164 Petter, W. and Laves, F. (1965) Naturwiss. 52, 617.

165 Phillips, V.A. and Hugo, J.A. (1970) Acta Metall. 18, 123.

166 Pierotti, A. (1967) in: Vacuum Microbalance Techniques, p. 1., ed. Czanderna, Plenum Press, New York.

167 Picard, C. and Dode, M. (1970) Bull. Soc. Chim. Fr. 2486.

168 Porter, V.R. (1965) Ph.D. Thesis, Pennsylvania State University, U.S.A.

169 Poulis, J.A., Massen, C.H. and Pelupessy, B. (1965) in: Vacuum Microbalance Technique, vol. 4, ed. Waters, Plenum Press.

170 Reed, T.B. (1970) in: "The Chemistry of Extended Defects in Non-Metallic Solids" ed. L. Eyring and M. O'Keefe, North-Holland. p. 21.

171 Reisman, A. and Holtzberg F. (1970) in: "High Temperature Oxides". ed. A.M. Alpen, Part 2, p. 217, Academic Press, New York.

172 Robens, E. (1971) in: Vacuum Thermobalance Technique, Vol. 8, p. 73, ed. Czanderna, Plenum Press, New York.

173 Rossini, F.D., Wagman, D.D., Kilpatric, J.E., Taylor, W.J. and Pitzer, K.S. (1945) J. Res. Nat. Bur. Standards, 34, 143.

174 Roth, R.S. and Coughanour, L.W. (1955) J. Res. Nat. Bur. Std. 55, 207.

175 Roth, R.S., Wadsley, A.D. and Gatehouse, B.M. (1964) Naturwiss. 51, 262.

176 Roth, R.S. and Wadsley, A.D. (1965) Acta Cryst. 18, 724.

177 Roth, R.S., Wadsley, A.D. and Andersson, S. (1965) Acta Cryst. 18, 643.

178 Roth, R.S. and Wadsley, A.D. (1965) Acta Cryst. 19, 32.

179 Rüdorff, W. and Lunginsland, H.H. (1964) Z. anorg. allg. Chem. 334, 125.

180 Sakata, K. (1969) J. Phys. Soc. Japan. 26, 1067.

181 Schäfer, H. (1964) "Chemical Transport Reactions" (Translated by Hans Frankfort), Academic-Press.

182 Schäfer, H. (1972) in: Preparative methods in Solid State Chemistry" ed. P. Hagenmuller, Academic Press.

183 Schäfer, H., Bergner, D. and Gruehn, R. (1969) Z. Anorg. Allg. 365, 31.

184 Schäfer, H. and Huesker, M. (1962) Z. Anorg. Allgem. Chem. 317, 321.

185 Schäfer, M.W. and Roy, R. (1958) Z. Krist. 110, 241.

186 Schäfer, H., Gruehn, R. and Schulte, F. (1966) Angew. Chem. (Int. Ed. Engl). 5, 40.

187 Schäfer, H., Schulte, F. and Gruehn, R. (1964) Angew. Chem. Internat. Edit. 3, 511.

188 Schäfer, H., Jacob, H. and Etzel, K. (1956) 286, 27.

189 Scherzer, O. (1949) J. Appl. Phys. 20, 20.

190 Schmalzried, H. and Pelton, A.D. (1972) in: "Annual Review of Materials Science" Vol. 2. ed. Robert A. Huggins.

191 Schottky, W. and Wagner, C.Z. (1930) Phys. Chem. B11, 163.

192 Sharp, W.B.A. and Mortimer, D. (1968) J. Sci. Inst. 2. 1, 843.

193 Sheasby, J.S. and Cox, B.G. (1968) J. Less-Common Met.

194 Skarnulis, A.J. (1977) J. Microsc. Spectrosc. Electron. Vol. 2, 461.

195 Skarnulis, A.J., Iijima, S. and Cowley, J.M. (1976) Acta Cryst. A32, 799.

196 Steensland, T. and Førland, K.S. (1966) in: Vacuum Microbalance Technique, Vol. 5, ed. Behrndt, Plenum Press - New York.

197 Steinheil. E. (1972) in: Progress in Vacuum Microbalance Technique, Vol. 1, p. 111. ed. T. Gast and E. Robens.

198 Stephenson, N.C., Beale, J.P. and Craig, D.C. (1972) N.B.S. Spec. Pub. 364, Solid State Chem., 165 (eds. R.S. Roth and S.J. Schneider) (Washington: Nat. Bur. Stand.).

199 Sundberg, M. (1977) Forth European Crystallographic Meeting, Oxford. U.K.

200 Tamura, S. (1972) J. Mater. Sci. 7, 298.

201 Taylor, A. and Doyle, N.J. (1957) J. Less-Common Metals 13, 331.

202 Terao, N. (1963) Japan J. Appl. Phys. 2, 156.

203 Terao, N. (1965) Japan J. Appl. Phys. 4, 8.

204 Thon, F. (1971) "Electron Microscopy in Materials Science" (New York-Wiley), ed. U. Valdré.

205 Thornber, M.R., Bevan, D.J.M. and Summerville, E. (1970) J. Solid State Chem. 1, 545.

206 Tilley, R.J.D. (1972) in: "Solid State Chemistry" ed. L.E.J. Roberts [Vol. 1 - MTP Internat. Review of Sci. Inorganic Chem. Ser. 1, Vol. 10] Butterworth.

207 Tilley, R.J.D. (1975) in: "Solid State Chemistry" ed. L.E.J. Roberts [Vol. 1, MTP Internat. Review of Sci. Inorganic Chem. Ser. 2, Vol. 10] Butterworth, London.

208 Thomas, J.M. and Poulis, J.A. (1963) in: Vacuum Thermobalance Technique. Vol. 3. ed. Berhrandt Plenum Press.

209 Van Landuyt, J. and Amelinckx, S. (1970) Mater. Res. Bull. 5, 267.

210 Volmer, M. (1931) Z. Physik. Chem. Bodenstein. Festb. 863.

211 Von Dreele, R.B. and Cheetham, A.K. (1974) Proc. Roy. Soc. Lond. A338, 311.

212 Ubbelohde, A.R. (1956) Brit. J. Appl. Phys. 7, 313.

213 Ubbelohde, A.R. (1966) J. Chem. Phys. 33.

214 U.S. Bureau of Mines (1950) - See Kelly, K.K., Bulletins Nos. 476 and 477.

215 Wadsley, A.D. (1955) Revs. Pur. & Appl. Chem. Australia) 5, 165.

216 Wadsley, A.D. (1961a) Acta Cryst. 14, 660.

217 Wadsley, A.D. (1961b) Acta Cryst. 14, 664.

218 Wadsley, A.D. (1964) in: "Non-Stoichiometric Compounds" ed. L. Mandekorn, Academic Press, New York.

219 Wadsley, A.D. and Andersson, S. (1970) in: "Perspective in Structural Chemistry", eds. J.D. Dunitz and J.A. Ibers. Vol. 3, (Wiley - New York).

220 Walker, R.F. (1961) in: Vacuum Microbalance Technique Vol. 1, Plenum Press, New York, p. 87.

221 Waring, J.L. and Roth, R.S. (1964) Acta Cryst. 17, 455.

222 Waring, J.L., Roth, R.S. and Parker, H.S. (1973) J. Research Nat. Bur. Stand. - A. Physics and Chemistry. Vol. 77A, No. 6.

223 Watanabe, D., Castles, J.R., Jostsons, A. and Malin, A.S. (1967) Acta Cryst. 23, 307.

224 Watanabe, D., Terasaki, O, Jostson, S.A. and Castles, J.R. (1970) in: The Chemistry of Extended Defects in Non-Metallic Solids" ed. L. Eyring and M. O'Keefe, North-Holland, Amsterdam.

225 Wheatley, P.J. (1955) Acta Cryst. 8, 224.

226 Webster, A.H. and Bright, N.F.H. (1961) J. Amer. Ceram. Soc. 44, 110.

227 Wenk, H.R. (1976) "Electron Microscopy in Mineralogy", Springer-Verlag, New York.

228 Yamawaki, M., Masayoshi, K. and Mukaibo, T. (1974) J. Less-Common Metals. 37, 257.